SELECTIVE MOLECULAR ADSORPTION ON GOLD CLUSTERS

A Thesis

Presented to

the Academic Faculty

by

William Todd Wallace

In Partial Fulfillment

of the Requirements for the Degree

Doctor of Philosophy in Chemistry

Georgia Institute of Technology

June 2003

SELECTIVE MOLECULAR ADSORPTION ON GOLD CLUSTERS

Approved:

Dr. Robert L. Whetten, Chairman

June 18, 2003

Date Approved

Dr. Mostafa A. El-Sayed

Dr. C. David Sherrill

Dr. Thomas M. Orlando

Dr. Phillip N. First

This thesis is dedicated to my mother,

Martha Lowe Hall,

who always believed.

ACKNOWLEDGEMENTS

Over the past four years, I have found that the ability to successfully make it through graduate school depends quite a lot on being able to survive all of the tough times, the (much) fewer good times, and all of those times when it seems that nothing at all is happening. This survival cannot be achieved without a good group of people who make life a bit easier and provide the necessary "pick-me-up" when the tough times never seem to be ending. In my case, I have been supported by a wonderful (as well as quite large) group of people.

To begin, I think that it is important to acknowledge the tremendous amount of support that I have received from my family. With my somewhat uneven path during my undergraduate years, I'm sure that they wondered if I would ever finish school. Even so, my choices were never seriously questioned, which is a fact for which I am extremely thankful.

Having the right advisor is perhaps the most important factor in navigating the graduate school waters. I have been extremely lucky in that I have had an advisor who understood my career goals and what I was willing to do to accomplish them. Dr. Robert Whetten has taught me a great deal over the past 4 years, and I want to thank him very much for all of his support and invaluable insight.

Without minimizing the contributions and support of anyone else, I feel that it is especially important to acknowledge the support and friendship of Dr. Andy Leavitt at the State University of West Georgia, who has been a constant source of advice and help, including talking me through some of my toughest times at Georgia Tech. Also, the use of the YAG laser from Dr. Farooq Khan at SUWG is greatly appreciated, as it allowed research to continue in this lab when our laser was useless.

I want to thank all past and present members of the Whetten group who may have helped me during my graduate career, in particular Dr. Brian Salisbury. Brian's assistance as I was starting in the group was invaluable, as was his knowledge of the laser and time-of-flight system used for all of my research. He helped me get off to a very fast start, which has been a continual aid.

I would be remiss if I did not thank the other members of my thesis committee. Dr. Mostafa El-Sayed, Dr. Thom Orlando, Dr. David Sherrill, and Dr. Phil First have all provided helpful assistance to me over the past 4 years, whether it be discussing research, future plans, or, in the case of Dr. First, typing a paper at the last minute in possibly the most user-unfriendly format ever, LATEX.

Finally, I would like to thank the "support system" mentioned above. It includes at Georgia Tech (in no particular order) Janine Herring, Chris Lane, Lauren Schwimmer, Dennis Robinson, Jim Captain, Lynn Capadona, Dr. Andy Bartko, Dave Hathcock, Dr. Christy Landes, Christy Vestal, Rich Wyrwas, Christine Conwell, Dr. Dave Gaul, and Pat Widener. To all others at Georgia Tech who I have forgotten in my haste or the non-

Georgia Tech friends that I have been blessed with, you are all very special and have made my life a little easier. Thank You and Good Night...

TABLE OF CONTENTS

LIST OF FIGURES

CHAPTER V: Carbon Monoxide Adsorption on Gold Cluster Anions

CHAPTER VI: Humidity and Temperature Dependence of CO Adsorption on Gold Cluster Anions

LIST OF TABLES

SUMMARY

Worldwide interest was raised by the discovery that gold could engage in catalytic activities. Previously viewed as essentially inert, it was found that small gold clusters highly dispersed on metal oxide substrates were active for reactions such as low-temperature oxidation of carbon monoxide, hydrogenation, and reduction of nitrogen oxides, among others. This discovery led to many studies on different forms of these systems, a common finding of which was that the catalytic activity was closely tied to the size of the gold clusters. However, a definitive understanding of the active species of the supported gold catalysts has remained a mystery. Therefore, studies on the gas-phase gold cluster species in the absence of the support material were necessary in order to indisputably determine whether the gold clusters or the support material, or a combination of the two, produce the catalytic activity.

This thesis concentrates on the study of gas-phase gold cluster anions with reactants that have been studied on the supported cluster catalysts. Molecular oxygen (important for oxygen-atom transfer reactions) is found to adsorb as a superoxo species, resulting from electron transfer from the gold cluster anions. Combined with CO adsorption, in which highly size-dependent adsorption and saturation characteristics are observed, this O_2 adsorption activity provides insight into the CO oxidation processes seen on the supported gold catalysts. Surprisingly, the presence of moisture was found to allow

adsorption of CO and O_2 on previously inactive clusters. When introduced together, the coadsorption properties of these two reactants are seen to be, in many cases, cooperative, and, for some of the clusters, lead to the loss of carbon dioxide, the result of CO oxidation.

CHAPTER I

INTRODUCTION

The fields of heterogeneous catalysis and surface science have long been intertwined. Whether it is the studies of Faraday on oxidation reactions over platinum surfaces, Langmuir's studies of the surface properties of catalysts, or even work performed in the present day on the abilities of different surfaces to act as catalysts, advances in surface science often lead to the development of new heterogeneous catalysts, just as the discovery of new catalytic properties push surface scientists to discern the origin of these properties.[1,2] Surface science has played a tremendous role in determining the mechanisms of bond breaking and molecular rearrangements occurring on catalysts, as well as the determination of the effects of surface structure on catalytic activity. For example, Somorjai and coworkers, in studying the synthesis of ammonia from hydrogen and nitrogen over iron surfaces with different crystal faces, found that the Fe (111) and Fe (211) surfaces were highly active, while the (100) and (210) surfaces were only

moderately active, and the (110) surface showed almost no reactivity.[1] They explained that the most active surfaces are the only ones out of this group that expose iron atoms with seven nearest neighbors to the incoming reactant gases, and theoretical work on the system suggested that these highly-coordinated iron atoms should show increased catalytic activity. This explains the lack of activity of the Fe (110) surface, which has no exposed seven-coordinate atoms.

Another catalytic reaction studied on a transition metal surface is that of carbon monoxide oxidation on platinum surfaces, a reaction that has both practical importance and a relatively simple mechanism.[3,4] Xu and Yates studied CO oxidation on the Pt (335) surface, which has 4-atom wide Pt (111) terraces separated by a Pt (100) step.[3] They found that both CO adsorption and dissociative O_2 adsorption are preferred at the step sites, but that the presence of adsorbed O will block CO adsorption. CO that is bound at the step sites is not as easily oxidized as CO on terrace sites, possibly due to the fact that adsorbed O on terrace sites does not possess a reactivity for CO oxidation equal to that of step-adsorbed O. Finally, while the sites leading to the highest oxidation probability of CO under high CO coverage conditions are ones in which the CO is adsorbed at terrace sites adjacent to O adsorbed at step sites, the most favorable configuration is not necessarily the one in which the adsorbates are closest together. The authors attributed this behavior to other geometric and energetic effects that could produce more positive reaction conditions.

Reports such as the ones described above show how surface structure and energetics can affect catalytic reactions, and more of these studies have been performed on a

multitude of different surfaces possessing every manner of crystal face for almost any catalytic reaction, as described in detail by Somorjai[1] and Zaera.[2] This experimental work has led, in turn, to many theoretical treatments of the reactions in question. Mavrikakis and coworkers recently presented a review of the theoretical techniques used in these studies, as well as a review of the latest activity in this field.[5]

From some of the earliest studies of transition metal clusters, a comparison between the gas-phase clusters and catalytically active bulk metal surfaces were incorporated in order to justify the need for gas-phase studies, as clusters can often be viewed as nanometer-scale surfaces due to their large number of surface atoms.[1,6-9] Indeed, many of the initial studies were concerned with reactant gas adsorption on clusters of known catalytically active metals. For instance, research groups in academic,[10-13] government,[6,14] and industrial[15-17] labs were all interested in the reactions taking place on clusters of iron. Another highly active bulk surface, platinum, was also the subject of many cluster studies.[7,9,18-21] Some of these early studies provided vital insight into possible mechanisms occurring during cluster reactions. Whetten *et al.* found that, for neutral iron clusters, there seemed to be a correlation between the adsorption activity of hydrogen and the electron binding energy of the clusters, measured by photoionization studies.[16] With this correlation in hand, they drew a direct comparison between their studies and the finding that electron transfer from the metal to the hydrogen molecule is the critical factor in hydrogen dissociation on transition metal surfaces. Whetten *et al.* proposed that the ability of the cluster to engage in simple electron transfer to the σ^*

orbital of H_2 could explain this observed correlation. Since the establishment of this idea of adsorption activity being directly related to electron binding energy, it has been invoked many times and has also been criticized as being neither a general nor specific description of the observed adsorption activity of reactant gases of interest on transition metal clusters.[10,11,22] While this may be true, after a massive amount of cluster reactivity studies, there have been no other proposed explanations to date that have been found to provide a general mechanism for adsorption based on electronic effects.

These early cluster studies were made easier by the development of new methods of cluster production. Prior to 1981, the production of metal clusters was mostly confined to the use of different types of oven sources, in which the entire source was simply heated above the boiling point of the metal to be studied.[23] These types of sources had been successfully used to study the properties of several different types of metal clusters, such as those of copper[24] and alkali metals.[25] However, oven sources are normally limited to metals with a somewhat low boiling point, and, even taking advantage of the cooling effects of supersonic expansions, do not provide extensive cooling of the internal rotational and vibrational modes of the clusters.[23] This lack of cooling, in turn, makes the identification of spectroscopic features more difficult, due to the presence of "hot bands", or transitions from excited states.[26] However, the combination of supersonic expansions with laser vaporization of a bulk target by Smalley and Bondybey brought the field of cluster science into a new era.[23,27] In this technique, a localized pulsed heating of the material to be studied is provided by focused laser radiation in the presence of an

inert carrier gas (normally He).[28] The material of interest is able to form larger species due to the ability to undergo stabilizing third-body collisions with the inert gas, which is much cooler than in earlier studies involving oven sources due to the fact that the heating of the material is localized rather than involving the entire cluster source (An additional benefit of the use of a pulsed source is the fact that the pumping requirements of this type of source are much less than that of continuous flow gas sources, resulting in lower costs). As the clusters and carrier gas leave the cluster source, in a nominal "cluster beam", a supersonic expansion serves to further cool the species in the beam. Early studies on the temperatures of these cluster species suggested that the rotational and translational temperatures of the clusters in these expansions were approximately 5 K,[28] while the unthermalized vibrational temperature was approximately 350 K. The ability of the clusters to undergo increasing third-body collisions has been shown to lead to even greater thermalization, i.e. close to room temperature.[29]

The initial development of these cluster sources enabled a wide variety of physical and chemical properties of clusters to be studied under much more favorable conditions than in the past. For instance, much higher resolution studies of excited cluster states were carried out as well as the determination of the ionization potentials of many cluster species. Another benefit of the so-called "Smalley" laser vaporization cluster source is the fact that, in addition to neutral clusters, significant abundances of cationic and anionic clusters are produced. This allowed the study of an even wider variety of properties, such as electron affinities and anionic cluster structures, as well as the chemical reactivities of all charge states of a given cluster species.

The past fifteen years have continued to see the comparison between cluster and bulk adsorption (and catalytic) activities, though the comparison is now based on somewhat firmer footing. Many studies have been carried out on the chemical properties of different commercial catalysts, which basically consist of transition metal clusters (of > 1 nm) grown on metal oxide supports.[30-32] Improved techniques of cluster growth have been developed in order to allow the researchers to obtain greater control over the sizes of clusters grown. Therefore, the change of catalyst efficiency can be studied as a function of cluster size. These effects led to a large number of experimental studies on "model" catalysts,[33-35] in which both the metal oxide surface and transition metal clusters are grown under well-defined, ultrahigh vacuum conditions. Such conditions also allow the catalysts to be amenable to traditional surface science techniques, such as x-ray photoelectron spectroscopy (XPS), auger electron spectroscopy (AES), low-energy electron diffraction (LEED), and scanning tunneling microscopy and spectroscopy (STM and STS), among others.[33]

One of the more recent developments in the studies of catalysts perhaps makes the strongest connection between gas-phase and condensed-phase research. This is the development of techniques allowing deposition of size-selected cluster species from the gas phase onto a surface under conditions in which the clusters are not destroyed upon landing.[36-48] In such a case, a direct connection can be drawn between gas-phase species and those on surfaces, providing an avenue for discussion of cluster active sites versus interstitial sites and electronic effects versus geometric effects as the determining factor for catalytic activity. There are concerns as to the ability of the clusters to retain

their structure and identity upon landing, as well the extensive times required to deposit sufficient amounts of clusters, but this technique or derivatives of it provide the best opportunity to develop "designer" catalysts, in which the ultimate activity of a catalyst can be achieved by placing the most active cluster on the surface.[44,49]

The ability of gold to act as a catalyst is one of the newer topics currently under study. Though generally considered an inert transition metal, catalysts (such as the commercial supported catalysts described above) containing gold clusters were found to be highly active in such processes as carbon monoxide oxidation, partial and complete oxidation of hydrocarbons, and reduction of nitrogen oxides, among others [50-52]. These catalysts were subsequently commercialized and have found an initial use as an ambient temperature air purification device. Though this discovery led to a multitude of studies on the "commercial" catalysts in an attempt to understand the nature of the catalytic activity,[52-60] studies on model gold catalysts,[34,61-65] those catalysts created using the soft-landing technique described above,[39-42,44] as well as theoretical studies of these systems,[39,63,66-74] have only recently begun in earnest. Several reviews covering the work performed on gold cluster catalysts have been published in the past few years.[52,75,76]

Studies of the properties of gold clusters in the gas phase have only recently begun to accelerate. This is due to the fact that gold has long been considered to be chemically inert[75] and also due to the fact that the methods of production of the larger clusters had not yet been developed.[77] Some of the earliest studies on gold cluster electronic

properties were performed by Lineberger and coworkers using photoelectron spectroscopy (PES),[78] but these only extended to the gold pentamer anion, as their experimental setup does not allow easy study of clusters higher in mass. However, the laser vaporization cluster sources of Smalley and others[23,27] made it possible to produce larger clusters and study their properties using PES and other techniques.[77,79-86] Some extremely interesting results were obtained for the gold cluster systems in these studies. For instance, in an attempt to find the effects of the addition (or subtraction) of a single atom, Taylor *et al.* measured the electron affinities (EA) of gold cluster anions using PES.[77] Their results indicated that the EAs varied in an odd-even manner, i.e. clusters with an even number of atoms possessed lower EAs than their neighboring odd-atom clusters. This behavior was compared to that shown by the spheroidal electron shell model, which was invoked and described extensively in the 1980s for other cluster species,[87-93] due to its ability to predict such physical properties as ionization potentials (IP), electron affinities, polarizabilites, and mass spectral abundances. An excellent review of the shell model was presented by deHeer.[94] Briefly, certain numbers of valence electrons create enhanced stability for different cluster species. For these clusters, the mass spectral abundance distributions (from photoionization mass spectrometry) are dominated by drop-offs following the peak arising from an especially stable cluster. This type of behavior has also been seen in positively and negatively charged clusters, hence the comparison by Taylor *et al.* For the smaller clusters studied ($N \leq 7$), the changes in EA with increasing cluster size did not mirror that predicted by the shell model, though the odd-even alternations were still present. In the case of this

oscillation, the shell model predicts that, even for situations in which an electronic shell is not closed, pairing of electrons can also produce enhanced stability, or higher EAs (as well as IPs), as also shown for other coinage metal clusters.[80,95-97] For clusters larger than 7 atoms, there was an excellent correlation between the measured electron affinities and the shell model. Their conclusion from this correlation was that, for the larger clusters, the valence electrons of gold could be well explained by the shell model. This interpretation provided a very simple basis for the discussion of the properties of gold clusters and has generally been successful in explaining these properties.

Until recently, very little attention had been given to the structural properties of free (gas-phase) gold clusters, other than a few studies concerning the shape of Au_6^-.[81,84,98] However, the past several years have seen a dramatic increase in the number of theoretical and experimental studies concerning gold cluster geometries. Theory has been especially productive, predicting both cluster geometric and electronic structures. An initial study by Häkkinen and Landman investigated the effects of cluster size on the structures of neutral and anionic gold clusters in the 2 to 10 atom size range.[99] They found that three-dimensional structures were favored for clusters greater than seven atoms (neutrals) and six atoms (anions) and suggested that the good agreement between the vertical detachment energies (the energy required to remove the most weakly bound electron) calculated for their structures and those measured earlier[77,78,81,82,84] provided support for their calculated structures. Subsequent ion-mobility measurements and density functional calculations performed by Kappes and coworkers on small Au_N^+ clusters ($N < 14$) indicated that three-dimensional structures were also favored for cations

of greater than 7 atoms.[100] However, further ion-mobility and density functional studies by the same group on small Au_N^- clusters (N < 16) suggested that the onset of three-dimensional structures reported by Häkkinen and Landman was too early. Instead, they found that planar structures were favored up to Au_{13}^-.[101] This result motivated Landman and coworkers to perform a more extensive density-functional study than their previous work, focusing entirely on Au_7^-.[102] In this study, they found that hybridization between the 6s and 5d orbitals indeed caused planar structures to be favored for this size cluster. In fact, the closest lying three-dimensional isomer was 0.47 eV higher in energy. They also noted that the calculated vertical detachment energies of the lowest energy planar and three-dimensional structures were very similar, as well as being very similar to the measured detachment energies, implying that it is not safe to make a definite determination of cluster structure based solely on these energies.

In general, there is not too much disagreement concerning the actual structures of small gold clusters at this point. After performing the calculations described above, Landman and coworkers[102] obtained minimum energy structures for Au_N^- clusters up to 13 atoms that correlated with the structures obtained experimentally by Furche *et al.*[101] Density functional studies carried out by Selloni and coworkers[103] on small (N < 7) gold clusters of all charge states were also in line with those calculated by Häkkinen and Landman[99] and experimentally measured by the group of Kappes.[100,101] Even so, there are still some who disagree with specific structures. For instance, Wells *et al.* continue to suggest that the lowest energy structures of the cationic, neutral, and anionic

forms of Au_{9-11} clusters are all three dimensional,[104] while Oviedo and Palmer actually proposed that the lowest energy structure of the Au_{13} cluster is amorphous.[105] Recently, exciting results were reported for the Au_{20}^- and Au_{20} clusters using PES and density functional calculations.[83] These studies implied that Au_{20} should be very stable and chemically inert, as an extremely large HOMO-LUMO gap was measured. Theory suggested that the most stable structure of the neutral was a tetrahedral structure. This high stability led the authors to propose that Au_{20} could be used as a possible building block for nanoscale materials, as has also been proposed for another highly stable cluster, buckminsterfullerene (C_{60}). Whether this ever occurs for Au_{20} remains to be seen, but the possibility is certainly exciting and will push research on gold clusters even further. Even with these few disagreements (or lack of secondary supporting work), it is obvious that a basic consensus is being approached concerning the lowest energy structures of gold clusters.

Prior to the work carried out in this thesis, only a few studies concerning the chemical properties of gold clusters in the gas phase had been attempted.[106-113] Therefore, with the information garnered from more recent studies of the commercial, model, and size-selected gold catalysts, more intensive studies of these chemical properties were performed under conditions not achievable in the previous work.

Chapter 2 first provides an overview of some of the different techniques that have been used to study cluster reactivity in the gas phase. Then, the experimental methods that were used to study the gas-phase chemical activities of negatively charged gold clusters in this work are discussed. This discussion includes a pulsed-helium, laser

vaporization cluster source developed previously in this laboratory, the variable-temperature fast-flow reactor, which allows near-atmospheric pressure studies to be performed on the gold clusters, and the reflectron-time-of-flight mass spectrometer used to measure the abundances of reaction products. Finally, results are presented from different types of clusters in order to show the abilities of this instrument.

The reactions of gold cluster anions with molecular oxygen (O_2) are described in Chapter 3. Though initial studies of this process had been performed earlier, this work provided some interesting results not attainable in the previous studies. Here, saturation coverages of O_2 on the clusters were achieved, allowing an adsorption mechanism to be suggested. This mechanism could be important in understanding the ability of gold cluster catalysts to efficiently oxidize carbon monoxide, even at low temperatures.

Chapter 4 discusses the effects of water on the O_2 adsorption activity on gold cluster anions. Studies on the commercial catalysts showed that the catalysts were not only tolerant of moisture, but some of their activities were even enhanced. Several explanations for this effect were suggested, but none sufficiently accounted for the moisture enhancement. The experimental results presented in Chapter 4 show that the adsorption of a hydroxide group on the cluster anions (resulting from water introduction in the system), significantly affects the O_2 adsorption activity. Accompanying theoretical work on this system performed by coworkers is also presented. The combination of these results provides support for the mechanism of molecular oxygen adsorption on bare gold cluster anions and also provides a possible explanation for the manner by which moisture could aid in the catalytic activity of supported gold clusters.

The interaction of gold cluster anions with carbon monoxide (CO) is described in Chapter 5. The results indicated that initial adsorption of CO seems to be dominated by the electronic structure of the cluster. Under higher CO partial pressures, saturation effects were seen on the clusters. Surprisingly, the saturation coverages obtained were quite low, and the maximum number of CO adsorbates began to decrease at relatively small cluster sizes. Results showing the relative ease with which some CO molecules simply fall off the clusters are also presented, indicating extremely weak binding energies.

The humidity- and temperature-dependence of CO adsorption on gold cluster anions is shown in Chapter 6. While the effects of water are not as dramatic as those presented for O_2 adsorption, they are nevertheless interesting. The major effect seen is that the presence of water makes previously inactive clusters active for CO adsorption, most likely by providing a means of releasing excess reaction energy. Studies of the temperature dependence of CO adsorption show that, like O_2, equilibrium conditions are achieved at temperatures close to room temperature and above, but kinetics play an important role at low temperatures.

The coadsorption properties of CO and O_2 on gold cluster anions are presented in Chapter 7. The presence of an individual reactant is seen to play a dramatic role in the ability of the other reactant to adsorb on the clusters, and several other interesting effects are seen, including the first experimental evidence of the gas-phase oxidation of CO by gold clusters. These results have presented new questions as to the active species in supported, gold cluster catalysts.

CHAPTER II

EXPERIMENTAL METHODS

2.1 Introduction

The study of charged metal clusters and their reaction complexes is inherently coupled to some sort of mass detection.[114] Therefore, improvements in the field of cluster science are often the result of improvements in mass spectrometry. There are several types of mass spectrometry that have found use in the study of gas-phase species. The different techniques used, and their methods of mass spectrometric detection will be discussed below.

A very popular technique of studying charged species uses the ability to store or "trap" ions using either fixed dc potentials augmented with sufficiently high ac potentials (Paul trap) or specific cyclotron frequencies (Penning trap).[115] By changing the conditions of the traps, the translational energies of the ions (Paul trap) or the cyclotron frequencies (Penning trap) can be increased to study the mechanism of dissociation using

collision-induced dissociation (CID) with the buffer gas also present in the trap. Alternatively, a secondary reaction gas (or gases) can be injected into the trap[116-124] in order to study any ion-molecule or cluster-molecule reactions. While an obvious benefit of these techniques is the ability to store ions for large amounts of time (many seconds) and their extremely high sensitivities, there are also some drawbacks. For instance, the quantity of ions able to be stored is limited due to space-charge effects in the miniscule volume of the traps (typically around 10^4 ions mm^{-3}).[117] Also, in the case of reaction studies, only small amounts of reaction gas can be used. The normal reactant partial pressure in a Fourier transform-ion-cyclotron resonance mass spectrometer (Penning trap) is on the order of 10^{-9}-10^{-8} mbar, though a novel technique of using pulsed gas valves allows the reactant pressure to be momentarily raised to approximately 10^{-5} mbar,[118] and reactant partial pressures for Paul traps are generally on the order of 10^{-2} mbar.[117] Therefore, while these techniques are useful for determining thermal rate constants and product lifetime measurements, they generally are not able to push reaction products towards their maximum values (saturation).

Another method that has found wide use for studying cluster reactions is that of the guided ion beam. While the specific methods used by different groups may be different, the general techniques are quite similar. In one use, clusters are formed using various methods (laser vaporization, ion sputtering, dc discharge) and are focused into a beam using quadrupole or octopole ion guides. Generally, a quadrupole mass filter is used to select a single ion of interest, which then enters a well-defined reaction zone where ion-(or cluster-) molecule reactions can take place under single-collision conditions.[125] By

adjusting the voltages between the source and reaction regions, the thermal velocities of the clusters can be varied, providing a wide range of kinetic energies under which reactions can occur, which allows the determination of reaction cross-sections. After leaving the reaction zone, the product species are filtered using a second quadrupole mass filter with their abundances being measured using highly sensitive detectors.[12,13,18,126-128]

A final method used to study cluster reactions, and the basis of this thesis, is that of the fast-flow reactor. This technique is relatively new, only being introduced in the past 20 years.[11,129] The fast-flow reactor is similar to the guided-ion beam technique described above, in that the methods of cluster production are similar, reactions take place in the presence of a dense, inert buffer gas, and product detection uses either time-of-flight or quadrupole mass spectrometers.[29] However, there are also some important differences. The most noticeable difference is the fact that the fast-flow reactor is attached directly to the cluster source. This provides both advantages and disadvantages for the study of cluster reactions. By being directly attached to the source, there is no requirement for a differentially pumped region containing a reaction vessel. This cuts down on pumping requirements (as well as space), and also has an added benefit. In conventional flow-reactor techniques, the majority of the initial buffer gas used for cluster growth is removed from the system prior to entering the flow reactor. Therefore, while the reactions take place in the presence of buffer gas, the pressures used are dictated by the pumping ability in the reaction chamber. This total pressure is normally much less than 1 Torr.[29,112,126] However, with the fast-flow reactor, the reactions take

place in the presence of the same buffer gas in which the clusters are grown. This reduces the additional amount of buffer gas needed in the reaction region. Due to the high buffer-gas pressures (normally between 10-1000 Torr) and fast flow (~ 10^5 cm/s) required to ensure efficient cluster growth and thermalization prior to entering the fast-flow reactor, reactions are normally carried out in the high-pressure limit under conditions of thermal equilibrium.[29] Calculations from several groups have indicated that the total pressure in the fast-flow reactor is on the order of 100 Torr,[129,130] yielding sufficient buffer gas collisions to ensure that unimolecular decay does not significantly contribute to the reaction, though the pressures are conceivably much higher.[131]

Mass selection presents a problem in the use of fast-flow reactors. In guided-ion beam reaction studies, individual species are selected for study prior to entering the reaction zone. This allows for the much easier observation of reaction processes resulting in fragmentation or neutralization of the parent cluster species. In fast-flow reactor studies, of course, there is no opportunity for mass selection prior to the reaction region. Therefore, in order to rule out the processes mentioned above, a careful accounting of signal intensity is required both with and without reactant gas added.[132,133] This will be discussed in more detail in Chapter 3. Combined with time-of-flight mass spectrometric techniques, which allows the study of a wide size range of clusters, the much higher reactant partial pressures available in the fast-flow reactor makes it a technique in which the advantages significantly outweigh the disadvantages.

Fast-flow reactors have been extremely useful in providing information on cluster reactivities since their inception. For instance, studies on nickel,[7,19,134-136]

platinum,[7,9,19] rhodium,[19] iron,[7,14-16] and copper clusters,[7,137] as well as other types of metal clusters,[8,138,139] have been performed using reactant molecules such as D_2, N_2, NH_3, CO, and others. Some recent review articles have discussed the reactions occurring on neutral[22] and charged[13] transition metal clusters. Additionally, fast-flow reactors have been used to study the chemistry occurring on ionic[29,140-142] and non-metal clusters[143-145] and have provided a wealth of information.

One of the more interesting uses of the fast-flow reactor is that of the "chemical probe" technique, pioneered by Riley and coworkers at Argonne National Laboratory.[139,146] Using the saturation coverages of different reactant molecules on nickel clusters possible using the fast-flow reactor, they determined the number of preferred binding sites on differently sized clusters and used that information to determine cluster structures. In the case of nickel[146] and copper clusters,[137] the clusters adopt geometric structures based on icosohedral packing. This technique has also been used on other types of clusters to determine their structures.[22] While the "chemical probe" method does not provide absolute proof of cluster structures, it is one of the more useful methods of determining cluster geometries, particularly in cases where the cluster size prohibits the use of spectroscopic probes.

In addition to the studies mentioned above and others (including those presented in the later chapters of this thesis), there are many studies still being carried out in fast-flow reactors. For instance, Knickelbein and coworkers are using a continuous-flow, fast-flow reactor to produce silver and gold clusters with individually adsorbed ethylene, ethanol,

and methanol and using infrared-photodissociation spectroscopy to gain insight into the bonding mechanisms of adsorbates on the clusters.[109,110,147] Also, metal oxide clusters are now particularly of interest, due to their role in catalytic[148-151] and atmospheric chemistry.[152,153] Obviously, the fast-flow reactor technique can be very useful in gaining a better understanding of these processes.

The remainder of this chapter will describe the experimental apparatus used for the studies described later in this thesis. Separate sections will describe the cluster source, fast-flow reactor, and different parts of the mass spectrometer, as well as the methods of gas introduction in the source and flow reactor. Finally, data obtained from a variety of materials in the instrument will be presented.

2.2 Complete Experimental Apparatus

A schematic of the entire experimental apparatus is shown in **Figure 2-1**. This picture shows both the source and detection chambers. The base pressure in the source chamber is normally less than $2x10^{-6}$ Torr, and the base pressure in the detector chamber is normally $2x10^{-10}$ Torr. Typical operating pressures are $3\text{-}7x10^{-5}$ Torr and $5\text{-}8x10^{-8}$ Torr, respectively, though these values can vary dramatically with the pulsed valve settings. Both chambers are maintained under vacuum using 8" turbomolecular pumps (Pfeiffer Vacuum, TPU 520) backed by mechanical pumps (Pfeiffer Vacuum, DUO 020 (source) and DUO 010 (detection)). Previous designs used for the experiments described

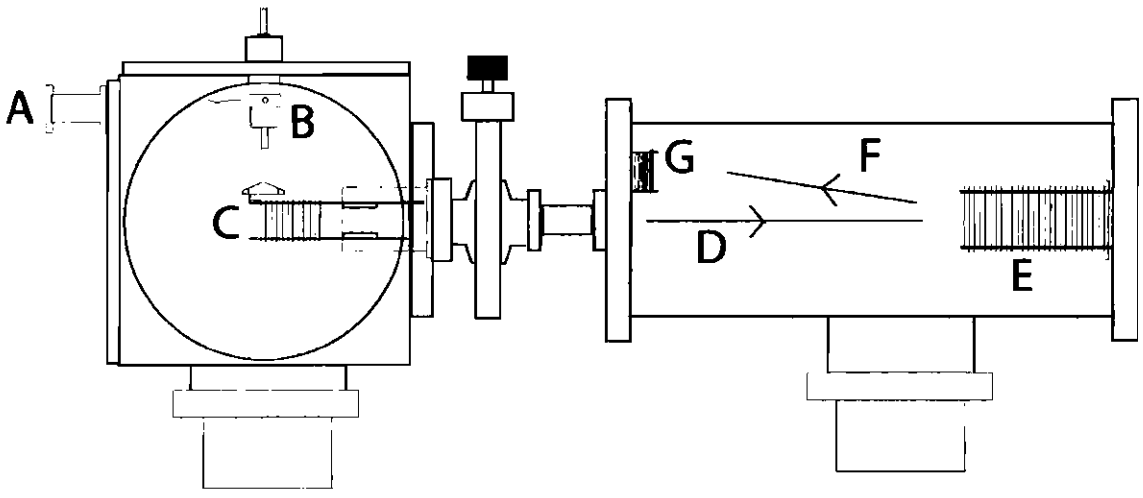

Figure 2-1: Reflectron time-of-flight mass spectrometer with laser ablation cluster source

A view of the entire experimental apparatus described in the text. (A) Rotary-motion feed-through for rotation and translation of the sample rod. (B) Laser ablation cluster source and fast-flow reactor. (C) Extraction region of the time-of-flight mass spectrometer. (D) The first field-free flight region of the mass spectrometer, with a flight length of 102 cm. (E) Reflectron assembly for energy focusing and reacceleration towards the detector. (F) Second field-free flight region, with a flight length of 50 cm. (G) Dual microchannel plates for the detection of clusters and reaction products. Adapted from references [132,154].

in chapters 3, 5, and 6 also incorporated a chamber between the source and detection chambers that contained ion optics for improved signal resolution. The pressure in that particular chamber eventually became too high, however, leading to degradation of the signal resolution, and it was subsequently removed.

2.3 Cluster Production and Growth

Clusters were produced for these experiments using a variation of the laser-vaporization cluster source developed by several groups in the early 1980s,[23,27] discussed in Chapter 1, and which has also been described in previous reviews of this instrument.[29,132] These sources have been used widely since their inception,[22] though improvements have been made by different groups.[155,156] A view of the entire cluster source and fast-flow reactor assembly is shown in **Figure 2-2**. Upon being triggered by a delay generator (Stanford Research Products), a short pulse of an inert gas (normally He) is released from a pulsed-gas valve (A, General Valve Series 9) into the laser vaporization block (B). The stagnation pressure behind the General Valve is normally 100 psig, though this can vary, as will be described later. Ablation of the material of interest (in the form of a 1/8" rod, as described previously)[132] is achieved using the 3rd harmonic output (355 nm) of a Nd:YAG laser (Continuum) triggered to arrive at the same time as the pulse of inert gas. The material released from the rod is swept along within the gas into a growth region of variable length (C). Within this region, the ablated

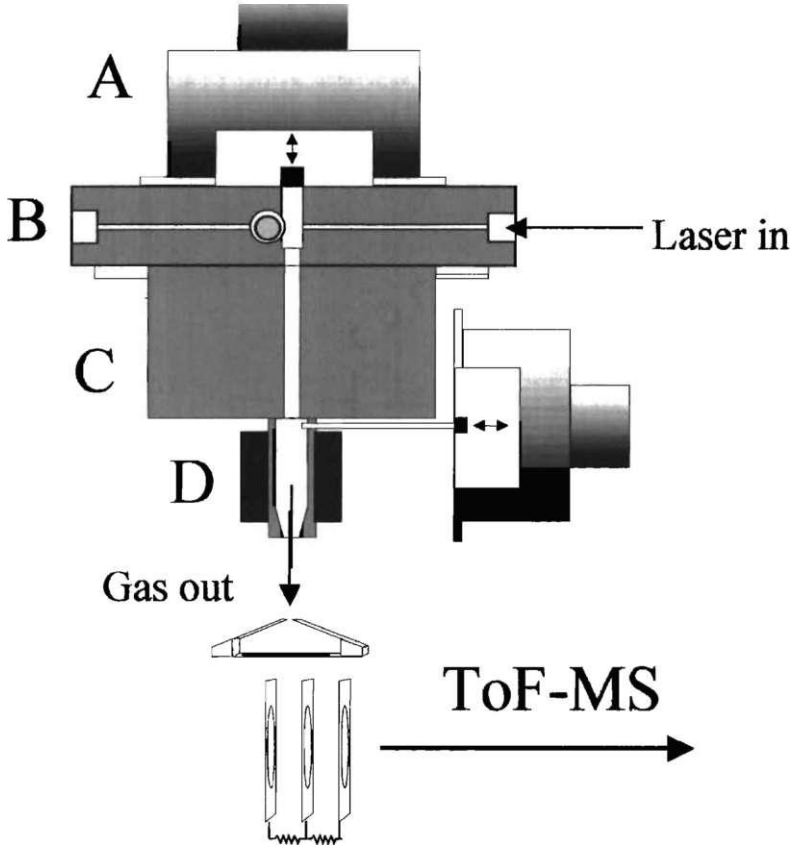

Figure 2-2: Laser ablation cluster source

(A) Pulsed valve for introduction of inert buffer gas into the source block (B), containing a 1/8" rotating and translating rod of the material to be studied. The 3rd harmonic output of a Nd:YAG laser to timed to arrive at the rod at the same instant as the gas pulse. The gas and material removed from the rod are swept into a growth region (C) where cooling and cluster formation occur. Cluster growth ends with the expansion of the gas into (D) the fast-flow reactor.

material condenses into clusters and thermalizes with the walls. While mostly neutral clusters are formed in this type of source, sufficient amounts of both cationic and anionic species are also produced for experimental reaction studies. The gas pulse undergoes an isothermal expansion from the 2mm-diameter channel of the growth region into the fast-flow reactor (D), at which point cluster growth is completed.

2.4 Variable Temperature Fast-flow Reactor

A closer view of the fast-flow reactor used for the majority of the experiments discussed here is shown in **Figure 2-3**. This reactor is constructed of stainless steel with an entrance diameter of 6 mm and that is choked down to 3 mm at the exit. The total length of the reactor is 25 mm. Immediately below the entrance of the reactor, a 1.55 mm hole allows for the introduction of a dilute mixture of reactant gas from a second General Valve through a 25 mm capillary tube of 1.5 mm diameter. This second valve (with a normal stagnation pressure of 30 psig) is triggered at a time that ensures the largest amount of reaction with the clusters. Alternatively, the timing could be adjusted so that there was no reaction occurring, which allows both reacted and unreacted mass spectra to be obtained under similar conditions. The total pressure in this reactor has been estimated to be approximately 150 mbar.[130] Other reactors were also constructed with different dimensions in order to raise the total pressure by reducing the volume. These brass reactors were 16mm, 25mm, and 37mm in length, with 4mm entrance diameters

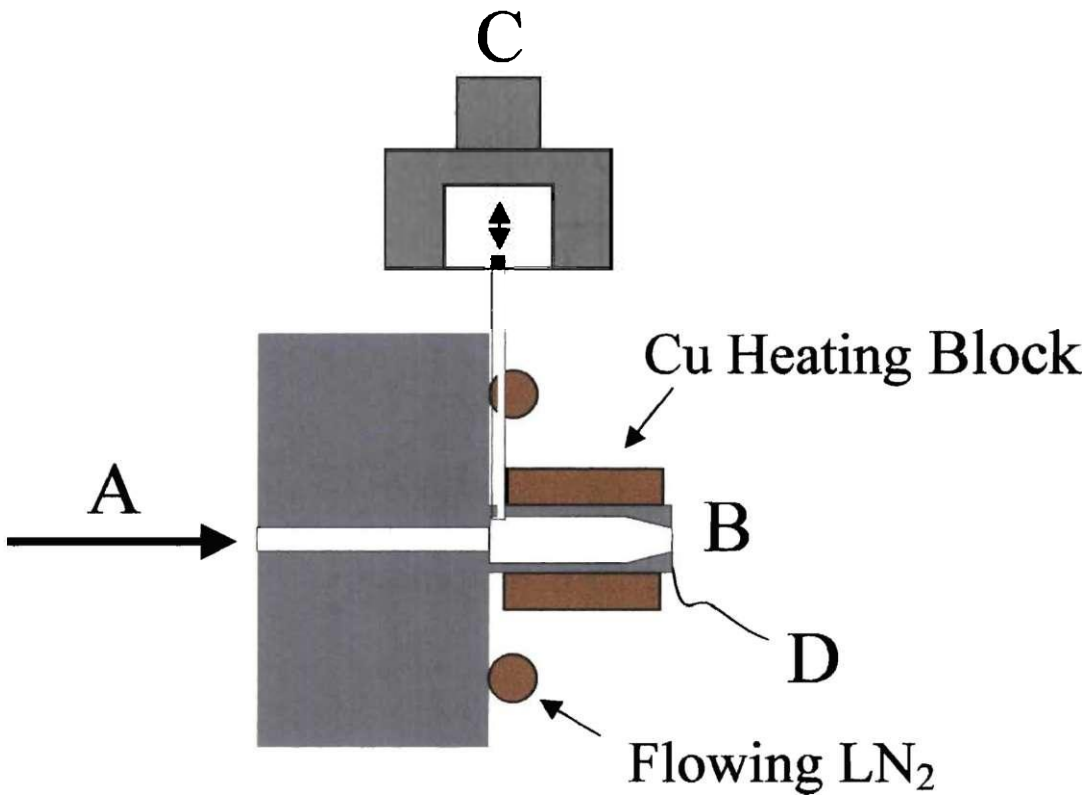

Figure 2-3: View of the reaction zone

A schematic of the area in which reactions take place during the experiments. The material ablated from the rod is swept by a high-pressure gas pulse (A) into the cluster growth region, where the clusters grow and thermalize prior to entering the fast-flow reactor (B). The reactor used for the majority of the experiments presented here is a 0.7 cm^3 stainless steel reactor of 25-mm length. Reactant gases are introduced into the flow reactor using a secondary pulsed valve (C). Cooling of the reactor is achieved using copper coils with flowing liquid nitrogen attached to the bottom of the growth region, while heating is accomplished using resistive heating of a copper block attached to the reactor. A thermocouple (D) is used to measure the temperature of the reactor.

choked down to 2mm at the exits. Scaling by volume, the total pressures obtained in these reactors were on the order of 680 mbar, 340 mbar, and 100 mbar, respectively. Pulse profiles measured using a fast-ion gauge (Beam Dynamics) are shown in **Figure 2-4**. This fast-ion gauge provides the best method by which optimal overlap between the main (cluster) pulse and the secondary (reaction) pulse can be determined. In this figure, the much larger full-width at half maximum (FWHM) of the reactant pulse can easily be seen. This larger width is due to the very constricted travel of this pulse through the capillary tube, which also serves to slow the travel of the pulse. In **Figure 2-4**, both the main and secondary valve are triggered at the same time, but they obviously do not reach the fast-ionization gauge at the same time. Due to this fact, the secondary valve must be fired approximately 500 microseconds prior to the firing of the main valve to achieve optimal overlap of the pulses.

Surrounding the reactor is a copper heating element with a tungsten wire within it. Using electrical vacuum feed-throughs, voltage can be applied to the tungsten wire (using a Sorensen DCS 40-25 power supply), thereby resistively heating the copper block and the fast-flow reactor. With temperature monitoring using a chromel-alumel thermocouple, the temperature of the flow reactor has been raised as high as 423 K.[145] Attached to the bottom of the growth region of the cluster source is a copper plate through which liquid nitrogen can flow and which has allowed for the cooling of the reactor to temperatures as low as 170 K. The ability to vary the temperature over such a wide range permits the determination of adsorbate binding energies on the clusters or activation barriers for adsorption or reaction. Upon leaving the flow reactor, the clusters

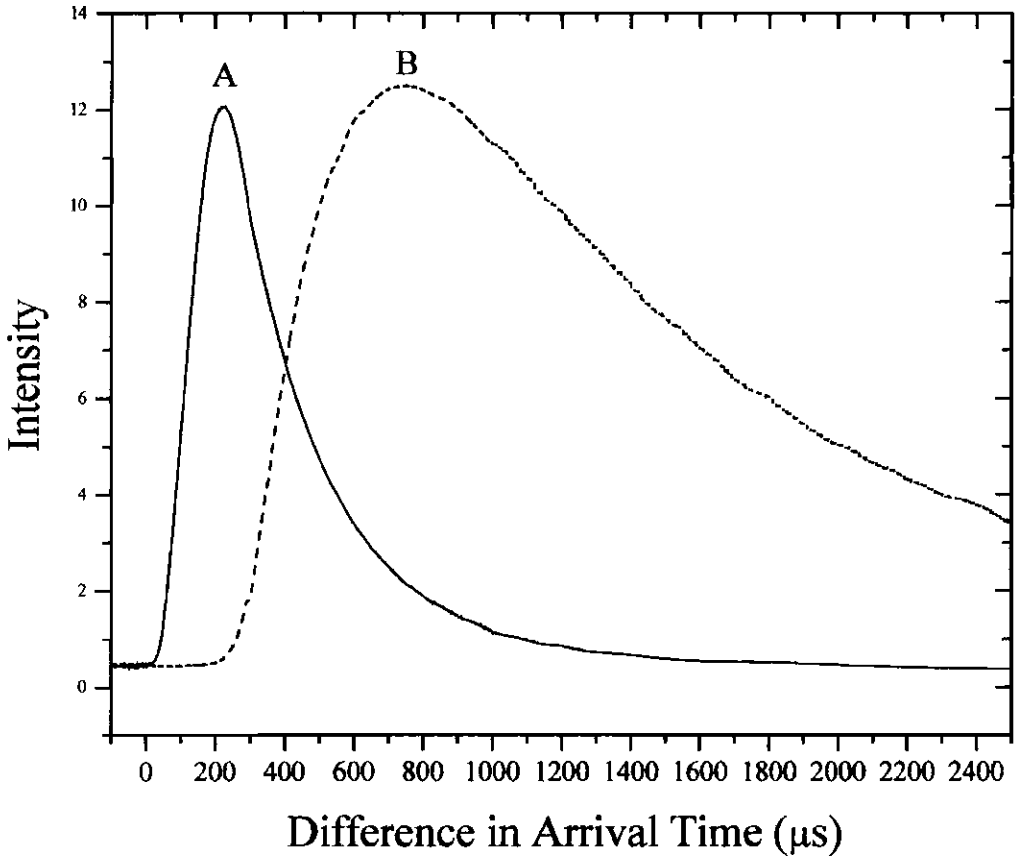

Figure 2-4: Pulse profiles of main and secondary gas valves

A plot of the difference in arrival time at the Beam Dynamics Fast-Ion Gauge between the main (A) and secondary (B) pulsed-gas valves when the valves are triggered at the same time. With this timing setup, the reactant gas pulse cannot achieve acceptable overlap with the main pulse, requiring that the secondary valve be pulsed~ 500 μs earlier than the main valve. The FWHM of the pulses are: (A) 335 μs and (B) 1400 μs.

and reaction products undergo a supersonic expansion into vacuum and are skimmed to collimate the beam prior to entering the time-of-flight mass spectrometer.

It is important to be aware of some of the assumptions and limitations of fast-flow-reactor measurements.[22,131] First, the gas temperature, T, is assumed to be that of the high-pressure, inert buffer gas (He). This temperature is further assumed to simply be equal to the wall temperature, T = 300 K, assuming there is sufficient helium to disperse the heat remaining from the laser ablation cluster source. However, the experiments lack an internal, fast thermometry, and higher temperatures are sometimes implicated. Secondly, the reactant partial pressure is variable over an extremely wide range (10^{-6} bar-1 bar). However, experiments using the fast-flow reactor lack an internal, fast barometer, and therefore require a known reaction, which serves as an internal calibration. This process is not simple, however, and the pressure values that are cited above are only best estimates of the pressures achieved in the flow reactor. Next, adsorption reactions may occur under equilibrium control if there is no large barrier to reaction (> 40 kT) and if there are sufficient helium collisions to remove the energy gained from adsorption, E_b. If the interactions between the adsorbate and the cluster are relatively weak, and there is no major structural rearrangement (which may be illustrated by the breaking of strong bonds), then these conditions are often met.[22] Finally, the actual measurement of the relative abundances of cluster-adsorbate complexes requires a transition to vacuum, which results in both an abrupt decrease in reactant partial pressure (loss of collisions with reactant molecules) and a coinciding decrease in temperature (de-energizing of

cluster-adsorbate modes) that together act to "lock in" the abundances determined by the equilibrium conditions.

2.5 Reflectron-Time-of-Flight Mass Spectrometer

2.5.1 Extraction Region

The time-of-flight mass spectrometer is oriented perpendicularly with regards to the incoming cluster beam. This orientation has been shown to lead to dramatically increased signal resolution due to the fact that it removes some of the kinetic energy spread of the ions arising from thermal conditions in the source region.[29] This particular mass spectrometer has been described in exhaustive detail elsewhere,[29,132] so only an overview of it will be given here.

The extraction region of the mass spectrometer is responsible for directing the ions away from their initial trajectory (i.e. in the direction of the initial gas pulse) and accelerating them towards the detector. This particular extraction region is a two-field acceleration region based on the original model of Wiley and McLaren,[157] consisting of 12 individual plates with holes in their centers (11 sub-regions, each with a hard-wired resistor). The first field region consists of the first 4 plates (3 sub-regions). By adjusting the voltage differences in this field with a variable resistor in parallel with the hard-wired resistors, it is possible to compensate for any differences in placement of two ions of the same mass in the first field region, which would cause them to receive unequal voltage

pulses. A cartoon of the extraction region is shown in **Figure 2-5** along with a plot of the voltage drops experienced by an ion for two different settings of the variable resistor and an overall voltage pulse of 2 kV. At the end of extraction region are two horizontal plates, controlled by a separate power supply and voltage divider, which serve to deflect the accelerated beam upwards towards the detector, removing their initial downward momentum. The magnitude of this deflection voltage determines the mass range observed in the experiments. At higher acceleration voltages (5 kV, for instance), this deflection voltage can be varied over a wide range (75-100 V) without much effect on the mass range, as the clusters are moving extremely quickly through the deflection region. However, at lower acceleration voltages (such as 2 kV), the ions spend much more time in this region, and the mass range observed becomes much more sensitive to deflection voltage changes, with a change of only ten volts leading to dramatic changes in mass range.

2.5.2 Reflectron and Detection

After being accelerated in the extraction region and traversing the deflection region, the ions leave the source chamber and entered the detection chamber. The low pressures present in this chamber help to ensure that degraded resolution and signal attenuation due to scattering from background gases are not a concern. Additionally, the low background interference makes it well suited for other techniques with relatively minor changes, such as spectroscopic (i.e. photoelectron, photodissociation, etc.) or scattering experiments such as surface-induced dissociation, for which it was used previously.[158,159] The

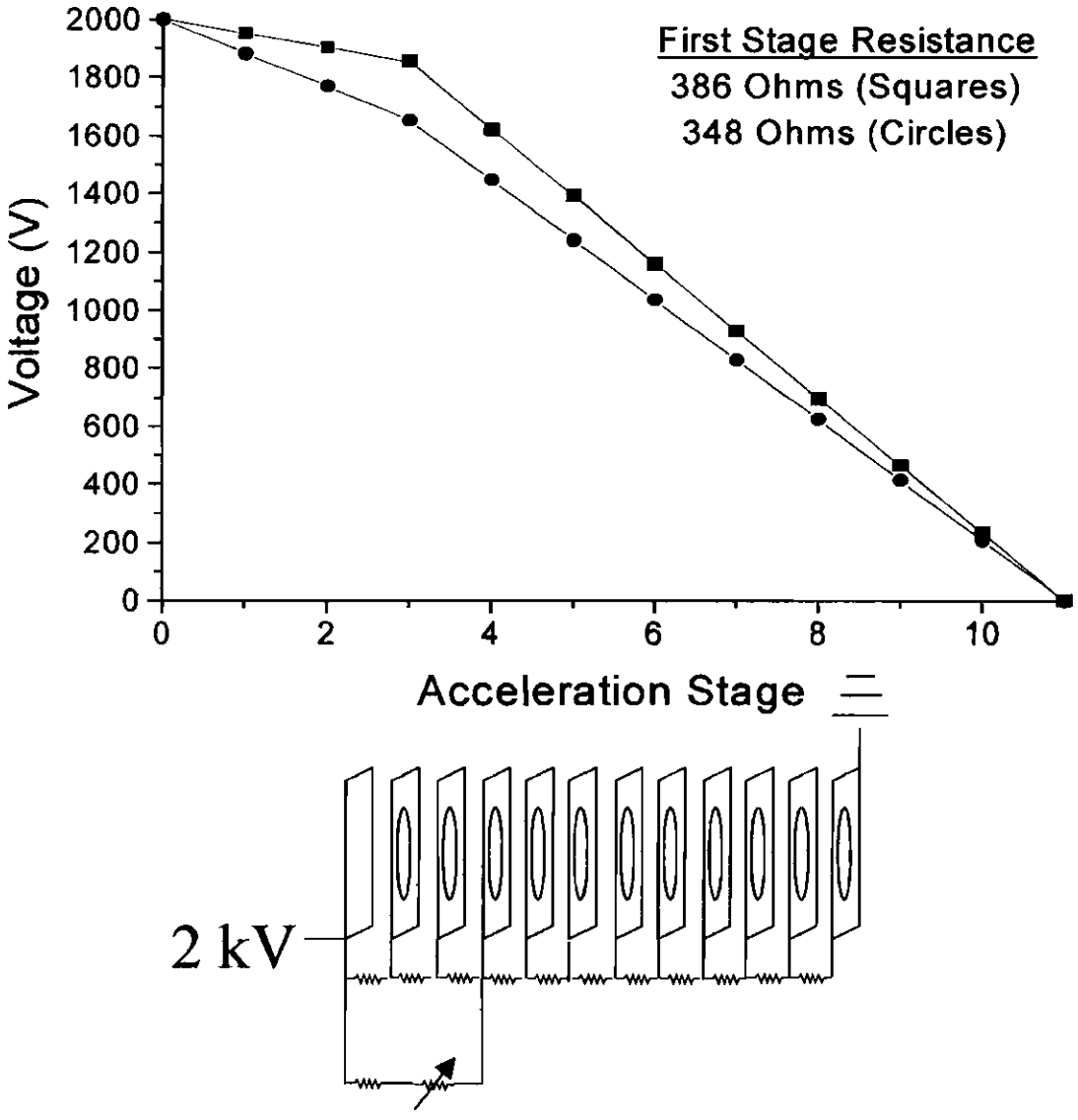

Figure 2-5: Extraction region and voltage drops

Bottom Frame: A schematic of the extraction region of the time-of-flight mass spectrometer. From the left, the first 3 stages between plates have 360 Ohms resistors in parallel with a variable resistor (600 – 15600 Ohms). The remaining stages have 600 Ohm resistors. Top Frame: Plots showing the voltage drops experienced by an ion when the variable resistor is set at 600 Ohms (squares) and 15600 Ohms (circles).

theory behind the use of a reflectron[160-163] and the design and construction of the reflectron used in this instrument have been described previously.[29,132] The reflectron basically serves as an ion mirror to redirect incident ions towards the detector, which is placed off-axis of the ion beam in the rear chamber. However, the reflectron, if used correctly, can also dramatically increase the mass resolution observed in a series of experiments. Ions of the same mass may have different kinetic energies arising from spatial effects in the acceleration region or thermal effects in the cluster source.[29,160] While the space focusing of the two-stage extraction region helps with some of these effects, the addition of the reflectron can almost completely remove them. Ions with greater velocities arising from any remaining energy spread penetrate deeper into the retarding and reacceleration regions of the reflectron than those ions of the same mass traveling more slowly, causing the faster-moving ions to spend a greater amount of time in the reflectron. By applying the correct voltages to the two stages of the reflectron (retarding and reacceleration), the ion beam could be focused on the detector both in space and time.

Starting from the rear of the reflectron (closest to the rear of the chamber), the overall voltage is set to be almost equal to that given to the ions in the extraction region, ensuring that no ions can simply travel straight through the reflectron and strike the back of the chamber. Starting from this rear plate, there are equal, and relatively small, voltage drops across the first 14 plates. In the remaining 4 plates, however, there is a very large voltage drop to ground potential. Therefore, incident ions encounter an extremely large retarding potential over a very short distance before encountering a much longer, more gradual

potential that then served to reaccelerate them towards the detector. The voltage increases in the reflectron for an initial 2 kV accelerating voltage are seen in **Figure 2-6**. Upon leaving the reflection region, the clusters are detected by a dual microchannel plate assembly. Voltages are supplied to the detector from a single power supply using an appropriate voltage divider, depending on the polarity of the species of interest.

2.6 Signal Acquisition and Data Analysis

The signal from the detector is amplified using a high-speed operational amplifier, displayed using any analog oscilloscope, and digitized and averaged using a 175 MHz LeCroy 9304M digital oscilloscope. Initially, the next step required that the digitized and averaged signal be transferred to an IBM PS/2 computer using modified LeCroy GPIB interface software, followed by another transfer to a computer used for analysis. This process did not allow for the rapid study of results needed for study of reaction species close in mass to possible contaminants or for on-line changes in applied voltages in attempts to improve signal resolution. Subsequent purchase and use of a faster microcomputer allowed for direct connection of the analysis computer to the LeCroy digital oscilloscope, significantly improving the ability to study results while also performing experiments. In both cases, however, results were analyzed using a version of Origin software (Microcal Software, Inc.).

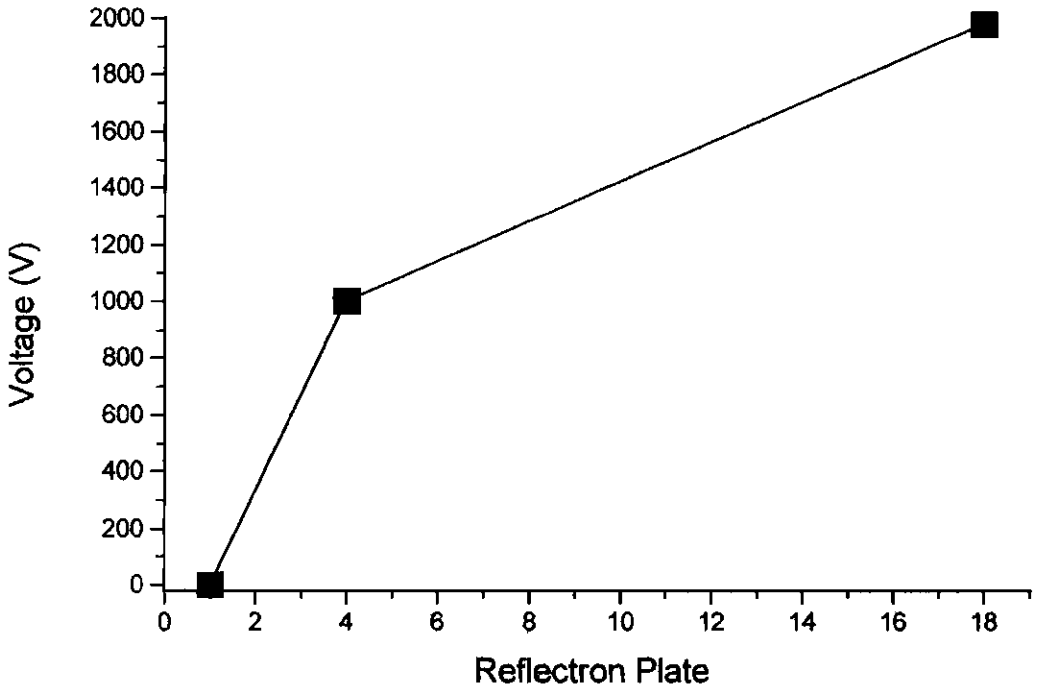

Figure 2-6: Voltage rise in reflectron region

Plot showing the voltage rise seen by an ion incident on the reflectron. In this case, the overall reflectron voltage is approximately equal to that of the extraction voltage used to accelerate the ions initially (2 kV). Incident ions initially see an extremely large potential rise over a short distance. The remaining potential rise takes place over a distance three times greater than that of the initial rise.

Several different materials were used to calibrate the mass spectrometer. Prior to removing the middle vacuum chamber, which required a subsequent decrease in acceleration voltage due to a dramatic reduction in path length, cesium iodide clusters ($Cs_NI_{N+1}^-$) were used routinely for mass calibration. These clusters are ideal for this task, as they very easily form very large clusters, allowing calibration to be performed over a wide mass range in a single experiment, and neither of the constituents possesses any significant isotopic distribution. Additionally, $Cs_NI_{N+1}^-$ clusters have been studied extensively, using a variety of different techniques, in this group and others.[164-166] A standard pulse train used to produce and study cluster reactions is presented in **Figure 2-7** and a representative mass spectrum of $Cs_NI_{N+1}^-$ clusters is shown in **Figure 2-8**.

With the removal of the middle vacuum chamber, the lower acceleration voltages used did not allow such a wide mass range of $Cs_NI_{N+1}^-$ clusters, with their large separations in mass (approximately 260 amu), to be observed, making it less suitable for a calibration tool. Fortunately, however, many studies have been performed on carbon cluster anions, C_N^-,[167-169] which made it possible to compare spectra obtained from this instrument with the published spectra in order to determine correlations. Subsequently, carbon clusters became the calibration tool of choice. Even with the lower acceleration voltages used, the small mass separations of carbon clusters (12 amu) allowed many more calibration points to be obtained. While not isotopically pure like $Cs_NI_{N+1}^-$, the relatively large abundance of ^{12}C made these clusters ideal as a calibration tool. Spectra obtained for several mass ranges are presented in **Figure 2-9**.

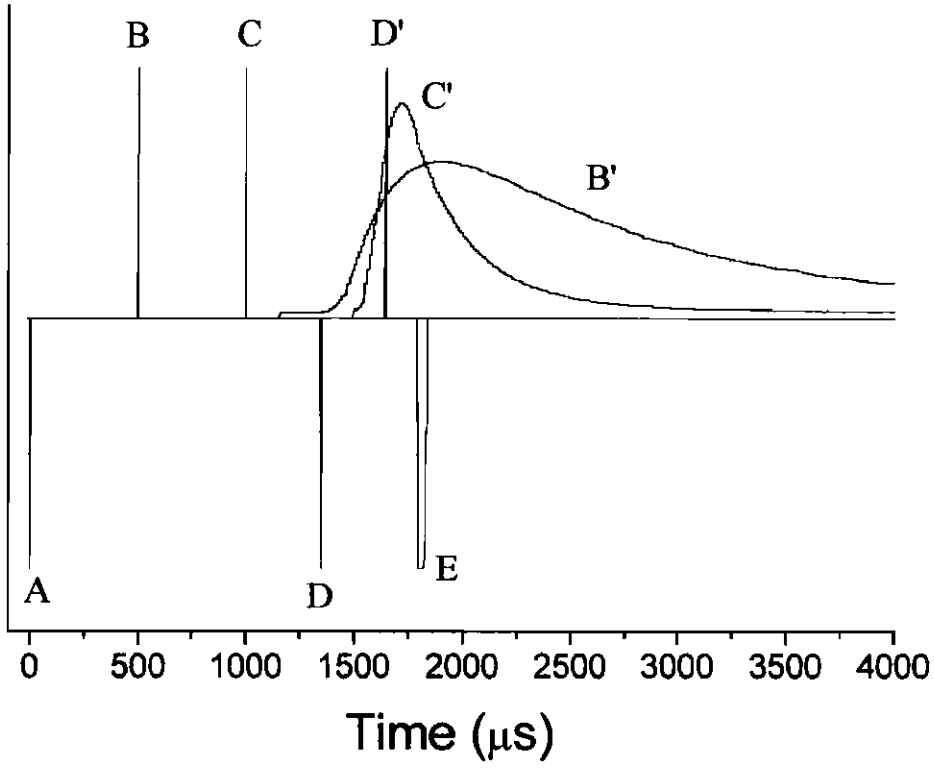

Figure 2-7: Standard pulse train for cluster studies

Pulse train used to generate clusters and study their reactivities. (A) Main system trigger, which drives subsequent pulses. (B) Secondary reaction valve trigger, triggered early to achieve maximum overlap with main cluster pulse. (B') Secondary reaction pulse. (C) Main pulsed-gas valve trigger. (C') Main gas pulse. (D) Trigger for Nd:YAG laser. (D') Laser firing. (E) HV pulse used for extraction of charged cluster species.

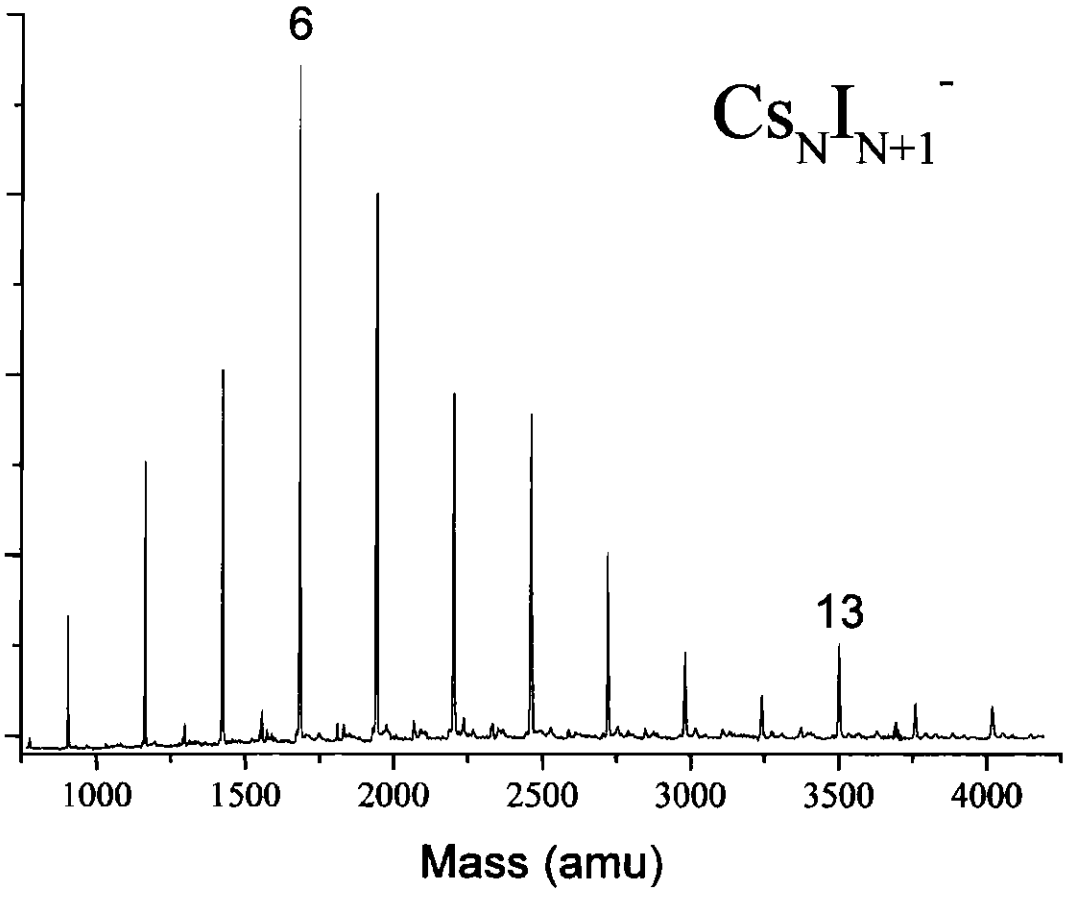

Figure 2-8: Cesium iodide mass spectrum

A representative mass spectrum of cesium iodide clusters, $C_NI_{N+1}^-$, used for mass calibration of the time-of-flight mass spectrometer, where N represents the number of atoms in the cluster of a particular element. With the longer mass spectrometer path length and higher acceleration voltage, $C_NI_{N+1}^-$ clusters provide many calibration points over a wide mass range.

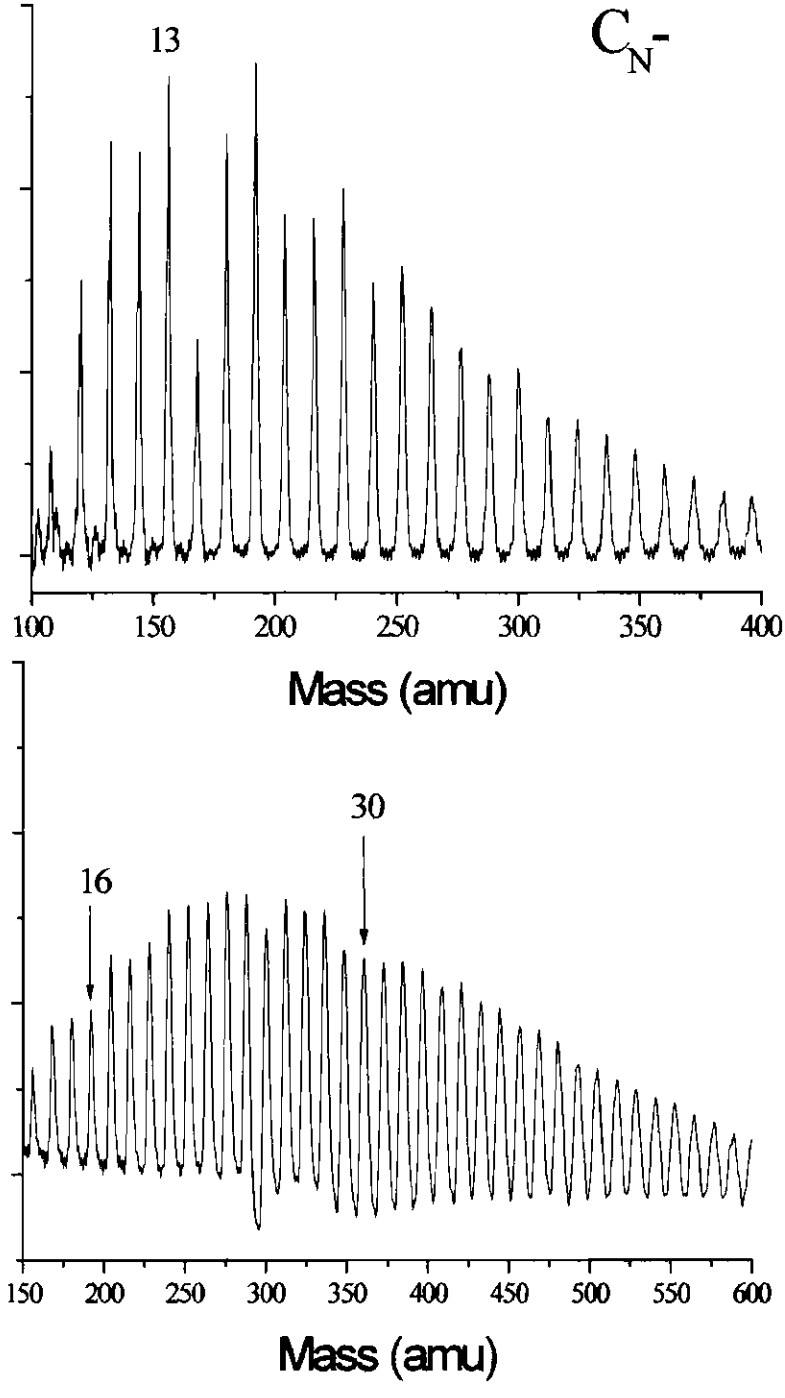

Figure 2-9: Carbon mass spectra

Representative mass spectra of different mass regions for carbon cluster anions, C_N^-.

CHAPTER III

ADSORPTION OF MOLECULAR OXYGEN ON GOLD CLUSTER ANIONS

3.1 Introduction

Due to its largely unreactive nature, gold has long been known as a "noble" metal, undergoing few of the reactions of its transition metal counterparts. Therefore, it has found much of its use as a null reaction system or as a support for self-assembled monolayers. However, this non-reactive nature is largely confined to bulk gold, as nanometer-scale gold clusters grown or deposited on metal-oxide supports have been shown to be quite active for a variety of reactions, including low-temperature combustion, hydrogenation and oxidation of hydrocarbons, and reduction of NO_x species.[34,39-42,50-52,55-59,61-63,65,66,75,170]

Cox and coworkers performed an early investigation into the room-temperature adsorption reactions of gas-phase gold clusters using helium flow-reactor

methods.[107,108] In this study, they found that the adsorption of several gas-molecules (H_2, CH_4, O_2) occurred on many of the clusters; remarkable considering that none of these gases had been observed to occur on bulk gold surfaces at room temperature or above.[171,172] Even so, the adsorption activity was found to be highly dependent on the size- and charge-state of the cluster. For instance, O_2 was found to adsorb on Au_{10}^+ and on many of the even-N Au_N^- clusters (no results were reported for the neutral gold cluster adsorption properties). Cox *et al.* indicated that the adsorption probability appeared to be correlated to the electron binding energies of the clusters, i.e. the electron affinity (EA) for the anions and the second ionization potential for the cation.

In studies subsequent to those of Cox and coworkers, Lee and Ervin measured the bimolecular rate constants of the $Au_N^- + O_2$ system ($N \leq 7$) in the low-pressure limit. Collision-induced dissociation studies were also performed in order to determine the binding energies of O_2 on the clusters.[113] As in the studies of Cox *et al.*, only the even-N Au_N^- clusters were shown to be reactive towards O_2 adsorption within their detection limit.[112]

This chapter describes a series of experiments on the adsorption of O_2 on Au_N^- clusters ($N < 23$), using high-pressure flow-reactor methods at ambient temperature. These experiments, carried out over a wider range of O_2 partial pressures than in other studies,[107,108,112,117,118] were motivated by the need to determine saturation coverages on the clusters and to establish equilibrium conditions for the adsorption-desorption processes. An additional motivation lay in the fact that a greater

understanding of the adsorption activity of gold clusters in the gas phase could provide information as to reaction mechanisms taking place on the nm-scale supported clusters.

3.2 Experimental Methods (Abbreviated)

The reactions between negatively charged gold clusters and molecular oxygen (O_2) were investigated using pulsed helium flow-reactor methods and instrumentation described in **Chapter 2**. Briefly, charged clusters were produced in a helium flow stream by pulsed laser vaporization, exposed to reactants, and detected by time-of-flight mass spectrometry using perpendicular pulsed extraction fields. Cluster growth and primary cooling occurred within the confined flow stream of the inert buffer gas; secondary cooling occurred upon expansion into vacuum. The resulting gas jet was skimmed to form a highly collimated cluster beam; the negatively charged components were extracted at right angles by the pulsed field of a reflectron-type time-of-flight mass spectrometer. Two configurations were used in these experiments. Normally, the reactant gas (O_2) was introduced downstream by a secondary pulsed valve; using this method with a concentration of 20% O_2:He, only the most reactive cluster (Au_6^-) could be completely reacted. By using this secondary pulsed valve to introduce the molecular oxygen, reactions occurred following the cluster growth and primary cooling stages and, therefore, had no effect on the growth of the clusters. In the event that the two valve pulses were not temporally overlapped, no oxygen adsorption was observed.

Alternatively, molecular oxygen was introduced into the primary flow stream by seeding the He buffer gas (upstream addition), and cluster growth took place in the presence of both He and O_2. This ensures the highest pressures and longest possible reaction times with the pre-formed clusters, thereby favoring the establishment of chemical equilibrium conditions. For example, a 20% O_2:He mixture, at 5 bar stagnation pressure, yields an O_2 partial pressure approaching 250 mbar in the vicinity of the metal vaporization zone, accounting for pressure drops due to an expansion in the channel diameter (1 mm to 2 mm). In this way, the reaction of even-N clusters (except N = 12, 16 and 22) could be driven to > 80% completion. Despite the transient high temperatures in the vaporization plasma zone, no evidence for processes involving oxygen atoms (or ozone) could be detected.

3.3 Results

Figures 3-1 and **3-2** show typical results for the reaction of gold cluster anions from 4 - 12 atoms with molecular oxygen, in which the O_2:He mixture was pulsed into the reactor by the secondary valve. If the two gas pulses are displaced temporally, by more than 1.0 ms, no adsorption is detected. When temporally overlapped, depletion of certain Au_N^- peaks is observed, accompanied by the appearance of the corresponding $Au_NO_2^-$ peak at 32 amu higher mass. These are attributed to the reaction process:

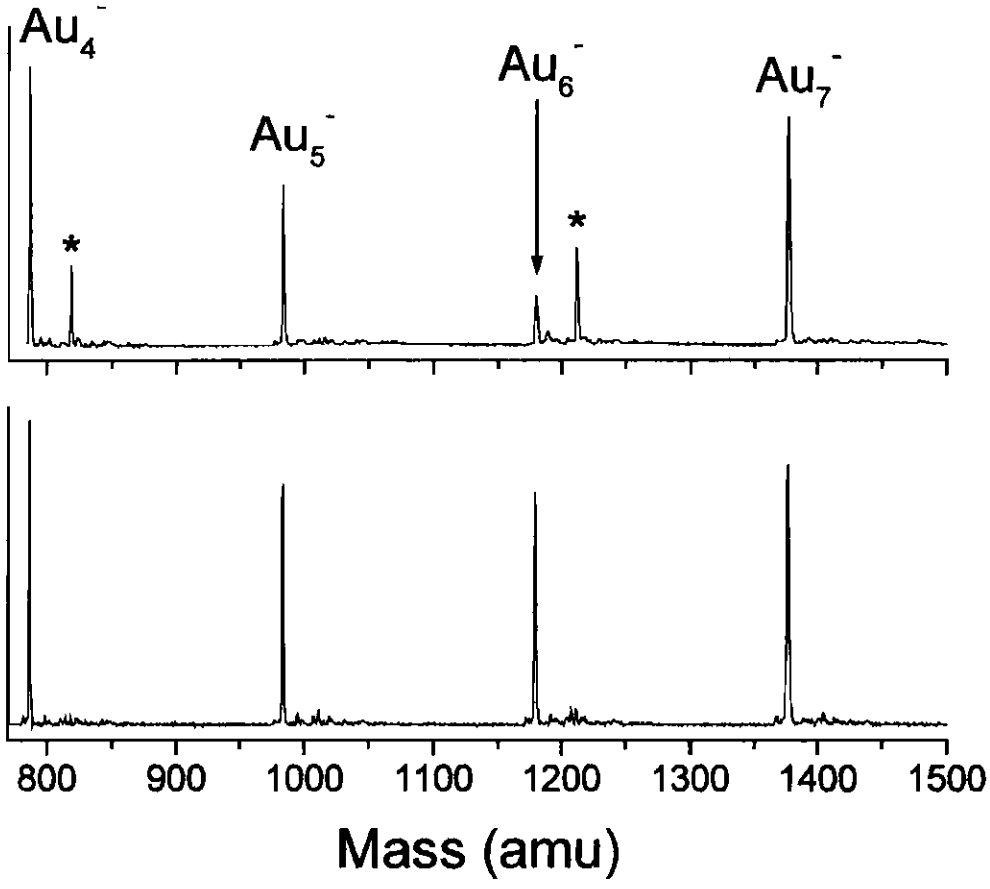

Figure 3-1: Initial adsorption of O_2 on gold cluster anions, Au_N^-

Plots showing the result of addition of molecular oxygen in the fast-flow reactor to smaller Au_N^- clusters ($N \leq 7$). Bottom frame: A mass spectrum obtained when the secondary (reactant) gas pulse is offset from the main (cluster) pulse. Top frame: The resulting mass spectrum when the main and secondary pulses are overlapped. New peaks (marked with asterisks) appear at 32 amu higher mass than the even-N peaks, corresponding to the molecular adsorption of O_2.

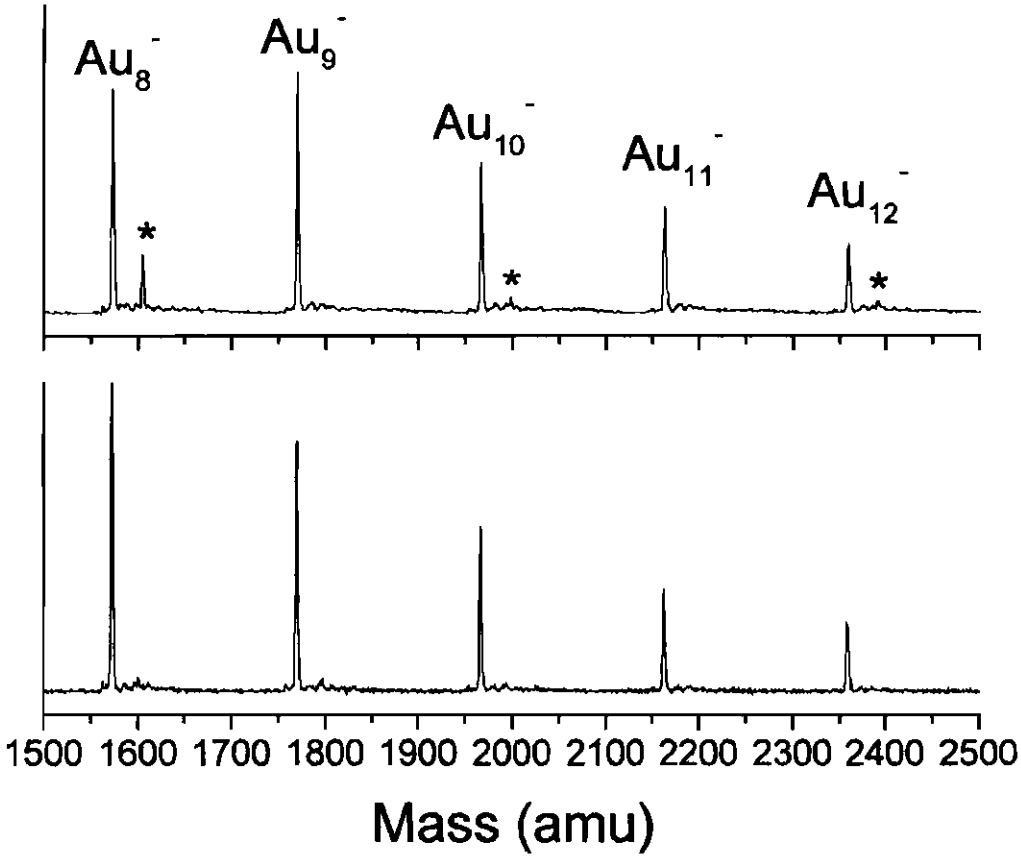

Figure 3-2: Initial adsorption of O_2 on gold cluster anions, Au_N^-

Plots showing the result of addition of molecular oxygen in the fast-flow reactor to larger Au_N^- clusters ($8 \leq N \leq 12$). Bottom frame: A mass spectrum obtained when the secondary (reactant) gas pulse is offset from the main (cluster) pulse. Top frame: The resulting mass spectrum when the main and secondary pulses are overlapped. New peaks (marked with asterisks) appear at 32 amu higher mass than the even-N peaks, corresponding to the molecular adsorption of O_2.

$$Au_N^- + O_2 \leftrightarrow Au_NO_2^- \quad (1).$$

An unusual feature that is readily apparent in **Figures 3-1** and **3-2** is the absence of evidence for secondary adsorption, to yield species such as $Au_6O_4^-$, a result that holds even when pure (undiluted) O_2 is used. These results are contrary to the reactions of molecular oxygen with other metal clusters. Specifically, nickel,[173] sodium,[174] vanadium,[175], silver,[112,116] and copper[112,137] clusters all show evidence for the adsorption of multiple oxygen molecules, a process that is normally interpreted as a dissociative chemisorption process.

A greater extent of reaction can be observed when molecular oxygen was introduced into the primary pulsed helium valve. This introduction results in a qualitative agreement with the size-dependent reactivity pattern seen in the case of downstream addition of O_2 in the reactor. As extreme cases, **Figures 3-3** and **3-4** show the distribution produced when a 20% O_2:He mixture is used upstream. Under these "saturation conditions", the mass spectrum assumes a very simple appearance, as the various clusters are either completely unaffected or almost completely converted. In **Figure 3-4**, the sole exception to this pattern is N = 10, which remained partially (~ 60%) converted.

In order to attribute the change in Au_N^- signal and the appearance of the corresponding $Au_NO_2^-$ peaks exclusively to the adsorption of molecular oxygen, other channels, such as reactive fragmentation or neutralization, had to be discounted. **Figure**

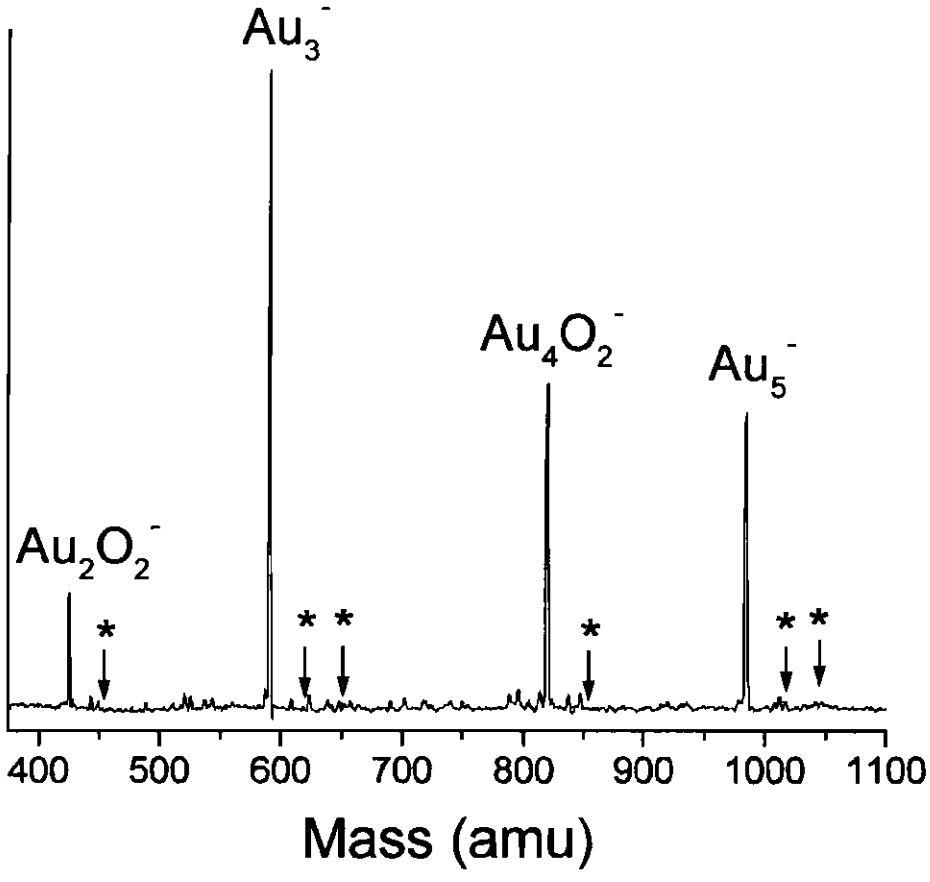

Figure 3-3: Saturation of gold cluster anions, Au_N^-, with O_2

Plots showing the result of adding molecular oxygen in the main pulsed gas valve while forming gold cluster anions, Au_N^- ($2 \leq N \leq 5$). The peaks corresponding to O_2 addition in **Figure 3-2** are now the only peaks present for the even-N clusters. Even under these extreme conditions, there is still no evidence of O_2 adsorption on any of the odd-N clusters. The arrows denote the positions at which a peak corresponding to the addition of a second O_2 molecule would appear on the even-N clusters and the positions at which both a first and second O_2 molecule would appear on the odd-N clusters.

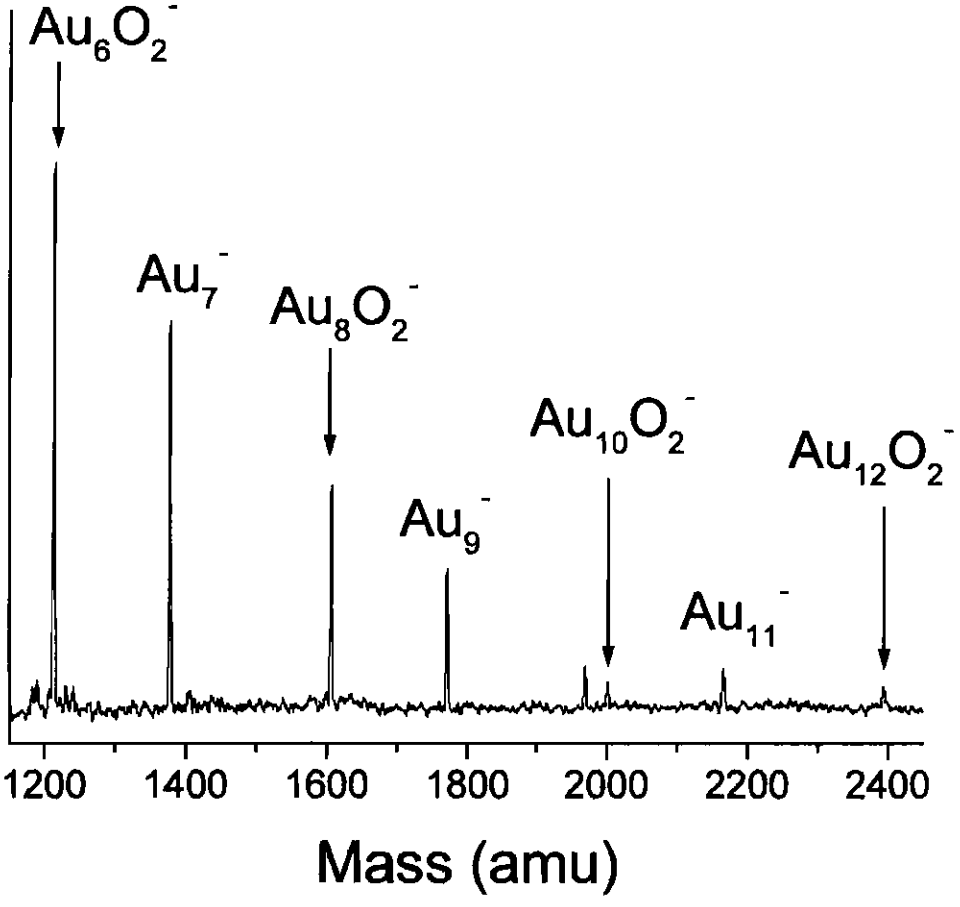

Figure 3-4: Saturation of gold cluster anions, Au_N^-, with O_2

Plots showing the result of adding molecular oxygen in the main pulsed gas valve while forming gold cluster anions, Au_N^- ($8 \leq N \leq 12$). The peaks corresponding to O_2 addition in **Figure 3-2** are now the only peaks present for the even-N clusters. Even under these extreme conditions, there is no evidence of O_2 adsorption on any of the odd-N clusters. As in **Figure 3-3**, there is no evidence of secondary adsorption on any of the clusters.

3-5 is a plot made to illustrate the conservation of signal intensity within the Au_N^- and $Au_NO_2^-$ peaks. A bare cluster spectrum was obtained before the addition of the oxygen and again at the end of the experiment. Due to intensity fluctuations, particularly at larger values of N, the mass distribution was not necessarily constant over the time required to complete the experiment. Therefore, a summed intensity was generated from:

$$\text{Summed Intensity} = \frac{[Au_N^-] + [Au_NO_2^-]}{[Au_{N-1}^-] + [Au_{N+1}^-]} \text{ for even N} \quad (2).$$

By weighting intensities of the reactive peaks to the neighboring unreactive peaks, variations in peak intensities in the spectrum as a whole could be separated from changes in intensity due to processes other than the addition of an O_2 molecule. The summed intensities depicted in **Figure 3-5** for Au_N^- (N = 6 – 12) represent several different O_2 concentrations and show well-conserved peak intensities over the wide range of O_2 partial pressures, leading to the conclusion that the only significant process resulting in the loss of Au_N^- signal is the adsorption of molecular oxygen.

Figure 3-6 plots the relative reactivities, or the extent of reaction, as defined by:

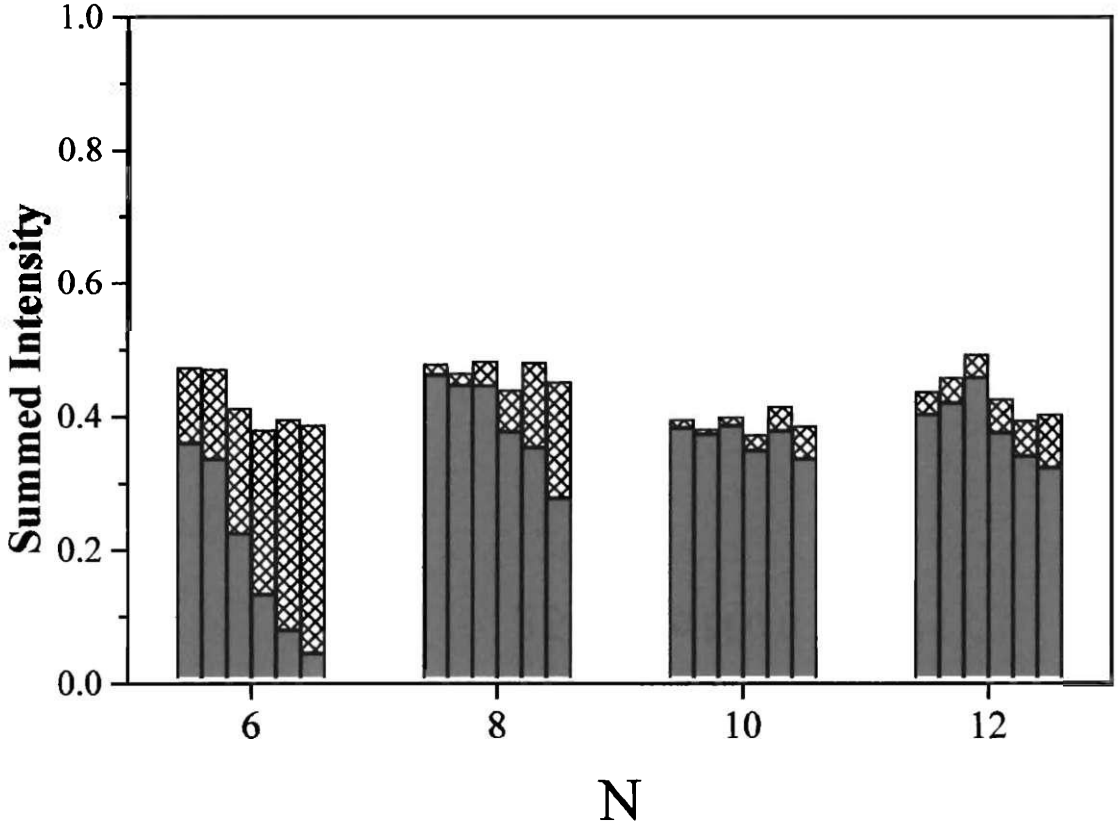

Figure 3-5: Summed signal intensity

A depiction of the conservation of cluster signal intensity over several different O_2 concentrations, indicating that Au_N^- clusters (gray) are not lost to other processes aside from the adsorption of O_2, leading to the production of $Au_NO_2^-$ clusters (cross-hatched). The summed intensity is calculated using equation (2). Adapted from Salisbury *et al.*[132,133]

$$\text{Extent of Reaction} = \frac{[Au_N O_2^-]}{[Au_N^-] + [Au_N O_2^-]} \qquad (3)$$

measured for a fixed O_2 concentration. Upper bounds on the extent of reaction for odd-N clusters, as well as N = 16 and 22, were calculated using the magnitude of the baseline noise as an extreme upper limit for the intensity of the associated O_2 peak. The conversion (or lack thereof) of the smaller cluster anions (N = 2 – 4) to their corresponding O_2 addition products as a function of reactant partial pressure is shown in **Figure 3-7**.

3.4 Discussion

3.4.1 Reactivity and saturation comparisons

The examples of the relative extents of reaction shown in **Figures 3-1**, **3-2**, and **3-5**, as well as the limiting or saturation cases displayed in **Figure 3-3** and **3-4**, can be compared with the previous studies carried out on the Au_N^-:O_2 system, as follows:

The Exxon group of Cox *et al.*,[107,108] employing pulsed flow-reactor methods very similar to those used to obtain **Figures 3-1** and **3-2** (downstream introduction of reactant), reported relative reactivities for the clusters N = 3 to 20. No results were given

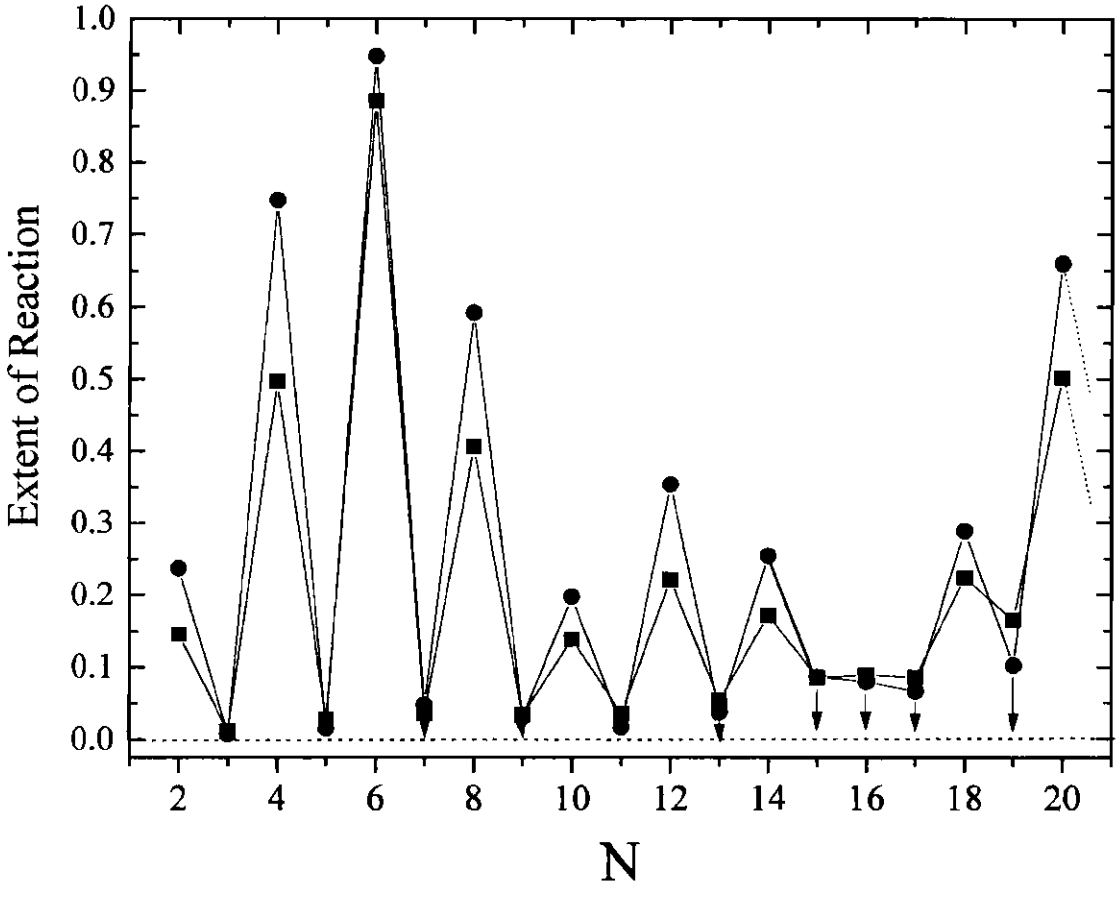

Figure 3-6: Extent of reaction

Size-dependence of the extent of reaction of Au_N^- clusters towards O_2, as defined in equation (3). The separate plots correspond to different O_2 concentrations. As in **Figures 3-1** to **3-4**, there is a striking odd-even reactivity, in which the even-N cluster anions (with the noticeable exception of Au_{16}^-) are highly active towards O_2 addition, while the odd-N clusters are inactive. Extents of reaction for Au_{16}^- and the odd-N clusters are upper limits.

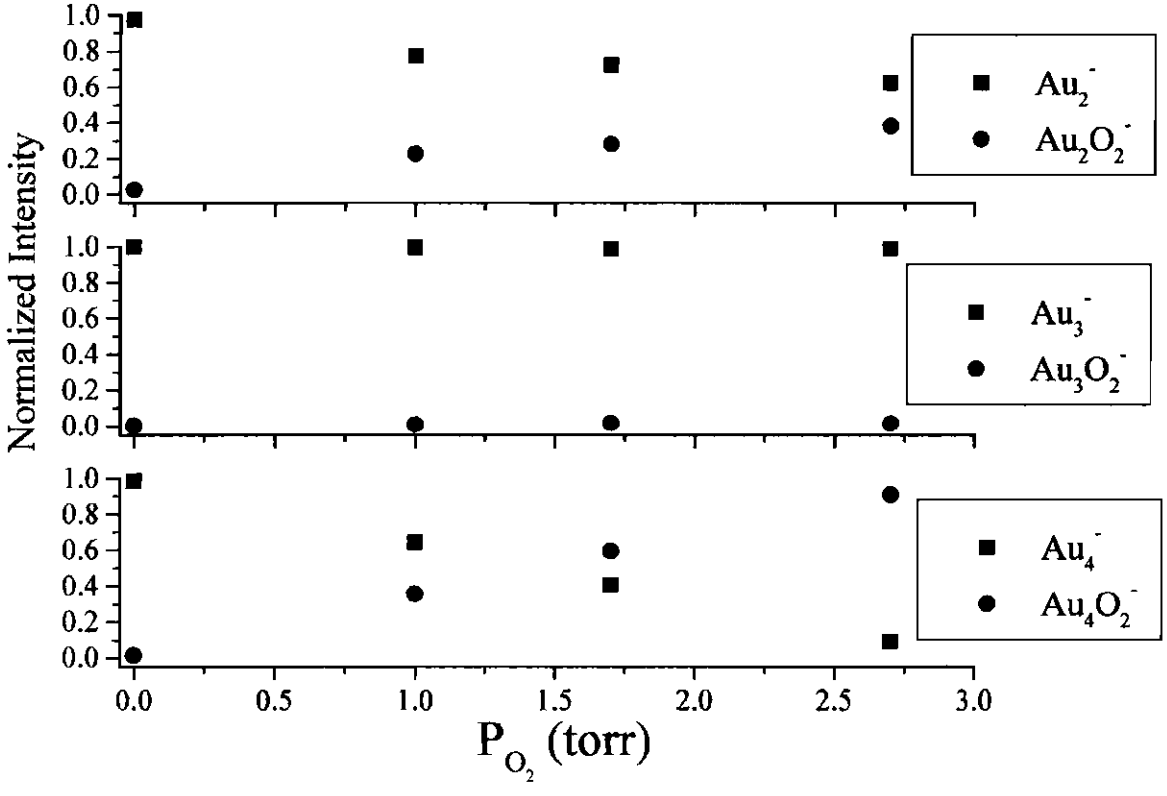

Figure 3-7: Pressure-dependence of O_2 addition to small Au_N^- clusters

Plots showing the normalized signal intensity of small Au_N^- and $Au_NO_2^-$ species (N = 2 – 4) as a function of O_2 partial pressure added in the fast-flow reactor using the secondary reaction valve. In this pressure regime, Au_4^- can be fully converted to its O_2 addition product, while Au_2^- is approximately 50% converted. As expected, Au_3^- remains unaffected over the full pressure range.

for N = 2, which is shown here to adsorb O_2 readily under higher reactant partial pressures, and to undergo complete conversion under the saturation conditions of **Figures 3-3** and **3-4**. Beyond the dimer, the high relative reactivities reported for N = 4, 6, 8, 14, and 20, in the descending reactivity order (N = 6 > 4 ~ 20 > 8 > 14 > 10), were in reasonable agreement with the results reported here. However, some strong discrepancies were also present, as no reactivity was reported for N = 18, and only a very slight extent of reaction was found for N = 12. In contrast, these results show that N = 12 and 18 are both very reactive, greater than N = 10 and comparable to N = 14. In agreement with these results, no reaction was detected for any odd-numbered cluster, nor for N = 16.

Cox and coworkers[107,108] did not mention saturation coverages in general, nor the more specific restriction of the single adsorption of an oxygen molecule. Due to the fact that their reaction conditions were limited to lower partial pressure, initial adsorption conditions, it is unlikely that they could approach the level of conversion seen in the present results, nor could they make a case for equilibrium conditions being met. The reactivity pattern observed was also attributed to activated dissociative chemisorption, in contrast to the interpretation of others.[39,112]

Employing low-pressure, guided-ion beam reactor methods, Lee and Ervin measured the effective bimolecular rate coefficients for the $Au_N^- + O_2$ (N = 1 - 7) reaction, as well as termolecular rate constants, obtained by varying the helium pressure.[112] The coefficient for Au_6^- was found to be very high, as, under the highest pressures used, it

was almost 5% of the Langevin (maximum) reaction cross-section. In comparison, where other silver clusters were found to be much more reactive than the same size gold clusters, Au_6^- was essentially as reactive as Ag_6^-. In contrast to the results shown in **Figure 3-6**, Lee and Ervin reported a much larger fall-off in reactivity for Au_4^- and Au_2^-. Reactions occurring in the low-pressure kinetic limit often have short complex lifetimes, possibly explaining this fall-off. As with the results of the Exxon group,[107,108] the authors were not able to achieve complete conversion and made no attempt to discuss saturation coverages.

3.4.2 Estimated free-energy variations and correlation to electronic structure

The results presented here were obtained at high partial pressures and moderate transit times (»10^{-5} s). In the absence of evidence for a barrier to adsorption, it is reasonable to assume, as opposed to being kinetically limited, that equilibrium conditions control the reaction processes. Therefore, variations in the relative equilibrium constants were calculated using selected results, using a form that omits the oxygen partial pressure:

$$K_N^{eq} = \frac{[Au_N O_2^-]}{[Au_N^-]} \qquad (4).$$

To compare these values with the electron affinity of the clusters, **Figure 3-8** gives the calculated adsorption free energies (left axis, squares), defined as:

$$-\Delta G_N = kT\ln(K_N^{eq}) \qquad (5),$$

where ambient conditions are assumed for kT (25 meV).

As already suggested by Cox *et al.*,[107,108] the pattern of the relative reactivities is similar to the variations observed[77,80] in the electron affinity of the bare gold clusters. These are included in **Figure 3-8** for comparison (right axis, triangles) with an energy scaling and offset that maximizes the visual agreement between the two quantities. The correlation between the two values is now even more apparent than previously assumed, with the reactivity of Au_{18}^- being found to be comparable to that of Au_{14}^- and not far below Au_{20}^-.

An explanation invoking the filling of spherical electronic shells and spheroidal subshells has often been invoked in order to explain the size-variation of the electron affinities of gold and other simple metal clusters.[77,82,94-97] The "islands" of high adsorption activity at N = 18 and N = 20 are particularly well correlated to the shell openings at 19 and 21 electrons, respectively, corresponding to $(1s^2 1p^6 1d^{10})2s^1$ and

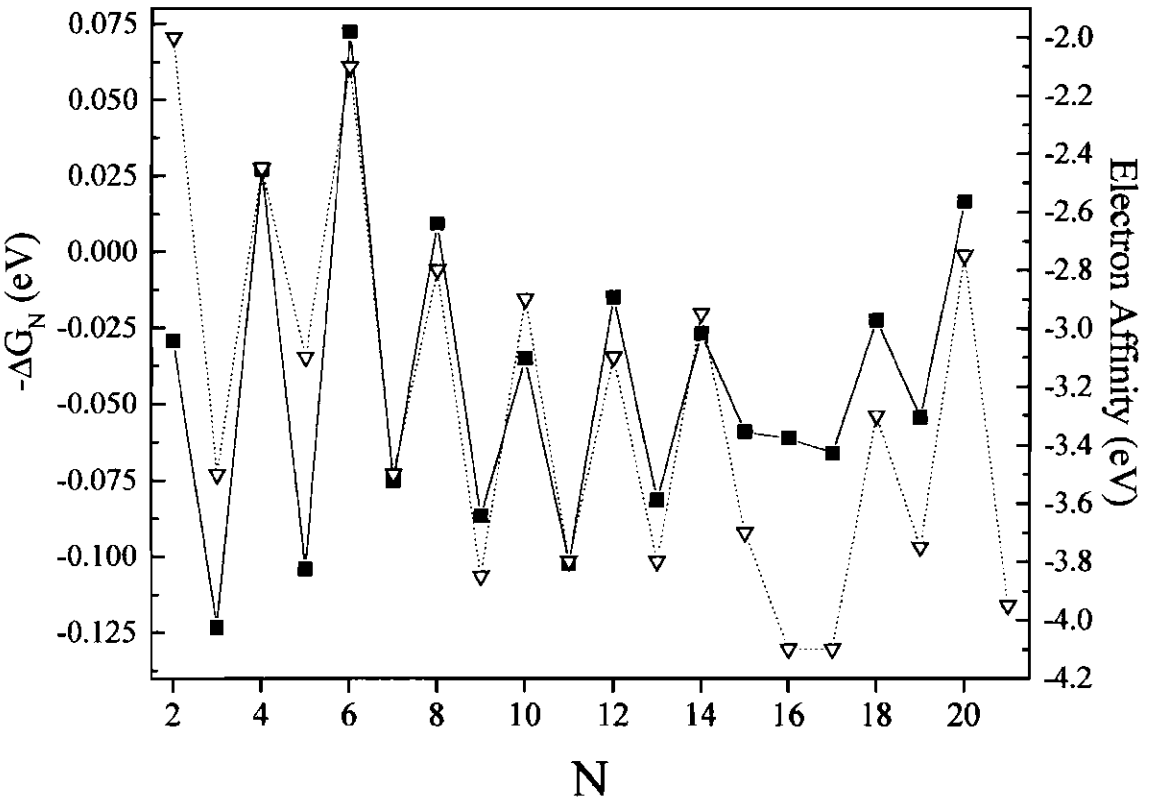

Figure 3-8: Correlation of adsorption free energy to electron affinity

Plot of the size dependence of the free energy of reaction, ΔG_N (solid lines, left axis), determined from equations (4) and (5), and the electron affinities measured by Chesnovsky *et al.* and Taylor *et al.* (broken lines, right axis).[77,80] A surprising correlation can be seen between these values. The free energies calculated for odd-N clusters represent upper bounds.

$(1s^2 1p^6 1d^{10})2s^2 1f^1$ electronic configurations.[22,89,94] Correlations have long been made between the size-dependent electron binding energies of metal clusters and their size-dependent reactivities. Even so, the correlations shown here do not necessarily imply that a long-range electron-transfer process is involved.

Some claim that the strict correlation between the strength of electron binding with reaction free energies is not entirely accurate, and have proposed other energy parameters.[10,22] For example, the trivial inverse-radius variation may be removed, equation (6):

$$EA^* = EA - (5.5 - 13.6/R^*)eV \qquad (6).$$

Here the expression in parenthesis is the classical variation of the electron affinity of a metal sphere of radius R (in atomic units) from its bulk value (the work function, 5.5 eV for gold). In practice, a radius R^* is used that exceeds the geometrical radius (calculated from the bulk density) by about an atomic unit. **Figure 3-9** shows a comparison between the reaction free energy variations (triangles) and this quantity (circles), in which only the even-N clusters are included, remembering, however, that Au_{16}^- is unreactive. In order to obtain this level of agreement, a large energy scaling is required.

Conceicao *et al.* have suggested that a more refined model for neutral clusters would compare the reactivity of different adsorbates to the difference between the ionization

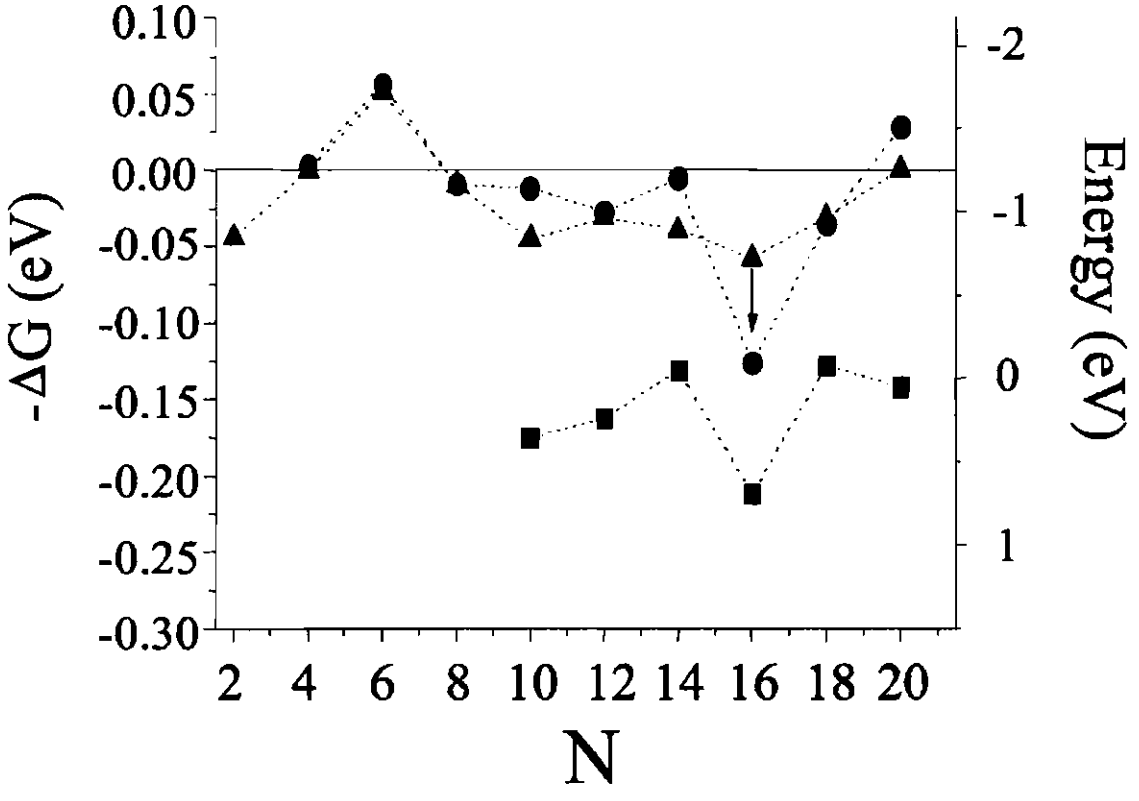

Figure 3-9: Comparison of different energy parameters

Size-dependence of the free energy of reaction (triangles, left axis) of the even-N Au_N^- clusters, compared with the specific electron binding energy (circles, right axis), calculated from equation (6), and with variations in the clusters' Pauli repulsion energy (squares, right axis), calculated from equation (7).

potentials (IP) of the individual clusters and their electron affinities. This assumes that the major barrier to adsorption is due to Pauli repulsion between the valence electrons of the potential adsorbate and the highest occupied molecular orbital (HOMO) of a cluster.[10,22] For negatively-charged clusters, this value can be estimated by the following relation:

$$P = EA - EA_2 - (27.2/R^*)eV \qquad (7).$$

Here EA_2 represents the second electron affinity, which Yannouleas and Landman estimated for doubly-charged gold cluster anions greater than nine atoms.[176] These values are plotted as squares in **Figure 3-9**. It is readily apparent that, in this case, the simple correlation of adsorption free energy with the electron binding energy (electron affinity) provides the much better match than the other proposed relations.

There is a simple mechanism that can be invoked that explains both the size-dependent variations in cluster reactivity as well as the saturation at one oxygen molecule. The gold clusters, attempting to obtain a closed-shell electronic configuration (pairing of electrons), donate an electron to the incoming O_2 molecule, which acts as a one-electron acceptor, generating a superoxide species, O_2^-. The donation of a single electron would leave odd-N (even electron-count) gold cluster anions unpaired,

explaining their inactivity. The same reasoning explains the inability of even-N clusters to adsorb a second O_2 molecule. Doing so would force the removal of an electron from a paired orbital, leaving the cluster in a less-stable electronic configuration. One might suggest that the odd-N clusters could retain a closed-shell configuration by simultaneously adsorbing two oxygen molecules and thereby donate a pair of electrons, but this would require the collision of three bodies simultaneously, which is highly unlikely, even under the high O_2 partial pressure used. Therefore, the restriction to either the adsorption of zero or one oxygen molecules is assured.

Alternative adsorption mechanisms could also be proposed. However, they each involve the transfer of an even number of electrons from the cluster and can not explain the correlation with the electron affinity. For instance, the simplest adsorption mechanism, physisorption, involves the transfer of zero electrons. The adsorption of oxygen as a peroxo species, –O–O–, would involve the transfer of two electrons to the π^* orbitals of the incoming molecule. Finally, in order for the oxygen to undergo a dissociative chemisorption process, a transfer of four electrons from the cluster to the π^* and σ^* orbitals of the oxygen molecule would be required. The capability of molecular oxygen to act as a one-electron acceptor is rooted in its open-shell (triplet) electronic configuration, which is unusual for stable molecules. Similar one-electron acceptor behavior can be found in the NO_x family of free radicals.[177]

An electrostatic model can be used to show the method by which the electron transfer process can be reconciled with the energetics of the individual gold cluster anions. If the gold cluster is approximated as a classical metal sphere and the oxygen molecule as a

point charge, the stability of the electron-transfer state can be estimated by the electrostatic potential energy including the induced polarization of the cluster. From these considerations, the binding energy of the electron-transfer state can be approximated by:

$$U = e^2a^3/2y^2(y^2 - a^2) \quad (8),$$

where a is the radius of the gold particle and y is the center-to-center separation. Using $y = 1.5\ a$ and a radius of 3 Å, a binding energy of ~2 eV is obtained. The potential energy curves resulting from this model are shown in **Figure 3-10**. Since the EA of O_2 is ~0.5 eV, the electron-transfer state will be stable (relative to the initial state) only if the EA of the Au_N^- cluster is less than 2.5 eV. While this value is in the same range as the measured EAs for small Au_N^- clusters, it is in no way a perfect model, as breakdowns in some of the assumptions are known to lead to somewhat inaccurate results. However, this model does provide evidence that the barrier between adsorbed and free molecular oxygen can be raised or lowered depending on the size-dependent change in cluster electron affinity.

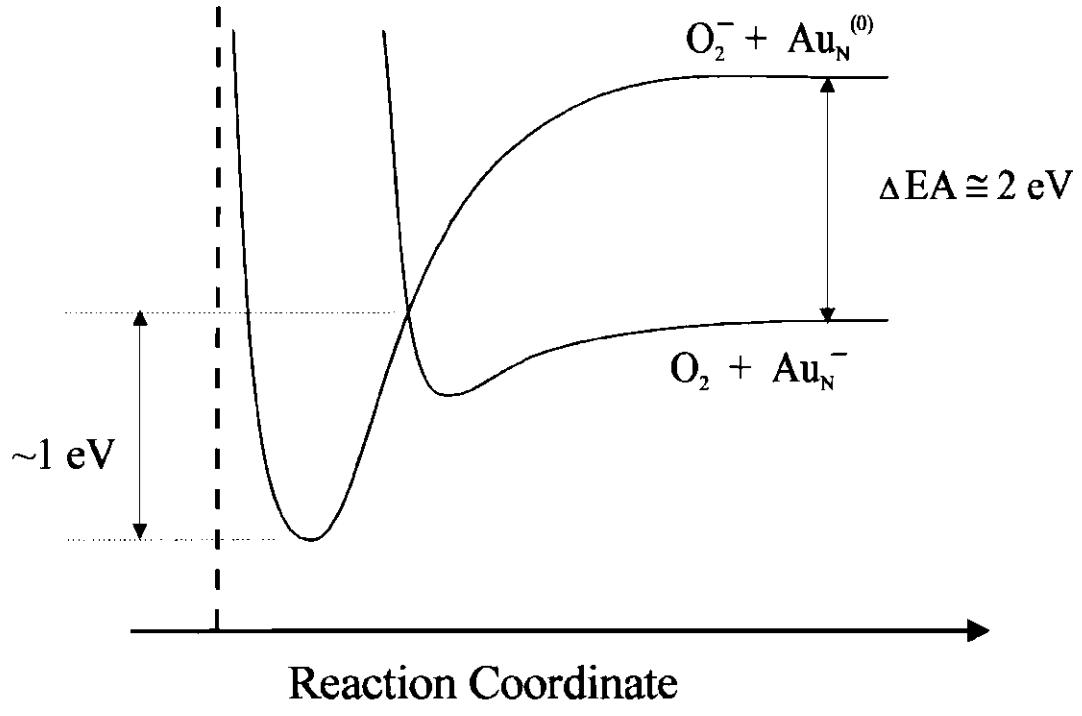

Figure 3-10: Potential energy surfaces from electrostatic model

Schematic illustration of the potential energy surfaces for interaction of O_2 with a Au_N^- cluster, as a function of the distance from the center of the cluster to the center-of-mass of the molecular oxygen. The vertical dashed line indicates the radius of the cluster. The curves as drawn are appropriate for a cluster anion whose electron affinity is approximately 2.0 eV, such as Au_6^-. The long-range attraction between the superoxide anion and the neutral cluster is described by equation (8), which uses the polarizability of a metal sphere.

3.4.3 Comparison with adsorption reactions and catalysis of supported gold clusters

The results and interpretations described above offer fascinating possibilities for correlation to the catalytic processes involving molecular oxygen on supported gold catalysts,[52] and even more so for the model systems recently investigated.[39,42,65] These will be described in more detail in Chapter 7. However, a short discussion here is helpful in providing evidence of the relevance of gas-phase studies. In the recent experiments of Sanchez *et al.*,[39] oxygen and carbon monoxide were co-adsorbed on mass-selected, supported gold clusters at cryogenic temperature. Upon heating, the yield of desorbed CO_2 was measured. They found that, while the reaction yield varied from zero to approximately two CO_2 molecules per cluster, none of the clusters studied, up to 20 atoms, showed CO_2 production that was significantly higher than 2. The stoichiometry shown in the present experiments (1 O_2 molecule per cluster) could explain this activity on the supported clusters, as the overall process ($O_2 + 2\ CO = 2\ CO_2$) yields two carbon dioxide molecules for each oxygen molecule consumed.

In these studies, the adsorption probabilities and energetics of molecular oxygen on the supported clusters was not measured. However, the agreement seen between the experiments of Sanchez *et al.* for CO_2 production and the present results for O_2 adsorption probability at least implies that the oxidation of CO on the supported clusters requires the type of activation of O_2 (lowering of bond order) seen in the gas phase. While there is only partial agreement between the two studies concerning the size-dependent oxygen adsorption activity (gas phase) and CO oxidation activity (supported clusters), the fact that there is any correlation at all makes it possible to argue that

perhaps the supported clusters are essentially anions. An theoretical study by Häkkinen, Barnett, and Landman which accompanied the experimental work of Sanchez and coworkers[39] found that this was indeed the case for the supported gold clusters localized on electron-rich F-center defects. Besides immobilizing the clusters, electron transfer from the defect sites was a crucial factor in the ability of the clusters to catalyze CO oxidation.

3.5 Conclusions

While it is not surprising to find that the O_2 adsorption activity on negatively-charged gold clusters is correlated to the clusters' electron affinities, the binary (0,1) adsorption activity under saturation conditions is very unusual and requires a unique explanation. The mechanism that best fits these results and those of others is that the oxygen molecule is adsorbing on the clusters as a one-electron acceptor, or as a superoxide species, while the clusters strive to obtain a closed-shell electronic configuration. While this mechanism seems to be the only possibility for O_2 adsorption on the gas-phase clusters under ambient conditions, it has found only begrudging acceptance, and is still openly questioned by some.[71,117,118,178,179] These criticisms will be discussed in more detail in Chapter 4. This proposed mechanism is supported by several sources, however. First, a superoxide bonding mechanism was proposed over 25 years ago for bonding of molecular oxygen to the neutral gold atom (open shell electronic configuration).[180,181]

Secondly, a recent photoelectron study of small $Au_NO_2^-$ clusters (N = 1 - 4) confirmed that O_2 was bound as a superoxide on Au_2^- (It must be noted, however, that peroxo-like bonding was found for Au_4^-, and O_2 adsorption was even found on the anionic monomer and trimer, though no explanation was given to explain these discrepancies).[182] Finally, the coadsorption properties of O_2 with other molecules on the Au_N^- clusters (Chapters 4 and 6) reinforce the validity of this proposed mechanism. Even so, further experiments using various other techniques could perhaps answer the question as to the bonding mechanism beyond any doubt.

CHAPTER IV

OXYGEN ADSORPTION ON HYDRATED GOLD CLUSTER ANIONS

4.1 Introduction

Supported gold catalysts for air purification function well even in humid environments; indeed, trace levels of moisture are considered essential in order for the optimal activity of the catalysts to be achieved.[51,183] One proposal is that the dissociation of oxygen is necessary for the reaction to occur, and that the presence of water aids in this dissociation.[56] However, it is also possible that the role of water simply is to maintain an appropriate termination of the oxide support. As the nature of the actual working catalysts remains a challenge to characterization, an understanding of the activity of selected gas-phase gold clusters towards reactants of interest (O_2, CO, etc.) needs to be achieved, in the presence of H_2O, in order to separate the contributions to the

catalytic activity of the gold clusters and the support material. Surprisingly, while several studies of water adsorption have been performed on clusters of other transition metals,[137,139,184-186] almost none have been carried out on gas-phase gold species. To date, the only studies of gold with water in the gas phase have concerned the adsorption of water molecules on the gold monomer cation.[187-189] This chapter, which explores the adsorption of O_2 on the predominant forms of gold-hydrate anions both experimentally and theoretically, takes a first step in understanding the effects of water on gold cluster anions.

The reactions of O_2 with gas-phase gold cluster anions have been described in detail in several reports and Chapter 3.[107,108,112,117,133] At room temperature, all previous experimental studies found that O_2 binds to Au_N^- in an even-odd manner, with odd-N clusters showing no activity towards O_2 adsorption, while the even-N clusters (except for N = 10 and 16) show a variety of relative reactivities and saturate at one molecule adsorbed.[133] This adsorption activity correlates well with the measured electron affinities of Au_N^-,[77] and was interpreted within a simple frontier orbital picture. In this explanation, the adsorption occurs via electron transfer from the cluster to the O_2 π^* orbital. For those clusters with an unpaired electron in their HOMO (even-N clusters, low electron affinities), this mechanism can yield strong binding (~1 eV) , but for those with a filled HOMO (odd-N clusters, high electron affinities), it is not accessible. This selective activity, as well as the correlation with the measured electron affinities, was explained by the suggestion that O_2 remains adsorbed molecularly (intact) as a one-electron acceptor, i.e. as a superoxo (O_2^-) adsorbate. The gold cluster possesses paired

electrons in its HOMO and is thus inactive toward secondary adsorption. A more complete discussion of this work is presented in Chapter 3.

Several theoretical studies concerning the Au_N^-/O_2 reaction system have been presented using density functional theory (DFT) methods.[71,104,178,190] These studies were generally in agreement with experiment, with odd-N clusters showing much lower O_2 binding energies than even-N clusters. However, compared to the experimental dissociation binding-energy estimates, the theoretical binding energies for O_2 to the even-N clusters were systematically higher in the literature, and significant (~0.5 eV) binding energies were even seen on the odd-N clusters.[71,104,178] Thomson and coworkers performed DFT calculations on the interaction of O_2 with Au_{9-11}^- and suggested that basis-set superposition error for the relatively small basis set used resulted in higher binding energies for O_2 on Au_{10}^-.[104] Mills *et al.* also performed more accurate coupled cluster calculations on the interaction of O_2 with Au_2^- and Au_3^-.[179] These calculations showed that the previously calculated O_2 binding energies were indeed too high for Au_2^- and addition of an O_2 molecule to Au_3^- became slightly unfavorable. However, the appropriate choice of functionals in the DFT procedure, in particular for the exchange part, and a sufficiently large AO basis set allows for an accurate description of binding energies of O_2 with metal clusters.[191]

A full CO oxidation cycle under low reactant coverage conditions was predicted for the gold dimer anion, Au_2^-,[190] and CO oxidation was seen on gold cluster anions as small as Au_6^- in fast-flow reactor experiments.[192] However, the question of the role of

moisture in enhancing the CO oxidation activity of the supported gold clusters has yet to be addressed in gas-phase studies. The presence of H_2O-derived adsorbates could significantly alter the O_2-adsorption activity and mechanism. Such coadsorption effects were already reported for the {CO, O_2} combination,[117,192] and this work extends this to {H_2O, O_2} coadsorption. In this case, an abundant anionic species has the composition, Au_NOH^-. The strongly electron-withdrawing OH group causes the odd-N gold subunits to be reactive towards binding of molecular oxygen.

4.2 Experimental Methods (Abbreviated)

The experimental techniques used to study the adsorption properties of O_2 on hydrated gold clusters were described previously[133] and in Chapter 2, so only a brief description will be given here. Charged gold clusters were formed and equilibrated by laser vaporization of a rotating and translating gold rod in a high-pressure helium/ ^2H_2O flowstream, produced using a pulsed valve with a stagnation pressure of approximately 3.5 bar. Prior to entering the stagnation region of the pulsed valve, the helium was bubbled through ^2H_2O, thereby saturating the helium with the vapor pressure of water at room temperature (~20 mbar). The clusters were then exposed to a gas pulse from a secondary pulsed valve containing a dilute reactant gas (approximately 20% O_2:He with a stagnation pressure of ~ 2 bar), expanded into vacuum, and were detected by time-of-flight mass spectrometry, using perpendicular pulsed extraction fields. With the addition

of a cooling sleeve (and heater) to the reactor, the effects of temperature on the reaction could be studied under a source temperature range of 220-330 K. A variety of products were detected, and the mass spectra were found to be stable for the duration of the experiments. All peak intensity was accounted for in order to rule out the contribution of decomposition reactions.

4.3 Theoretical Methods

The group of Bonačić-Koutecký performed concurrent theoretical studies on this system using DFT methods[191,193] with Becke's hybrid three parameter non-local exchange functional combined with the Lee-Yang-Parr gradient corrected correlation functional (B3LYP).[194-196] Calculations were carried out with the 19-electron relativistic effective core potential (19-RECP) from the Stuttgart group for the gold atom and the [9s7p5d1f]/[7s5p3d1f] AO basis set.[100,197] For oxygen and hydrogen atoms, the 6-311 G(d,p) triple-ζ split valence basis set was employed.[198,199]

The accuracy of the results obtained for O_2 binding on small Au_N^- clusters using this method were compared to the collision-induced dissociation (CID) data of Lee and Ervin.[113,131,200] For $Au_2O_2^-$, the calculated binding energy of 1.06 eV agreed very well with the CID energy of 1.01 ± 0.14 eV. The calculations for $Au_4O_2^-$ agreed less favorably with the CID data, giving a binding energy of 0.64 eV, compared to the dissociation energy of 0.91 ± 0.14 eV. It must be remembered, however, that CID does

not account for the presence of reverse activation barriers. Therefore, the values obtained from that method are upper bounds. The calculated binding energy for this system compared very favorably with the experimentally estimated binding energy of 0.5 eV (discussed below). From the comparisons with the experimental results, Bonačić-Koutecký and coworkers determined that the proper treatment of the exchange part of the density functional, combined with an accurate basis set, is needed for a reliable description of the bonding between gold and oxygen. In this case, their DFT calculations yielded results of comparable accuracy to coupled cluster methods, in contrast to the statements published by Varganov *et al.*,[179] which stated that DFT methods are not able to accurately model oxygen binding to metal clusters. All the structures reported were fully optimized using a gradient-based minimization method, and the character of the stationary points was checked by performing vibrational analysis. In order to study the electron transfer from the gold clusters to the oxygen, the natural bonding orbitals (NBO) analysis also was carried out.

4.4 Hydrated gold cluster anions, $Au_n \cdot OH^-$

4.4.1 Experimental

Gold cluster anions in the size regime of 2 - 11 atoms were produced using the methods described above in order to determine the effects of water presence on the adsorption activity of the clusters. **Figures 4-1** and **4-2** show mass spectra obtained when

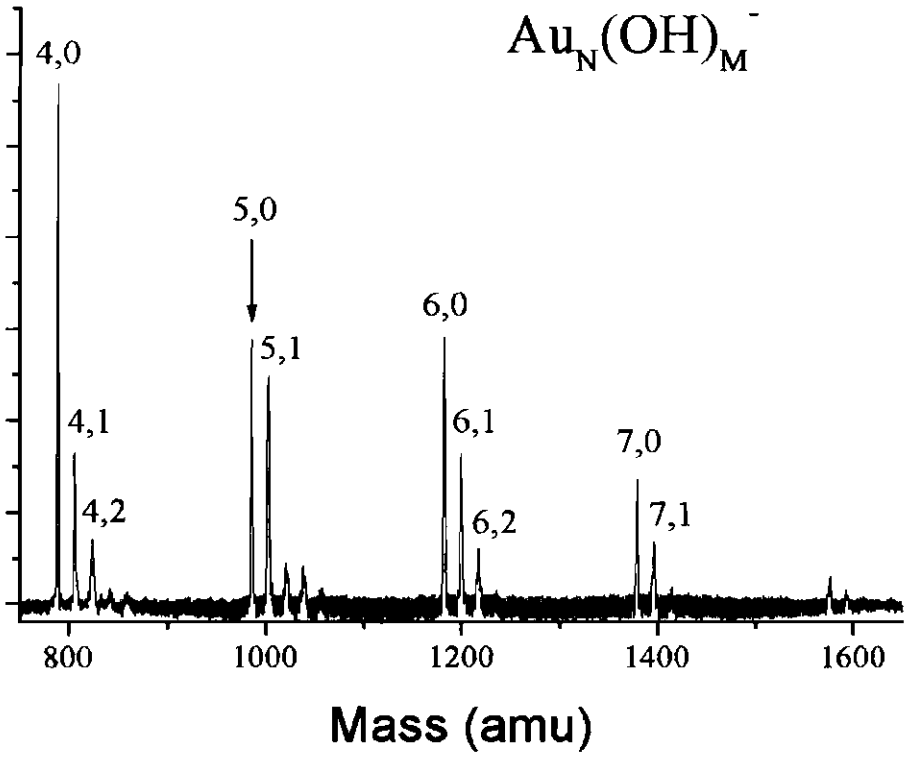

Figure 4-1: $Au_N(OH)_M^-$ species produced at room temperature

Mass spectrum obtained when H_2O-seeded helium is used as a buffer gas. Under these conditions, the dominant anionic species are complexes corresponding to the form, $Au_N(OH)_M^-$, though there are also generally smaller amounts of species corresponding to $Au_N(OH)_M(H_2O)_L^-$. The numbering scheme refers to the number of gold atoms and hydroxide adsorbates, respectively.

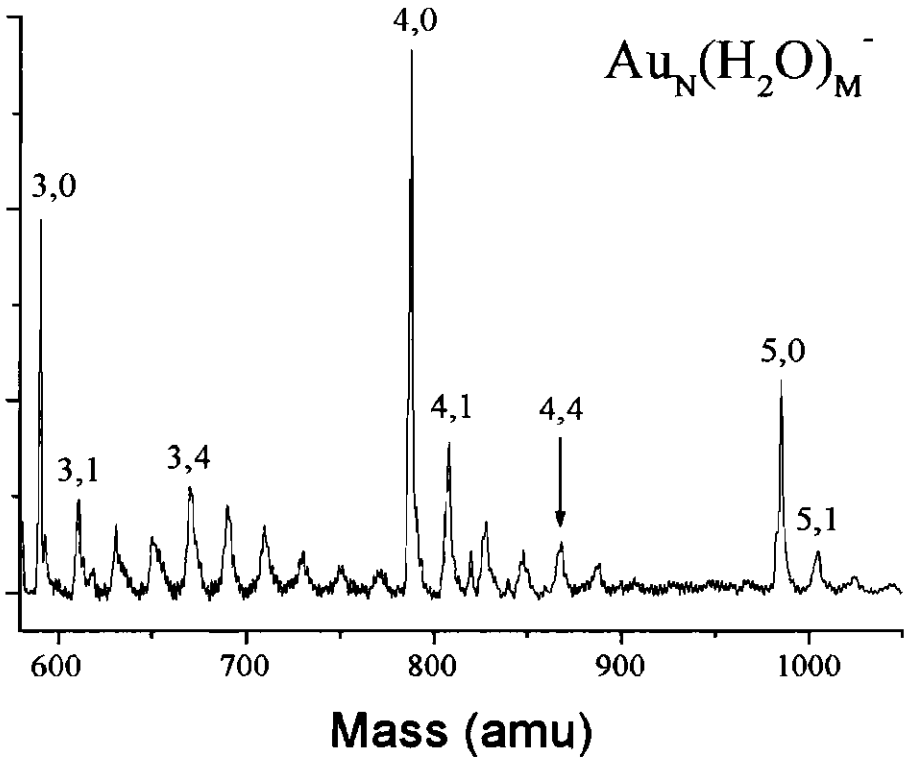

Figure 4-2: $Au_N(H_2O)_M^-$ species produced at low temperature

Mass spectrum showing the effect of lowered temperatures in the laser-ablation source region when H_2O-seeded helium is used as a buffer gas. Instead of forming clusters with attached hydroxide species (as in **Figure 4-1**), these conditions lead to the formation of gold cluster anions with adsorbed water molecules. This mass spectrum was obtained at a source temperature of approximately 200 K. The numbering scheme refers to the number of gold atoms and water molecues, respectively.

^2H_2O-seeded He buffer gas was used in the cluster source and the secondary (reactant) pulse was offset temporally from the main pulse at room temperature and low temperature, respectively. In addition to bare gold cluster anions, Au_N^-, several other species are obtained by this method, namely products corresponding to the formula, $Au_N(OH)_{0,1,2}(H_2O)_{0,1,2}^-$. While the Au_NOH^- products seem to be the only strongly bound (non-displaceable) species at room temperature (**Figure 4-1**), lowering the temperature of the cluster source produces conditions in which the $Au_N(H_2O)^-$ species are dominant (**Figure 4-2**). In general, though, the results presented here are insufficient to determine unequivocally what the compositions are of any typically favored hydration compositions. Overall, the production of $Au_N(OH)_{0,1,2}(H_2O)_{0,1,2}^-$ species is highly dependent on the laser fluence, with higher fluences producing large amounts of the hydrated species. Being able to control the amount of these species simply by changing laser fluence is extremely helpful when trying to perform studies on bare gold cluster anions, as the hydrates tend to overwhelm the mass spectrum. Obviously, gaining a much more detailed understanding of the mechanisms involved in the production of these anionic cluster species could be extremely helpful in ongoing research on gold clusters.

4.4.2 Theoretical

The structural and electronic properties of Au_NOH^- clusters (N = 2 - 5) were systematically investigated using the theoretical methods described above by Bonačić-Koutecký and coworkers. Their optimized structures are shown in **Figure 4-3** and the properties of the cluster species are summarized in **Table 4-1**. In all cases, they

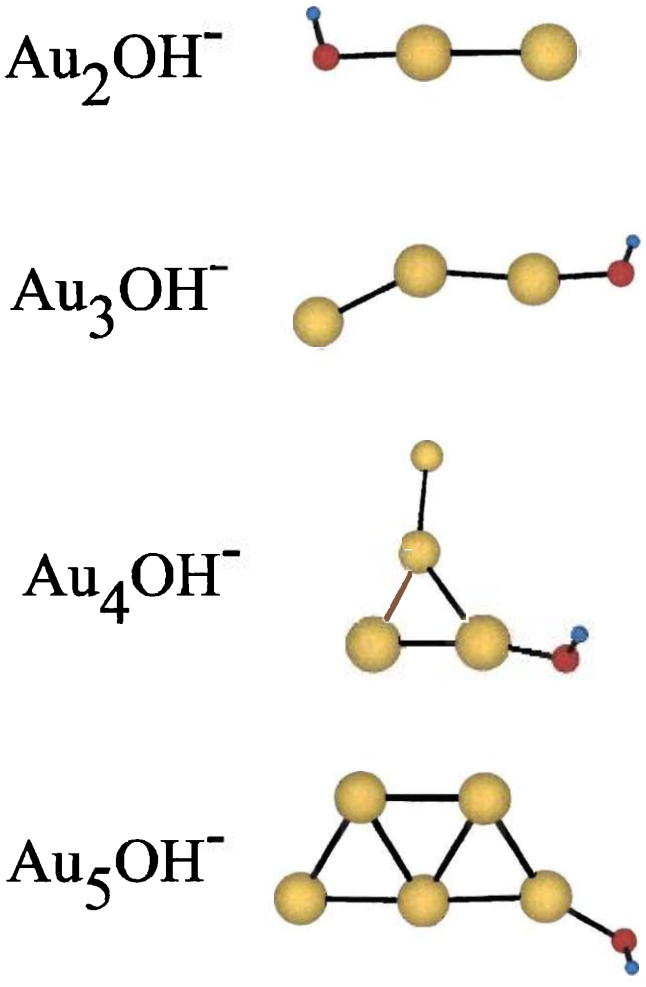

Figure 4-3: Calculated structures of Au_NOH^- complexes (N = 2 - 5)

Lowest-energy structures calculated for the Au_NOH^- system using the theoretical methods described in the text. Oxygen and hydrogen atoms are labeled by large red and small blue circles, respectively. For other higher-energy structural isomers, see the original text.[193]

Table 4-1: Ground-state energies and properties of optimized Au_NOH^- (N = 2 - 5) clusters

Au_nOH^- n=2-5	Symm.(State)	Energy a.u	ΔE^a eV	$E_b{}^b$ eV	NBO Charge	
					Au_n	OH
Au_2OH^-	C_s ($^1A'$)	-347.514326		3.16	-0.35	-0.65
$Au_3OH^-(I)$	C_1 (^2A)	-483.314557		1.84	-0.63	-0.37
$Au_3OH^-(II)$	C_s ($^2A''$)	-483.313657	-0.02			
Au_4OH^-	C_1 (^1A)	-619.158765		3.00	-0.38	-0.62
Au_5OH^-(I)	C_1 (^1A)	-754.961885		2.30	-0.65	-0.35
Au_5OH^-(II)	C_1 (^1A)	-754.955443	-0.17			
Au_5OH^-(III)	C_1 (^1A)	-754.944645	-0.47			
$Au_2O_2^-$	C_1 (^2A)	-422.054480		1.06		
$Au_3O_2^-$	C_1 (^3A)	-557.869781		0.015		
$Au_4O_2^-$	C_1 (^2A)	-693.694330		0.64		
$Au_5O_2^-$	C_{2v} ($^3A_2$)	-829.497109		-0.06		

Energies and properties obtained using DFT with the B3LYP method; [a]Energy difference with respect to the most stable structure; [b]Binding energy for the Au_NOH^- complexes is defined by $E_b = E(Au_NOH^-) - E(Au_N^-) - E(OH)$, and for the $Au_NO_2^-$ complexes as $E_b = E(Au_NO_2^-) - E(Au_N^-) - E(O_2)$.[193]

determined that the OH group was bound at a peripheral position, which Mills *et al.* also found for O_2 binding on small gold cluster anions.[178] However, as OH groups are generally more reactive than oxygen molecules, the binding of the OH group to the gold clusters was found to be stronger. In general, the binding energies of complexes with the OH group and with molecular oxygen were found to oscillate as a function of size, but the absolute binding energies were much higher for those with the OH group (for instance, see the top frame of **Figure 4-4**). This explains the presence of odd-N Au_NOH^- clusters in the experimental results, whereas no evidence of odd-N $Au_NO_2^-$ species was found. In the case of the Au_2OH^- species, the binding energy was calculated to be 3.16 eV, and a significant amount of electron transfer from the gold subunit to the OH group takes place, as can be seen from calculated natural bonding orbital (NBO) charges in **Table 4-1**.

Since the Au_3^- cluster has an even number of electrons, it was expected that the binding energy towards the molecular oxygen and hydroxide groups would be much lower. As opposed to the complex with O_2, Au_3OH^- was very stable, having a binding energy of 1.84 eV. The lowest energy structure is shown in **Figure 4-3** (For the other isomer, see reference . In the lowest energy isomer, the OH group was bound at the peripheral atom of the almost linear structure, while in the second isomer the OH group was bound to the triangular gold subunit. Weaker bonding in Au_3OH^- was also reflected in significantly less electron transfer to oxygen than in the case of Au_2OH^-, showing that the charge remains mainly localized on the Au_3 subunit.

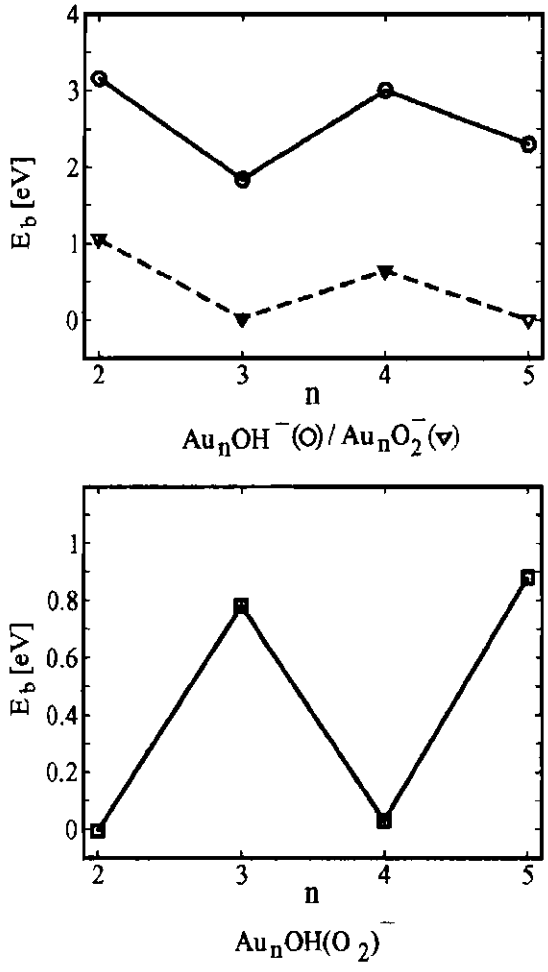

Figure 4-4: Binding energies on Au_N^- clusters

(Top frame) Binding energies of O_2 (triangles) and OH (circles) on Au_N^- clusters (N = 2-5). For stable structures of Au_nOH^- complexes, see **Figure 4-3**. $Au_N^- \cdot O_2$ complexes have common structures with those published previously.[178] (Bottom frame) O_2 adsorption energies on Au_NOH^- cluster complexes (N = 2-5). For stable structures of $Au_NOH(O_2)^-$, see **Figure 4-10**.

For the most stable structure of Au_4OH^-, Bonačić-Koutecký and coworkers determined that the gold subunit assumed a T-form and the OH group was bound to a gold atom that is part of the triangular subunit. The calculated binding energy of 3.16 eV was close to that of Au_2OH^-, and the negative charge was located at the OH group as well.

The most stable structure of Au_5OH^- was found to be composed of a planar trapezoidal Au_5 subunit with an OH group placed at the peripheral position. The binding energy of Au_5OH^- was larger than Au_3OH^-, and electron transfer was reduced with respect to the complexes with an even number of gold atoms.

4.5 Adsorption of molecular oxygen on hydrated gold cluster anions, $Au_NOH(O_2)^-$

4.5.1 Experimental

When a secondary gas pulse containing dilute O_2:He was overlapped with the main (cluster) pulse in the experiments, mass spectra of the type shown in **Figures 4-5** and **4-6** (top frames) were obtained. As can be seen, overlap of the pulses results in the depletion of several peaks in the mass spectrum as well as the growth of new peaks at 32 amu higher mass. For the even-N clusters, O_2 addition proceeds as expected, with the adsorption of a single molecule on the bare cluster, as in

$$Au_{N(even)}^- + O_2 \rightarrow Au_{N(even)}O_2^- \qquad (1).$$

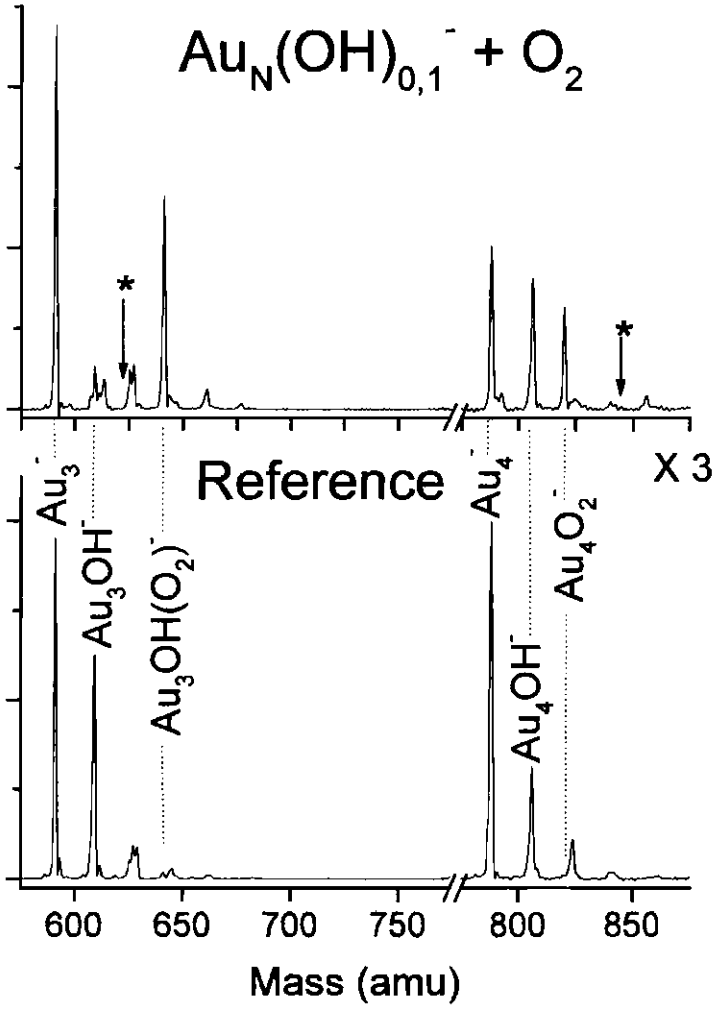

Figure 4-5: Reaction of O_2 with Au_NOH^- clusters (N = 3,4)

(Bottom frame) Mass spectrum of negatively-charged gold clusters, Au_N^-, and various hydrates of the form, Au_NOH^- generated when the cluster and reactant gas pulses are temporally offset. (Top frame) Mass spectrum obtained when the secondary gas pulse containing ~20% O_2:He is temporally overlapped with the main pulse. The asterisks indicate the position in which peaks corresponding to $Au_3O_2^-$ and $Au_4OH(O_2)^-$ would be present.

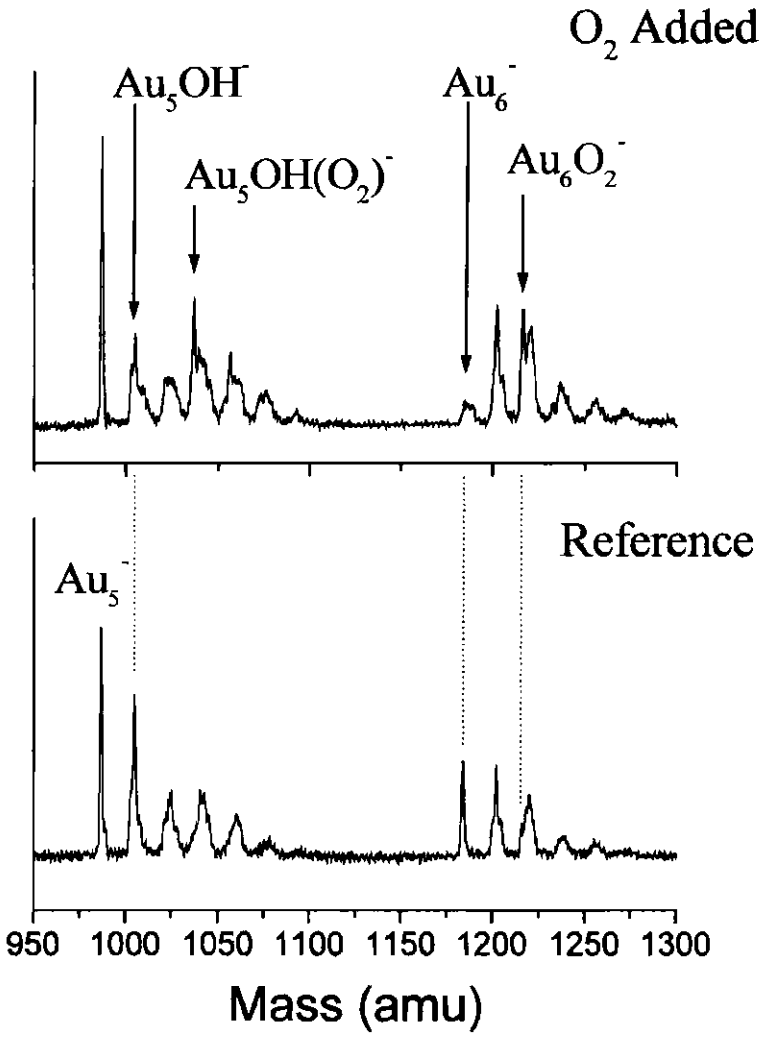

Figure 4-6: Reaction of O_2 with Au_NOH^- clusters (N = 5,6)

(Bottom frame) Mass spectrum of negatively-charged gold clusters, Au_N^-, and various hydrates of the form, Au_NOH^- generated when the cluster and reactant gas pulses are temporally offset. (Top frame) Mass spectrum obtained when the secondary gas pulse containing ~20% O_2:He is temporally overlapped with the main pulse.

For the odd-N clusters, however, rather surprising results are seen. As no O_2 adsorption had been seen on these clusters in the past and no or extremely weak binding had been calculated (for instance, see **Figure 4-4** and **Table 4-1**), it is not surprising to find that no complexes of the type, $Au_{N(odd)}O_2^-$, are present in the mass spectrum. However, on odd-N clusters of the type, $Au_{N(odd)}OH^-$, adsorption of a single O_2 molecule is found, according to the reaction,

$$Au_{N(odd)}OH^- + O_2 \rightarrow Au_{N(odd)}OH(O_2)^- \qquad (1').$$

In contrast, on $Au_{N(even)}OH^-$ clusters, no O_2 adsorption activity is detected. The normalized intensities of these major peaks are plotted in **Figure 4-7** for N = 2 - 6, both when the O_2 pulse is temporally offset from the main pulse (bottom frame) and overlapped (top frame). This figure clearly shows that reaction (1') is the only significant process for O_2 addition to odd-N clusters, while even-N clusters simply add O_2 to the bare clusters, as in reaction (1). An extension to N = 11 confirms that this pattern applies up to at least the N = 11 cluster.

The size-dependent adsorption activity of the different cluster species can be quantitatively described by some simple calculations. Using the normalized cluster intensities shown in **Figure 4-7**(top frame), the relative reactivities, or extent of reaction, of the various clusters at a fixed O_2 concentration are calculated by:

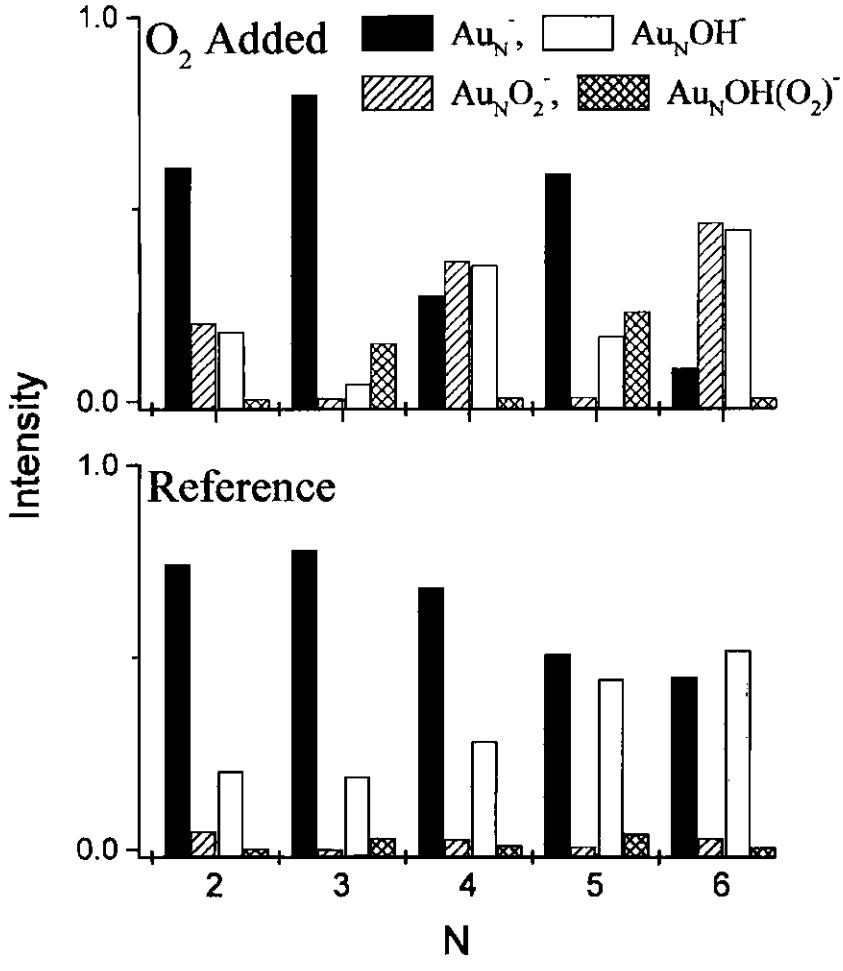

Figure 4-7: Bar-graph representation of the normalized cluster intensities of Au_N^- and Au_NOH^- with and without O_2 addition

Intensities obtained when the secondary gas pulse is temporally offset (bottom frame) and overlapped (top frame) with the main cluster pulse. This shows that reaction (1') is the only significant process for O_2 addition to odd-N clusters while the presence of an –OH group on the even-N clusters causes them to lose all activity for O_2 addition.

$$\frac{[Au_N O_2^-]}{[Au_N O_2^-]+[Au_N^-]} \qquad (2)$$

for the bare clusters, or by

$$\frac{[Au_N OH(O_2)^-]}{[Au_N OH(O_2)^-]+[Au_N OH^-]} \qquad (2')$$

for the hydrated clusters. The extents of reaction for different O_2 concentrations are plotted in **Figure 4-8** according to equation (2) in the bottom frame and equation (2') in the top frame. Upper bounds for the reactivity of the even-N Au_NOH^- clusters and odd-N Au_N^- clusters are plotted using the magnitude of the baseline noise as an upper limit for the corresponding O_2 peak intensity. **Figure 4-9** shows the extents of reaction for N = 6 - 11 obtained with a single O_2 partial pressure using equation (2'). Just as in **Figure 4-7**, these figures readily indicate the even-odd activity of the $Au_NOH^- + O_2$ reaction system. What is also interesting to note is the extremely high reactivity of Au_3OH^- at lower O_2 partial pressures, which approaches (and even exceeds) the activity of Au_6^-, the most active bare gold cluster, at lower O_2 partial pressures.

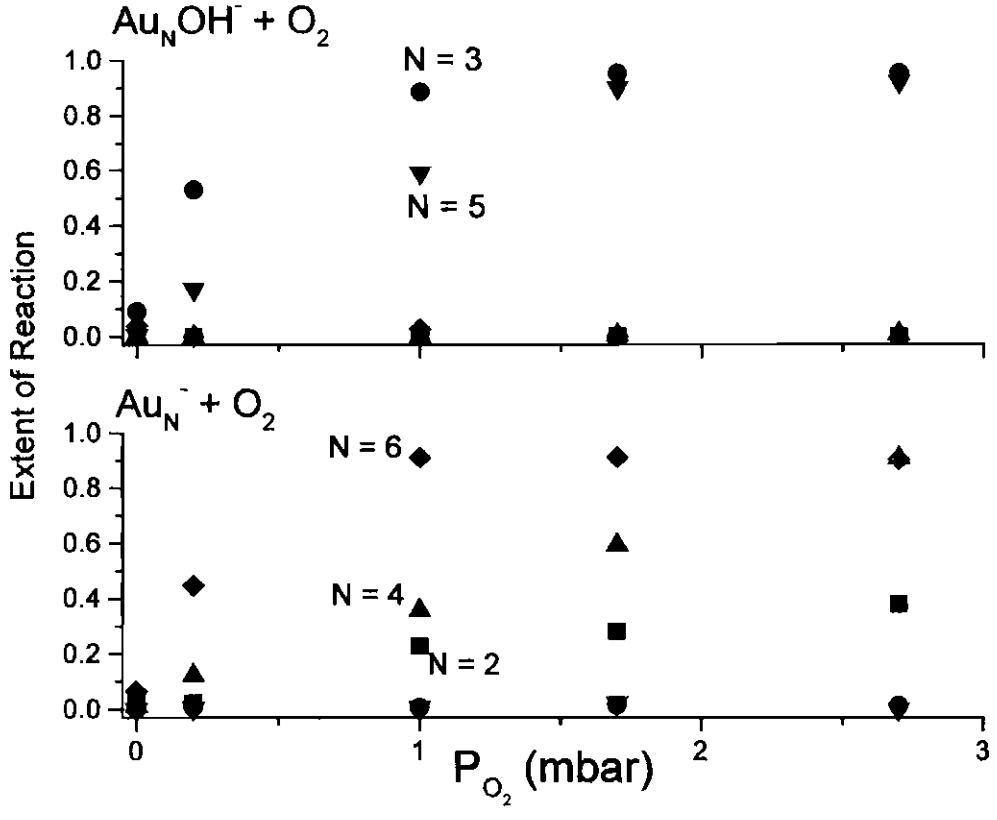

Figure 4-8: Cluster size-dependence of the extent of reaction

Extents of reaction for the addition of O_2 to Au_N^- and Au_NOH^- clusters (N = 2 - 6), as defined in equation (2) (bottom frame) and equation (2') (top frame), for different partial pressures of O_2 in the reactor. These pressures are calculated from the overall pressure in the reactor (~150 mbar), the difference in average pressure achieved when the secondary valve fires, as well as the difference in pulse length, and the known dilutions of O_2:He. The extents of reaction for odd-N Au_N^- clusters and even-N Au_NOH^- clusters are upper limits.

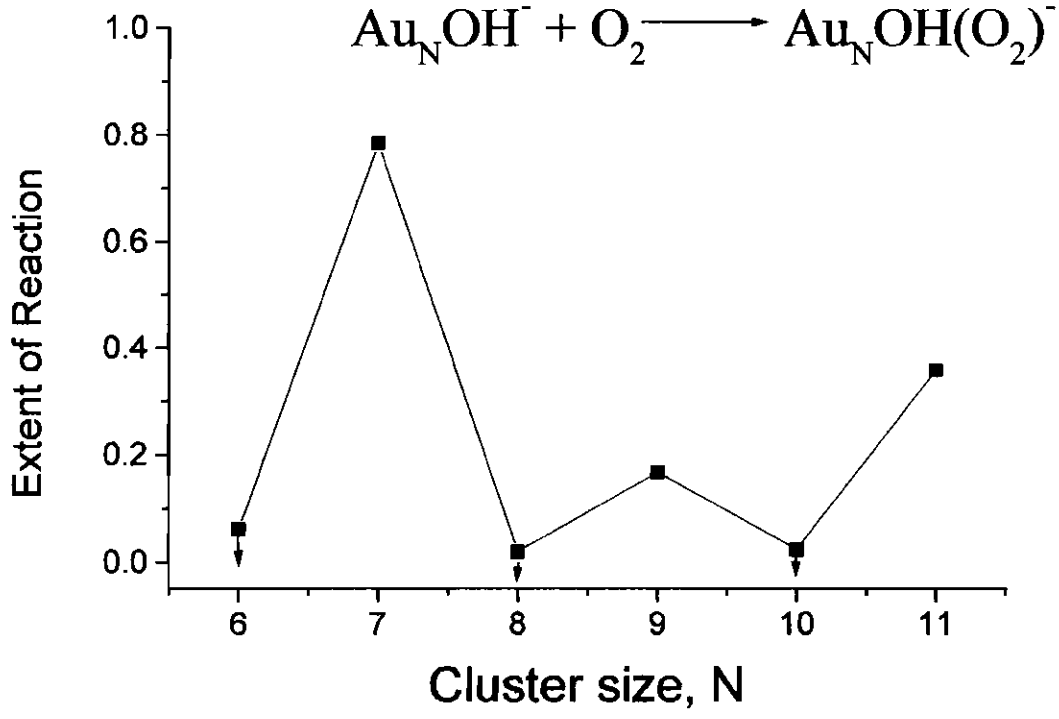

Figure 4-9: Cluster size-dependence of the extent of reaction

Extents of reaction for the addition of approximately 1 mbar O_2 to Au_NOH^- clusters (N = 6 - 11), as defined in equation (2'). The extents of reaction for the even-N Au_NOH^- clusters are upper limits.

4.5.2 Theoretical

Bonačić-Koutecký and coworkers determined the structures (**Figure 4-10**) and stabilities (**Table 4-2**) of $Au_NOH(O_2)^-$ species in order to investigate the reactivity of Au_NOH^- complexes towards molecular oxygen (also shown in **Figure 4-4**). Their calculations confirmed that the addition of the hydroxide moiety caused the O_2 adsorption activity to reverse. In contrast to the strong binding of O_2 to Au_2^-, the binding of molecular oxygen to Au_2OH^- is not energetically favorable (**Figure 4-4**). The NBO analysis shows that there is almost no electron transfer from the Au_2 subunit to the O_2 molecule (**Table 4-2**). In contrast, Au_3OH^- was found to strongly bind O_2, and a significant amount of electron transfer from the Au_3 subunit takes place. In this species, O_2 is found to be in the form of a superoxide subunit, as determined from the NBO charge and the length of the bond between the oxygen atoms, which was significantly longer than that of molecular oxygen. The stable $Au_3OH(O_2)^-$ complex has a triangular structure with OH and O_2 bound at the neighboring Au atoms. They also found that the binding of O_2 to Au_4OH^- is very weak, explaining why it is not be observed in the experiments. No significant electron transfer from the gold subunit to O_2 was found, leading to a shorter oxygen-oxygen bond.

In the most stable structure of $Au_5OH(O_2)^-$, the O_2 molecule bridges two gold atoms of a trapezoidal Au_5 subunit. The binding energy of 0.88 eV is only slightly higher than that of $Au_3OH(O_2)^-$ (0.78 eV). Again, stronger interaction with the Au_5 subunit is reflected in the electron transfer and in the oxygen-oxygen bond length. The trapezoidal

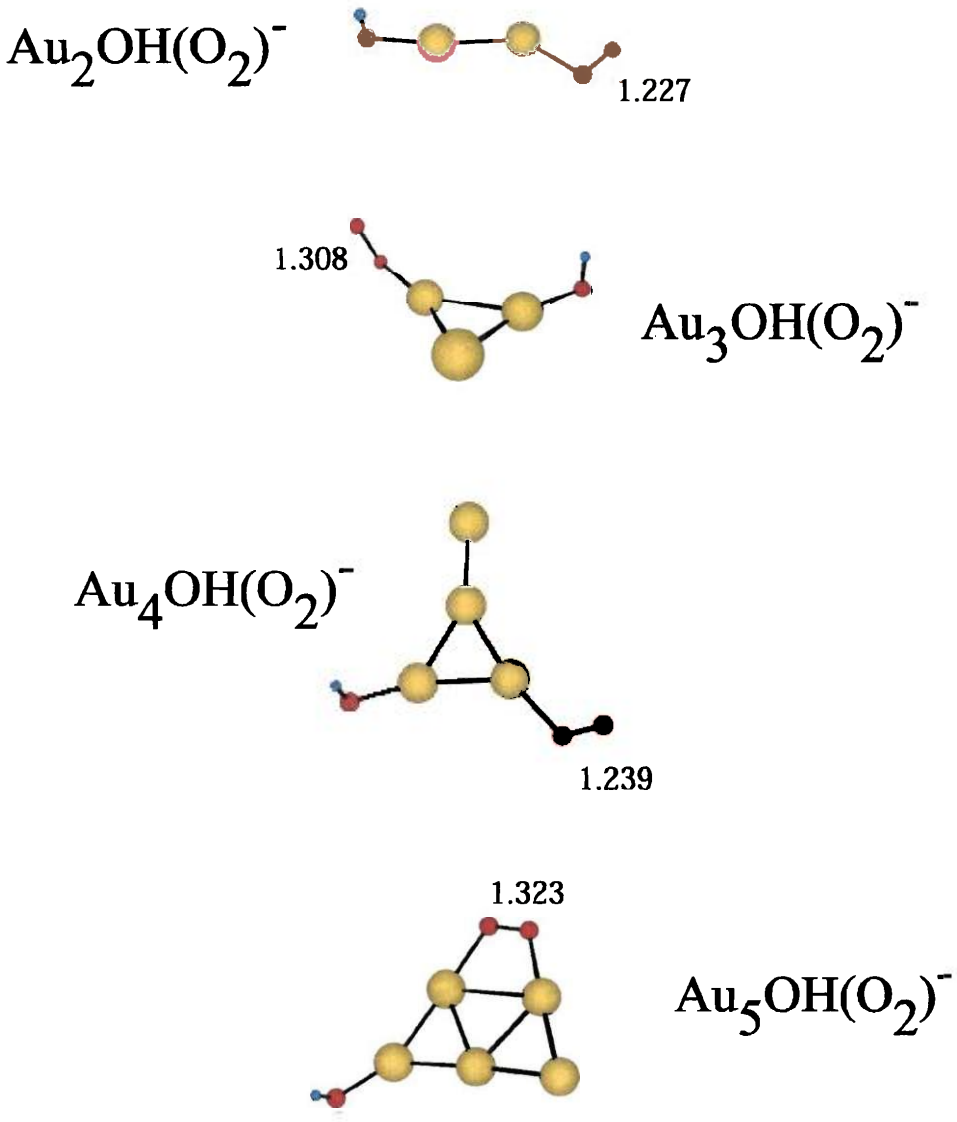

Figure 4-10: Calculated structures of $Au_NOH(O_2)^-$ complexes (N = 2 - 5)

Lowest-energy structures calculated for the $Au_NOH(O_2)^-$ system using the theoretical methods described in the text. Oxygen and hydrogen atoms are labeled by large red and small blue circles, respectively, and O_2 bond lengths are listed in angstroms. For other higher-energy structural isomers, see the original text.[193]

Table 4-2: Ground-state energies and properties of optimized $Au_NOH(O_2)^-$ (N = 2 - 5) clusters

$Au_nOH(O_2)^-$ n=2-5	Symm.(State)	Energy a.u	ΔE eV	E_b eV	NBO Charge		
					Au_n	OH	O_2
$Au_2OH(O_2)^-$	C_1 (^{3}A)	-497.883874		-0.006	-0.195	-0.638	-0.167
$Au_3OH(O_2)^-(I)$	C_1 (^{2}A)	-633.713091		0.78	0.154	-0.310	-0.844
$Au_4OH(O_2)^-$	C_1 (^{3}A)	-769.529684		0.03	-0.174	-0.606	-0.220
$Au_5OH(O_2)^-$(I)	C_1 (^{2}A)	-905.364643		0.88	0.114	-0.322	-0.835
$Au_5OH(O_2)^-$(II)	C_1 (^{1}A)	-905.351662	0.353				
$Au_5OH(O_2)^-$(III)	C_1 (^{1}A)	-905.350389	0.388				
$Au_5OH(O_2)^-$(IV)	C_1 (^{1}A)	-905.341137	0.640				

Energies and properties obtained using DFT with the B3LYP method; [a]Energy difference with respect to the most stable structure; [b]Binding energy for the $Au_NOH(O_2)^-$ complexes is defined by $E_b = E(Au_NOH(O_2)^-) - E(Au_NOH^-) - E(O_2)$.[193]

Au_5 subunit was slightly positively charged due to the complete electron transfer to the OH and O_2 subunits.

4.6 Determination of binding energies from the temperature dependence of the equilibrium constant

In an attempt to determine the binding energies of O_2 on the reactive gold cluster species and to facilitate a comparison with the theoretical values of binding energies, the temperature of the reaction system was varied between the range of 258 K to 318 K. Using this method, the binding energies can be determined using the equation

$$\Delta \ln K = \frac{-\Delta_r H}{R} \Delta \frac{1}{T} + \frac{\Delta S}{R} \qquad (3),$$

in which $\Delta_r H$ is the binding energy of O_2 on the cluster, ΔS is the entropy of adsorption, R is the gas constant, and the apparent equilibrium constant, K, at a constant O_2 concentration is defined by

$$K = \frac{[Au_N O_2^-]}{P_{O_2}[Au_N^-]} \quad (4)$$

for even-N clusters. For odd-N clusters, Au_N^- would be replaced by Au_NOH^- and $Au_NO_2^-$ would be replaced by $Au_NOH(O_2)^-$. Representative plots of lnK v/s 1/T obtained from equation (3) are shown in **Figures 4-11** and **4-12** for Au_3OH^- and Au_4^-, respectively, for two different partial pressures of O_2. Linear fits for the high temperature data are also shown in the figures. For simple adsorption behavior, the relative equilibrium constant should continue to increase with decreasing temperature. As is readily apparent from **Figures 4-11** and **4-12**, this is not the case for the two species shown. In the case of Au_4^-, a linear fit can only be made for temperatures above room temperature (RT, ~298 K), the slope of which gives an approximate O_2 binding energy (ΔH_r) of 0.53 ± 0.01 eV, which is lower than the value determined by Lee and Ervin in their collision-induced dissociation experiments by approximately 0.5 eV.[113,131,200] At temperatures lower than room temperature, however, the value of the apparent equilibrium constant becomes much less steep. A tentative interpretation of this behavior is that the gradual slope at lower temperatures may be indicative of a parallel binding process, in which O_2 interacts with Au_4^- in a weakly bound, loosely held structure. However, this activity still is not well understood. Therefore, these discussions will focus on the high-temperature activity ($\geq$ RT).

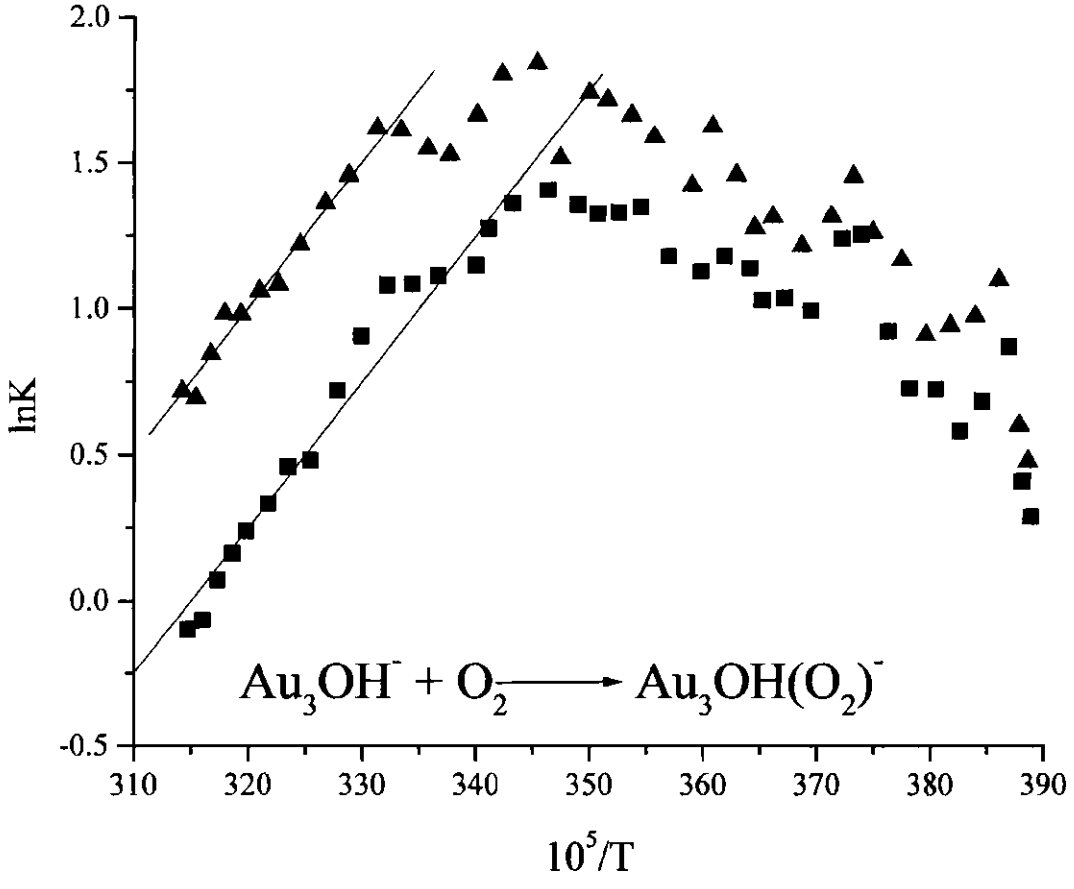

Figure 4-11: Temperature-dependence of the apparent equilibrium constant of the $Au_3OH^- + O_2$ reaction

Plots of the gas-phase temperature-dependence of the apparent equilibria $Au_3OH^- + O_2$ obtained from equation (3) for two reactant concentrations. The plots correspond to ln K v/s 1/T. At higher temperatures, the lines are a linear fit to the data, yielding the binding energies described in the text.

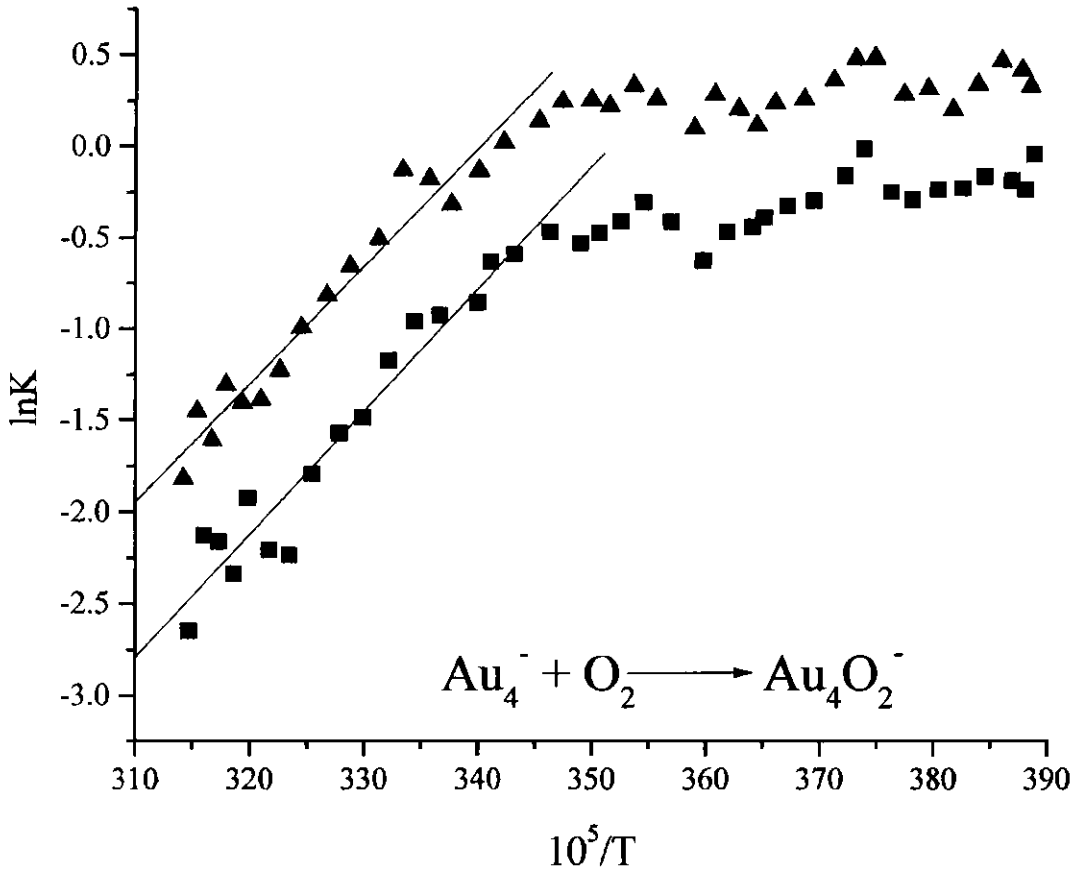

Figure 4-12: Temperature-dependence of the apparent equilibrium constant of the $Au_4^- + O_2$ reaction

Plots of the gas-phase temperature-dependence of the apparent equilibria $Au_4^- + O_2$ obtained from equation (3) for two reactant concentrations. The plots correspond to ln K v/s 1/T. At higher temperatures, the lines are a linear fit to the data, yielding the binding energies described in the text.

The behavior of Au_3OH^- is also not simple. Up to temperatures just below room temperature, the value of the apparent equilibrium constant is actually *increasing*, suggesting that an effective energy barrier must be overcome for O_2 to bind to the cluster. Only beginning immediately below room temperature does the value of the apparent equilibrium constant begin to decrease with increasing temperature. From a linear fit to this data, a binding energy of approximately 0.47 ± 0.05 eV can be obtained. While these binding energies are significantly different from those calculated here and measured experimentally (by Lee and Ervin[113,131,200]), the plots still give important qualitative information, namely that, at lower temperatures, kinetics may play an important role and an equilibrium treatment of these systems may not be applicable.

4.7 Discussion

The easiest (and perhaps most pleasing) explanation for the selective activity of the Au_NOH^- species towards O_2 adsorption draws on a comparison to the activity of the bare Au_N^- clusters. As described above, with the high electron affinity of OH (~ 1.8 eV), the electron transfer from the even-N clusters to OH becomes highly favorable, and causes transfer from the odd-N clusters to become stable. In such a case, the electronic structure of the gold clusters reverses from the situation seen for bare clusters, i.e. the bare, odd-N Au_N^- clusters have no unpaired electrons, while the odd-N Au_NOH^- clusters now have an

unpaired electron on the gold cluster. In this case, in an attempt to once again pair electrons, the open-shell cluster complexes can adsorb O_2 as a one-electron acceptor.

An analysis of the experimental and theoretical results provided in this chapter support this bonding mechanism for the Au_3OH^- cluster and is described as follows: First, the OH group binds to a closed shell Au_3^- cluster having a linear geometry.[78] Due to the high electron affinity of the OH group, electron transfer from Au_3^- to the OH takes place, resulting in an essentially neutral Au_3 subunit (having a bent configuration,[191,193] though the actual ground state geometry has not been agreed upon[78,79,103]), which then, due to its open shell structure, strongly binds O_2. In the resulting complex, the gold subunit has a positive charge and a triangular geometry,[191] and the negative charge is mainly localized at the O_2 superoxide subunit.

With this mechanism in mind, a greater understanding of this system could be provided by further studies of the activity of the neutral gold clusters, Au_N. In this case, subsequent O_2 adsorption depends on the ionization potential (IP) of the neutral cluster species. Several experimental and theoretical values of Au_N IPs are collected in **Table 4-3**. An analysis of these values provides additional insight into the observed extents of reaction. While the absolute values of the cluster IPs are somewhat different, the *overall trends* are consistent. Beginning with Au_2, a strong even-odd oscillation in cluster IP is seen (as with the measured extents of reaction), with the even-N clusters having significantly higher IPs than the odd-N clusters. Within the odd-N clusters studied, the IP value for Au_5 is higher than that for Au_3, which is consistent with the lower extent of reaction for Au_5 (**Figure 4-8**).

Table 4-3: Experimental and Theoretical Values for Au_N (N = 2 - 6) Ionization Potentials

	Au_2	Au_3	Au_4	Au_5	Au_6
IP (eV) [a]	9.50	7.50	8.60	8.00	8.80
IP (eV) [b]	9.16 ± 0.10	7.27 ± 0.15		7.61 ± 0.20	
IP (eV) [c]	9.41	7.06	7.98	7.46	
IP (eV) [d]					7.60
IP (eV) [e]	9.63	7.30	8.09	7.68	8.37

(a) Experimental values;[93] upper limits for IP, (b) Experimental values;[106] no value reported for Au_4 or Au_6, (c) Theoretical values;[201] no value reported for Au_6, (d) Theoretical value;[202] Au_6 is the smallest cluster reported. (e) Theoretical values[203,204]

While a separate understanding of the adsorption properties of {O_2, CO, etc.} are important to gain an understanding of the CO oxidation activity of free anionic gold clusters, it is their coadsorption properties that may play the largest role. Studies using the methods described for the current experiments were used to study the coadsorption of {CO, O_2} on small gold cluster anions, Au_N^- ($N \leq 10$).[192] Those experiments showed that, in many cases, CO and O_2 adsorb cooperatively on Au_N^-. Instead of lowering the probability of subsequent adsorption, the presence of a preadsorbate increases the ability of the cluster to bind an incoming molecule. This activity holds when either CO or O_2 is the preadsorbate. Very recent work by the group of Wöste also provided exciting results on the reactions of Au_{2-3}^-.[117] Using a temperature-controlled ion trap, they found that only Au_2^- showed activity towards O_2 adsorption over the temperature range of 100 K to 350 K. Under 250 K, however, *when CO is preadsorbed*, Au_3^- shows the addition of both one and two O_2 molecules, in the form $Au_3(CO)(O_2)^-$ and $Au_3(CO)(O_2)_2^-$. Only under conditions in which CO was preadsorbed, and at low temperatures, was O_2 adsorption able to be seen on this odd-N cluster anion, reinforcing the concept of cooperative coadsorption. The results presented in this chapter show that the coadsorption properties of {H_2O, O_2} on Au_N^- are equally interesting and suggest the need for further studies on the {H_2O, CO} and {H_2O, O_2, CO} coadsorption systems.

CHAPTER V

CARBON MONOXIDE ADSORPTION ON GOLD CLUSTER ANIONS

5.1 Introduction

The adsorption of carbon monoxide (CO) has been cited as the most extensively investigated chemisorption process on gold, though its sticking probability on bulk surfaces is extremely small at room temperature.[75] Even under low coverage conditions on stepped surfaces, the interaction energy is only ~ 55 kJ/mol, with the binding energy decreasing with increasing coverage.[205,206] Nevertheless, further study was motivated by several compelling factors, not the least of which regards the manner in which the size-, structural-, and electronic state of gold clusters and nanoparticles affects CO adsorption properties. The investigation of CO adsorption processes of gas-phase, negatively charged gold clusters,

$$Au_N^- + M \bullet CO \rightarrow Au_N(CO)_M^- \qquad (1),$$

referred to as (N,M) in future discussion, were motivated by several considerations described below.

A variety of oxygen-atom transfer reactions are catalyzed by small metal-oxide supported gold clusters. These include a class of carbon (C1) transformations and their reverse reactions that are of great importance in both the scientific and technical arenas. These include:

$$CO + \frac{1}{2}O_2 \rightarrow CO_2 \qquad \textit{combustion}$$

$$CO + NO \rightarrow \frac{1}{2}N_2 \qquad NO_x \textit{ reduction}$$

$$CO + H_2O \rightarrow CO_2 + H_2 \qquad \textit{water-gas shift}$$

$$CO + 2H_2 \rightarrow CH_3OH \qquad \textit{methanol synthesis}$$

For each of these reactions, comparable activities to the existing standards were shown by supported gold catalysts, with both a reduced operating temperature and/or activation energy.[52,75] Studies found that the activity of these catalysts depended quite highly on the average size of the supported gold particles, though the catalysts are highly diverse structurally. Strong evidence was presented showing that small gold clusters are immobilized at surface oxide vacancies of the support.[39,44,72,73] These defects are sites of localized electron density that can be transferred to the highly electronegative gold clusters,[39,44] and it is this negative charge transfer that is the basis for the study of gold cluster anions, Au_N^-. Studies of such species with reactants of interest (i.e. CO) are important in gaining a better understanding of the effective activity of the supported clusters.

Relatively few studies have focused on the chemical properties of gas-phase gold clusters in the size range described below, while a great deal of work has focused on their electronic properties.[77,80-82,106,207] In many cases, these properties have been found to depend on cluster size and charge, in a manner consistent with an electron-shell model.[77] An early report that was mainly concerned with the interaction of CO on copper cluster cations also briefly mentioned that the initial CO adsorption activity on gold cluster cations is only weakly dependent on the size of the cluster, though the complexes Au_7CO^+ and $Au_{19}CO^+$ showed greater resistance to fragmentation.[111] More recently, Lee and Ervin performed a much more encompassing analysis of the CO adsorption properties of Au_N^- clusters, measuring the rate of initial CO adsorption on

Au_N^- (N = 2 - 7) using low-pressure continuous-flow tube methods. They reported a reaction rate that was extremely small for sizes $N \leq 4$, but then increased dramatically and monotonically with increasing cluster size.[112,113] Only Au_7^- appeared to approach the high-pressure limit of bimolecular reactions, and their accessible pressure range (described in Chapter 2) did not allow them to determine any type of saturation behavior.

As described in Chapters 3 and 4, a binary-like adsorption behavior was found for the $Au_N^- + O_2$ reaction system (and, equivalently, the $Au_NOH^- + O_2$ system), in that either zero or one O_2 molecule adsorbs on the clusters at saturation. This was explained by assuming that O_2 acts exclusively as a one-electron acceptor, while the gold-cluster subsystem strives to pair its valence electrons. If the adsorption of CO was also to be controlled by this sort of valence-electron-count driven activity, then the CO molecule should act as a two-electron donor, as is normally assumed in inorganic chemistry.[22] In this case, the $Au_7(CO)_1^+$ and $Au_{19}(CO)_1^+$ complexes described above[111] would represent 8- and 20-electron shell closings, since each (neutral) gold atom contributes one electron.

The experiments in this chapter describe the pressure-dependence of CO adsorption on gas-phase gold cluster anions. With the far-reaching goal of showing gas-phase carbon monoxide oxidation on the clusters (as shown on supported clusters), it is important to determine the pressure-dependent coverage of each reactant in order to determine the feasibility of catalytic cycles occurring on the clusters. Only then can a parallel be drawn between the processes occurring on the clusters and those taking place on heterogeneous catalysts.

5.2 Experimental Methods (Abbreviated)

The CO adsorption activity and saturation of gold cluster anions were measured using a pulsed helium flow-reactor and detected by time-of-flight mass spectrometry. The method and instrument have been described in Chapter 2, so only a brief summary of its performance characteristics is given here. Negatively charged gold clusters were produced by laser ablation of a gold rod, underwent growth and cooling in the helium pulse entrained in the growth region of the cluster source, and then entered the fast-flow reactor where they interacted with a dilute CO:He pulse introduced using a secondary pulsed valve. At the end of the reactor region, the merged gas pulses sprayed into vacuum, were collimated by a skimmer, and entered the extraction-field region of the time-of-flight mass spectrometer.

As described in Chapter 2 for the adsorption of O_2 on Au_N^- clusters, the CO/He mixture was introduced into the system via two methods. First, using a CO/He mixture that was varied in composition from 1-20%, the reactant was introduced into the fast-flow reactor using the secondary pulsed valve. Alternatively, the reactant mixture (usually no more than ~1% CO/He) was introduced into the main gas valve, allowing much longer reaction times for the clusters and reactants. Combining these methods allowed for the observation of a much wider range of adsorption activity.

Lee and Ervin measured the absolute bimolecular rate constant for the room-temperature reaction $Au_7^- + CO = Au_7CO^-$, which has a ~ 5 $Å^2$ reaction cross-section as the high-pressure limit is approached.[112,113] This reaction cross section made it

possible to use the reaction as an internal reference (as described in Chapter 2) to calculate the CO partial pressures used in the experiments below. The CO partial pressure was calculated to range from approximately 0.01 to 0.2 mbar. Using a 1% CO/He mixture in the main valve, a CO partial pressure in the reactor of approximately 1 mbar was estimated. In either case, the total helium pressure is estimated to approach 150 mbar in the reactor, yielding ~ 1 ns between buffer gas collisions for Au_7^-.

5.3 Results

The initial adsorption activity of CO on Au_N^- clusters was studied using the secondary pulsed gas valve to introduce small amounts of the reactant mixture into the fast-flow reactor. **Figure 5-1** shows typical mass spectra obtained for N = 4 - 18 both when the main and secondary gas pulses are temporally offset (top frame) and overlapped (bottom frame). As can be seen in the top frame, introducing an offset between the pulses results in only the clean gold clusters, Au_N^-, being detected. Overlapping the gas pulses results in a (small) depletion of the bare cluster peaks and the growth of new peaks in the mass spectra, each displaced by multiples of 28 amu from each parent peak. These new peaks are described as having the composition $Au_N(CO)_M^-$ = (N,M), and are marked with asterisks in the bottom frame of **Figure 5-1**. The relative amounts of CO added to the various clusters are quite dissimilar. These differences in activity will be described below.

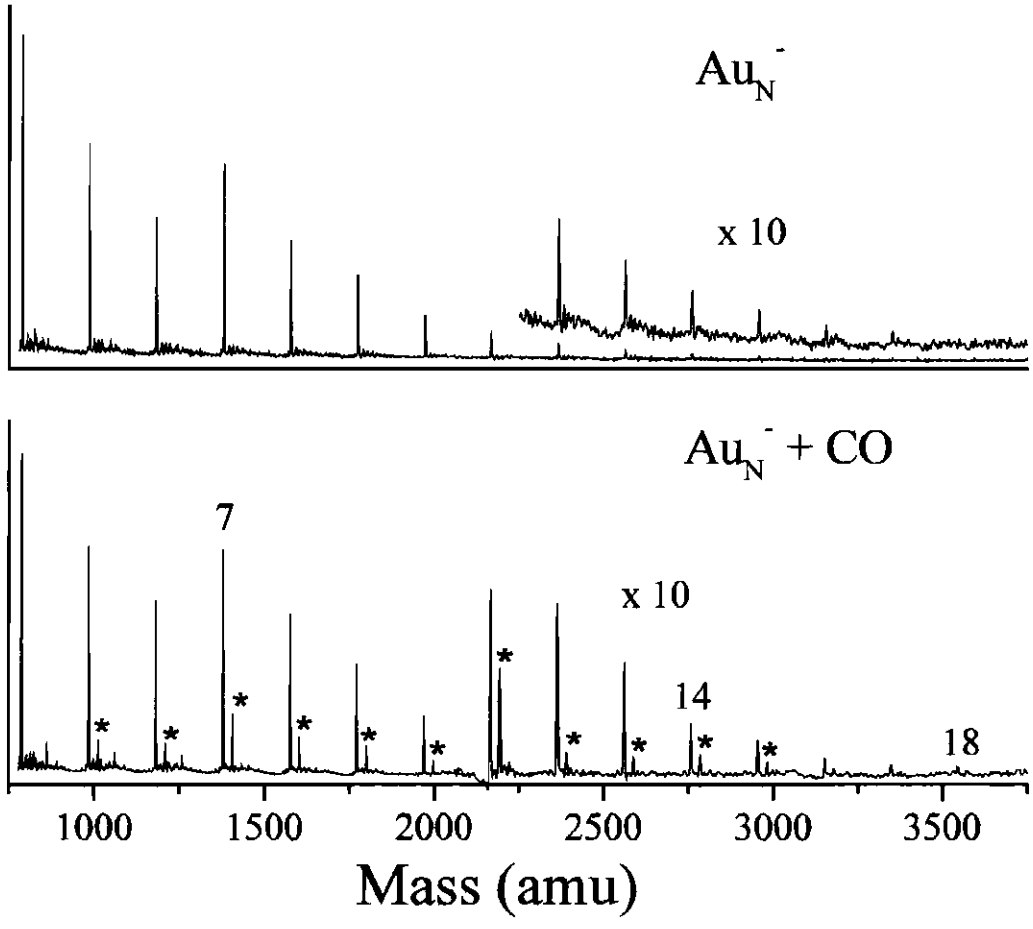

Figure 5-1: Initial adsorption of CO on Au_N^- clusters

(Top Frame) Mass spectrum obtained when the secondary gas pulse was temporally offset from the main (cluster) pulse, resulting in a "clean" mass spectrum, i.e. only bare gold cluster anions with no adsorbed CO. (Bottom Frame) Mass spectrum obtained when the gas pulses were overlapped, resulting in the depletion of the parent clusters and the appearance of new peaks at +28 amu intervals above the depleted parent peaks.

As the amount of reactant gas is increased in the flow reactor, additional peaks spaced 28 amu apart begin to appear, and the parent (bare) cluster peak becomes even more depleted. A typical mass spectrum obtained under these conditions is shown in **Figure 5-2** for N = 4 - 15. In all cases, the intensities for each parent cluster and its adsorbate complexes seem to be well conserved throughout all pressure dependent studies. This is important, as described in Chapter 3, in order to attribute all observed reactions simply to adsorption of CO, as opposed to other processes such as fragmentation of the clusters upon adsorption of CO. The intermediate conditions shown in **Figure 5-2** are significant in that, as opposed to single adsorption of varying activity, product distributions resulting from the adsorption of multiple CO molecules can be observed. None of the clusters show truly statistical behavior in their adsorption patterns, in which a binomial distribution of adsorption products would be assumed. Additionally, several of the clusters show preferential adsorption species, in which the mass spectrum in a certain size range is dominated by a single peak. For instance, certain (N,M) compositions corresponding to (5,1), (11,1), (15,1) and (15,2) are all significant in their intensity in relation to other peaks in their (N,M) family. These "special compositions" are collected in **Table 5-1**.

At the higher CO partial pressures of **Figure 5-3**, in which CO was seeded into the main pulsed gas valve, evidence of saturation is obtained for many cluster sizes. In these cases, certain (N,M) compositions predominate and subsequent addition of CO does not lead to further reaction. Examples some of the saturation peaks are marked in **Figure 5-3**, and the saturation compositions (N,M_{max}) are collected in **Table 5-2**. It should also be

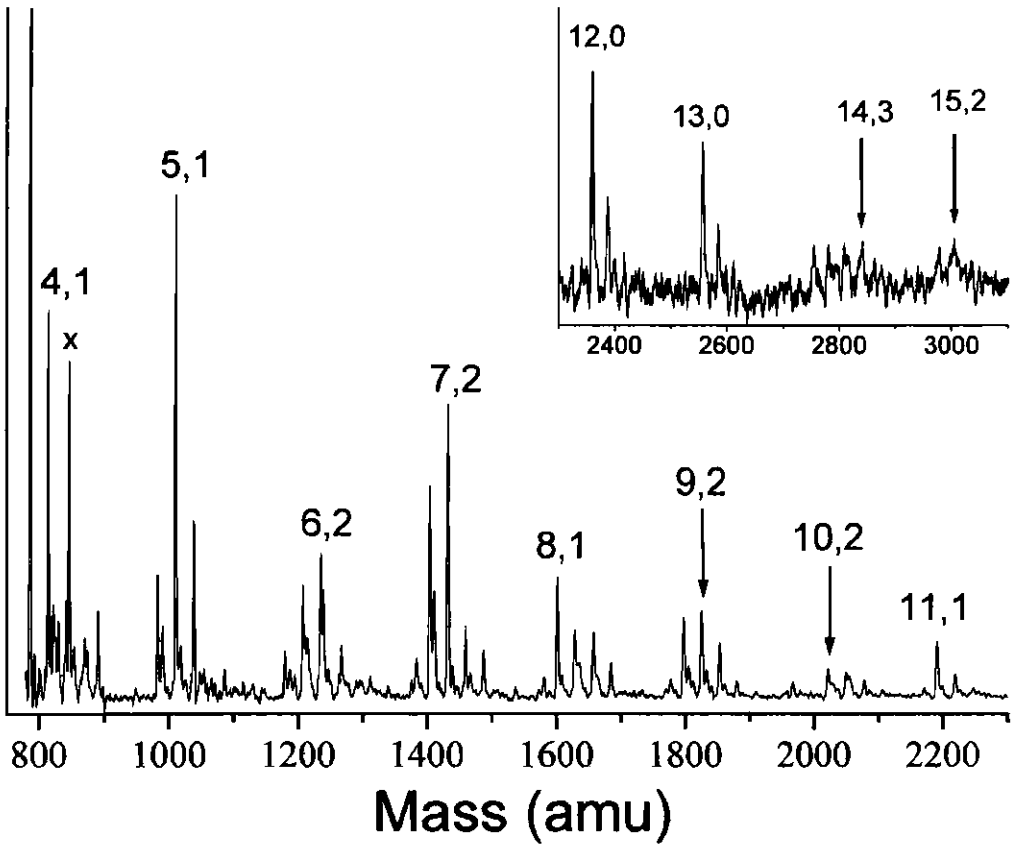

Figure 5-2: Intermediate adsorption of CO on Au_N^- clusters

Mass spectrum obtained as in **Figure 5-1** (introduction of reactant using the secondary pulsed gas valve), but now with much higher CO partial pressure. Most of the peaks have added a second (or third) CO adsorbate, and some evidence of especially stable cluster species can now be seen (as described in the text). The peak marked with an "x" to the right of Au_4^- is the result of trace O_2 contamination in the system, as it corresponds to CO_3 (+60 amu).

Table 5-1: Special compositions, $Au_N(CO)_M^{\pm}$ = (N,M, ±) and electron counts

(N,M,±)	[a]N_e	[b]Configuration	Source
(5,1,-)	8	$1S^2 1P^6$	Fig. 5-2
(7,1,+)	8	$1S^2 1P^6$	Ref. 111
(11,1,-)	14	$1S^2 1P^6 (t2g)6$	Fig. 5-2
(15,1,-)	18	$1S^2 1P^6 1D^{10}$	Fig. 5-2
(15,2,-)	20	$1S^2 1P^6 1D^{10} 2S^2$	Fig. 5-2
(19,1,+)	20	$1S^2 1P^6 1D^{10} 2S^2$	Ref. 111

(a) Electron counts, N_e, are from equation (8). (b) Configurations are described by deHeer,[94] and octahedral symmetry can account for the 14 electron subshell.

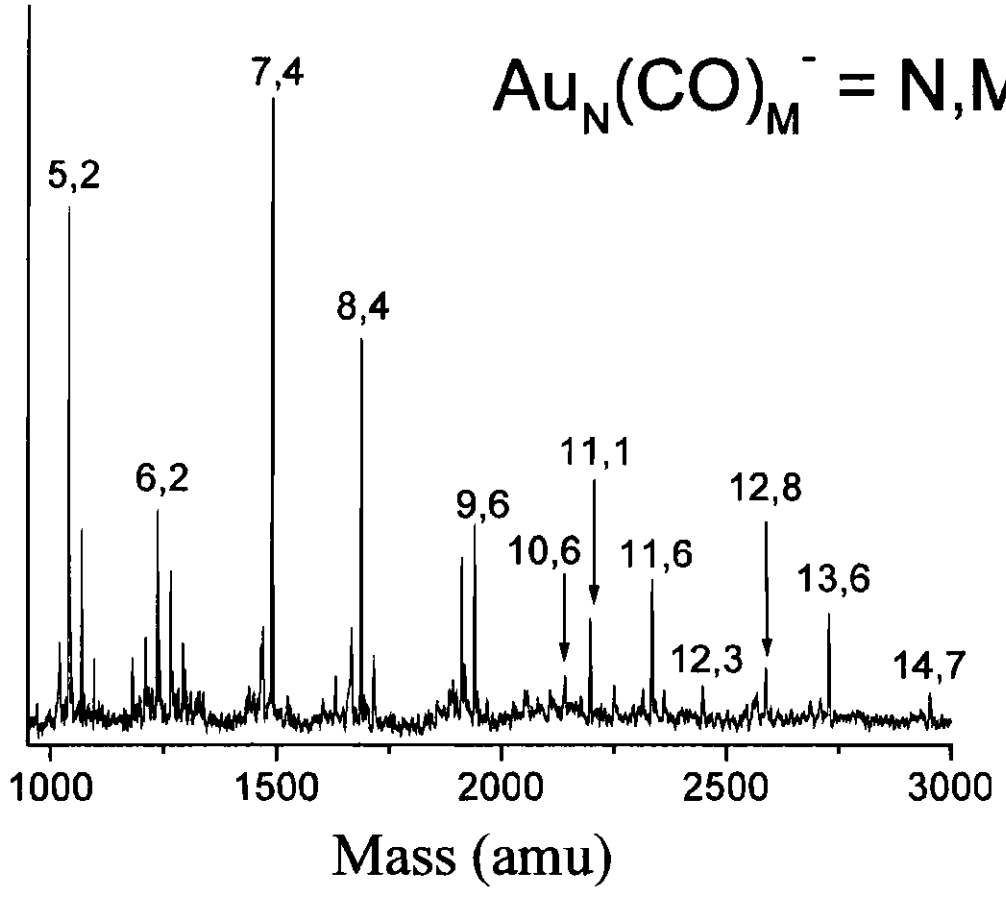

Figure 5-3: CO adsorption on Au_N^- clusters (upstream addition)

Mass spectrum resulting from the introduction of a 1% CO/He mixture in the primary pulsed gas valve. A much wider distribution of products is seen than in **Figures 5-1** and **5-2**, and several of the clusters have become resistant towards further CO addition.

Table 5-2: Saturation compositions (N,M_{max})

N	M_{max}	other $M^{(a)}$	$M_{max}(O_2)^{(b)}$
4		1	1
5	4	1-3	0
6	4	0-3	1
7	4		0
8	5	4	1
9	6	5	0
10	6		1
11	6	1	0
12	8	3	0,1
13	6		0
14	7		1

(a) Other compositions still prominent at conditions approaching saturation. (b) From Salisbury *et al.*[133]

noted that mass spectra obtained under these extreme conditions (and, to a certain extent, under intermediate conditions) are complicated by peaks that appear in between each CO-adsorbate peak. These peaks will be discussed in greater detail in Section 5.4.

5.4 Discussion

5.4.1 Initial Adsorption Activity

The size-dependent adsorption activity, defined by equation (1), of a series of clusters at room temperature can be described quantitatively with the aid of a few simple calculations. First, the peak intensities $I_{N,M}$ within each pattern are normalized, so that they can be expressed as (fractional) abundances,

$$f_{N,M} = \frac{I_{N,M}}{\Sigma_M I_{N,M}} \qquad (2)$$

where the sum runs from M = 0 (the unreacted cluster) to M_{max} (the saturation adsorption). Then, assuming kinetic control of the adsorption (i.e. irreversible sequential

adsorption steps), the reactivity R_N can be defined in terms of the depletion of the unreacted cluster abundance,

$$R_N = -\ln [f_{N,M=0}] \qquad (3).$$

Reactivity plots for different CO partial pressures are shown in **Figure 5-4**. Each of the reactivity values have been normalized to that of Au_7^-,

$$R_N^* = \frac{R_N}{R_7} \qquad (3').$$

Assuming kinetic control of the reactions, these relative reactivities should not depend on the concentration of CO in the reactor.

A more appropriate method to determine the actual extent of reaction of a given cluster species is to observe the change in average adsorption as a function of reactant partial pressure. **Figures 5-5** and **5-6** provide plots of the change in mean CO adsorption on individual clusters as a function of the CO/He pulse duration, a measure of

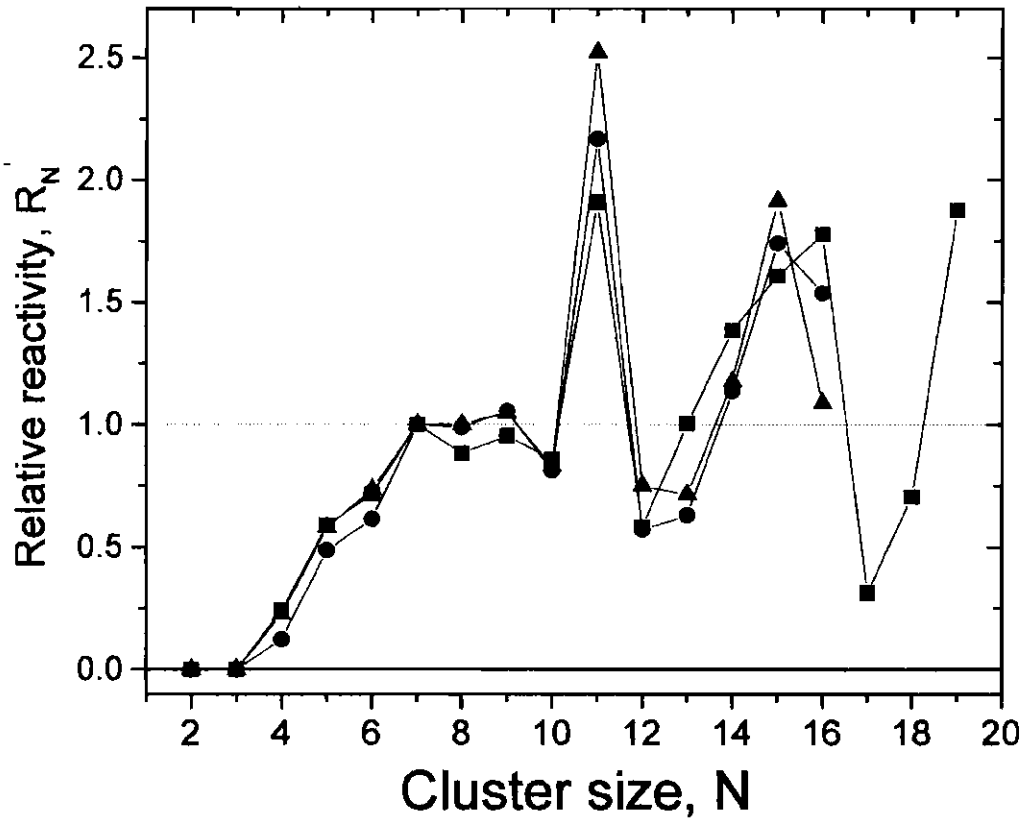

Figure 5-4: Relative activity of Au_N^- clusters towards CO adsorption

Variations in the (relative) initial activity of Au_N^- clusters towards CO adsorption as a function of size, N, as defined in equations (3) and (3'). The different plots correspond to different CO concentrations in the flow reactor in the increasing order of squares, circles, and triangles.

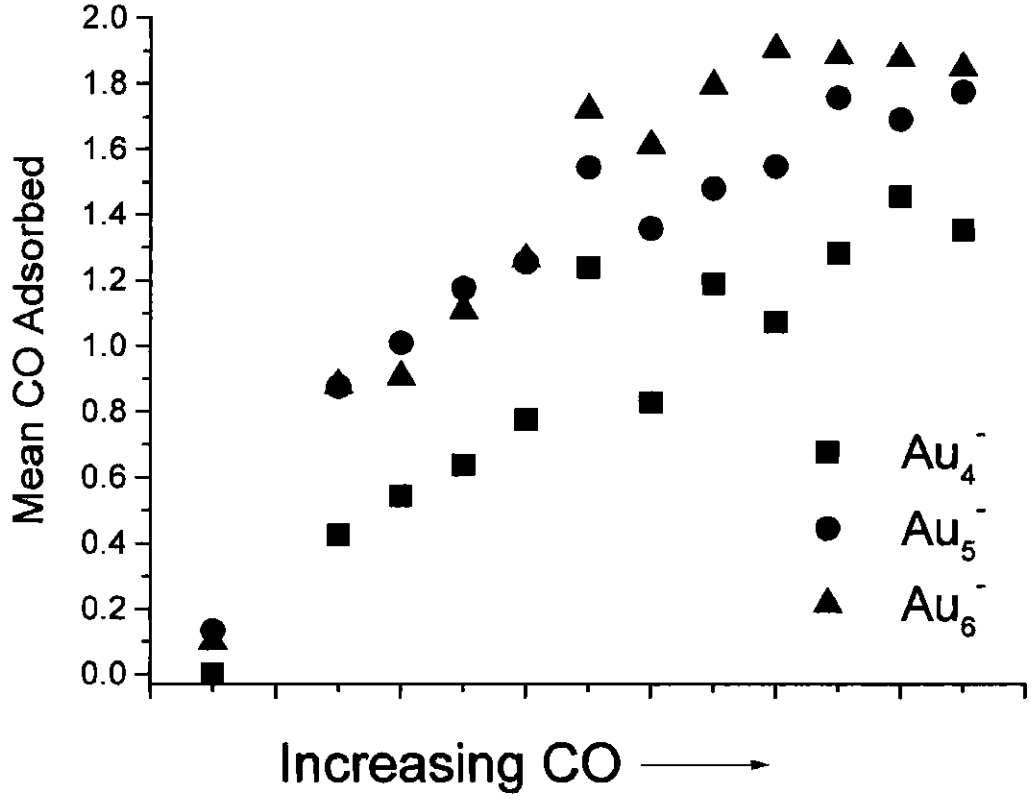

Figure 5-5: Mean CO adsorption on selected Au_N^- clusters

Plot showing the variable adsorption of CO on gold cluster anions (N = 4 - 6). By linearly varying the duration of the CO/He pulse (lower axis), the mean number of CO adsorbates on the various clusters can be increased. While the mean number of adsorbates on Au_4^- and Au_5^- continue to increase with longer pulse lengths, the adsorption "isotherm" of Au_6^- seems to level off at higher pressures, possibly suggesting that its saturation coverage has been achieved.

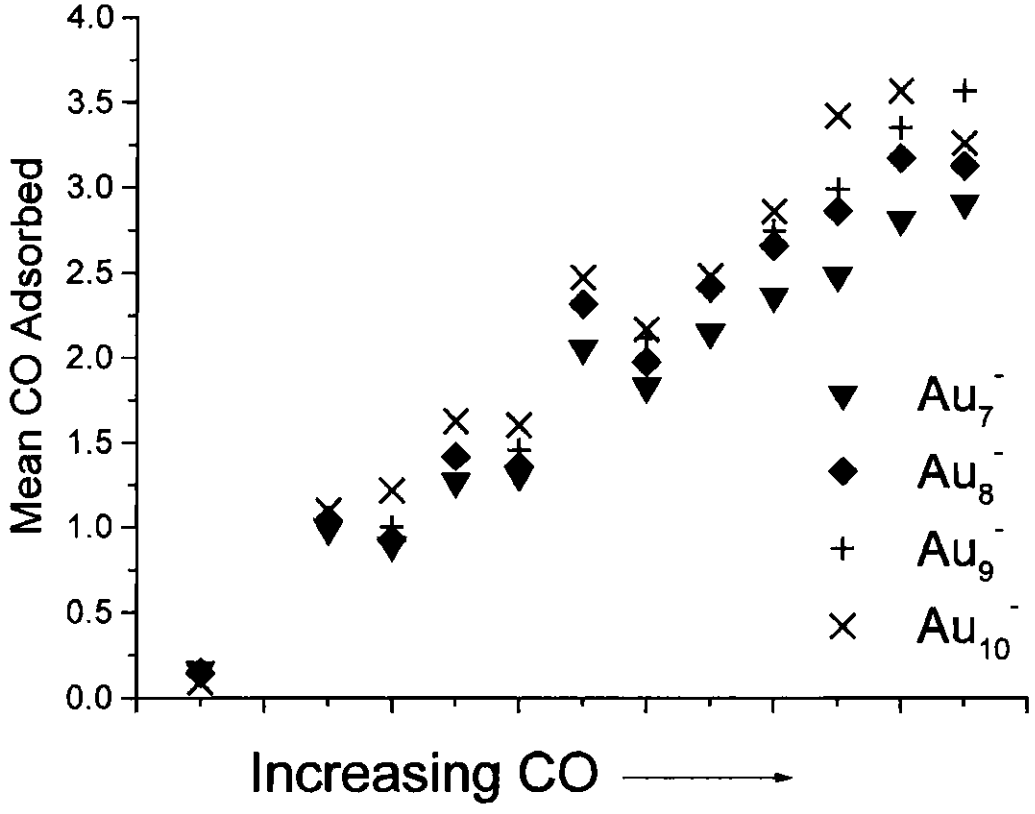

Figure 5-6: Mean CO adsorption on selected Au_N^- clusters

Plot showing the variable adsorption of CO on gold cluster anions (N = 7 - 10). By linearly varying the duration of the CO/He pulse (lower axis), the mean number of CO adsorbates on the various clusters can be increased. With increasing cluster size, an increase in the mean number of adsorbates also increases in this size range.

the CO partial pressure in the flow reactor. For the majority of the cluster species shown in these figures, increasing the partial pressure of CO causes an increase in the mean number of CO adsorbates. For Au_6^-, however, after an initial rise in average adsorption, the slope of the plot levels off, and further CO introduction does not lead to a larger mean number of adsorbates. This could indicate that Au_6^- has approached its saturation point, which is interesting, as the members of this cluster family have not been completely converted to a single species (as seen for some of the other clusters), but instead maintain a relatively flat distribution.

As is more often the case with simple adsorption processes (defined by a negligible barrier to adsorption and no metastable precursor states), reaction processes such as that show in (1) are under equilibrium control. In this case, the appropriate measure of initial activity is the adsorption free-energy, expressed by the logarithm of the stepwise equilibrium constant $K_{N,\,M=0,1}$,

$$\ln K_{N,M=0,1} = \ln \left[\frac{(f_{N,M=1})}{(f_{N,M=0})P_{CO}} \right] \qquad (4),$$

where P_{CO} is the partial pressure of carbon monoxide, which may be removed by normalizing to that of K_7, the equilibrium constant for Au_7^-,

$$K_N^* = \frac{K_N}{K_7} \qquad (4').$$

Again, such relative adsorption free energy values should not depend on the CO dose used, assuming equilibrium control. These values are plotted in **Figure 5-7**.

The main features of the results collected in **Figures 5-4** and **5-7** can be summarized by a few points. Even under the saturation conditions of **Figure 5-3**, there is no evidence of the room temperature adsorption of CO on either Au_2^- or Au_3^-. Au_4^- is the smallest cluster to show measurable adsorption activity. There is a large increase in activity with Au_5^-, which adsorbs CO readily. Part of this high initial activity may be attributed to the special stability of the Au_5CO^- product, as suggested by its reluctance to undergo further CO adsorption. The activity in the N = 6 to 10 range varies within a narrow band, with a weakly superimposed trend toward an even odd-alteration, with odd-N (even electron) clusters more active than their neighboring even-N (odd electron) clusters. While it may seem odd (in light of the results presented in Chapters 3 and 4) for the even-N clusters to be less reactive, as a two-electron donor, CO will have a repulsive interaction with the highest occupied molecular orbital of the even-N cluster anions, which possesses a single electron. Therefore, it is more important to observe the relative energies of the lowest unoccupied molecular orbital of the clusters in relation to CO. The highest level of activity is seen with N = 11, which is the most active of the larger clusters. In fact, only N = 15 approaches the high level of adsorption activity shown by Au_{11}^-, and several of

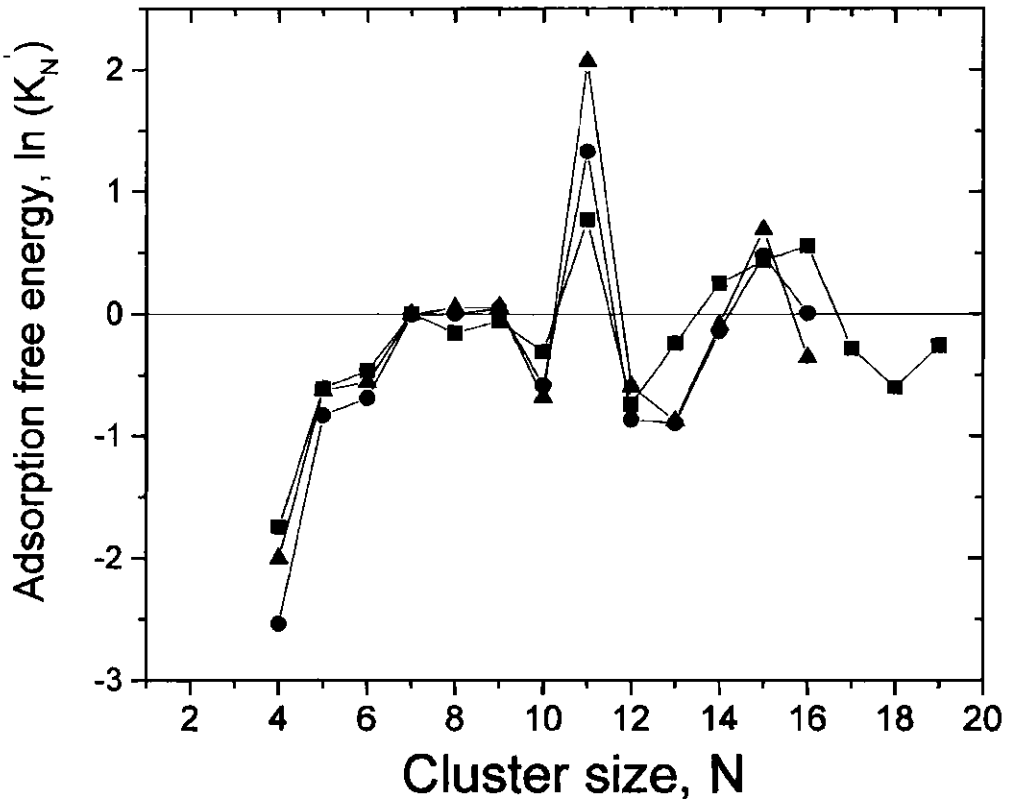

Figure 5-7: Free energy of adsorption of CO on Au_N^- clusters

Relative first equilibrium constants (K_N') of CO adsorption on Au_N^- clusters as a function of size obtained at room temperature. The equilibrium constants are calculated using equations (4) and (4'). The different plots indicate varying CO partial pressures in the flow reactor in the order: squares (lowest concentration) < circles < triangles (highest concentration)

the larger clusters (N = 12, 13, 17) are consistently below N = 7. Finally, these results do not provide enough information with which to decide between kinetic and equilibrium limits.

5.4.2 Higher Coverages, Saturation, and Metastability

Due to the small size range presented in these experiments, it is not possible to determine how these results would relate to CO adsorption on macroscopic gold surfaces, which have negligible sticking probabilities at room temperature. Yet it is certainly sufficient to conclude that the adsorption probability fails to continue to rise with increasing size. (The collision cross-section varies little across this size-range, since the increase in the cluster's geometrical cross-section, which nearly doubles on going from N = 7 to N = 20, is largely cancelled by the enhanced long-range ion-dipole interaction for smaller clusters.[112])

There is clear evidence, in the patterns shown in **Figure 5-3**, that subsequent adsorption steps are even more selective with respect to cluster-size than is the initial adsorption process. Without evaluating these trends quantitatively, one may yet conclude that: (i) N = 5 and 11 are relatively reluctant to adsorb a second CO molecule, while N = 15 acts similarly against the third adsorption. (ii) Approaching saturation, there is a pronounced odd-even alternation across the N = 6 to 13 range, as "evens" remain partially unsaturated while "odds" rush toward saturation values. The latter effect may be appreciated by considering the size-dependences of the mean coverage and especially its

standard deviation, **Figure 5-8**. This behavior is very far indeed from that of a "structure-insensitive reaction", as CO adsorption has often been described.[7,112,113]

As mentioned earlier, under higher CO partial pressure conditions, the mass spectra became complicated by peaks appearing between each successive CO-adsorption peak. In lieu of these peaks arising from contamination or other processes taking place in the reaction zone of the cluster source, the ``extra" peaks could be due to products of metastable decay processes taking place in the first free-flight region of the mass spectrometer. This type of process would correspond to the reaction:

$$Au_N(CO)_M^- \rightarrow Au_N(CO)_{M-y}^- + y \cdot (CO) \qquad (5).$$

For y=1, these ``satellite" peaks appear approximately 20 amu lower in mass than each $Au_N(CO)_M^-$ complex. This idea is relatively simple to test both theoretically and experimentally. Using the same reasoning described previously,[208] the difference between the residence times of the parent and daughter ions in the reflectron can be derived. In a simplest calculation, the stopping and turn-around time in the reflectron, given by

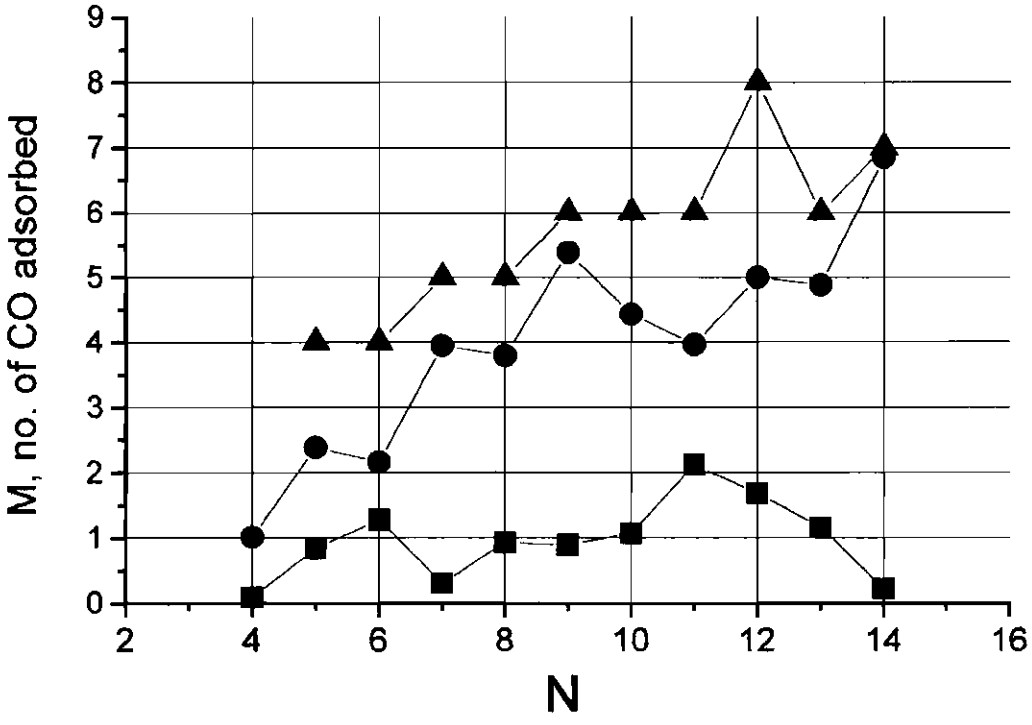

Figure 5-8: CO product distributions at saturation

The mean (circles) and standard deviation (squares) of the product distribution, M, calculated for under conditions such as those shown in **Figure 5-3**, in which many of the clusters have been completely converted to their saturation compositions. The triangles represent the maximum number of CO adsorbates, M, observed.

$$t = \left(\frac{2mK}{e^2E^2}\right)^{\frac{1}{2}} \qquad (6),$$

where K is the kinetic energy of the ion, m is the mass, and E is the electric field in the turn-around region, will be different for two masses, where m'< m and K'< K,

$$\Delta t = t - t' = \left(\frac{2mK}{e^2E^2}\right)^{\frac{1}{2}}\left(1-\left(\frac{m'}{m}\right)^{\frac{1}{2}}\right) \qquad (7).$$

Of course, in order to account for both the entrance into and the exit from the turn-around region, $2\Delta t$ must be found. In the settings of the reflectron used for these studies, E = 2072 V/ 8.9 cm and K could be approximated to be 2900 eV under the circumstances that the initial kinetic energy of the ions was nearly 5000 V and the first reflectron stage dissipated 2100 V. Using the mass of the $Au_6(CO)_l^-$ cluster, 1210 amu, and its metastable decay counterpart, Au_6^-, 1182 amu, the difference in the time of arrival at the detector for the two species wasfound to be ~ 523 ns. The experimental results showed a Δt of approximately 400 ns with a spread in the peaks of ~ 200 ns (FWHM). An additional test of whether or not the additional peaks were actually due to metastable

decay was to reduce the voltage in the turn-around region of the reflectron and monitor the change in the mass spectrum. If the extra peaks were in fact resulting from metastable decay processes in the first free-flight region of the mass spectrometer, a decrease in the reflectron voltage would result in the decrease of the parent mass peaks, leaving only the metastable peaks. As can be seen in **Figure 5-9**, this relative enhancement of the metastable peaks indeed occurred as the reflectron voltage was reduced. In this figure, the mass spectrum of the Au_7^- series of peaks is plotted with decreasing voltage in the turn-around region. The disappearance of the parent-mass peaks provides clear evidence that the extra peaks in the mass spectra of the $Au_N(CO)_M^-$ complexes are due to decay processes, as opposed to contamination or other reactions. While the reason behind the metastability in this system is not perfectly understood, as metastable decay may result from the internal energy of the ion as it leaves the source, or it may be caused by collisions with background gas in the flight path, it does show the relatively weak binding of CO on Au_N^- clusters.

5.4.3 Special Compositions and Electron Counting

Table 5-1 presents all those compositions that have been identified as having enhanced stability, either with respect to their accumulation as intermediate products or as the observed saturated compositions. Also listed is the valence electron count[94] of the gold clusters for each of these compositions, namely

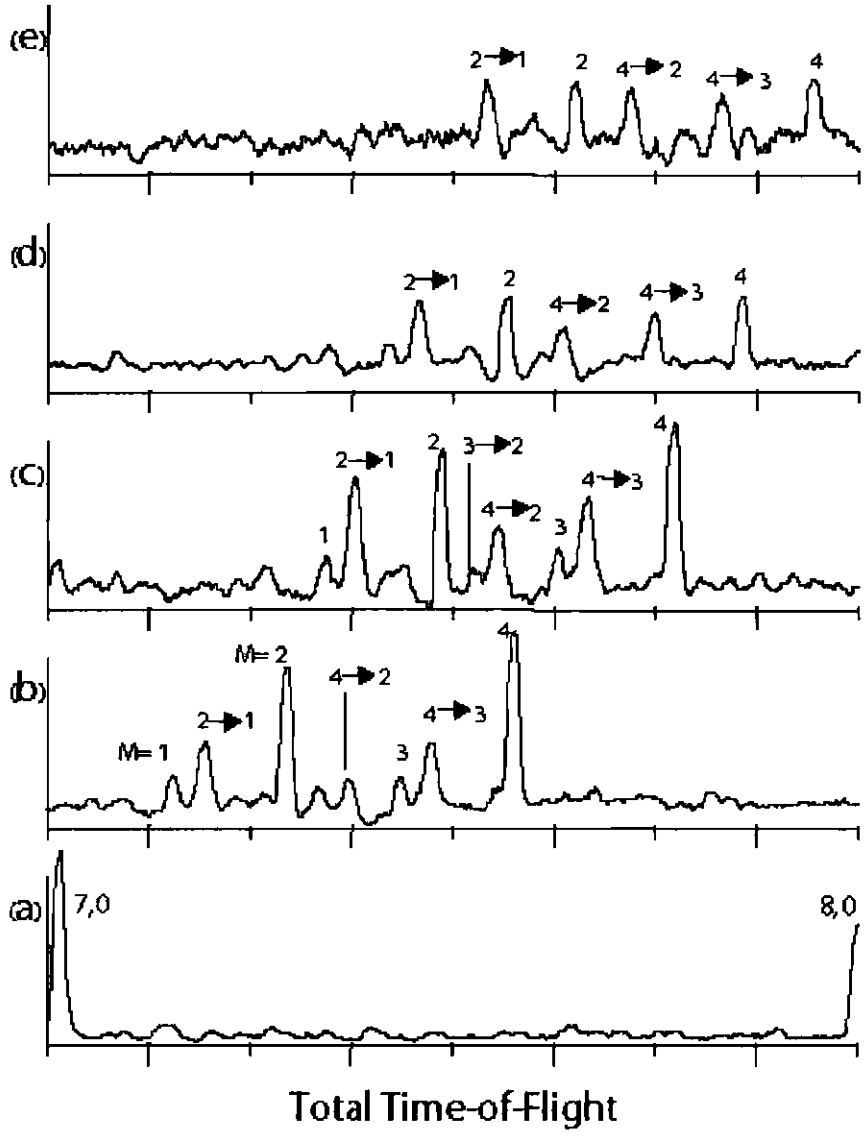

Figure 5-9: Metastability of $Au_7(CO)_M^-$ Complexes

(a) Mass spectrum with no CO added in the flow reactor. (b) CO added in the flow reactor, resulting in multiple adsorption. For (b) through (e), the voltage applied to the second stage of the reflectron is reduced. The voltages are: (b) 2072 V (c) 1945 V (d) 1895 V (e) 1845. The labels indicate both stable complexes as well as metastable decay products (with an arrow identifying the decay process).

$$N_e = (N + 1) + 2M \qquad (8)$$

where the negatively charged gold cluster contributes the parenthetic quantity, and it is assumed, following convention, that CO acts exclusively as a two-electron donor. It is seen that the special intermediate compositions identified can each be explained in terms of the known stability of the 8, 14, 18 and 20 electron shell fillings. However, to constitute a sufficient explanation of the entire pattern, one would also need to find additional special compositions, e.g. (9,2), (13,2), (13,3).

The propensity for even-M values in the saturation compositions (**Table 5-2**) raises the further question as to whether the CO groups, as adsorbed on gold clusters, might not actually be paired, e.g. as glyoxylate adsorbates, —C(=O)—C(=O)—, in which case only a single electron is donated per CO adsorbed. The saturation compositions of $Au_{11}(CO)_6^-$ and $Au_{13}(CO)_6^-$ could then coincide with 18 and 20 electron shell-closings, respectively.

Regardless of the physical basis of the saturation coverages — whether they lie in the number of structural "active sites" or in electron-counting — the most obvious conclusion to be drawn is that they are much lower than one would expect, given the size of the clusters. While they may seem incredibly low, particularly as compared with the familiar geometrical saturation achieved by platinum-group metals, consider e.g. $Ni_{38}(CO)_{36}$, or $Pt_{38}(CO)_{44}$.[134,209] However, it should be remembered that no such cluster compounds are known for gold clusters (or any other coinage metal clusters). Also, it is well

established from surface-science investigations that Au (and Cu) surfaces saturate at low CO coverage (~ 17% of the geometrical coverage), even at low temperature.[205,206] Such low fractional coverages, although never explained, are thus intrinsic to metallic gold surfaces, and are more consistent with the saturation values presented here. (A pertinent comparison has been drawn by the Exxon group of Cox *et al.*[107,108] for the case of H_2 and CH_4 saturation chemisorption on gold versus other transition-metal clusters.[19])

5.5 Conclusions

Recent experiments have been performed by Bondybey and coworkers on the CO adsorption properties of Au_N^- clusters in an ion-cyclotron-resonance mass spectrometer.[118] In this study, they measured the absolute bimolecular rate constants for the CO addition at pressures much lower than even those of Lee and Ervin.[112,113] The results showed that, while the overall pattern of adsorption was in relative agreement with the earlier studies, the absolute magnitudes of the rate constants were several orders of magnitude lower. Also, this group noted that the electron-shell model often invoked to explain physical[77] and chemical[107,108,133,192,193] properties of gold clusters could explain some of their results, but other results seemed to contradict this model. This description is not terribly different from the results presented above, in that some of the initial CO-adsorption complexes could be explained by the shell model (for instance,

{N,M} complexes corresponding to {5,1}, {11,1}, {15,1}, and {15,2}), but other highly-abundant complexes present at saturation could not be as easily explained (such as {12,3}, {11,6}, and {13,6}).

The pressure-dependent adsorption activity of CO presented in this chapter, in combination with the activity of the O_2:Au cluster system presented earlier,[132,133] could provide a better understanding of the reaction mechanisms of supported-gold catalysts,[52,75] in addition to the model catalysts studied more recently.[39-42,65] The combination of the O_2 rules presented in Chapter 3 and elsewhere[133] (none or one adsorbed at a time, for each cluster) and the limitations placed here on CO adsorption has interesting consequences that may survive 'translation' to the case of the supported clusters. More generally, the electron-counting interpretations above are consistent with the work of Goodman and coworkers[65], which showed that the global electronic structure characteristics of the supported gold clusters may be as important as local structural characteristics in determining the ability of the clusters to catalyze reactions. In the case, though, that the geometry and size of the clusters could be important, the geometrical unsaturation shown here could be significant in allowing for co-adsorption and activation of other molecules, such as O_2, NO, H_2, or H_2O.

CHAPTER VI

HUMIDITY AND TEMPERATURE DEPENDENCE OF CO ADSORPTION ON GOLD CLUSTER ANIONS

6.1 Introduction

Gold clusters highly dispersed on transition metal oxides have been found to be extremely active for a variety of reactions, including low-temperature combustion, hydrogenation and oxidation of hydrocarbons, and NOx reduction, among others.[50-52,76,183,210] A surprising finding was that not only are the gold catalysts tolerant of moisture, but their activity is even enhanced in many cases by moisture.[51,183] For the oxidation of carbon monoxide, Boccuzzi and coworkers proposed that the presence of water aids in the dissociation of molecular oxygen at the gold-support interface, a necessary step in order for the reaction to occur.[56] However, it is also possible that the role of water simply is to maintain an appropriate termination of the oxide support. As

the complete understanding of the actual working catalysts (as well as the related model systems) is still very much a topic of hot debate,[33,34,39-42,44,48,50-56,58-63,65-70,72,73,75,76,170,183,210] it is important to attempt to gain an understanding of the activity of selected gas-phase gold clusters towards reactants of interest (O_2, CO, etc.), in order to separate the contributions to the catalytic activity of the gold clusters and the support material. The role of moisture is certainly important in the gas phase, as was shown recently.[193] Surprisingly, while several studies of water adsorption have been performed on clusters of other transition metals,[137,139,184-186] almost none have been carried out on gas-phase gold species. To date, the only studies of gold with water in the gas phase have concerned the adsorption of water molecules on the gold monomer cation.[187-189] This chapter, which explores the adsorption of CO on gold-hydrate anions helps to provide a further understanding of the effects of water on the adsorption activity of gold cluster anions.

In contrast to the many studies concerned with the binding of O_2 on free gold cluster anions, Au_N^- (described in Chapters 3 and 4), the adsorption properties of CO have been studied in much less detail. Lee and Ervin performed an early study on the reactions of gold cluster anions with CO using flow tube experiments.[112] They found extremely slow reaction rates for the smaller cluster anions ($N < 5$), but, at $N = 5$, a large increase in rate was seen which continued to $N = 7$, the largest cluster able to be studied within their detection limits. This general trend was also seen by Bondybey and coworkers to extend to higher mass before beginning to decrease, though O_2 contamination was found to

cause a break in the trend at N = 6.[118] Studies performed using high-pressure, fast-flow reactor techniques also confirmed these findings, with the relative size-dependent reactivities showing a dramatic increase with N = 5.[130] A suggested mechanism that accounts for some of the spikes in relative rates and reactivities is that CO acts as a two-electron donor, as is standard in organometallic chemistry, and especially stable cluster-adsorbate electron counts lead to larger reaction rates.

Much more recently, Hagen *et al.* studied the temperature-dependent coadsorption of CO and O_2 on small Au_N^- clusters (N < 4), which necessarily also allowed them to observe the temperature-dependent CO adsorption behavior.[117] Their results indicated that it was indeed possible to adsorb up to 2 CO molecules on Au_2^- and Au_3^- at cryogenic temperatures. However, above 250 K, no adsorption products were observed, in agreement with the high-pressure flow reactor studies.[130] Those same studies by Hagen *et al.* showed that the coadsorption properties of CO and O_2 were also very interesting. For instance, O_2 was found to bind on $Au_3(CO)^-$ at low temperatures (T < 250 K), in contrast to bare Au_3^-, on which O_2 does not bind. In other words, the preadsorption of CO aided in the ability of O_2 to bind to the cluster, i.e. cooperative coadsorption. Concurrent studies by Wallace and Whetten using high-pressure, fast-flow reactor techniques also indicated that, in many cases, the coadsorption properties of CO and O_2 were cooperative.[192]

While these studies have provided a great deal of insight into the possible mechanisms of CO oxidation on gold clusters in the gas phase, there remains the question of the exact role of moisture in this process. Recent experimental and theoretical results

have shown that the presence of a hydroxide group on Au_N^- clusters causes previously inactive clusters to become highly active for O_2 adsorption.[193] It would be interesting to discover exactly what effect that this reversed activity might have on the ability of the gas-phase clusters to catalyze CO oxidation. However, it is important to also find what kind of effect that the presence of moisture may have on the ability of the clusters to adsorb CO. The work presented in this chapter discusses how moisture affects the CO adsorption activity of Au_N^- clusters and also shows the temperature dependence of the CO adsorption process, allowing preliminary CO binding energies to be obtained.

6.2 Experimental Methods (Abbreviated)

The experimental techniques used to study the moisture and temperature dependent adsorption properties of CO on gold clusters were described previously[133] and in Chapter 4, so only a brief description will be given here. Charged gold clusters were formed and equilibrated by laser vaporization of a rotating and translating gold rod in a high-pressure helium/ D_2O flowstream, produced using a pulsed valve with a stagnation pressure of approximately 3.5 bar. Prior to entering the stagnation region of the pulsed valve, the helium was bubbled through D_2O, thereby saturating the helium with the vapor pressure of water at room temperature (~20 mbar). The clusters were then exposed to a gas pulse from a secondary pulsed valve containing a dilute reactant gas (approximately 20% CO:He with a stagnation pressure of ~ 2 bar), expanded into vacuum, and were

detected by time-of-flight mass spectrometry, using perpendicular pulsed extraction fields. With the addition of a cooling sleeve (and heater) to the reactor, the effects of temperature on the reaction could be studied under a reactor temperature range of ~ 220 K - 330 K.

6.3 Results

In an attempt to study the moisture dependence of CO adsorption, hydrated gold cluster anions were produced using the methods described in Chapter 4 and elsewhere.[193] The mass spectra obtained at room temperature using this method are shown in the bottom frames (labeled "Reference") in **Figures 6-1** and **6-2**. As can easily be seen in **Figure 6-1**, the hydrate of the gold dimer anion is readily formed under these conditions, with quite a bit less of the hydrated trimer anion being formed. In **Figure 6-2**, the relative lack of hydrates on Au_4^- and Au_5^- is obvious, begging the question as to why the dimer anion seems to hydrate quite easily, while the process becomes less favorable with increasing size. A possible explanation is that the highly localized charge present in the dimer anion induces a slight polarization of the incoming water molecule, leading to stronger (though still very weak) binding. With the charge on the larger clusters being more diffuse, the induced polarization may not be sufficient to lead to strong enough binding.

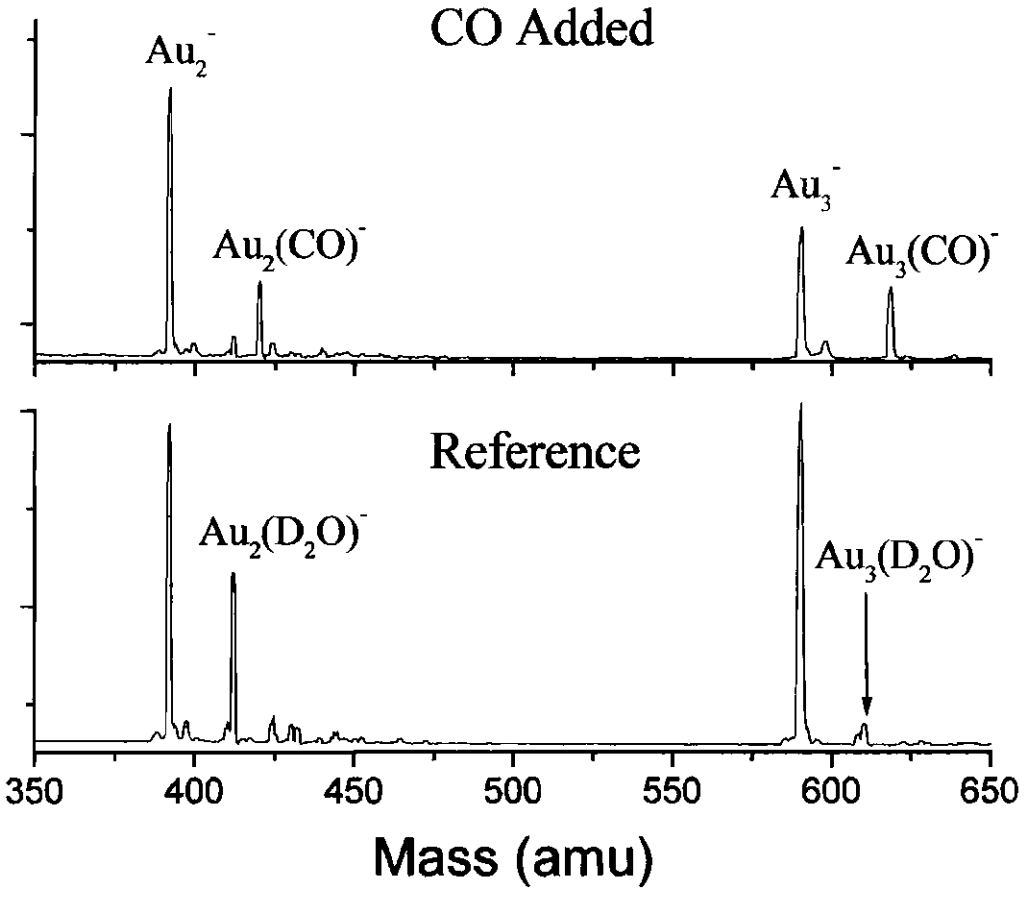

Figure 6-1: Moisture-dependent CO adsorption on Au_N^- and $Au_N(D_2O)^-$

(Bottom Frame) Bare and hydrated gold cluster anions (N = 2,3) produced at room temperature using the methods discussed in Chapter 4. No CO is added in the flow reactor. (Top Frame) Mass spectra resulting from the addition of 20% CO/He in the flow reactor. The use of H_2O as opposed to D_2O had no effect on the results.

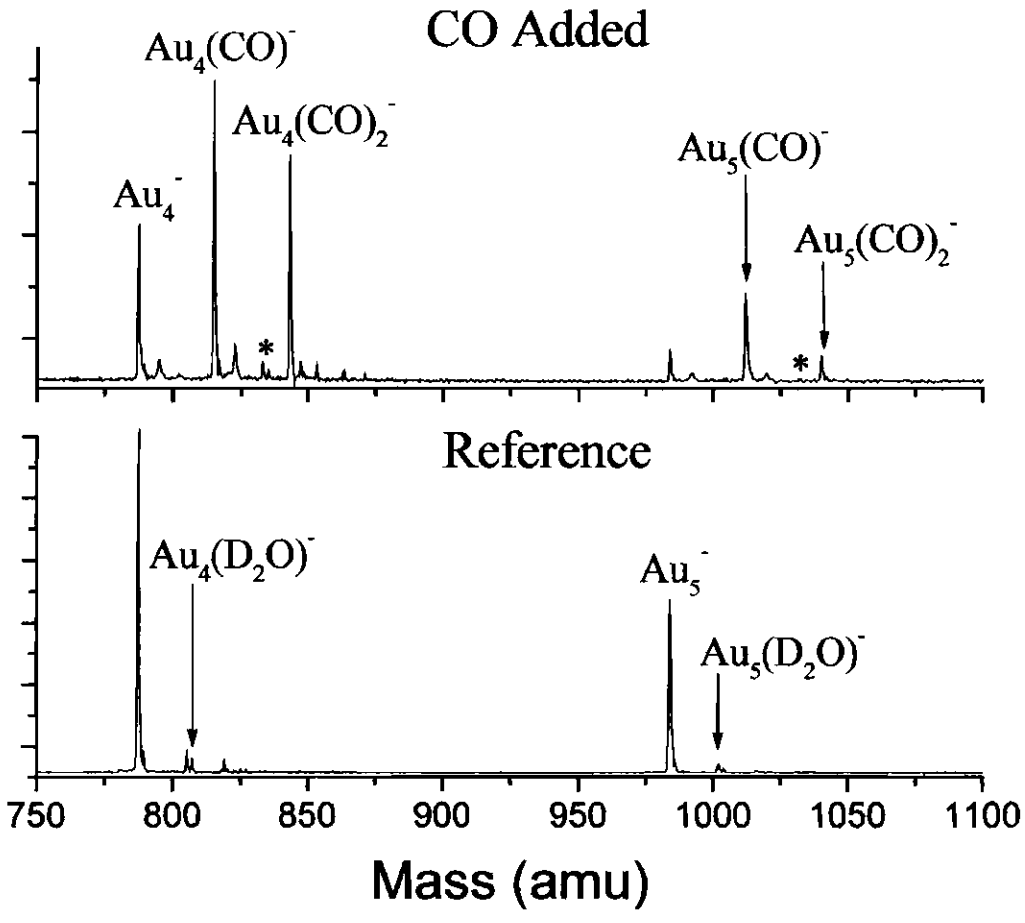

Figure 6-2: Moisture-dependent CO adsorption on Au_N^- and $Au_N(D_2O)^-$

(Bottom Frame) Bare and hydrated gold cluster anions (N = 4,5) produced at room temperature using the methods discussed in Chapter 4. No CO is added in the flow reactor. (Top Frame) Mass spectra resulting from the addition of 20% CO/He in the flow reactor. The use of H_2O as opposed to D_2O had no effect on the results. The peaks marked with asterisks correspond to hydrated CO adsorption products, $Au_N(D_2O)(CO)^-$.

When a secondary valve is used to introduce dilute CO:He in the reactor and the main and secondary pulses are overlapped, spectra of the type shown in the top frames (marked "CO Added") of **Figures 6-1** and **6-2** are obtained. The addition of CO in the reactor results in the appearance of complexes corresponding to $Au_N(CO)^-$ in this size range (N = 2 – 5) as well as $Au_N(CO)_2^-$ (N = 4,5). The implications of these results will be discussed below.

The temperature-dependence of the CO adsorption reactions on the small gold cluster anions were studied by varying the temperature of the cluster source and flow reactor in the range of ~ 230 K to 315 K, leading to the mass spectra shown in **Figures 6-3** and **6-4** (low temperature) and **Figures 6-5** and **6-6** (high temperature). At low temperatures, introduction of CO in the fast-flow reactor (bottom frames) results in the production of Au_N^- clusters with bound CO, corresponding to the equation

$$Au_N^- + M \bullet CO \rightarrow Au_N(CO)_M^- \qquad (1).$$

Additionally, there are also species in which CO is bound to the hydrated clusters, corresponding to

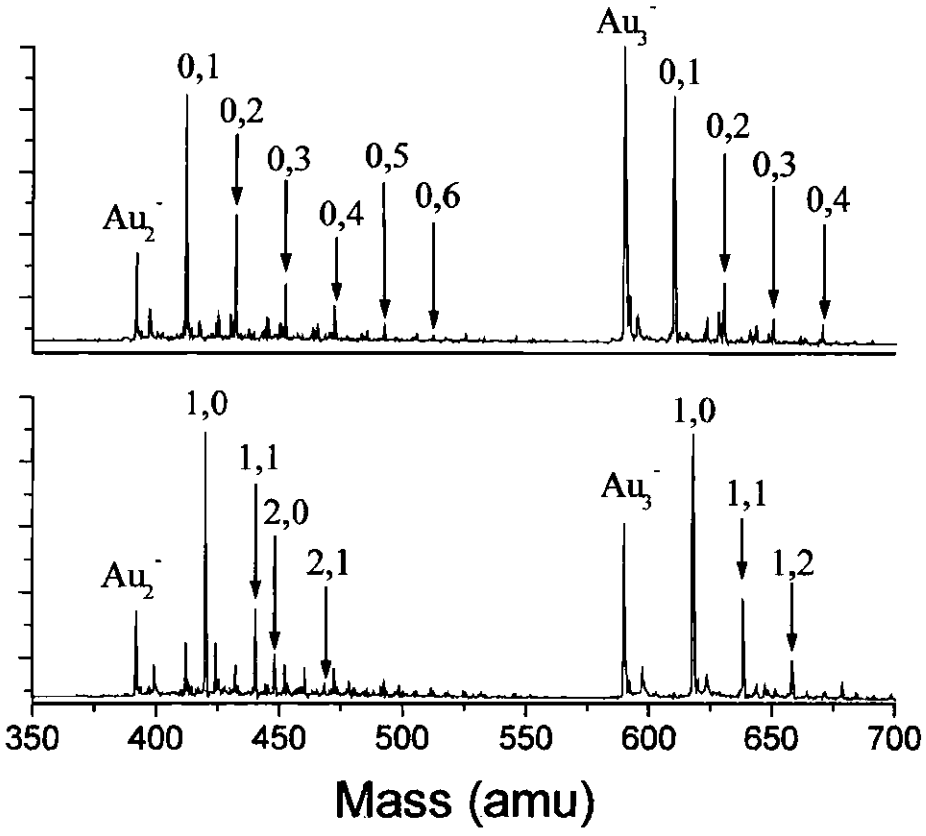

Figure 6-3: Low-temperature addition of CO to Au_N^- and $Au_N(D_2O)^-$

(Top Frame) Bare and hydrated gold cluster anions (N = 2,3) produced using the methods discussed in Chapter 4 (T = 231 K). No CO is added in the flow reactor. The numbering scheme to the right of each parent cluster refers to the number of CO and D_2O adsorbates, respectively. (Bottom Frame) Mass spectra resulting from the addition of 20% CO/He in the flow reactor at a reactor temperature of 237 K. The use of H_2O as opposed to D_2O had no effect on the results. Peaks not marked in the mass spectra are simply higher hydrates of the form $Au_N(OD)_M(D_2O)_L^-$ or peaks arising from slight O_2 contamination (for the Au_2^- species).

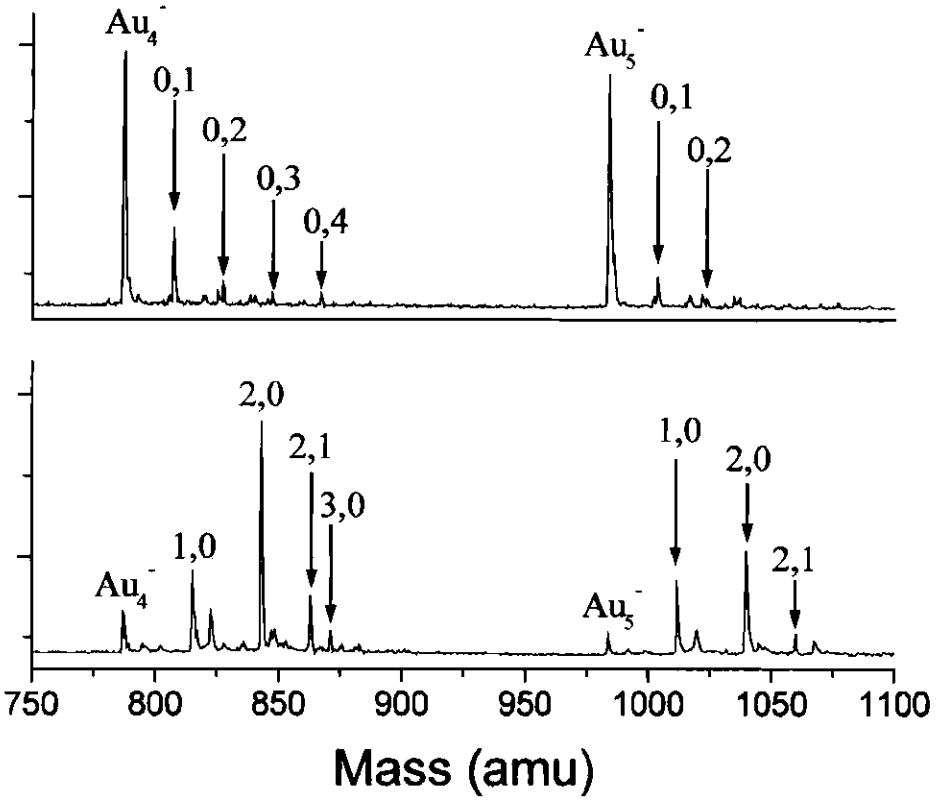

Figure 6-4: Low-temperature addition of CO to Au_N^- and $Au_N(D_2O)^-$

(Top Frame) Bare and hydrated gold cluster anions (N = 4,5) produced using the methods discussed in Chapter 4 (T = 232 K). No CO is added in the flow reactor. The numbering scheme to the right of each parent cluster refers to the number of CO and D_2O adsorbates, respectively. (Bottom Frame) Mass spectra resulting from the addition of 20% CO/He in the flow reactor at a reactor temperature of 238 K. The use of H_2O as opposed to D_2O had no effect on the results. Peaks not marked in the mass spectra are simply higher hydrates of the form $Au_N(OD)_M(D_2O)_L^-$ or peaks arising from slight O_2 contamination (for the Au_4^- species).

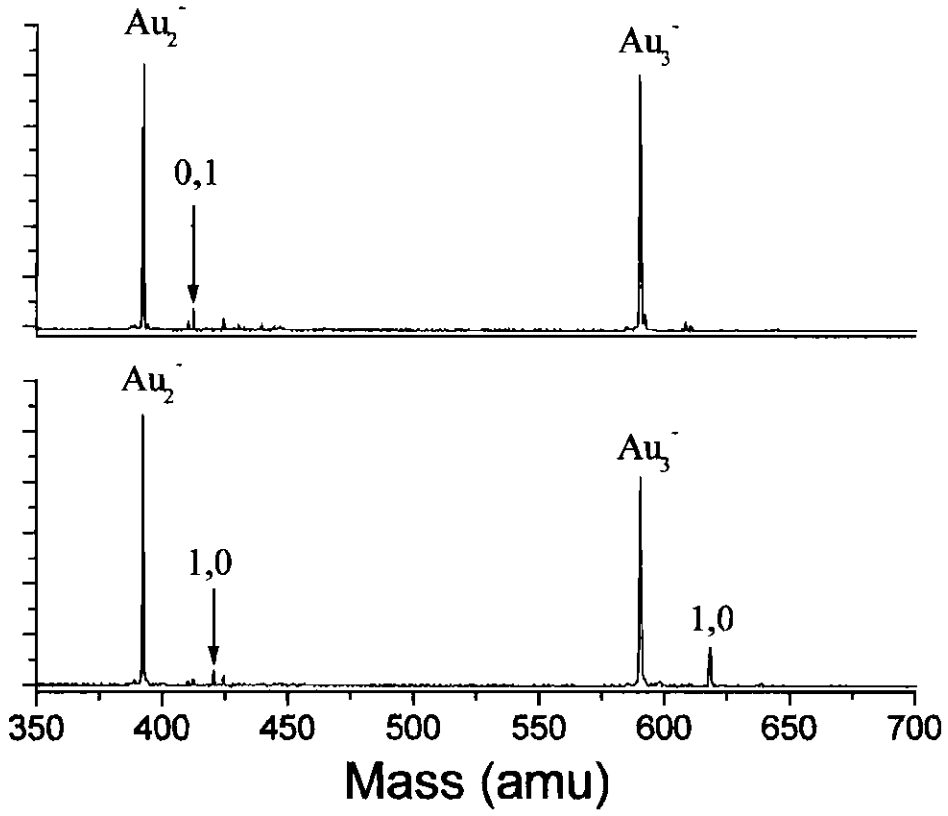

Figure 6-5: High-temperature addition of CO to Au_N^-

(Top Frame) Bare gold cluster anions (N = 2,3) produced using the methods discussed in Chapter 4 (T = 313 K). No CO is added in the flow reactor. The numbering scheme to the right of each parent cluster refers to the number of CO and D_2O adsorbates, respectively. (Bottom Frame) Mass spectra resulting from the addition of 20% CO/He in the flow reactor at a reactor temperature of 315 K. The use of H_2O as opposed to D_2O had no effect on the results. Peaks not marked in the mass spectra are simply hydrates of the form $Au_N(OD)_M(D_2O)_L^-$ or peaks arising from slight O_2 contamination (for the Au_2^- species).

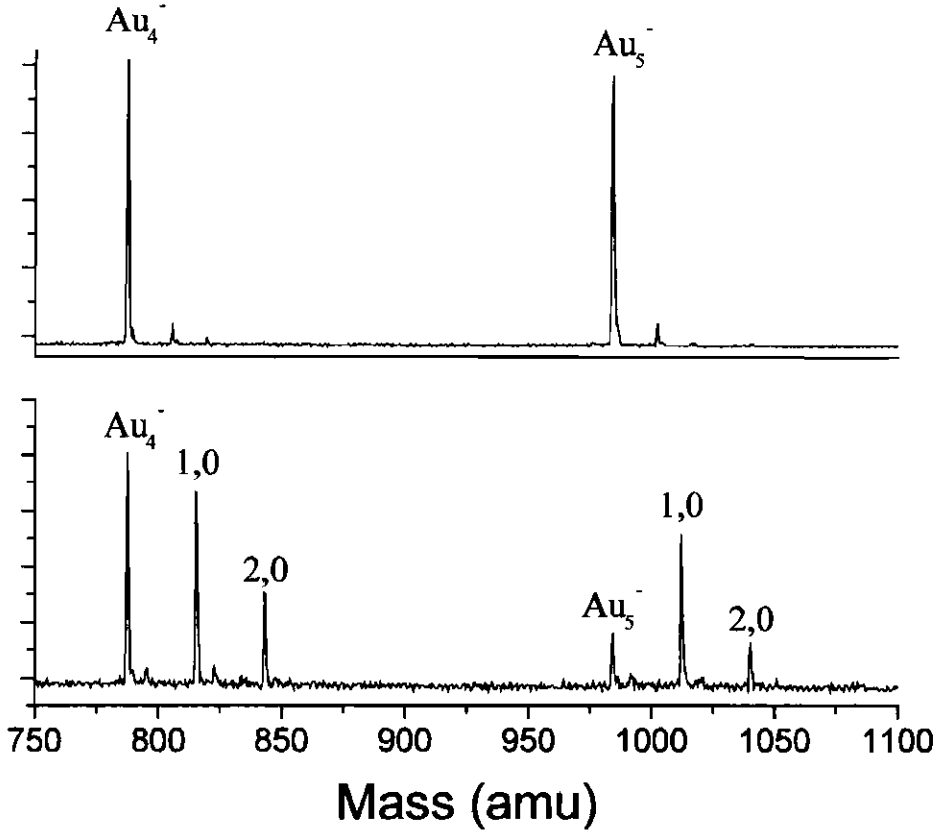

Figure 6-6: High-temperature addition of CO to Au_N^-

(Top Frame) Bare gold cluster anions (N = 4,5) produced using the methods discussed in Chapter 4 (T = 312 K). No CO is added in the flow reactor. The numbering scheme to the right of each parent cluster refers to the number of CO and D_2O adsorbates, respectively. (Bottom Frame) Mass spectra resulting from the addition of 20% CO/He in the flow reactor at a reactor temperature of 313 K. The use of H_2O as opposed to D_2O had no effect on the results. Peaks not marked in the mass spectra are simply hydrates of the form $Au_N(OD)_M(D_2O)_L^-$ or peaks arising from slight O_2 contamination (for the Au_4^- species).

$$Au_N(D_2O)_L^- + M{\bullet}CO \rightarrow Au_N(D_2O)_L(CO)_M^- \qquad (2).$$

While the main focus of this study was the energetics of CO adsorption, the D_2O adsorption distributions on the clusters are interesting in their own right, with the small clusters adsorbing 4 or more molecules at low temperatures, while, in this admittedly limited range, the larger cluster (Au_5^-) seems to adsorb far fewer.

With increasing temperature, major changes are seen in the adsorbate distributions. First, the majority of the D_2O adsorbates are lost at the higher temperatures, leading to a much cleaner mass spectrum. More importantly, higher temperatures dramatically decrease the probability of CO adsorption on the clusters. For instance, there is almost no evidence of CO adsorption on Au_2^- under the high temperature conditions, and the CO adsorption complex of Au_3^- is also greatly diminished. For N = 4 and N = 5, large amounts of CO adsorption complexes are still present, but the relative amounts of CO are decreased. For instance, at lower temperatures, the dominant CO adsorption peaks for these clusters correspond to $Au_4(CO)_2^-$ and $Au_5(CO)_2^-$. However, at the highest temperatures used, the dominant cluster complexes become $Au_4(CO)^-$ and $Au_5(CO)^-$, and the abundances of the bare cluster anions are also increasing.

6.4 Discussion

As mentioned earlier,[117,130] at room temperature CO adsorption was not seen on the gold dimer and trimer anions. However, it is readily apparent from **Figure 6-1**, that CO is adsorbed to both of these clusters when water is present. In general, this adsorption of CO on Au_2^- and Au_3^- cannot be simple adsorption, but is more likely a displacement of the water molecule already bound, as the appearance of a peak corresponding to $Au_2(CO)^-$ or $Au_3(CO)^-$ primarily results in the depletion of the $Au_2(D_2O)^-$ and $Au_3(D_2O)^-$ peaks, though some of the $Au_3(CO)^-$ peak must be attributed to simple addition of CO to the bare cluster anion. This activity ascribed to displacement could be explained as such: It is possible that not all reactions occurring in the fast-flow reactor are in the high pressure limit, especially for smaller species not possessing sufficient modes to dissipate excess reaction energy. In this case, a third body would be required to remove the excess energy. For $Au_2(D_2O)^-$ and $Au_3(D_2O)^-$, the bound water molecule could serve as the third body, desorbing from the cluster upon CO adsorption. In **Figure 6-2**, this behavior is not nearly as apparent (or present at all) for Au_4^- and Au_5^-. These clusters obviously are able to dissipate the energy gained from adsorption without needing any further third body stabilization than is already present in the helium jet. The addition of CO to the four and five atom cluster anions (both bare and hydrated) simply results in complexes corresponding to $Au_{4,5}(CO)_M^-$ or $Au_{4,5}(D_2O)(CO)_M^-$. Regardless of how the cluster-adsorbate species were formed, once present, studies could be performed using temperature variations to determine the binding energies of CO on the clusters.

In **Figures 6-7** through **6-11**, the normalized intensities of the observed bare and CO-ligated clusters are plotted (on a logarithmic scale to better show the extent of change) as a function of temperature. The major feature of these plots is the fact that, in general, changing the temperature does not dramatically affect the measured abundances. This is surprising, even for a molecule expected to be as weakly bound as CO. While the final two temperature points for the Au_2^- (**Figure 6-7**) and Au_3^- (**Figure 6-8**) systems do show a fairly substantial break in behavior from the earlier points, it is difficult to make an absolute determination as to whether this is a real effect (a change in adsorption just above room temperature) due to the extremely low signal intensity for the product peaks (see, for instance, **Figure 6-5**). Ideally, raising the temperature of the reactor would provide more information, but, in this case, no remaining product intensity makes further temperature increases ineffective.

As described in Chapter 4, by plotting the natural logarithm of the (stepwise) equilibrium constant versus the change in inverse temperature, the binding energy of an adsorbate on a cluster can be determined from the equation,

$$\Delta \ln K = \frac{-\Delta_r H}{R} \Delta \frac{1}{T} + \frac{\Delta S}{R} \qquad (3),$$

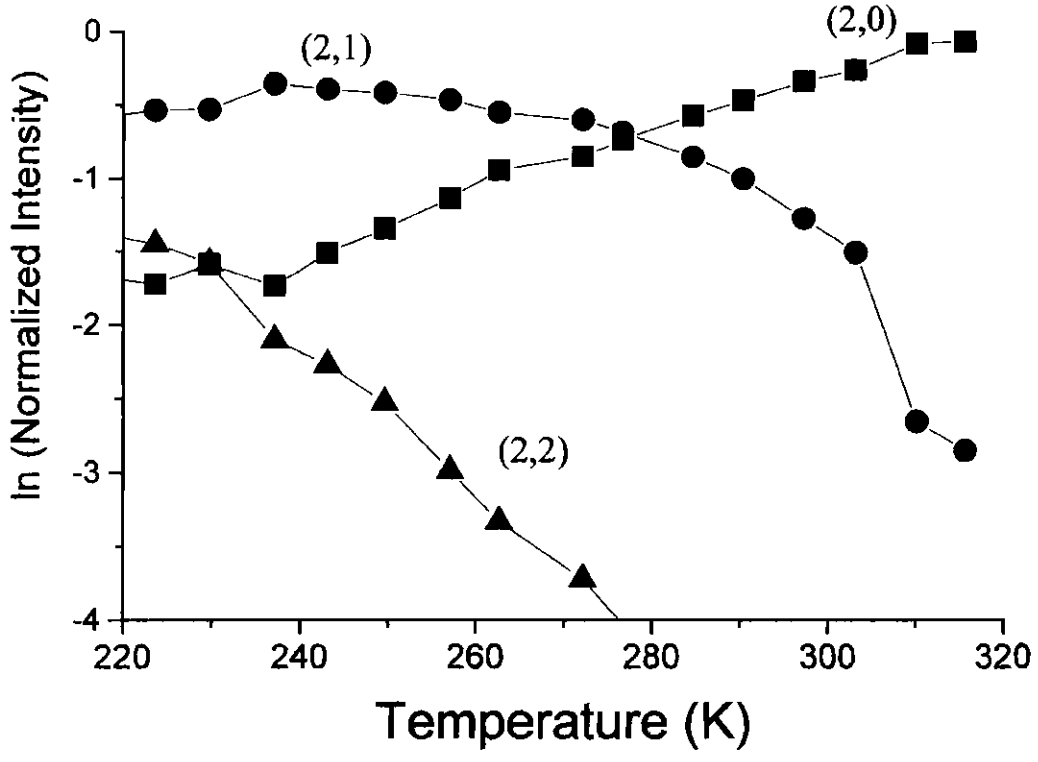

Figure 6-7: Temperature-dependent adsorption of CO on Au_2^-

Plot showing the change in parent and product intensity for the Au_2^- + CO system [designated by $Au_N(CO)_M^-$ = (N,M)] as a function of temperature. The final two points (at ~ 310 K and ~ 315 K) may show real behavior changes in the bonding of CO on the cluster, but it is more likely that they are simply anomalies due to the low signal levels for the product peaks at these temperatures.

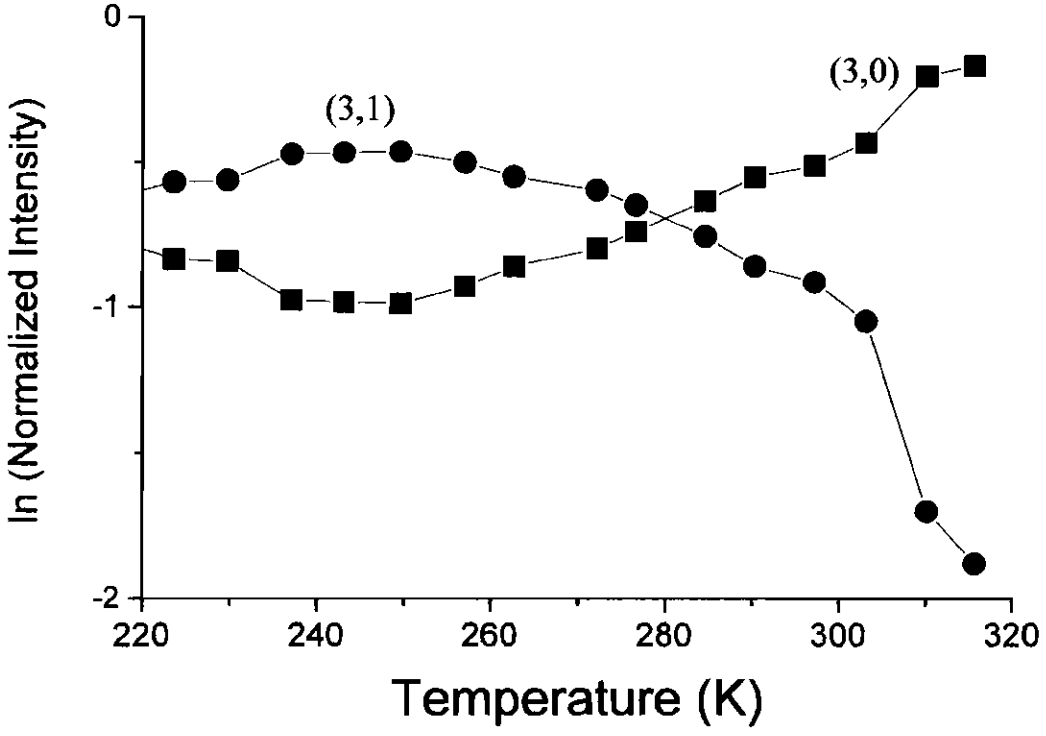

Figure 6-8: Temperature-dependent adsorption of CO on Au_3^-

Plot showing the change in parent and product intensity for the Au_3^- + CO system [designated by $Au_N(CO)_M^-$ = (N,M)] as a function of temperature. The final two points (at ~ 310 K and ~ 315 K) may show real behavior changes in the bonding of CO on the cluster, but it is more likely that they are simply anomalies due to the low signal levels for the product peaks at these temperatures.

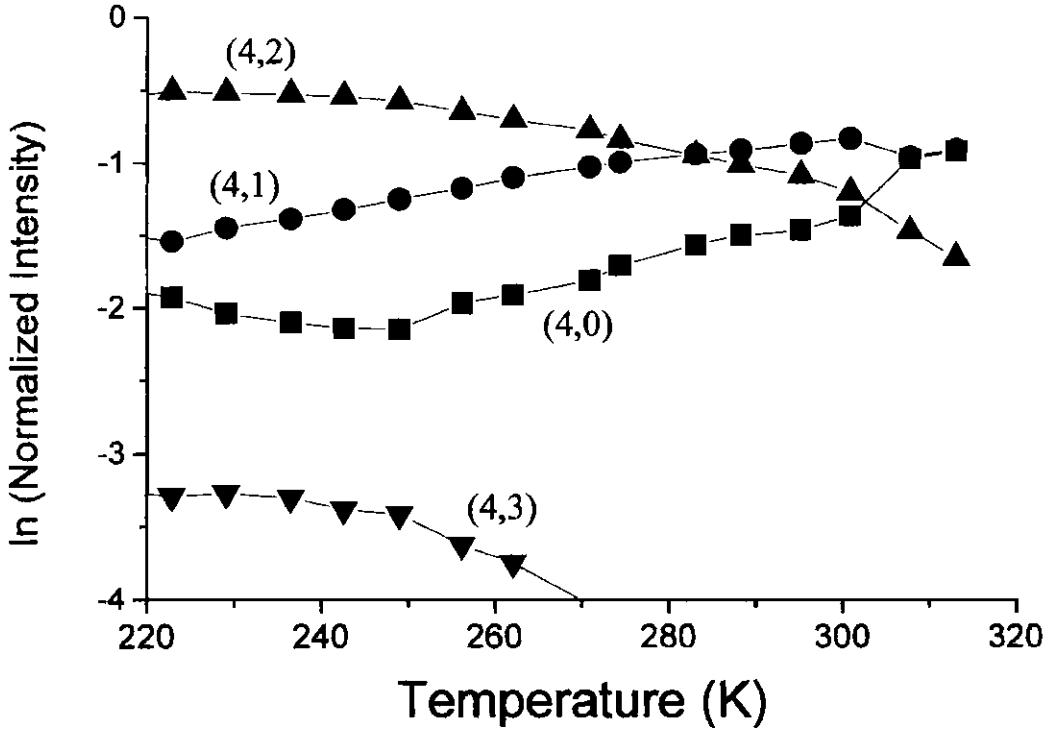

Figure 6-9: Temperature-dependent adsorption of CO on Au_4^-

Plot showing the change in parent and product intensity for the Au_4^- + CO system [designated by $Au_N(CO)_M^-$ = (N,M)] as a function of temperature.

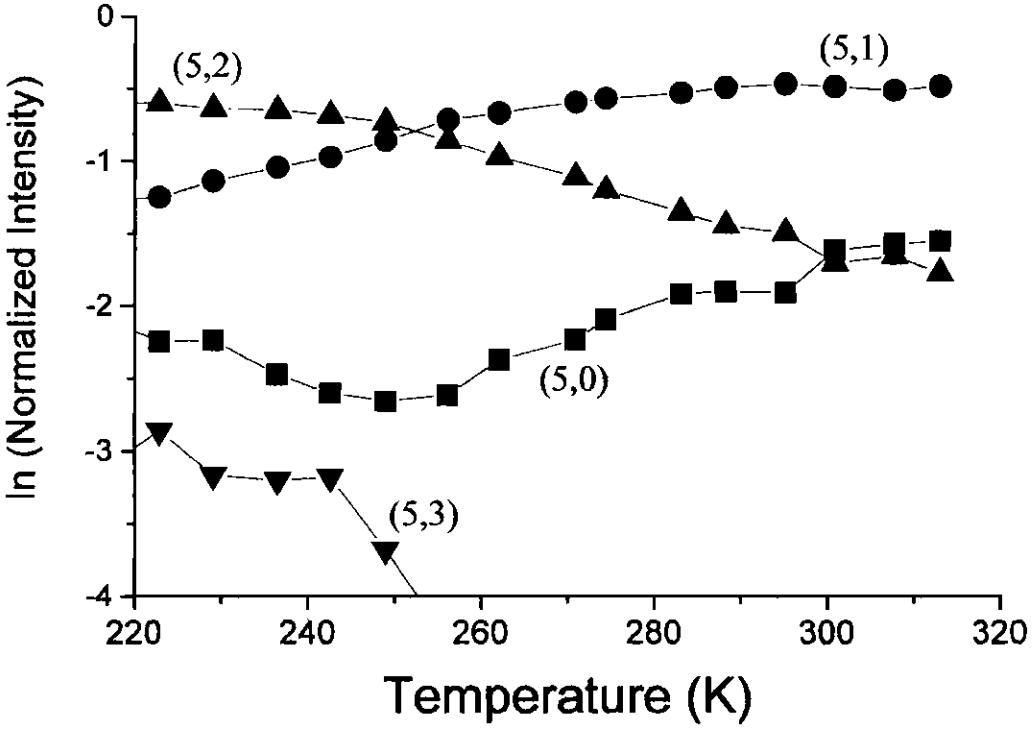

Figure 6-10: Temperature-dependent adsorption of CO on Au_5^-

Plot showing the change in parent and product intensity for the Au_5^- + CO system [designated by $Au_N(CO)_M^-$ = (N,M)] as a function of temperature.

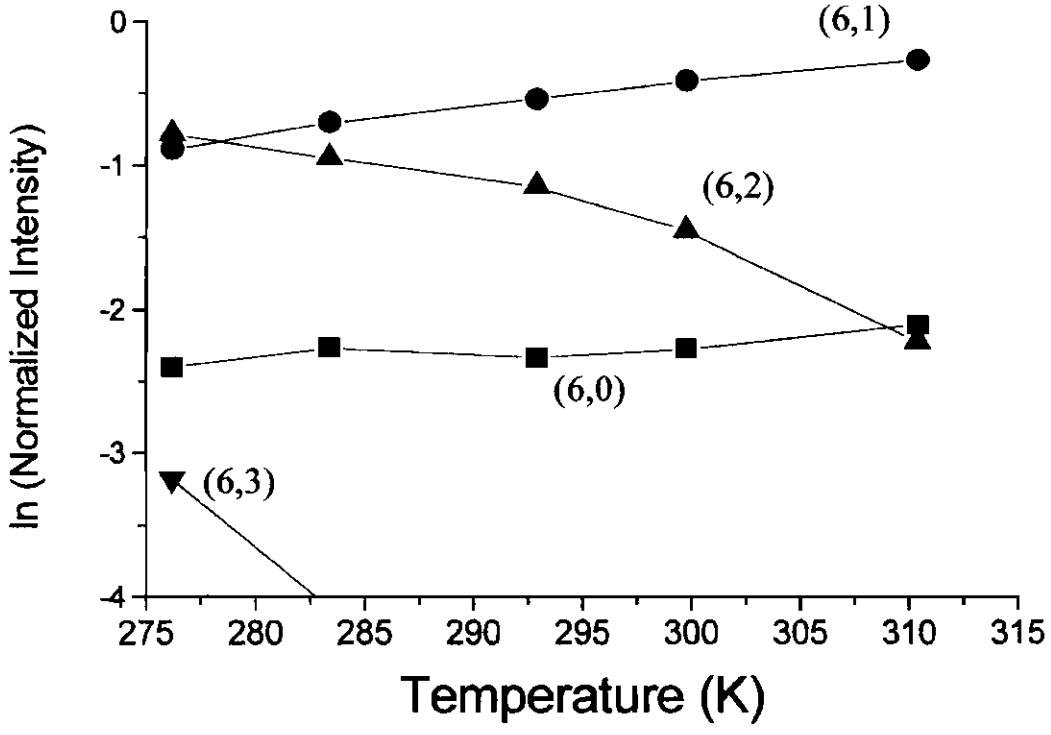

Figure 6-11: Temperature-dependent adsorption of CO on Au_6^-

Plot showing the change in parent and product intensity for the Au_6^- + CO system [designated by $Au_N(CO)_M^-$ = (N,M)] as a function of temperature.

where $\Delta_r H$ is the binding energy of CO on the cluster, ΔS is the entropy of adsorption, and R is the gas constant. Additionally, these plots can provide information as to the presence of adsorption barriers. **Figure 6-12** shows the plots representing the first addition of CO to the smaller gold cluster anions (N = 2 - 5), while **Figure 6-13** illustrates the effect of changing temperature on the second equilibrium constant for Au_4^- and Au_5^-. From **Figure 6-12**, it is apparent that, at low temperatures, equilibrium conditions do not control the reaction processes, as the value of the equilibrium constant should decrease with increasing temperature for processes under equilibrium control. This suggests the presence of an activation barrier to CO adsorption at these lower temperatures. At higher temperatures, however, the slope of the equilibrium constant becomes negative, i.e. an increase in temperature leads to a decrease in adsorption products. From this higher temperature data, linear fits can be made in order to obtain possible CO binding energies. These binding energies are collected in **Table 6-1**. The values presented in the table, of course, seem incredibly low when compared to the binding energy of CO on the bulk gold surface, which is already very weak under low-coverage conditions (~ 0.5 eV).[205,206] Also, theoretical calculations on Au_2^- have shown a CO binding energies of 0.96 eV[190] and 0.78 eV,[103] while photon-induced thermal desorption of the $Au_2(CO)^-$ complex gave a binding energy of ~ 0.9 eV.[20] Even considering the tendency of density-functional theory to sometimes overestimate binding energies when carrying out calculations involving gold cluster anions[131,179,193] and the inability of dissociation techniques to account for possible reverse activation barriers (making binding energies gained from these techniques upper limits),[127] the binding

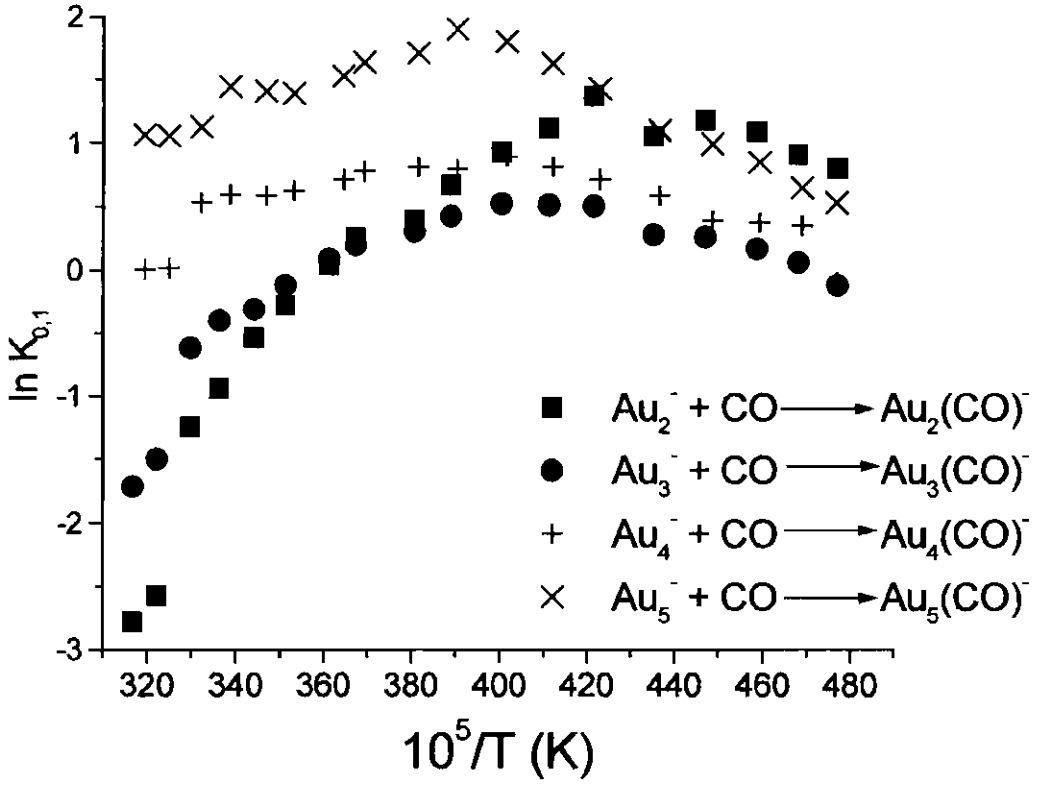

Figure 6-12: Temperature-dependence of the apparent equilibrium constant of the Au_N^- + CO reaction

Plots of the temperature-dependence of the apparent equilibrium constants of the Au_N^- + CO system (N = 2 - 5) obtained from equation (3) for a single CO partial pressure. Each of the plots indicate that, at very low temperatures, equilibrium conditions do not control the reaction processes, as the value of the apparent equilibrium constant is actually increasing. At higher temperatures, when equilibrium behavior is suggested for all of the species presented here, a linear fit to the data can be made in order to determine CO binding energies, as described in the text.

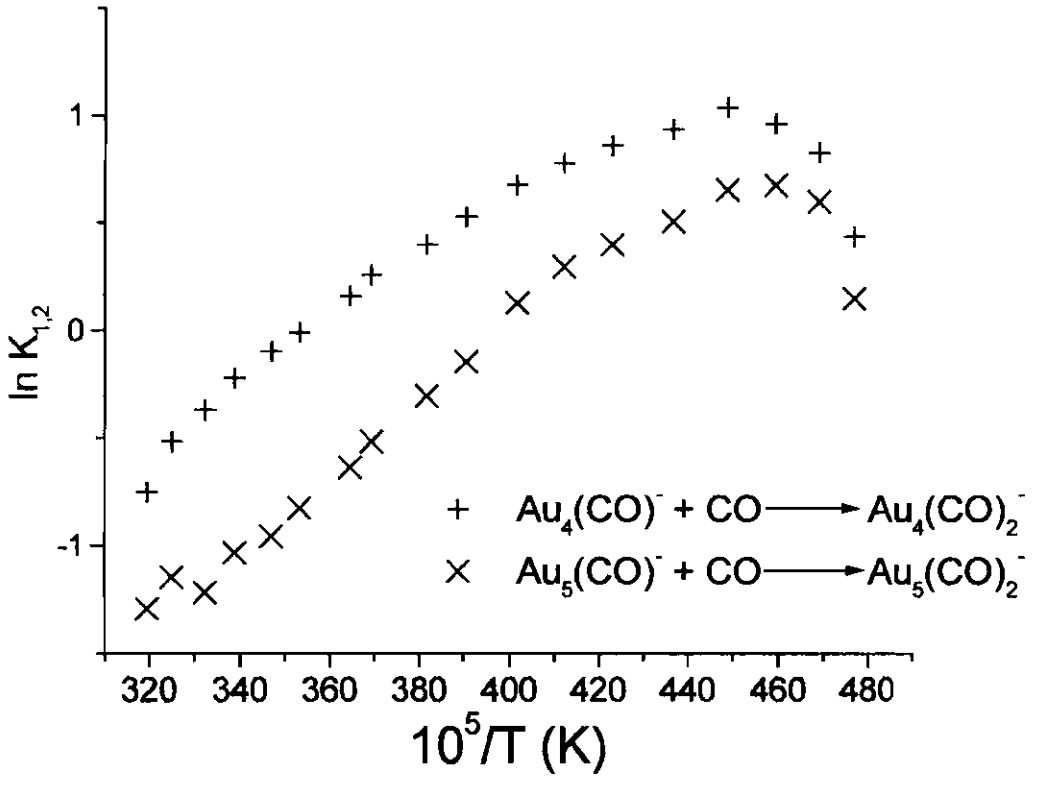

Figure 6-13: Temperature-dependence of the apparent equilibrium constant of the $Au_N(CO)^-$ + CO reaction

Plots of the temperature-dependence of the apparent equilibrium constants of the $Au_N(CO)^-$ + CO system (N = 4,5) obtained from equation (3) for a single CO partial pressure. Both plots indicate that, except at very low temperatures, equilibrium conditions seem to dominate the second addition of CO to these clusters.

Table 6-1: Binding energies of CO on selected Au_N^- clusters

Parent Cluster	Binding Energy of Primary[(a)] or Secondary[(b)] CO (eV)
[(a)]Au_2^-	0.26 ± 0.04
[(a)]Au_3^-	0.17 ± 0.04
[(a)]Au_4^-	0.06 ± 0.02
[(a)]Au_5^-	0.09 ± 0.01
[(b)]$Au_4(CO)^-$	0.10 ± 0.02
[(b)]$Au_5(CO)^-$	0.12 ± 0.02

Binding energies of CO on various gold cluster anions calculated from equation (9) and **Figures 6-12** and **6-13**. (a) Binding energies of primary CO adsorption. (b) Binding energies of secondary CO adsorption.

energies presented here cannot be considered correct, much like those presented in Chapter 4 for the adsorption of O_2 on Au_4^-. In that case, the binding energy obtained was approximately 0.5 eV lower than the dissociation energy measured by Lee and Ervin.[113,200] Using that value as a scaling factor would bring the binding energies presented much closer in line with those presented earlier.[20,103,190] It is dangerous to assume that a similar scaling factor could be used, considering the differences in adsorption mechanisms between CO and O_2, but, in this case, it may be acceptable, as the dissociation energies of $Au_4(CO)^-$ and $Au_3(CO)^-$ were reported to be 0.85 ± 0.09 eV and 0.36 ± 0.07 eV, respectively.[113] As in the case with O_2 binding, though, the temperature-dependent plots in **Figures 6-12** and **6-13** provide important qualitative information as to temperature regions where kinetic and equilibrium control of the CO adsorption processes occur.

6.5 Conclusions

The effects of moisture and temperature on the CO adsorption properties of gold cluster anions were studied using pulsed-helium flow reactor techniques and time-of-flight mass spectrometry. While having no effect on the ability of the larger clusters (N = 4,5) to adsorb CO, preadsorbed D_2O was found to allow Au_2^- and Au_3^- carbonyls to be formed. This process most likely occurs through displacement of the water molecule and indicates that a possible reason for the lack on carbonyls formed on the bare dimer and

trimer anions is that they are not able to sufficiently dissipate the reaction energy. Studies of the temperature dependence of the CO adsorption process suggest that equilibrium conditions do not control the reaction over the entire temperature range. While equilibrium seems to be achieved at higher temperatures, activation barriers must be overcome at lower temperatures.

CHAPTER VII

COADSORPTION OF CO AND O_2 ON SELECTED GOLD CLUSTERS

7.1 Introduction

In the late-1980s, the group of Haruta in Osaka, Japan[50-52,183] discovered that a family of gold-based catalysts, consisting of highly dispersed gold clusters on various metal oxide supports, facilitate a wide range of oxygen-atom transfer reactions, including the combustion of amines and carbon monoxide. This discovery led to worldwide interest[49,211,212] in the properties of the catalysts and they have already been commercialized for use in air purification.[52,75,76]

Catalysts formed by the precipitation methods described by Haruta and others[50-52,54-60,76,170,183] possess countless inhomogeneous structural features. However, measured correlations between the catalysts' activity and their observable structure (usually obtained via transmission electron microscopy) indicated that the

highest activity seemed to occur when the gold particles were in the size range of 1 - 3nm in diameter. Special significance has been attributed to sites along the oxide-gold perimeter, for instance, for the activation of O_2.[52,75,183]

While studies on the commercial catalysts have been ongoing since Haruta's pioneering work and many technical advances have been made, only recently have intense studies began on related "model" catalysts, with two studies being of particular note. In the first study, Valden *et al.* prepared a model Au:TiO_2 catalyst by evaporating gold onto a monocrystalline TiO_2 substrate and annealing to form a distribution of gold nanostructures,[34,65] The average size of the Au nanocrystals was controlled by varying the amount of evaporated metal. Scanning tunneling microscopy/spectroscopy measurements carried out in order to correlate the observed CO oxidation rates with the structural and electronic properties of the nanocrystals indicated some important factors for activity. The clusters with the highest activity were found to be two layer structures of ~ 2nm in diameter (two atomic layers of ~ 50 atoms each). These structures also possessed a tunneling gap of several hundred millivolts each, indicating the importance of a specific electronic requirement in their CO oxidation activity.

Another study of model catalysts was performed by Heiz and coworkers, in which they prepared their Au:MgO catalyst by soft landing mass-selected Au_N clusters on the monocrystalline MgO substrate.[39-42,44] They measured CO oxidation activity using the technique of temperature-programmed reaction (TPR), in which CO and O_2 were coadsorbed at cryogenic temperatures, followed by a temperature increase to detect CO_2 generation. While highly size-dependent activity was seen from N = 8 - 22, the observed

activity was negligible if the F-center (oxide vacancy) defects were removed from the metal oxide surface prior to cluster deposition. An accompanying theoretical treatment of the Au_8:MgO-defect system described the low-energy pathways for adsorption, reaction, and desorption of O_2 and CO, as well as the role of electron transfer, from the F-center defect to the cluster and then to the oxygen molecule, in facilitating the reaction.[39]

While many experimental and theoretical studies concerning the individual adsorption properties of CO and O_2 on gas-phase gold cluster anions have been presented,[20,71,103,104,107,108,112,113,118,130-133,154,178,179,182,190,193] few results have been communicated concerning their coadsorption properties. Very recent work by the group of Wöste provided quite interesting results on the $\{O_2,CO\}$ coadsorption activity of Au_{2-3}^-.[117] Using a temperature-controlled ion trap at low reactant partial pressures, they found that only Au_2^- showed activity towards O_2 adsorption over the temperature range of 100 K to 350 K. Under 250 K, however, *when CO is preadsorbed*, Au_3^- shows the addition of both one and two O_2 molecules, in the form $Au_3(CO)(O_2)^-$ and $Au_3(CO)(O_2)_2^-$. Only under conditions in which CO was preadsorbed, and at low temperatures, was O_2 adsorption able to be seen on this odd-N cluster anion.

The experiments presented in this chapter extend the understanding of the O_2 and CO adsorption properties of gold clusters and provide insight into their coadsorption effects. Under the high reactant partial pressures unique to this experimental setup, CO and O_2 are found to adsorb cooperatively on gold cluster anions, and the first evidence of gas-phase CO oxidation by gold clusters is shown.

7.2 Experimental Methods (Abbreviated)

Studies of the coadsorption of CO and O_2 on gold cluster anions were performed using pulsed-helium flow-reactor techniques at room temperature as described in Chapter 2. For these experiments, several combinations were used to introduce the reactants. In one series of trials, O_2 was seeded into the buffer gas, while CO was subsequently introduced in the reactor. For another series, the order of reactant introduction was reversed. This allowed for studies of the effects that a particular adsorbate may have on the subsequent adsorption of another type. Finally, the reactants were mixed in various concentrations and introduced into the reactor using the second pulsed valve. The heating and cooling system attached to the growth region of the source allowed for the variation of the temperature over the range of 235 K to 321 K. In all cases, the mass spectra were observed to be stable for the duration of the experiments. In order to determine that decomposition reactions make a negligible contribution to the reaction systems, all peak intensity was accounted for, as described earlier,[133] in order to determine whether mass-spectral intensity had been lost or gained across cluster sizes, N.

7.3 Results

With the knowledge of CO and O_2 adsorption properties established in Chapters 3 through 6, the question of their effects on the adsorption of each other could be explored.

When CO was first introduced "upstream" (in the source valve), and O_2 was introduced "downstream" (in the secondary valve), spectra of the type shown in **Figure 7-1** were obtained. As can be seen, the bottom frame represents Au_N^- (N= 6 - 8) saturated with CO, without the introduction of any O_2. As the amount of O_2 is increased, additional peaks begin to appear in the spectra, corresponding to the addition of an O_2 molecule to a cluster already possessing *M* CO adsorbates (note the presence of the peak corresponding to $Au_7(CO)_4^-$ whose intensity remained constant throughout the experiment, representing stable conditions). This is most notably exhibited by the appearance and growth of a post-CO saturation peak corresponding to $Au_6(CO)_4O_2^-$ and which is marked in the top frame. Reversing the order of reactant introduction and plotting for the same mass range as in **Figure 7-1** led to spectra of the type shown in **Figure 7-2**. In this figure, the even-N clusters were saturated with O_2 (bottom frame), and increasing amounts of CO were introduced in the reactor (middle/top frames). Once again, new peaks appear in the mass spectrum corresponding to coadsorption complexes.

By varying the temperature of the fast-flow reactor from ~235K to ~320K, the effects of temperature on the coadsorption processes were studied. **Figure 7-3** presents three spectra taken at the temperature extremes and median values. As in the higher-pressure, room-temperature spectra, the addition of O_2 to clusters containing a high amount of CO at low temperature led to a variety of CO/O_2 coadsorption peaks. Note, for instance, the presence of the $Au_6(CO)_4(O_2)^-$ peak, the post-CO saturation peak for Au_6^- present even when Au_5^- is only approaching its saturation value. As the temperature is increased, the higher-M (CO) peaks begin to disappear, leaving behind clusters with a smaller

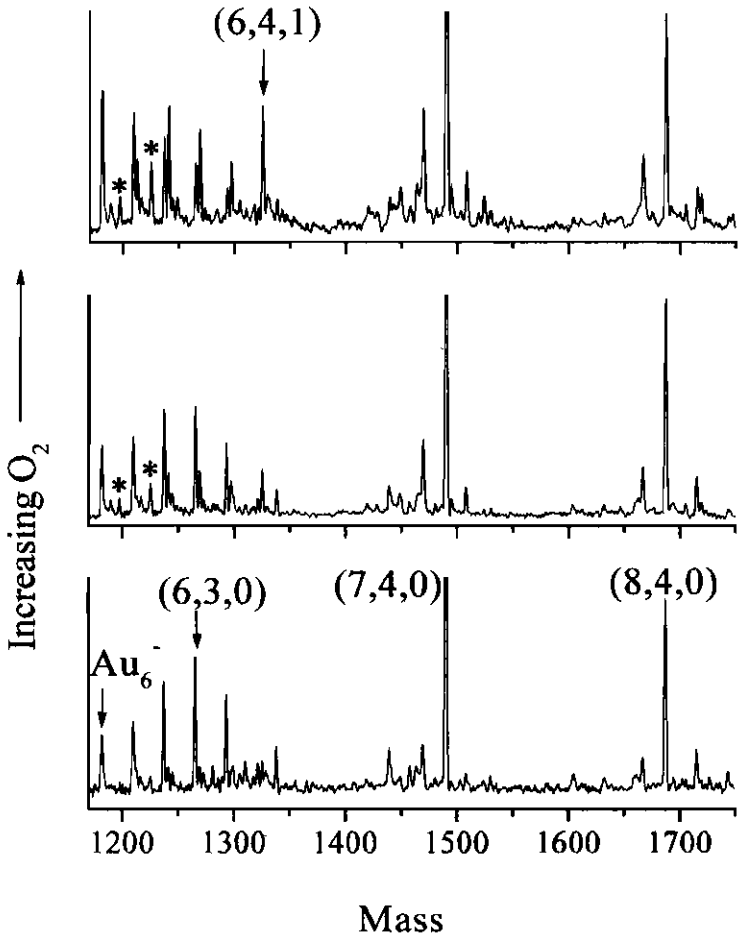

Figure 7-1: O_2 adsorption on CO-saturated Au_N^- (N = 6 - 8)

A series of spectra resulting from increasing the partial pressure of O_2 in the reactor region in which the bottom frame represents Au_N^- (N = 6 - 8) saturated with CO, without the introduction of any O_2. Increasing O_2 causes additional peaks to appear, mostly belonging to the addition of an O_2 molecule to a cluster already possessing *M* CO adsorbates, most notably exhibited by the growth of a peak corresponding to $Au_6(CO)_4O_2^-$, which is marked in the top frame. Peaks arising from processes (4) and (5) are marked with asterisks.

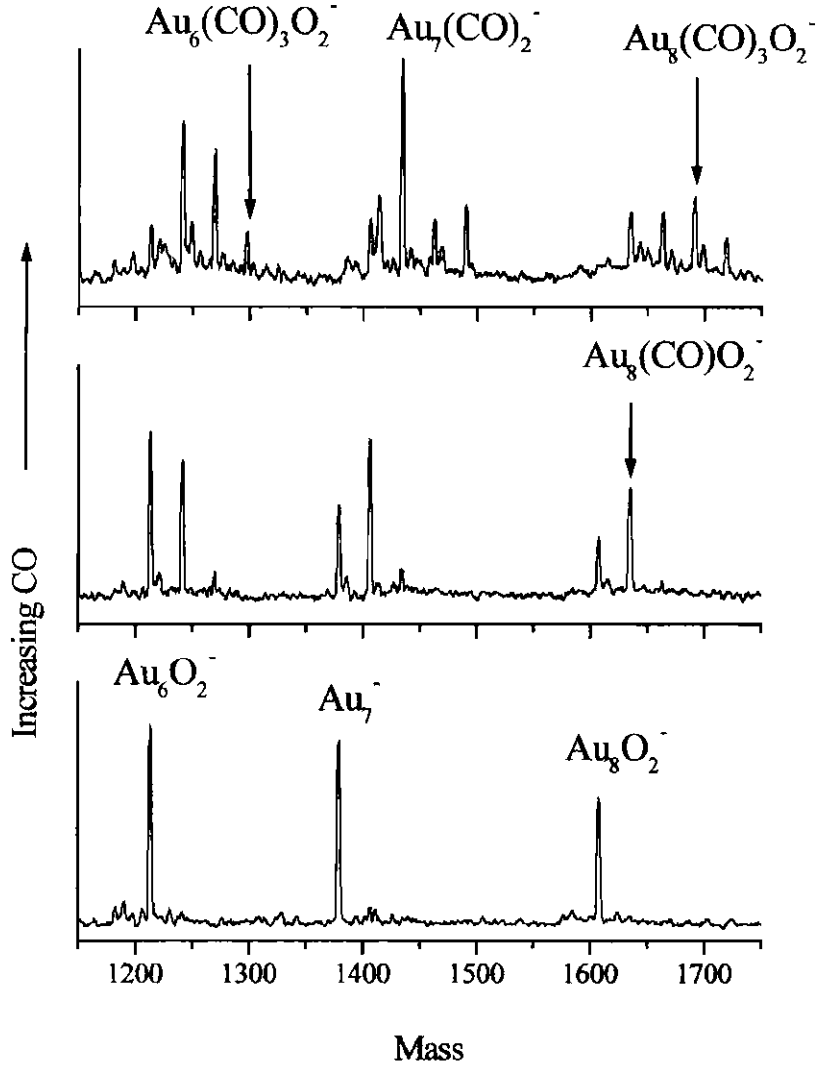

Figure 7-2: CO adsorption on Au_N^- (N = 6 - 8) with preadsorbed O_2

A series of spectra resulting from increasing the amount of CO in the reactor when O_2 is preadsorbed on the Au_N^- clusters (N = 6 - 8). The bottom frame shows the even-N clusters saturated with O_2 while Au_7^- remains inactive towards O_2 addition. Increasing the amount of CO in the reactor leads to both $Au_N(CO)_M^-$ peaks and, for the even-N clusters, $\{O_2,CO\}$ coadsorption peaks, as described for **Figure 7-1**.

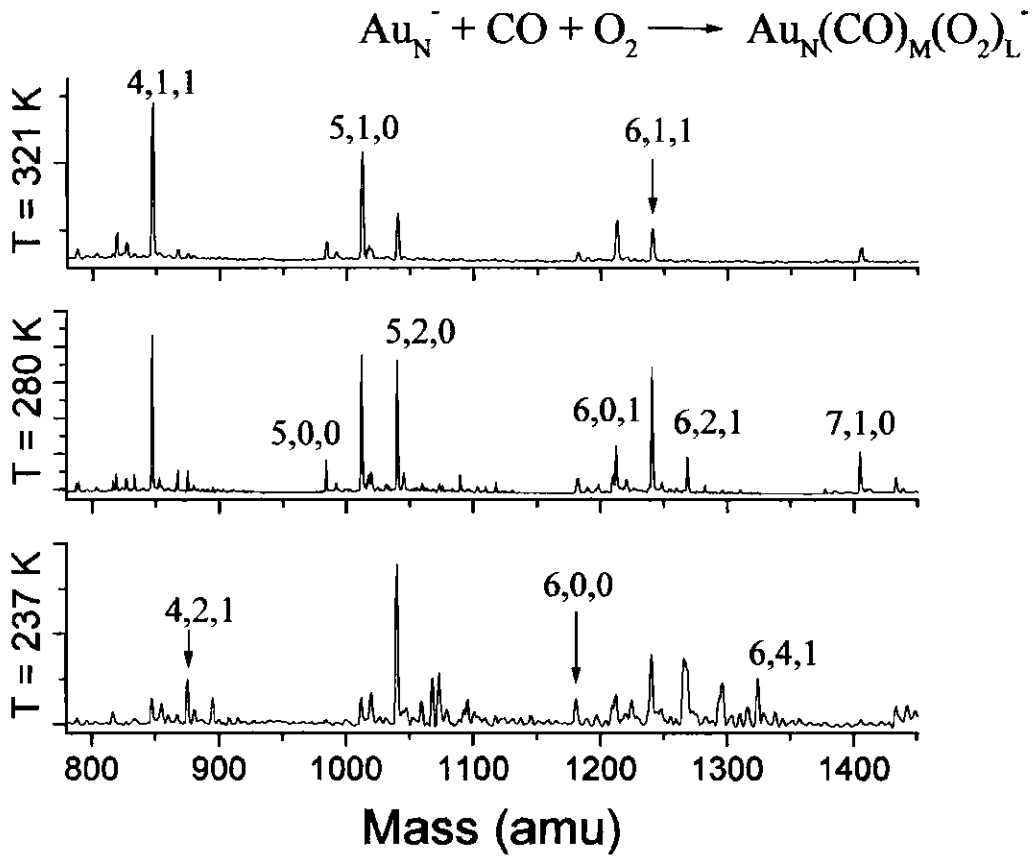

Figure 7-3: Temperature-dependence of CO and O_2 coadsorption

(Bottom frame) Mass spectrum of gold cluster complexes (N = 4 - 7) formed with 10% CO:He added upstream and ~ 0.3 mbar O_2 in the reactor at 237K. (Middle frame) As in the bottom frame, but now at a temperature of 278K. Increasing temperature has led to a decrease in the number of high-M complexes. (Top frame) Mass spectrum obtained at a reactor temperature of 321K. The majority of M > 1 complexes have now disappeared, leaving behind especially stable CO-adsorption complexes (N = 5,7) and CO/O_2 coadsorption complexes (N = 4,6).

distribution of adsorbates. At the highest temperatures studied, only a few peaks are left behind for each of the clusters shown. The possible reasoning for their survival will be discussed below.

7.4 Discussion

7.4.1 Pressure Dependence

The new peaks shown in **Figures 7-1** and **7-2** can provide an opportunity to ascertain the exact nature of coadsorption between these molecules, whether it is competitive, non-competitive, or cooperative. By studying the mass spectra and determining the relative equilibrium constants (as described in Chapters 3 - 6), an interesting and quite unexpected result arises. While the normal view of coadsorption on surfaces may assume that adsorbates will compete for binding sites, it is not necessarily the case. As can be seen in **Figure 7-4**, by studying the relative effects of a preadsorbate on the step-wise equilibrium constants of a series of even-N cluster peaks, described by

$$\text{Effect of Preadsorbates} = \ln \frac{K_n}{K_{n-1}} \qquad (1),$$

it is found that the presence of adsorbed CO (O_2) may actually enhance the subsequent adsorption of O_2 (CO) on the cluster. For example, the presence of a preadsorbate on the Au_4^- cluster enhances the binding probability of the second adsorbate by a factor of approximately 18:1. Likewise, a dramatic increase in adsorption efficiency can be seen for the Au_{10} anion. When O_2 is preadsorbed on Au_{10}^-, the equilibrium constant for subsequent CO adsorption is greater than 5, as opposed to a value of ~0.7 for CO adsorption on bare Au_{10}^-. The effect of cooperative coadsorption is even more dramatic in the case of Au_2^-. As described in Chapter 5, this size cluster shows no isolated adsorption of CO in the absence of a third body that can remove excess reaction energy, even under conditions that lead to saturation of the larger cluster anions. However, when O_2 is preadsorbed on the cluster, a CO molecule is seen to adsorb with a relative equilibrium constant of ~0.27. This result is shown in **Figure 7-5**.

While, for instance, the presence of two preadsorbate molecules may cause the coadsorption process to show no effect or to become competitive, it must be noted that the probability of cooperative coadsorption does not simply continue to decrease with added preadsorbates. On the contrary, Au_6^- shows an increase in cooperative coadsorption with increasing numbers of preadsorbates. This type of cooperative adsorption could help to explain how, on the supported gold clusters, large rates of CO_2 production can be seen when neither of the reactant molecules is known to readily adsorb on bulk gold surfaces. However, though the effects of preadsorbed CO may lead to high

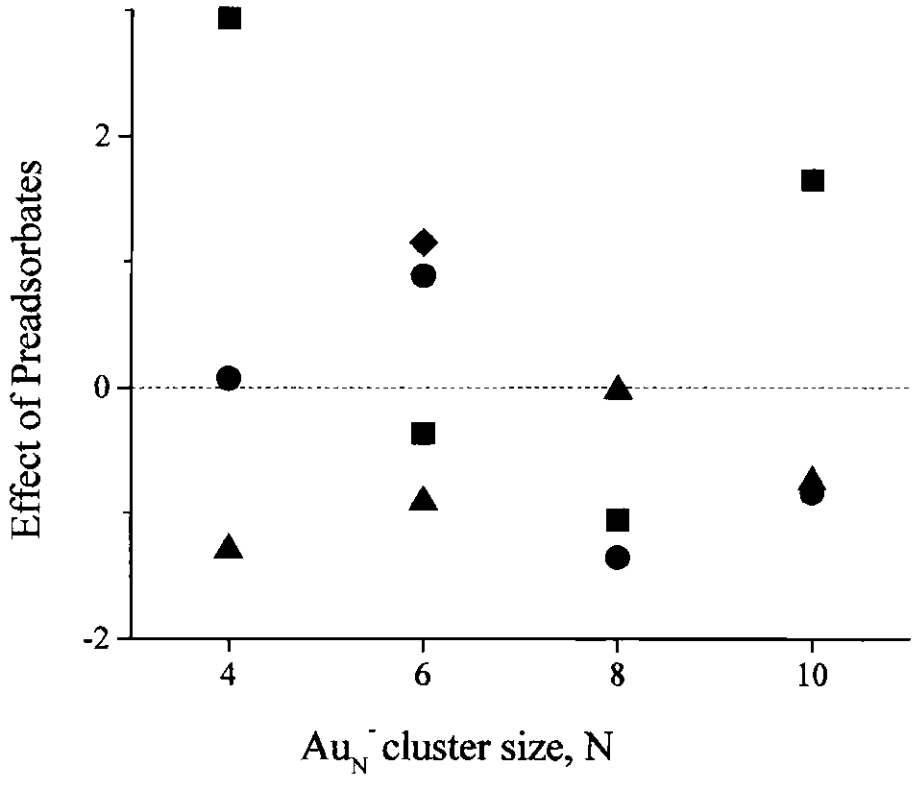

Figure 7-4: Effect of preadsorbates on secondary adsorption

A series of log plots denoting the change in equilibrium constants with the presence of a preadsorbate on several even-N clusters, described by equation (1). Cooperative coadsorption is defined by a ratio of equilibrium constants (on a log scale) greater than 0, while competitive coadsorption has a ratio of less than 0. The black squares represent the effect of a single preadsorbate on the subsequent adsorption of another molecule. The triangles and circles represent the effect of 2 and 3 initial preadsorbates, respectively. The effect of 4 preadsorbates on the subsequent adsorption of another molecule on Au_6^- has also been plotted as a diamond. A dotted line has been placed at a ratio of 0 (no effect) in order to differentiate between the competitive and cooperative processes.

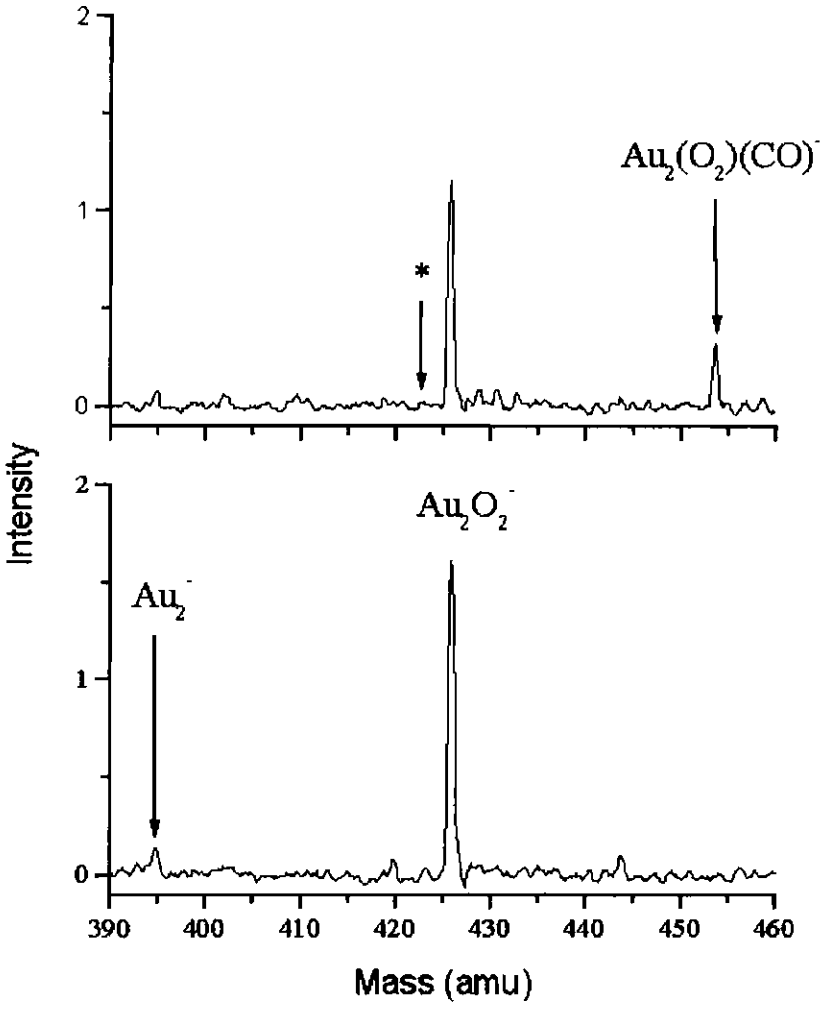

Figure 7-5: Cooperative coadsorption of CO and O_2 and Au_2^-

Mass spectra indicating the effect of cooperative coadsorption in the Au_2^- system. In the bottom frame, Au_2^- is almost completely converted to $Au_2O_2^-$ by upstream addition of O_2. In the top spectrum, CO has been added in the reactor. No individual adsorption of CO can be seen (the asterisk marks the point at which this would occur), but CO adsorbs on the $Au_2O_2^-$ cluster, resulting in the $Au_2(O_2)(CO)^-$ complex.

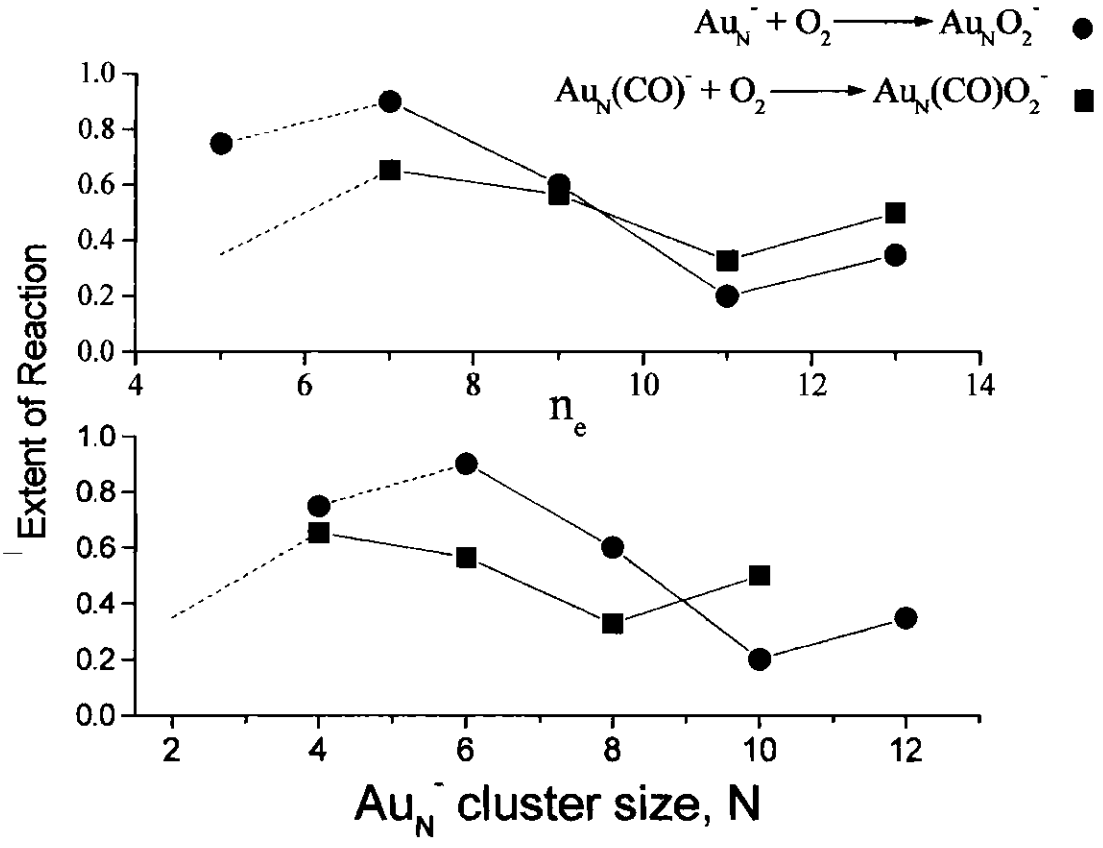

Figure 7-6: Effect of preadsorbed CO on O_2 adsorption

A comparison of O_2 adsorption activity on bare clusters (circles) and those possessing a preadsorbed CO molecule (squares). The bottom frame shows the extent of O_2 adsorption plotted versus cluster size, N. The top frame presents the extent of reaction plotted against the number of valence electrons, n_e, of the cluster or cluster:CO complex, as defined by (2) and (3). The addition of two electrons from a preadsorbed CO molecule causes an approaching O_2 molecule to treat a $Au_N(CO)^-$ cluster as if it were Au_{N+2}^-.

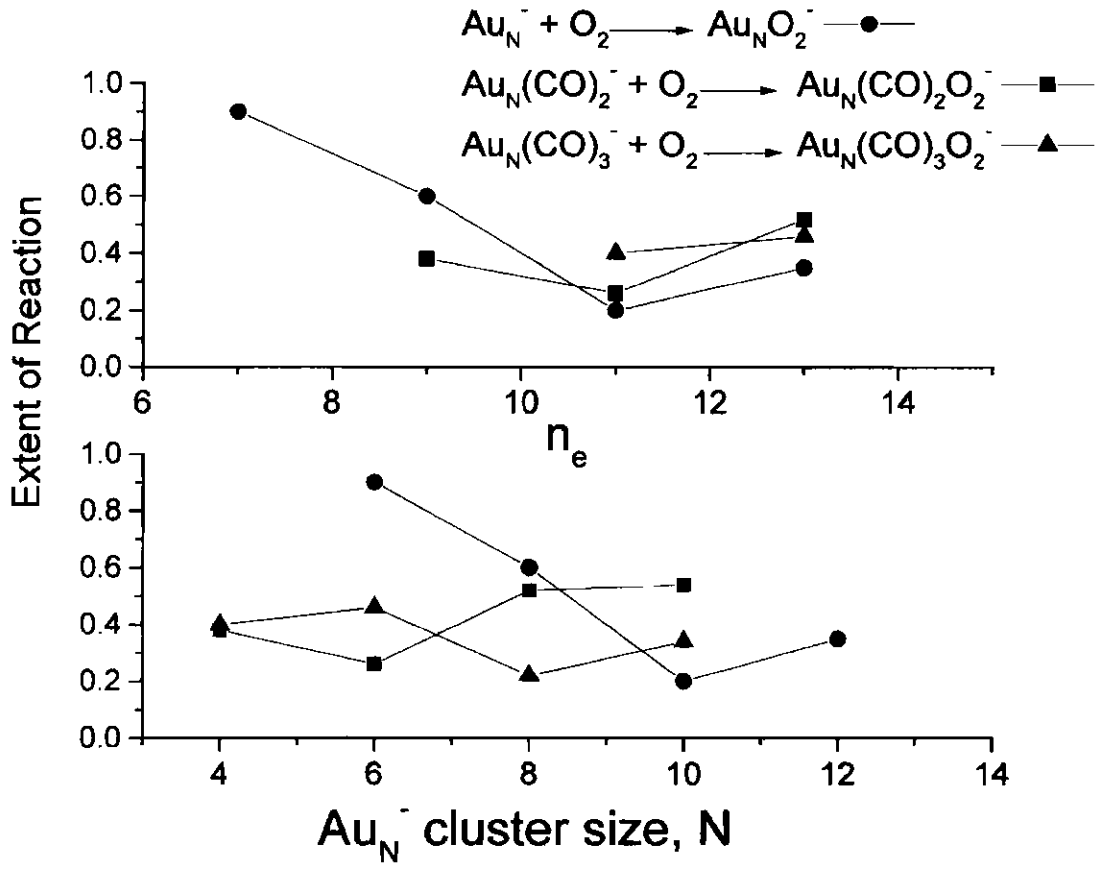

Figure 7-7: Effect of preadsorbed CO on O_2 adsorption

A comparison of O_2 adsorption activity on bare clusters (circles) and those possessing two (squares) and three (triangles) preadsorbed CO molecules. The bottom frame shows the extent of O_2 adsorption plotted versus cluster size, N. The top frame presents the extent of reaction plotted against the number of valence electrons, n_e, of the cluster or cluster:CO complexes, as defined by (2) and (3).

probability of O_2 binding on a cluster (or O_2 enhancing subsequent CO adsorption), they do not relax the forbidden nature of an odd-N cluster gaining an O_2 adsorbate or for a second O_2 molecule adsorbing on an even-N cluster.

A possible explanation for this coadsorption activity is that the first adsorbate affects the electronic structure of the cluster, causing it to appear electronically different to the second approaching molecule. A recent theoretical study of the gas-phase catalytic oxidation of CO by Au_2^- provides some insight into this possibility.[190] CO binds much more tightly to neutral Au_2 than to the anion (1.60 eV versus 0.96 eV). Assuming that this also applies to the larger cluster sizes, a Au cluster anion with a preadsorbed O_2 will appear to be neutral to the approaching CO molecule due to the charge transfer that takes place from the Au_N^- cluster to the O_2. A test of this prospect is to compare the reactivity of a second adsorbate on both the bare cluster and a cluster with a preadsorbate. For instance, the extent of reaction for O_2 adsorption on Au_N^- may be different than adsorption on $Au_N(CO)^-$. An analysis of this possibility is provided in **Figures 7-6** and **7-7**. In the bottom frame of **Figure 7-6**, O_2 adsorption on Au_N^- (circles) and on $Au_N(CO)^-$ (squares) is plotted as a function of cluster size. In the top frame, the extent of reaction is plotted again, but as a function of the number of valence electrons:

$$n_e = N + 1 \qquad (2)$$

for bare Au_N^- clusters or

$$n_e = N + 2M \tag{3}$$

for Au_N^- clusters with preadsorbed CO molecules (acting as two electron donors). As can be seen, the extent of reaction of O_2 changes with the presence of a preadsorbed CO. In fact, the addition of two electrons from the CO causes the adsorption behavior of O_2 toward the cluster to mirror that of a bare cluster two atoms larger. **Figure 7-7** provides the same comparison of O_2 adsorption activity on Au_N^- clusters and $Au_N(CO)_2^-$ (squares) and $Au_N(CO)_3^-$ (triangles) clusters. It is readily apparent that the presence of additional CO adsorbates causes the O_2 adsorption behavior to mirror that of a bare cluster 4 atoms larger (2 CO adsorbates) and 6 atoms larger (3 CO adsorbates).

Under coadsorption conditions, evidence for CO_2 elimination depends on the appearance of peaks of the type, $Au_N(CO)_MO_1^-$, which is attributed to the process:

$$Au_N(CO)_{M+1}(O_2)_1 \rightarrow Au_N(CO)_MO + CO_2 \tag{4}$$

as well as to the recovery enhancement of $Au_N(CO)_{M-1}^-$ peaks, from

$$Au_N(CO)_MO \rightarrow Au_N(CO)_{M-1} + CO_2 \qquad (5).$$

This reaction "cycle" under low-coverage conditions is shown in Scheme 1.

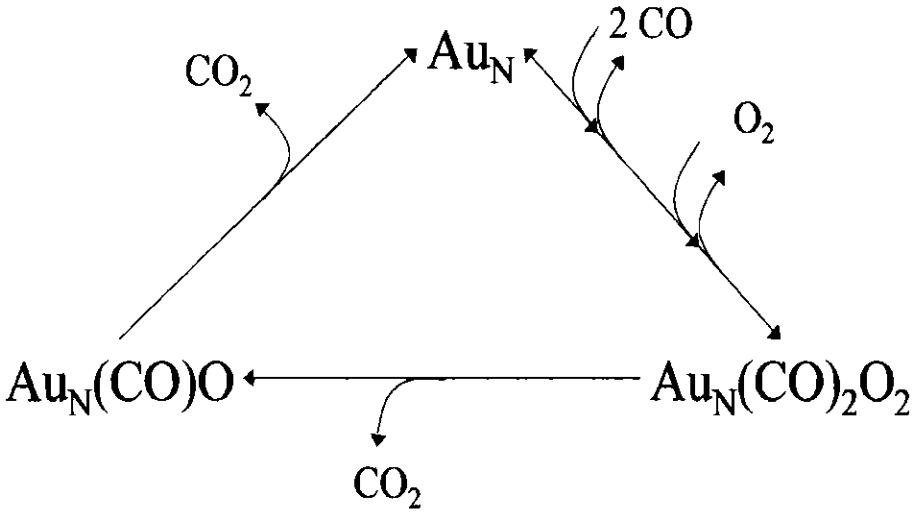

Scheme 1

Figure 7-8 presents the results of coadsorption experiments on Au_6^-, organized for convenient viewing, when CO and O_2 are introduced sequentially. As can be seen, the cluster is first saturated with CO, giving a relatively flat distribution of $Au_6(CO)_M^-$ complexes. As O_2 is introduced in the secondary reactor, the initial peaks that appear are due to $CO:O_2$ coadsorption products. However, with increasing amounts of O_2 being introduced, new peaks begin to appear at irregular intervals. Upon closer inspection, the mass of these peaks corresponds to that which would be expected if a CO_2 molecule were lost from the cluster. Similarly, in **Figure 7-9**, it can be seen that reversing the method of reactant introduction continues to lead to the appearance of CO_2-loss peaks. These peaks are also marked with asterisks in **Figure 7-1**. A glance at **Figure 7-9** shows that much smaller amounts of the CO_2-loss peaks are present when O_2 is preadsorbed on the cluster. There are two possible explanations for this result. First, the stronger binding described above for CO adsorption on neutral gold clusters (Au_2 versus Au_2^-) could be to blame. Assuming that this behavior holds for larger clusters, then CO binding on a $Au_NO_2^-$ cluster (in which the cluster is essentially neutral) may be too strong in order for the CO molecule to find the adsorbed O_2. A second possible explanation is that introduction of CO into the reactor using the secondary pulsed valve may not provide sufficient CO partial pressures for greater amounts of CO_2 loss to be observed.

The information gained on the adsorption of CO and O_2, as well as that presented here for the case of coadsorption, provides an opportunity to propose a mechanism for the gold cluster-catalyzed oxidation of CO, which, while exothermic, is marked by a sizable activation barrier under non-catalyzed conditions. One proposal, based on detected

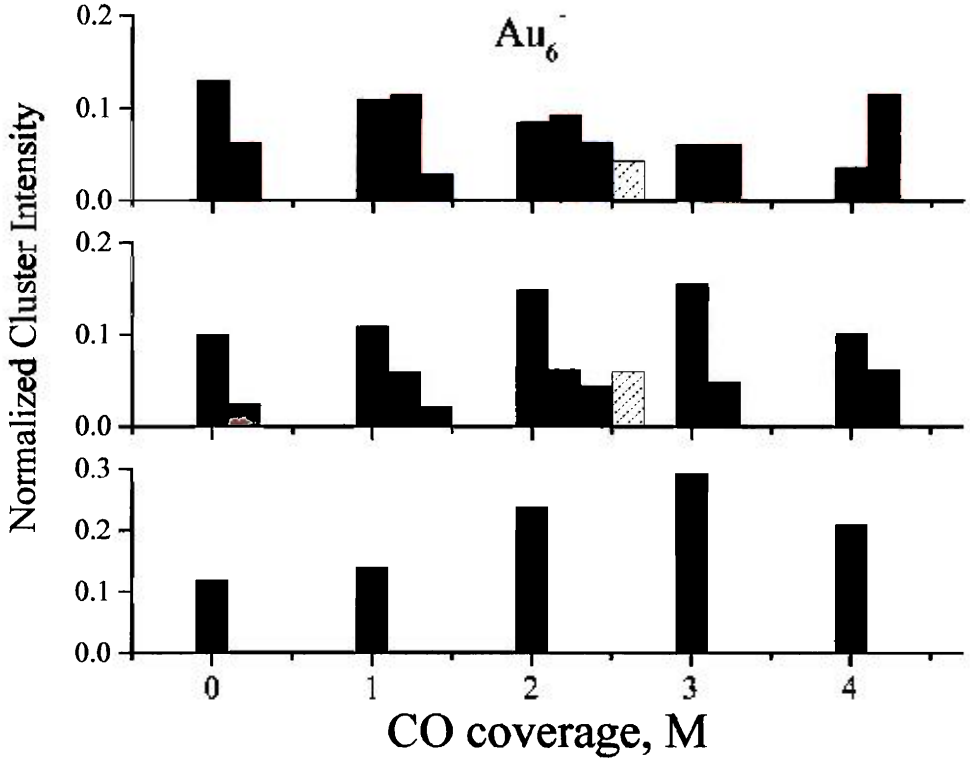

Figure 7-8: Abundances of coadsorption species

Relative abundances of various Au_6X^- species are grouped according to their CO coverage, and plotted as bar graphs. The lower frame represents a reference mass-spectrum with no O_2 introduced downstream, showing only the distribution of CO coverage (added upstream), M, $Au_6(CO)_M^-$, as black bars. The middle and upper frames represent conditions under which O_2 is added downstream at ~0.5 mbar and ~1.1 mbar, respectively. Red bars indicate co-adsorption species, $Au_6(CO)_MO_2^-$, eliminating CO_2 from which gives the primary reaction product, $Au_6(CO)_{M-1}O^-$, represented by blue bars. This species may eliminate a second CO_2 to give the secondary product, $Au_6(CO)_{M-2}^-$, an estimate of which is represented by the cross-hatched bars.

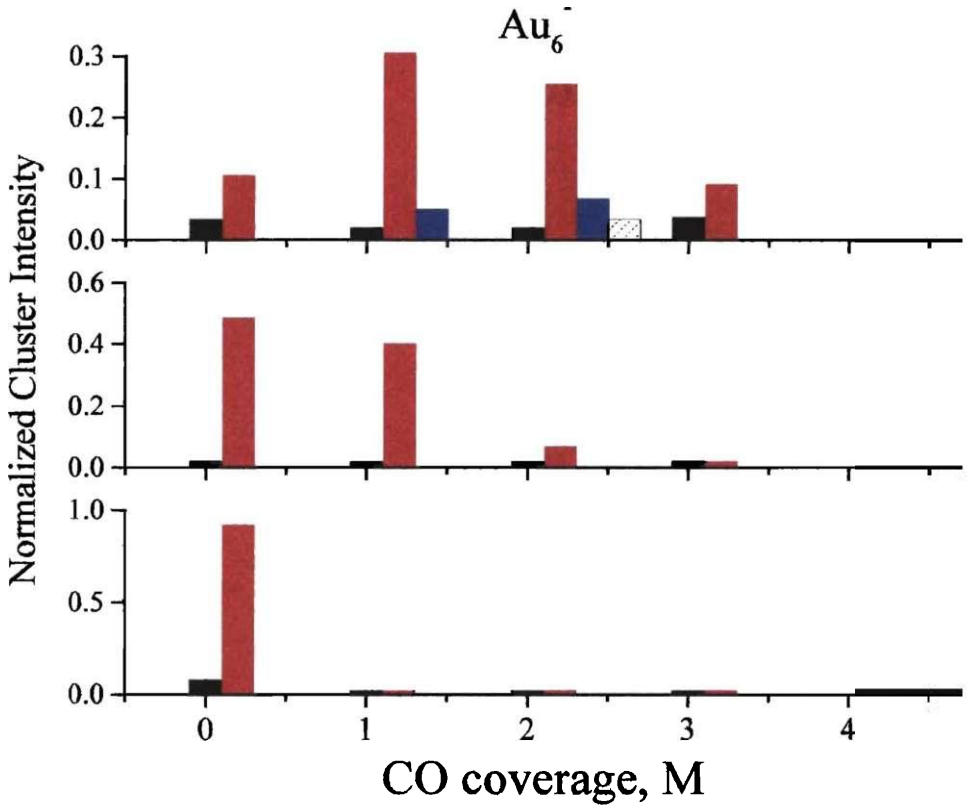

Figure 7-9: Abundances of coadsorption species

Relative abundances of various Au_6X^- species grouped according to their CO coverage, and plotted as bar graphs. The lower frame represents conditions under which no CO is introduced downstream, showing as a reference only the nearly complete conversion of Au_6^- to $Au_6O_2^-$ resulting from up-stream addition of O_2 (main red bar). The middle and upper frames represent conditions under which CO is added downstream at ~0.3 mbar and ~0.9 mbar, respectively. The format of the bars is the same as that given in **Figure 7-8**.

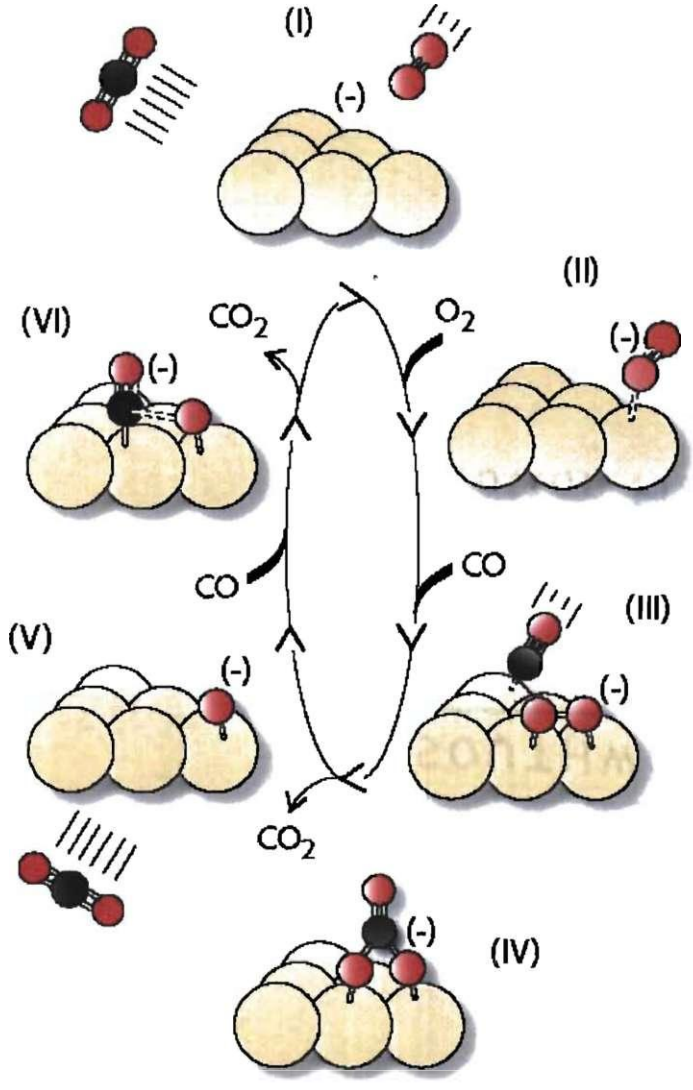

Figure 7-10: Possible CO oxidation mechanism under low coverage

Schematic representing a possible CO oxidation mechanism on gas-phase gold cluster anions. (I) The bare Au_6^- cluster, in its calculated equilibrium structure, adsorbs molecular oxygen, in the superoxo form (II). Subsequent co-adsorption of CO yields a $Au_6O_2(CO)^-$ species (III), which may rearrange to produce the very stable CO_3^- adsorbate (IV). Elimination of CO_2 yields Au_6O^- (V). Adsorption of a second CO yields the $Au_6CO_2^-$ mass (VI), which may desorb a second CO_2 and return the Au_6^- catalyst.

species in these experiments and illustrated for low coverage conditions, is described by **Figure 7-10**: The bare Au_6^- cluster (I), in its calculated equilibrium structure,[99] adsorbs O_2 in the superoxo form (II). Upon subsequent adsorption of a CO molecule, providing a cluster complex with a mass corresponding to $Au_6(CO)_1O_2^-$ (III), a rearrangement occurs to form a stable CO_3^- intermediate (IV). The presence of this stable form can be inferred from the lack of a metastable decay species in the mass spectrum arising from the loss of CO in the free-flight region of the mass spectrometer, which was described in Chapter 5. Studying the higher CO-coverage complexes, evidence of metastable decay can be seen from the coadsorbate complexes, indicating that a single CO is being stabilized by an interaction with the coadsorbed O_2 molecule. Following the loss of a CO_2 molecule, a Au_6O^- complex (V) is detected, as in process (3). The adsorption of a second CO molecule leads to a complex possessing the $Au_6(CO_2)^-$ mass (VI), which may desorb a second CO_2 molecule and return the bare Au_6^-.

There are several points in this process at which obstacles could possibly arise. Inefficient adsorption and coadsorption of CO and O_2 on the cluster would not allow the reactants to be held long enough for the reaction to occur. Secondly, a large barrier to diffusion will not allow the reactants to find each other on the surface of the cluster, as described above for CO adsorption on an O_2-saturated Au_6^- cluster. Once the O_2 and CO molecules have interacted, too large a barrier to reaction will not allow the production of CO_2. Also, in order for the reaction products to be seen, there must not be a large interaction between the CO_2 and the cluster. Otherwise, the barrier of reaction for desorption of CO_2 will be too large to overcome. Finally, side-reactions and destructive

processes must be avoided. For instance, besides being highly active, the cluster must have a high selectivity for CO_2 production as opposed to other reactions. One such reaction is the poisoning of the cluster by impurities. Each of these obstacles must be avoided for each CO_2 production process on a cluster, whether an impinging CO encounters an O_2 on the surface or it encounters an O atom left behind following the earlier production of a CO_2. The final, and perhaps most pressing point, though, is whether the high exothermicity of the reaction could lead to the destruction of the cluster. This is obviously a valid concern, considering that, in the case of Au_6^-, the energy required to dissociate a single gold atom[99] is very nearly the same as that released from CO oxidation (~2.8 eV). It has been noted for CO oxidation on Pt surfaces, however, that only ~ 0.6 to 0.8 eV of the reaction energy is deposited into the surface,[213] and as mentioned above, a summation of the intensities of parent and product peaks involved in the experiments show no loss of ion signal due to cluster dissociation. Therefore, it is likely that the excess energy released from the reaction is dissipated by the desorption of a "hot" CO_2 molecule or through collisions with the He buffer gas.

Previously, Shi and Ervin presented results indicating that platinum cluster anions are capable of catalytically oxidizing carbon monoxide.[21] While this work is exciting in its own right, several questions arise. First, the lack of coadsorption species in the mass spectra leads to the question as to whether the CO is ever adsorbed on the cluster in the reaction process. Secondly, the fact that the order of reactant addition could lead to cluster fragmentation and much lower product yields indicates that these cluster "catalysts" could be easily poisoned or even destroyed. Finally, the low reactant

coverages studied do not allow the effect of adsorbate saturation on the catalytic activity to be determined. In contrast, the results here show that, under reactant saturation conditions, easily identifiable coadsorption and product peaks are found for anionic gold clusters and that the order of reactant introduction does not lead to either cluster fragmentation or loss of catalytic ability.

While the results of O_2 and CO adsorption alone present a favorable avenue for discussion of the relevance of gas-phase cluster reactions to those carried out on supported clusters, the appearance of the CO_2 elimination peaks due to the processes, (4) and (5), provide several opportunities. These consist of the opportunity to gain a more detailed understanding of the role of the support material, as well as to compare the relative rate of CO_2 elimination on the gas-phase clusters with those achieved on the model systems and the actual supported-gold catalysts. In the work of Sanchez *et al.* on size-selected gold clusters supported on MgO,[39] it was noted that, if the F-center (oxygen vacancy) defects on the surface were removed, the CO oxidation activity was almost non-existent. As these surface defects provide a large amount of localized electron density, it was suggested that charge-transfer from the surface to the cluster was responsible for the activation of O_2, the rate-limiting step in CO oxidation. The results presented earlier (Chapter 3) reinforce this explanation in that O_2 adsorption is seen from the gold anions, while it was previously reported that gold cations, with the exception of Au_{10}^+, did not show any O_2 adsorption activity.[107,108] The excess electron clearly is necessary in order for the reaction to occur, and the neutral supported clusters acquire the electron via charge transfer from the surface. The results of Sanchez *et al.* also noted a

tendency towards an even-odd N dependency for CO_2 oxidation activity, in agreement with the results for O_2 adsorption. The only contradiction with the gas-phase results is the fact that the smallest supported cluster to show significant activity was Au_8, while Au_6^- was found to show extremely high activity.

Though the results presented for the size-selected supported clusters provide important information as to the reaction mechanism that is taking place for CO oxidation, they provided no information as to the rate of CO_2 production, only stating that 1-2 CO_2 molecules were seen in the range of 8 to 20 Au atoms. The turnover frequency (t.o.f.) of these supported clusters is important if they are ever to be used as improved catalysts. The initial studies of Haruta[52] showed a t.o.f. of ~0.2 CO_2 per exposed Au atom per second for supported gold particles under 2 nm in diameter. Further studies on model gold cluster catalysts by Valden *et al.*[65] showed a t.o.f. of approximately 2 CO_2 molecules per total gold atoms per second. In both cases, the gold catalysts were exposed to $CO:O_2$ mixtures, and the resulting CO_2 production was measured. By noting that the reaction time (τ) in the present experiments is 100-200 μs (transit time through the reactor region) and determining the fraction of Au_N clusters (f_r) detected in a form due to the processes, (4) and (5), a rough estimate of the gas-phase turnover frequency can be formed:

$$\textbf{turnover frequency (t.o.f.)} = f_r / N * \tau \qquad (5).$$

Assuming a reactive fraction of 10% from a ten-atom gold cluster, this formula estimates a turnover frequency of ~100 CO_2 per Au atom per second, two orders of magnitude greater than that seen for the present commercial gold catalysts. It must be noted, though, that the gold cluster anions have undergone only a single reaction cycle at most, while the model catalysts of Goodman[34,65] and the commercial catalysts of Haruta[50-52,183] have been exposed to many cycles. Indeed, the efficiency of a real catalyst must be measured as an average over thousands of reaction cycles. Even with the concerns over the ability of the gold clusters to undergo multiple reaction cycles and to dissipate the excess energy produced in the reaction, though, these estimates of t.o.f. show the possible capabilities of small gold clusters and provide an incentive for further study in order to improve the efficiency of supported gold cluster catalysts.

7.4.2 Temperature Dependence

Considering the ability of the supported gold catalysts to efficiently oxidize carbon monoxide even at low temperatures, it is important to gain an understanding of the temperature dependence of these reactions in the gas phase. As seen in **Figure 7-3**, at lower temperatures, a variety of coadsorption peaks are present. However, as the temperature of the system is raised, only certain cluster-adsorbate compositions survive. In the case of the N = 4 and N = 6 systems, these special compositions correspond to clusters containing both single CO and O_2 adsorbates. As described above, the adsorbates may form a CO_3^- species on the cluster, possibly providing extra stability as the temperature is raised. In the case of Au_5^-, the largest peak remaining corresponds to

$Au_5(CO)^-$. The reluctance of this cluster-adsorbate complex to undergo further adsorption in pressure-dependent studies previously was attributed to the fact that this species corresponds to an electronic shell filling (8 electrons).[130] This highly stable behavior likely helps the complex to survive at higher temperatures when higher-CO species do not.

Figure 7-11 presents the temperature-dependence of the apparent equilibrium constant of the addition of O_2 to a primary gold-carbonyl, in a reaction denoted by:

$$Au_4(CO)^- + O_2 \rightarrow Au_4(CO)(O_2)^- \qquad (6).$$

The positive slope of this plot indicates that the formation of a coadsorption species on this particular cluster requires the surmounting of an activation barrier. This may be expected, as, if an especially stable CO_3^- species is truly being formed, a decrease in entropy arising from the formation of a single species from two different species could lead to the appearance of an activation barrier. Of course, it is also possible that any CO molecules not being stabilized via interaction with O_2 are simply desorbing from the clusters in the flow reactor. This action could cause the $Au_4(CO)(O_2)^-$ peak to appear especially intense, even if it is not the primary peak in an equilibrium distribution.

As Au_6^- has been shown to efficiently oxidize CO, it is interesting to observe the temperature dependence of this reaction. **Figures 7-12** and **7-13** show the change in the apparent equilibrium constants of the reactions

$$Au_6(CO)(O_2)^- \rightarrow Au_6O^- \quad (7)$$

and

$$Au_6(CO)_2(O_2)^- \rightarrow Au_6(CO)O^- \quad (8)$$

as a function of temperature. Just as the supported cluster catalysts have been shown to be active for CO oxidation at temperatures as low as -70 °C, these plots indicate that there is no barrier to CO_2 generation from Au_6^- in the temperature range studied. This behavior continues to at least -60 °C (not shown). To what temperature extremes this exothermic CO_2 production continues is unknown, due to the loss of cluster intensity at high temperatures and the inability to consistently cool the reactor to temperatures below those described here. It is pleasing to note, though, that the slopes of these van't Hoff plots are

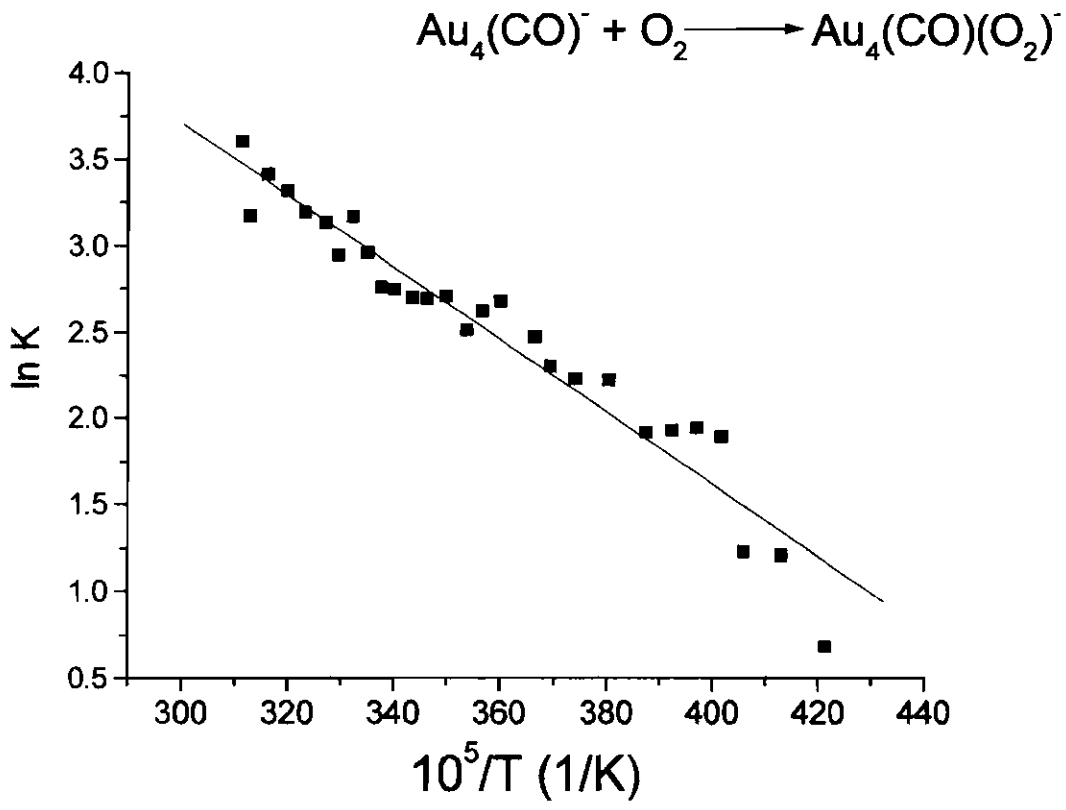

Figure 7-11: Temperature-dependence of the adsorption of O_2 on $Au_4(CO)^-$

Plot showing the change in apparent equilibrium constant for the addition of O_2 to $Au_4(CO)^-$ with increasing temperature. The positive slope with increasing temperature indicates that this process is activated.

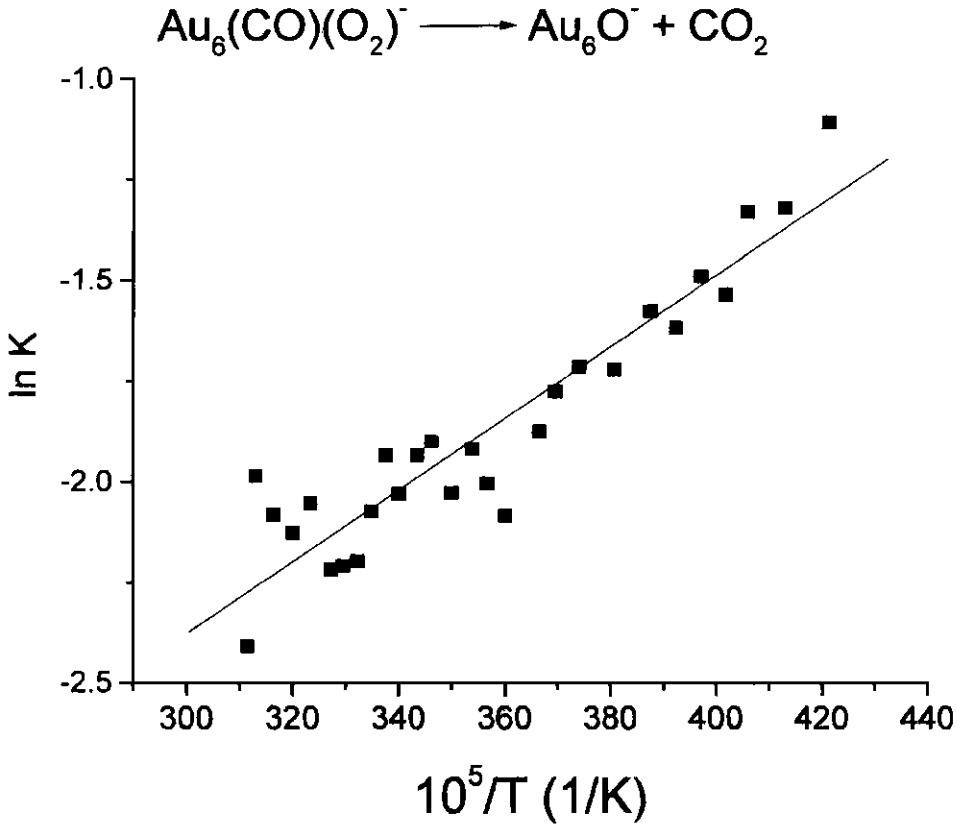

Figure 7-12: Temperature-dependence of CO_2 loss from $Au_6(CO)(O_2)^-$

Plot showing the effect of increasing temperature on the production of CO_2 from a Au_6^- cluster with a single CO and O_2. The plot indicates that, even at temperatures well below room temperature, this process is not activated.

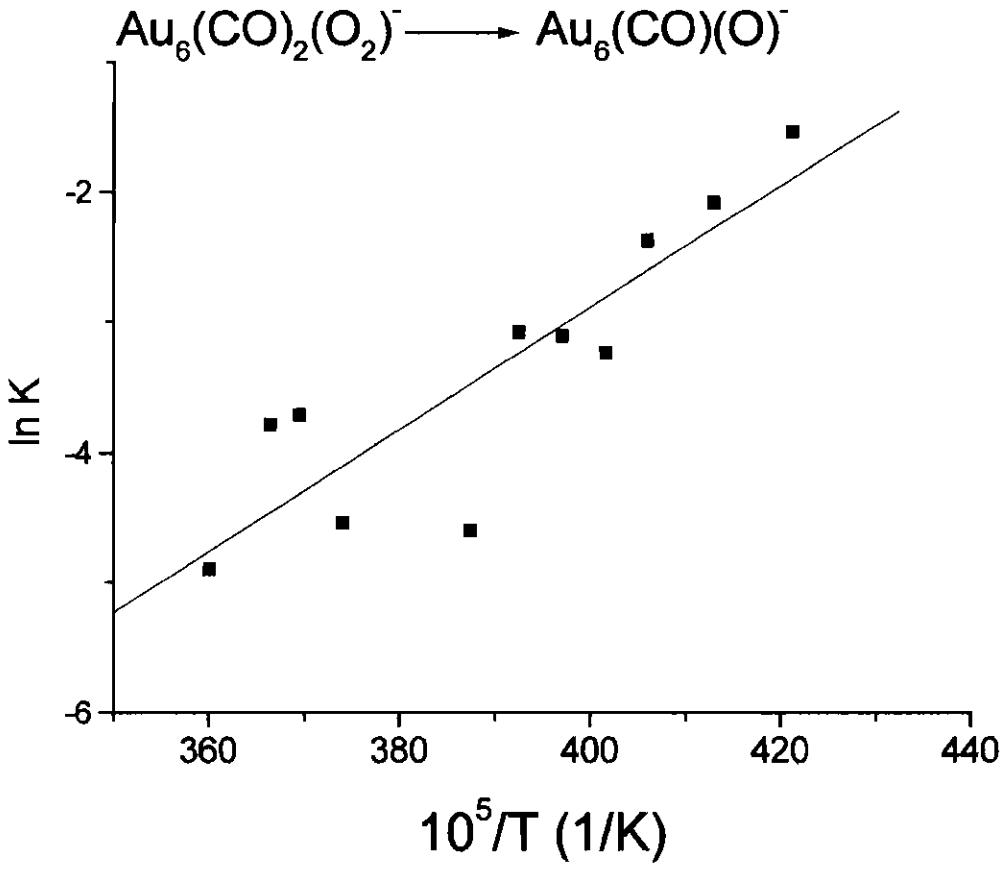

Figure 7-13: Temperature-dependence of CO_2 loss from $Au_6(CO)_2(O_2)^-$

Plot showing the effect of increasing temperature on the production of CO_2 from a Au_6^- cluster with two CO adsorbates and O_2. As with the generation of CO_2 from $Au_6(CO)(O_2)^-$, this process is not activated, even at temperatures well below room temperature.

almost identical for the production of CO_2 from two different starting species, indicating that there is a similar starting point. In this case, the starting point could be the proposed CO_3^- species and any excess CO simply would simply act as a spectator.

7.5 Conclusions

While the adsorption mechanisms of CO[118] and O_2[71,104,178,182] individually continue to be debated, the results presented here indicate that the reactants do not necessarily compete for reaction sites on gold cluster anions, Au_N^-. On the contrary, in many cases the presence of a preadsorbate aids in further adsorption on the clusters. Additionally, the coadsorption of these species on several of the clusters has been shown to lead to the oxidation of CO, i.e. the production and desorption of CO_2. Whatever the actual mechanism of the CO oxidation, the ability of the clusters (in particular Au_6^-) to catalyze CO oxidation at the temperatures studied, in the absence of the metal oxide support, lends further credence to the belief that the gold cluster is the active species in supported gold cluster catalysts.

Further studies will continue to provide more information as to the exact nature of the interaction of O_2 and CO, together and separately, with gold clusters. For instance, the development[214,215] of electron diffraction of mass selected clusters provides an opportunity to study the structural characteristics of the $Au_N(CO)_M^-$ system at each stage of adsorption and reaction with O_2. Furthermore, infrared spectroscopy has been used

with success on the supported gold cluster systems[53-56] to distinguish between different forms of CO binding, and the use of recently-improved methods of infrared absorption-dissociation on a mass selected cluster beam or in an ion trap could provide important information as to the bonding characteristics of the CO and O_2 adsorbates and their reaction products.[109,110,124,147] Combined with the information on reactivity, these types of techniques could aid in the determination of the reaction mechanisms of adsorption of O_2 and CO, as well as provide information concerning the production of CO_2 on a step-by-step basis.

APPENDIX A

ADSORPTION OF SULFUR DIOXIDE ON SELECTED GOLD CLUSTER ANIONS AND THEIR HYDROXIDES

A.1 Introduction

Sulfur dioxide is a major pollutant arising from the combustion of fossil fuels, such as coal, natural gas, and oil in homes, automobiles, and energy production.[216] Its removal from the atmosphere is important for several reasons. First, as SO_2 is used for the industrial production of sulfuric acid, H_2SO_4, similar process can occur in the atmosphere, leading to acid rain. Additionally, for many catalytic metal surfaces, the presence of SO_2 can drastically decrease their catalytic activity. SO_2 has been shown in the inorganic literature[217,218] to act as a σ-donor and π-acceptor, much as CO. However, with a much higher electron affinity than CO (1.1 eV versus -1.8 eV), SO_2 is expected to act as a much stronger π-acceptor. On many transition metal surfaces {Fe, Rh, W, Ni, Pd, Pt, Cu, and Zn}, SO_2 shows spontaneous or thermally activated

decomposition.[216,219-221] A notable exception is Ag, on which SO_2 adsorbs and desorbs molecularly. This has been explained by the reasoning that the 4d orbitals of Ag are too low in energy to take part in bonding with the LUMO of SO_2, which would aid in S-O bond cleavage.[216,222]

Sulfur containing molecules are one of the few species known to adsorb on gold surfaces at room temperature.[52] This ability has been exploited to create self-assembled monolayers, and the adsorption characteristics of thiols,[223] hydrogen sulfide,[224] and other sulfide containing compounds[225] have been well studied. Surprisingly, however, very little work has been carried out to understand the adsorption properties of SO_2 on gold surfaces. A recent study by Haruta and coworkers dealt with the effects of SO_2 on CO oxidation over supported gold cluster catalysts.[60] They found that the supported Au catalysts showed extreme attenuation in CO oxidation activity when SO_2 was included in the reactant gas feeds. After subsequently removing SO_2 from the gas feeds, they found that the CO oxidation activity of the catalysts did not recover. Also, the oxygen adsorption activity of the catalysts was significantly reduced after sulphation. As the perimeter sites between the Au cluster and the substrate have been suggested as the active sites of the catalysts,[53,54] it was proposed that, since SO_2 binds more strongly to metal oxide surfaces than to metallic surfaces, SO_2 is likely to bind at the gold/metal oxide interface. With these sites occupied, O_2 is not able to adsorb and become activated, thereby halting the CO oxidation activity of the catalysts.

More recent findings have been published dealing with the subject of SO_2 adsorption on a metallic gold surface.[222] In this study, thermal desorption spectroscopy (TDS) and high-resolution x-ray photoelectron spectroscopy (XPS) were used to study the chemistry of SO_2 and several other compounds on the Au (111) surface. TDS showed that the SO_2 desorption process is entirely molecular, with only a single desorption peak at low SO_2 coverages and a peak assigned to condensed multilayers of SO_2 at higher coverages. Analysis of the main desorption peak yielded a desorption activation energy of approximately 0.3 eV. XPS carried out at various temperatures confirmed the TDS data, with the loss of sulfur-related XPS signal at the desorption temperature seen in the desorption spectra. The small (~15 K) difference between the main and multilayer desorption peaks was interpreted to indicate extremely weak bonding between the gold surface and SO_2. As with the interpretation made for SO_2-Ag(bulk) bonding,[216] it was suggested that the gold d-electrons are much too strongly bound to play any part in a more attractive bonding interaction with SO_2.

More recently, the same group formed gold clusters on a TiO_2 (110) substrate by standard methods and studied the interaction of SO_2 with the Au/TiO_2 (110) system using high-resolution photoemission experiments.[63] In contrast to the adsorption characteristics of SO_2 on bulk gold (described above) or on TiO_2 (110), in which surface sulfate-like species are formed, the photoemission studies show a clear increase in atomic sulfur intensity, due to the complete dissociation of SO_2, upon dosing onto the Au/TiO_2 (110) system at room temperature. Increasing amounts of gold on the surface (up to ~0.5 ML) resulted in increasing amounts of atomic sulfur, and preannealing of the sample

prior to introducing SO_2 led to even greater extent of dissociation. It was also noted that these supported gold clusters adsorb and dissociate SO_2 with an activity comparable to that of several other highly active transition metal surfaces. While the research of Rodriguez *et al.* showed that the Au/TiO_2 system is highly efficient in cleaving the S-O bonds of SO_2 and could thereby find use as desulfurization catalysts,[63] in light of the work of Haruta and coworkers,[60] one is faced with a dilemma. Using these catalysts in applications to remove sulfur-compounds would significantly hinder their ability to act as CO oxidation catalysts.

In the work presented here, the interactions of SO_2 on small ($N \leq 8$) gold cluster anions, Au_N^-, and their hydrated derivatives, Au_NOH^- were studied. Using pulsed-helium flow reactor techniques, studies were performed to observe the activities and approach to saturation of the different cluster species, some of which are surprising and in contrast to common assumptions.

A.2 Experimental Methods (Abbreviated)

The experimental techniques used to study the adsorption properties of SO_2 on both bare and hydrated gold clusters at ambient temperature have been described previously[193] and in Chapter 4, so only a brief description will be given here. Charged gold clusters were formed and equilibrated by laser vaporization of a rotating and translating gold rod in a high-pressure helium/ ^2H_2O flowstream, produced using a pulsed

valve with a stagnation pressure of approximately 3.5 bar. Prior to entering the stagnation region of the primary pulsed-gas valve, the helium was bubbled through ^2H_2O, thereby saturating the helium with the vapor pressure of water at room temperature (~20 mbar). The clusters were then exposed to a gas pulse from a secondary pulsed valve containing a dilute reactant gas (approximately 10% SO_2:He with a stagnation pressure of ~ 2 bar), expanded into vacuum, and were detected by time-of-flight mass spectrometry, using perpendicular pulsed extraction fields.

A.3 Results

The methods described above were used to study the adsorption characteristics of SO_2 on bare and hydrated gold cluster anions, Au_N^- and Au_NOH^-, respectively. Providing a temporal offset between the main (cluster) pulse and the secondary (reactant gas) pulse produced mass spectra of the type shown in the bottom frame of **Figure A-1**. By overlapping the two gas pulses, spectra of the type shown in the top frame of **Figure A-1** were obtained. In this figure, $Au_N(OH)_M(SO_2)_L^-$ clusters are shown and are denoted by the formula N,M,L. As can be seen in the bottom frame, when the gas pulses are temporally offset, only peaks corresponding to bare and hydrated gold cluster anions are acquired. By overlapping the gas pulses, peaks corresponding to the addition of SO_2 molecules to the clusters are obtained, corresponding to the formula

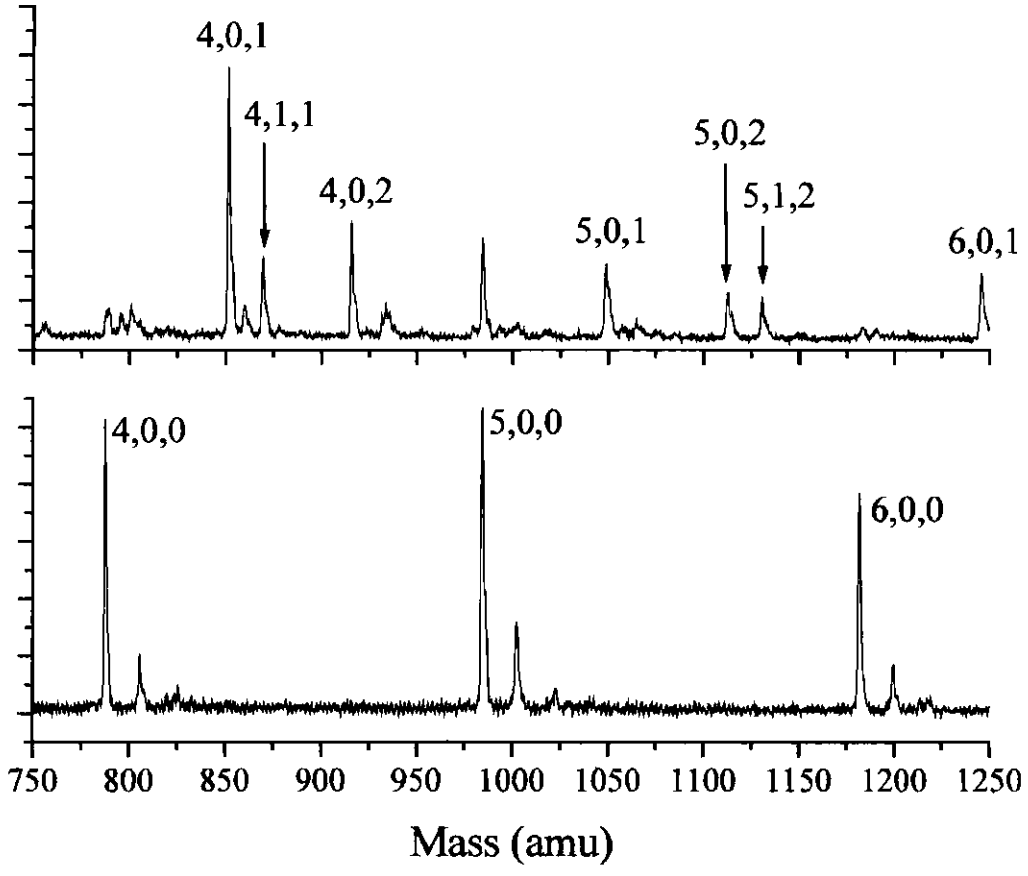

Figure A-1: SO_2 Adsorption on bare and hydrated gold cluster anions

(Bottom frame) A mass spectrum obtained when the main (cluster) and secondary (reactant) gas pulses are temporally offset, leading to no reaction. The numbering scheme refers to $Au_N(OH)_M(SO_2)_L^-$ = N,M,L. (Top frame) Mass spectrum obtained when the two gas pulses are overlapped with an SO_2 partial pressure of ~0.5 mbar. This overlap results in the depletion of the Au_N^- and Au_NOH^- peaks and the growth of peaks corresponding to the primary and secondary adsorption of SO_2.

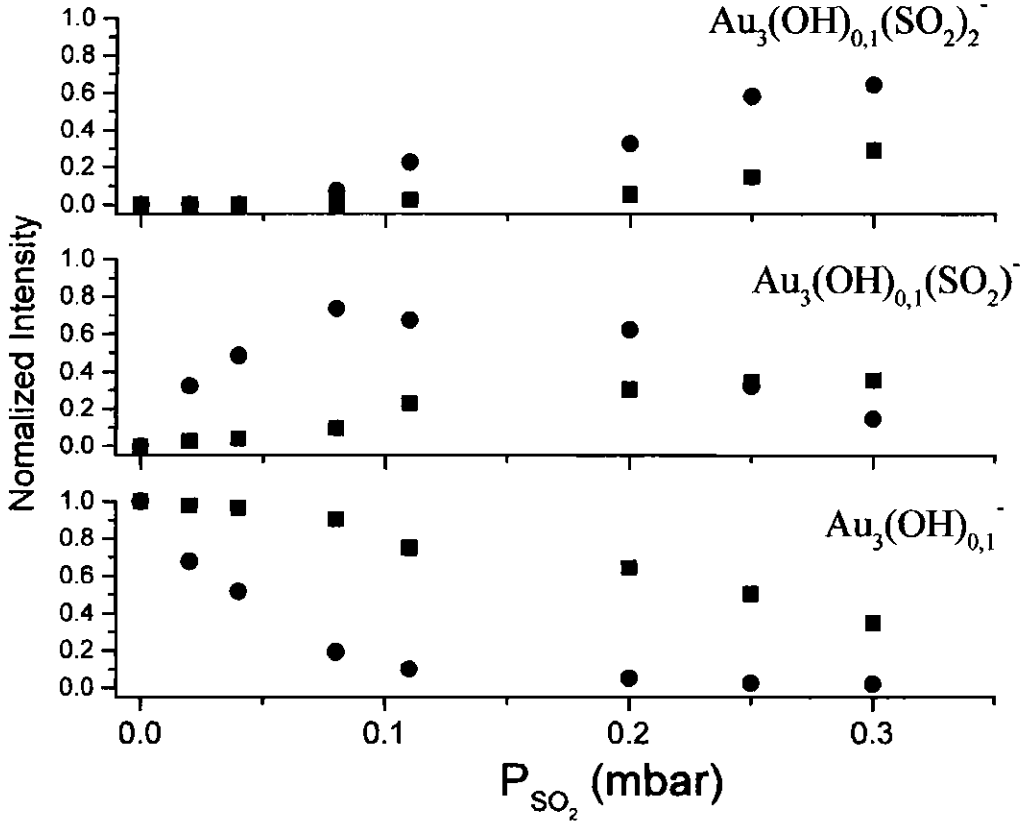

Figure A-2: Comparison of bare and hydrated cluster activity

A direct comparison of the activities of $Au_3(OH)_{0,1}^-$ (zero OH: squares; one OH: circles) species towards SO_2 adsorption as a function of reactant partial pressure in the lower pressure regime. (Bottom frame) Parent cluster intensity (Middle frame) Intensity of clusters with a single SO_2 adsorbate (Top frame) Intensities of clusters with two SO_2 adsorbates. At lower partial pressures, the hydrated cluster, Au_3OH^-, is much more active. This initial higher activity persists over the entire cluster size range studied.

$$Au_N(OH)_M^- + L \bullet SO_2 \rightarrow Au_N(OH)_M(SO_2)_L^- \quad (1).$$

Relatively small amounts of SO_2 (approximately 0.5 mbar) lead to the addition of up to 2 SO_2 molecules to all of the bare and hydrated clusters discussed here with the exception of Au_8OH^-.

By performing pressure dependent experiments, the activities of the bare clusters in relation to the hydrated clusters could be compared. **Figure A-2** provides a direct comparison of the normalized cluster intensities of the Au_3^- (squares) and Au_3OH^- (circles) systems. The bottom frame shows the depletion of bare cluster signal with increasing amounts of SO_2 in the flow reactor. With the addition of very little reactant, Au_3OH^- begins to quickly adsorb an SO_2 molecule, while the bare cluster remains relatively inactive. For all of the clusters studied here, the hydrated clusters are initially more active for SO_2 addition.

Increasing the reactant partial pressure in the flow reactor leads to further SO_2 adsorption on the clusters. A more extensive pressure dependence for the bare (N = 1 - 7) and hydrated (N = 2 - 5) clusters than in **Figure A-2** is shown in **Figures A-3** through **A-13**. Here, the normalized cluster intensities of all of the species present for a specific cluster size, N, are plotted as a function of SO_2 partial pressure. A representative mass spectrum obtained under the highest-pressure conditions used in these figures is shown in **Figure A-14** for the same mass range as **Figure A-1**. The mass spectra obtained under these conditions are complicated by the growth of new peaks between the bare and

hydrated clusters and their adsorbate complexes. These are due to the metastable loss of a water molecule in the first free-flight region of the mass spectrometer, as described previously.[130,154] Further increase in SO_2 partial pressure leads to little more reaction for many of the clusters. One method of observing this behavior is to study the maximum number of adsorbates on the different clusters. These maximum numbers of adsorbates under three different reactant partial pressures are presented in **Figures A-15** through **A-17** (With each partial pressure jump, the mass range decreased, as increasing amounts of both reactant and buffer gas tended to attenuate the higher mass signal). However, these values do not tell the entire story, as their mere presence does not indicate how statistically significant a role they may play in the analysis of cluster reactivity and saturation. A statistical measure of determining the extent of adsorption of SO_2 on the clusters (as well as to determine the relative importance of the "maximum" number of adsorbates) is to observe the average (mean) number of adsorbates. The mean number of adsorbates on Au_N^- clusters are plotted as a function of SO_2 partial pressure in **Figures A-18** (N = 1 - 4) and **A-19** (N = 5 - 7), while the mean number of adsorbates on the Au_NOH^- clusters are plotted in **Figure A-20** (N = 2 - 5).

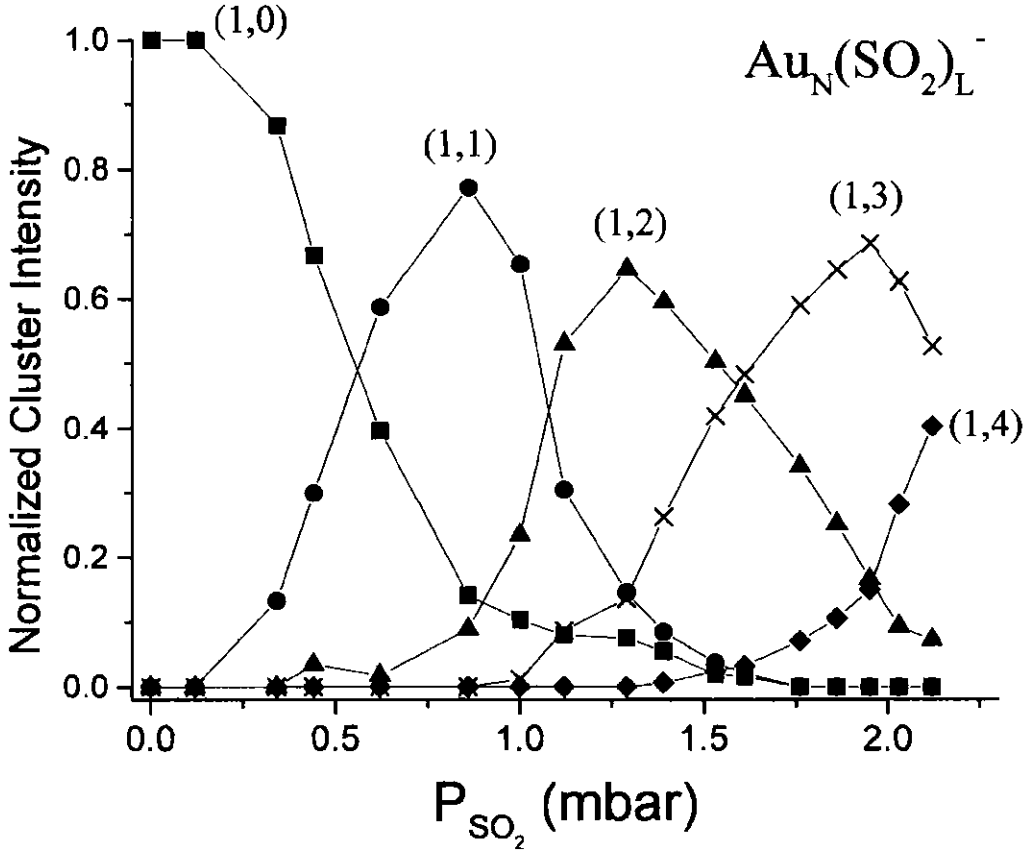

Figure A-3: SO_2 adsorption on Au^-

Normalized cluster abundances produced with increasing amounts of SO_2 in the flow reactor. The numbers in parenthesis correspond to the number of gold atoms (N) and SO_2 adsorbates (L).

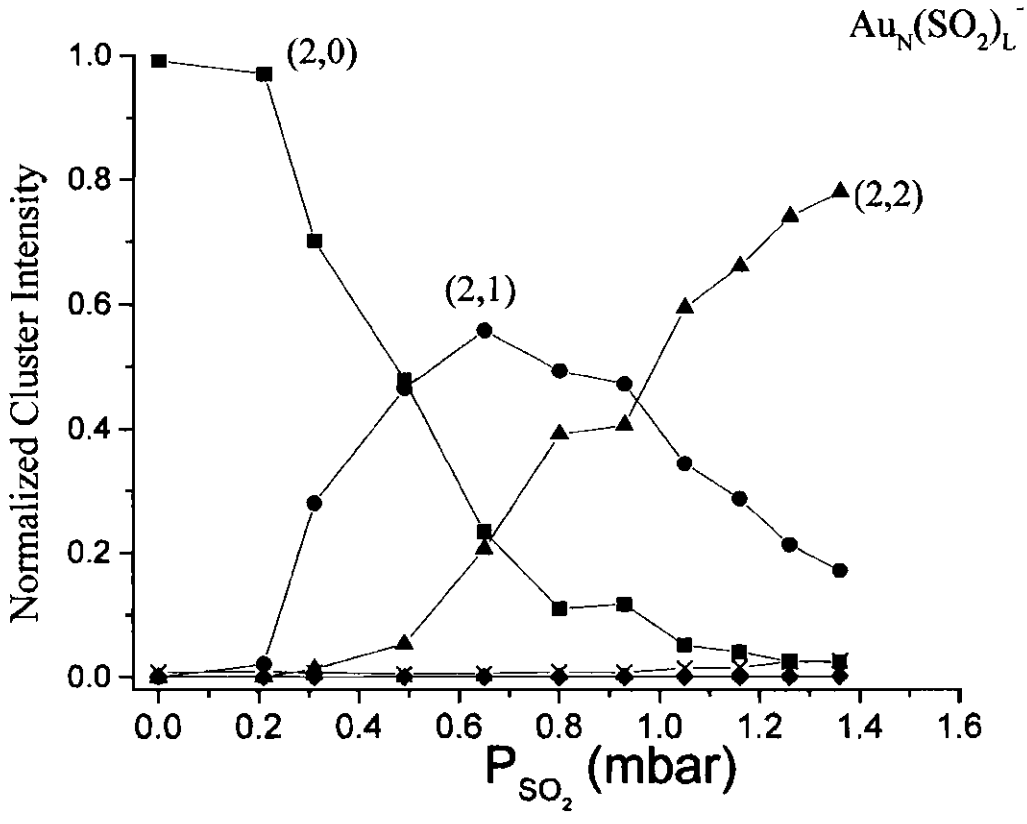

Figure A-4: SO_2 adsorption on Au_2^-

Normalized cluster abundances produced with increasing amounts of SO_2 in the flow reactor. The crosses represent the abundances arising from the addition of a third SO_2 molecule and the diamonds represent the addition of a fourth adsorbate. The numbers in parenthesis correspond to the number of gold atoms (N) and SO_2 adsorbates (L).

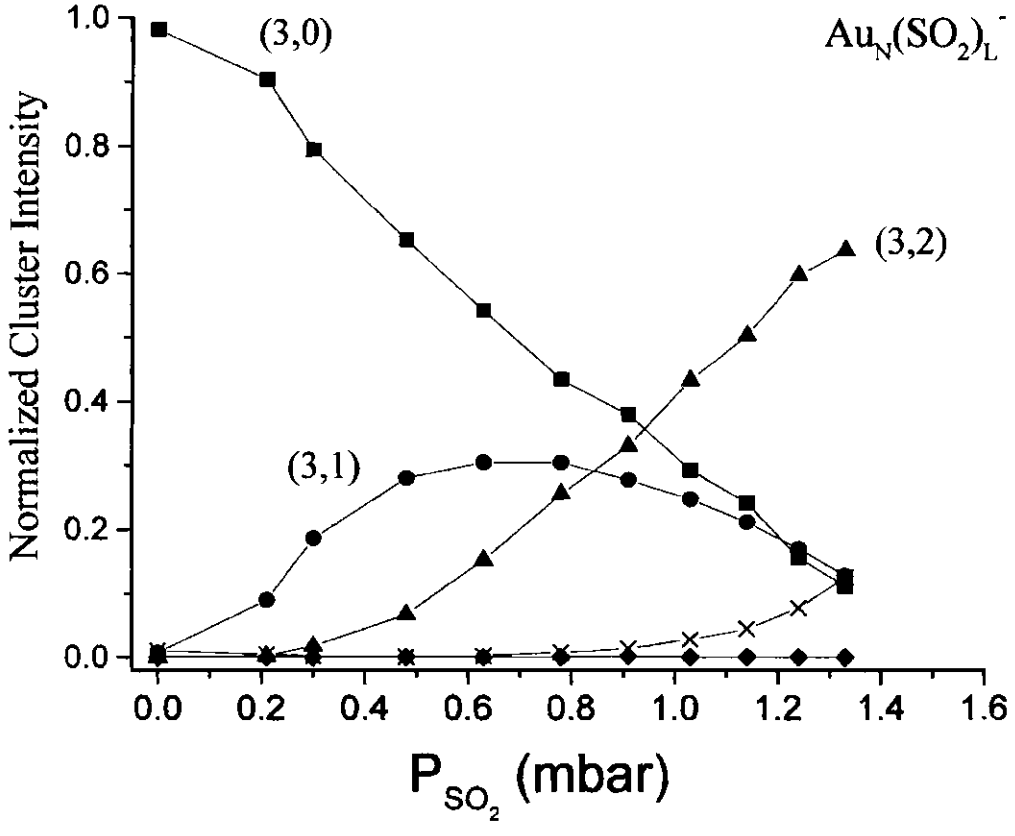

Figure A-5: SO_2 adsorption on Au_3^-

Normalized cluster abundances produced with increasing amounts of SO_2 in the flow reactor. The crosses represent the abundances arising from the addition of a third SO_2 molecule and the diamonds represent the addition of a fourth adsorbate. The numbers in parenthesis correspond to the number of gold atoms (N) and SO_2 adsorbates (L).

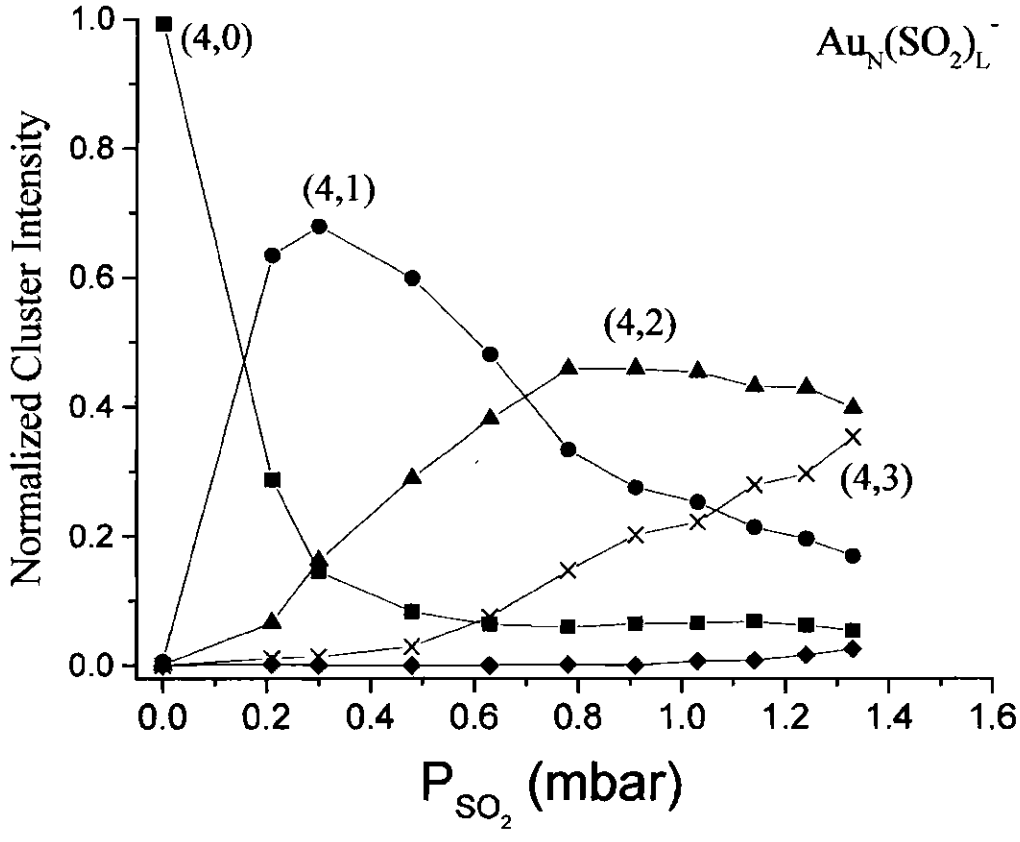

Figure A-6: SO_2 adsorption on Au_4^-

Normalized cluster abundances produced with increasing amounts of SO_2 in the flow reactor. The diamonds represent abundances arising from the addition of a fourth SO_2 adsorbate. The numbers in parenthesis correspond to the number of gold atoms (N) and SO_2 adsorbates (L).

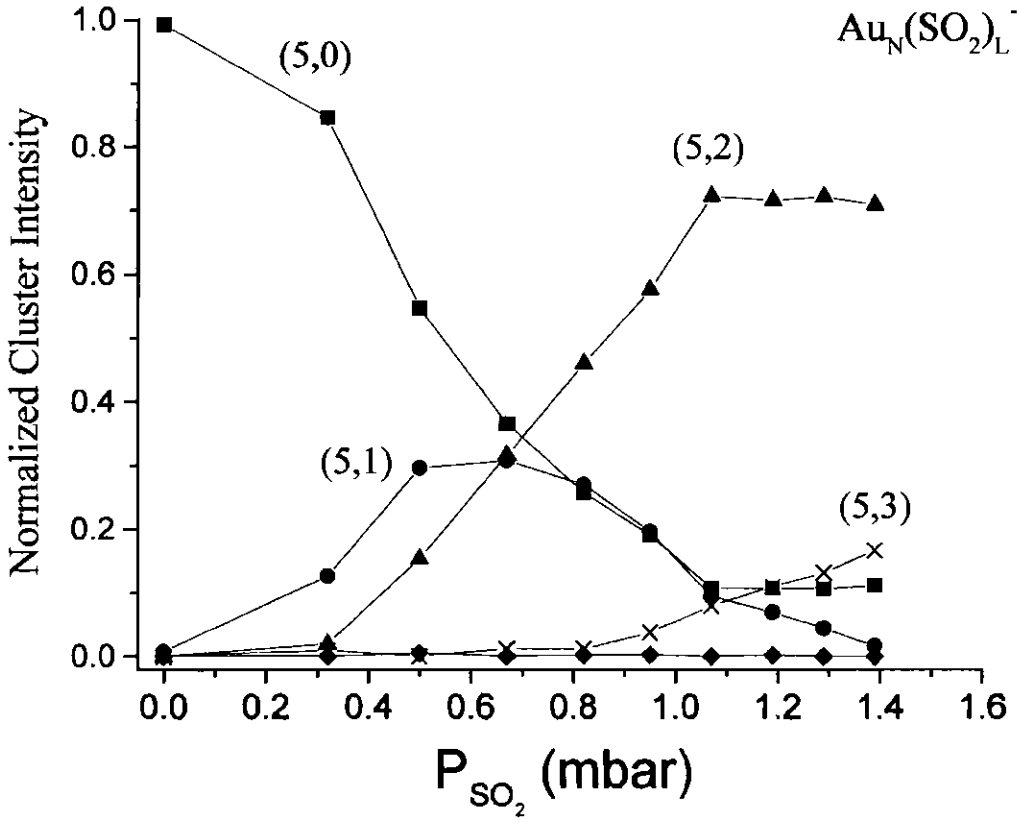

Figure A-7: SO_2 adsorption on Au_5^-

Normalized cluster abundances produced with increasing amounts of SO_2 in the flow reactor. The diamonds represent abundances arising from the addition of a fourth SO_2 adsorbate. The numbers in parenthesis correspond to the number of gold atoms (N) and SO_2 adsorbates (L).

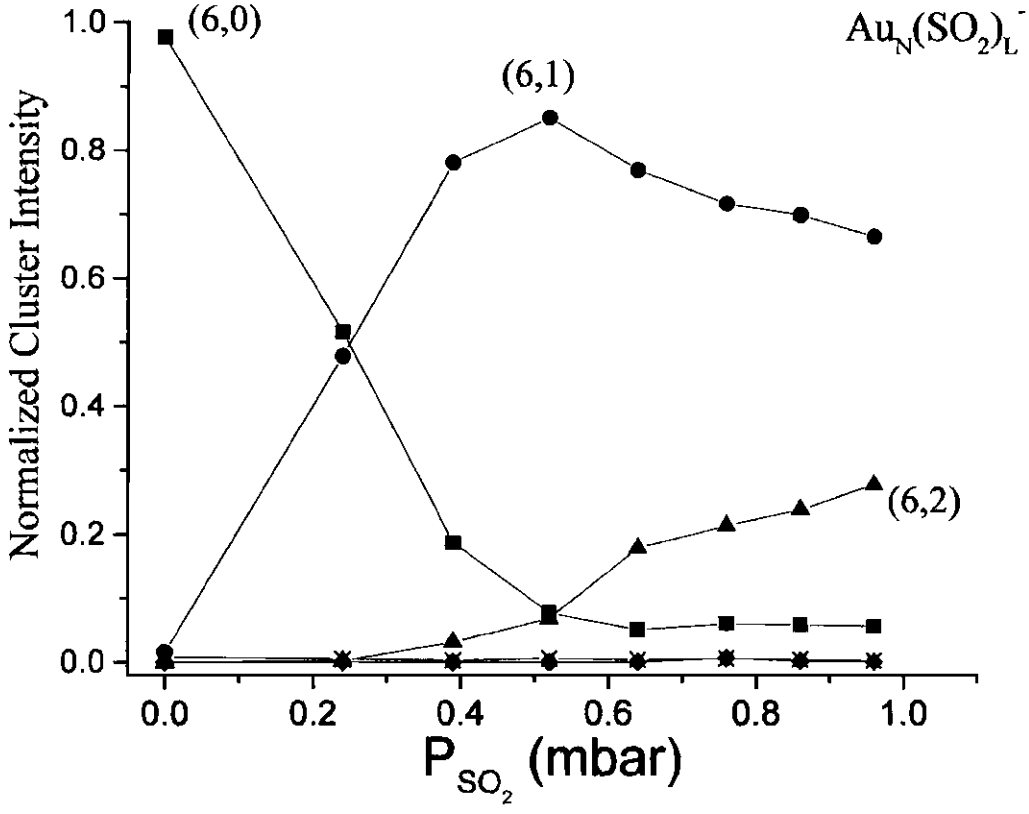

Figure A-8: SO_2 adsorption on Au_6^-

Normalized cluster abundances produced with increasing amounts of SO_2 in the flow reactor. The crosses represent the abundances arising from the addition of a third SO_2 molecule and the diamonds represent the addition of a fourth adsorbate. The numbers in parenthesis correspond to the number of gold atoms (N) and SO_2 adsorbates (L).

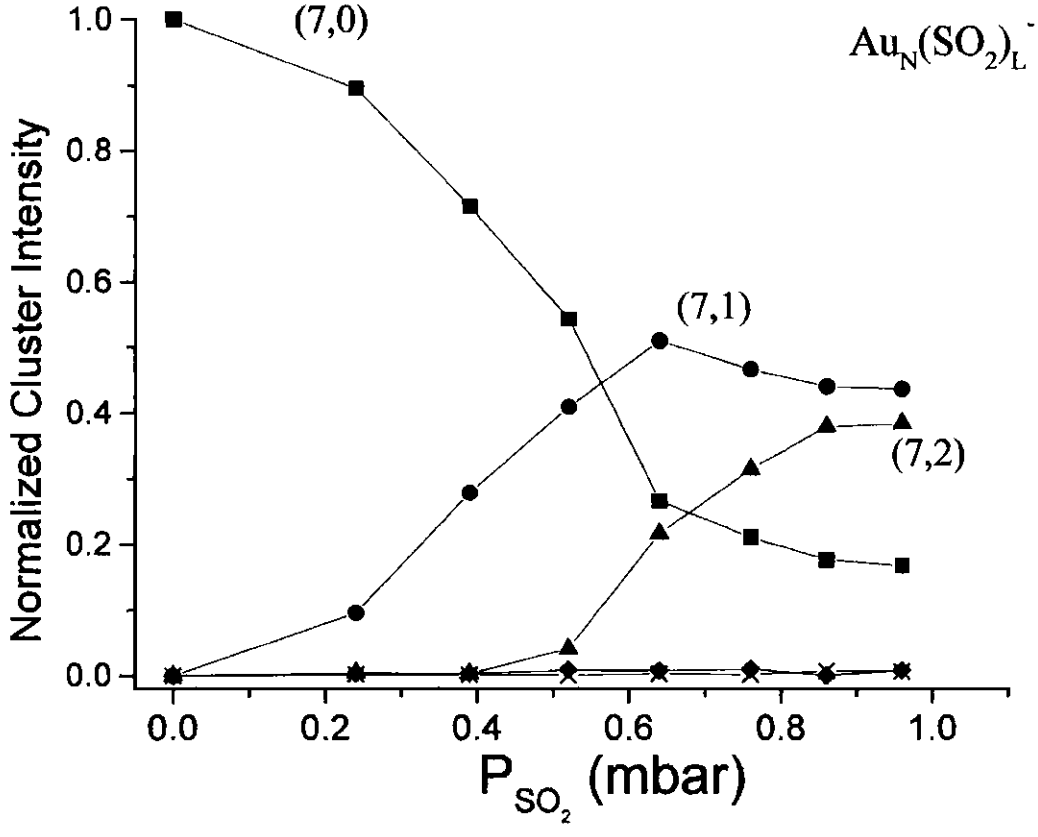

Figure A-9: SO_2 adsorption on Au_7^-

Normalized cluster abundances produced with increasing amounts of SO_2 in the flow reactor. The crosses represent the abundances arising from the addition of a third SO_2 molecule and the diamonds represent the addition of a fourth adsorbate. The numbers in parenthesis correspond to the number of gold atoms (N) and SO_2 adsorbates (L).

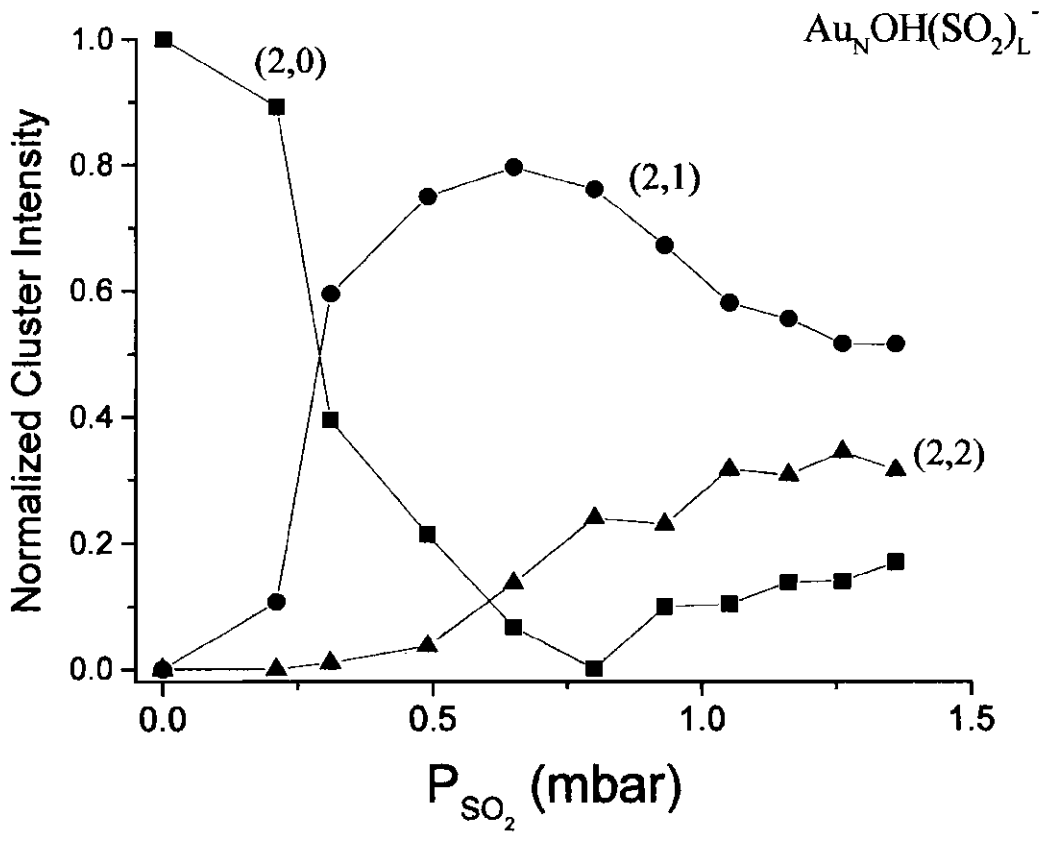

Figure A-10: SO_2 adsorption on Au_2OH^-

Normalized cluster abundances produced with increasing amounts of SO_2 in the flow reactor. The numbers in parenthesis correspond to the number of gold atoms (N) and SO_2 adsorbates (L).

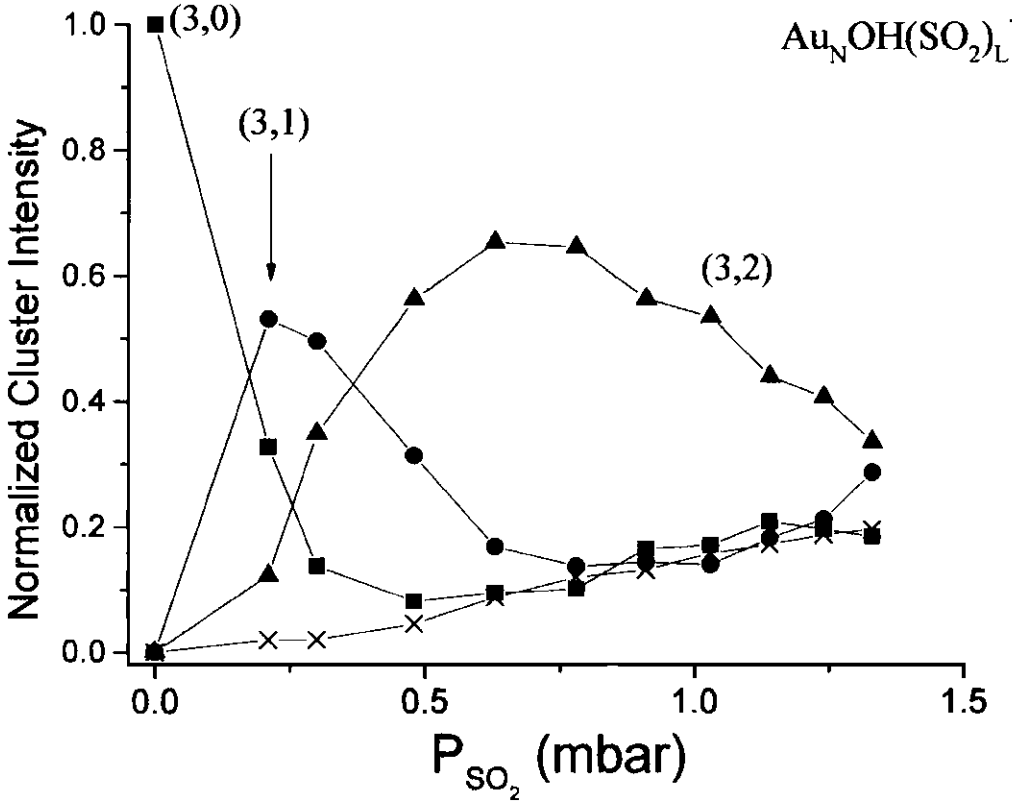

Figure A-11: SO_2 adsorption on Au_3OH^-

Normalized cluster abundances produced with increasing amounts of SO_2 in the flow reactor. The crosses represent the abundances arising from the addition of a third SO_2 molecule and the diamonds represent the addition of a fourth adsorbate. The numbers in parenthesis correspond to the number of gold atoms (N) and SO_2 adsorbates (L).

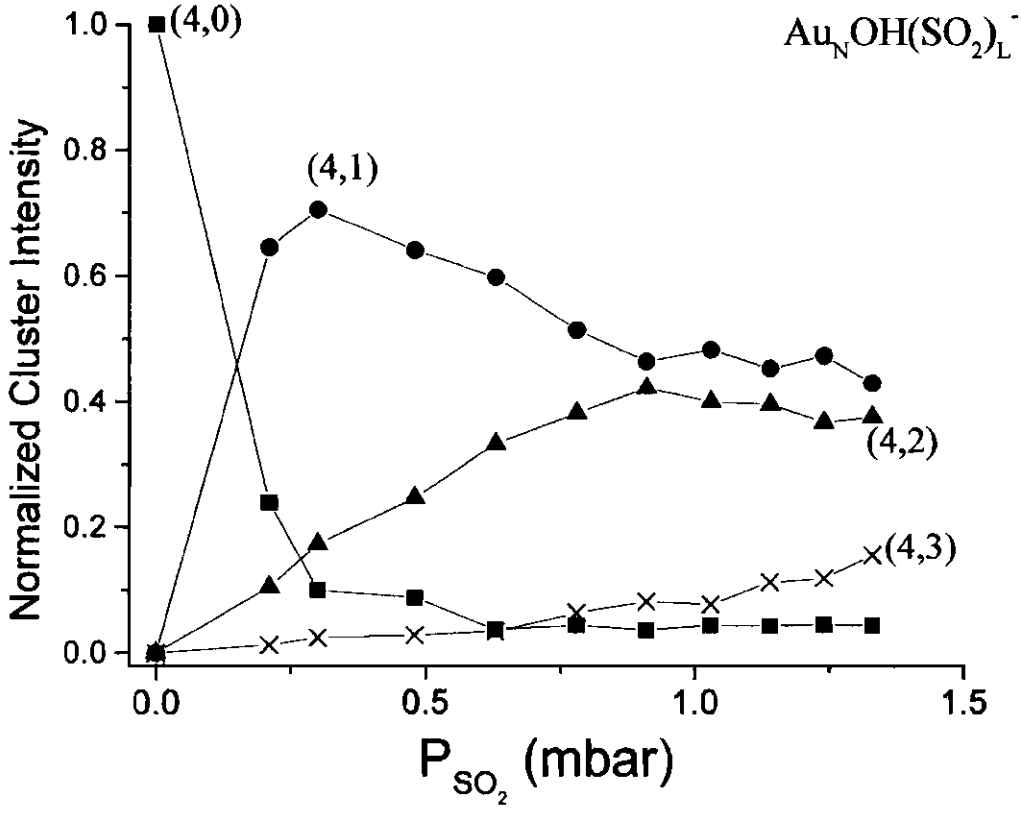

Figure A-12: SO_2 adsorption on Au_4OH^-

Normalized cluster abundances produced with increasing amounts of SO_2 in the flow reactor. The diamonds represent the abundances arising from the addition of a fourth SO_2 molecule. The numbers in parenthesis correspond to the number of gold atoms (N) and SO_2 adsorbates (L).

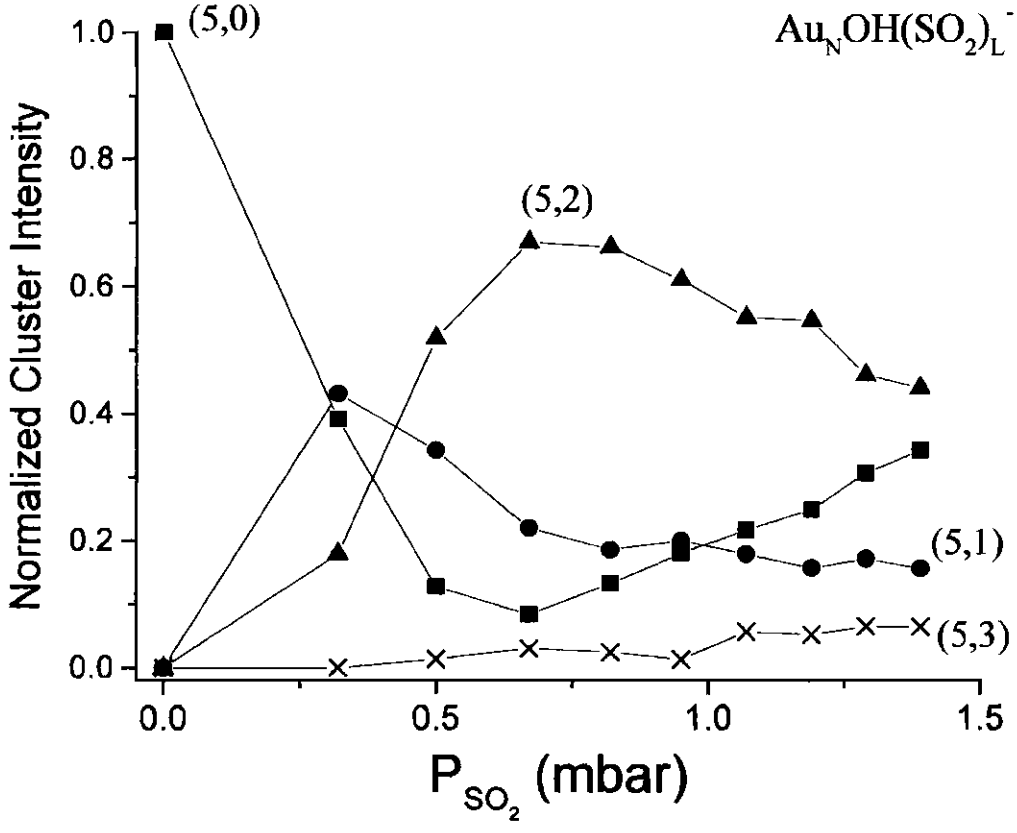

Figure A-13: SO_2 adsorption on Au_5OH^-

Normalized cluster abundances produced with increasing amounts of SO_2 in the flow reactor. The numbers in parenthesis correspond to the number of gold atoms (N) and SO_2 adsorbates (L).

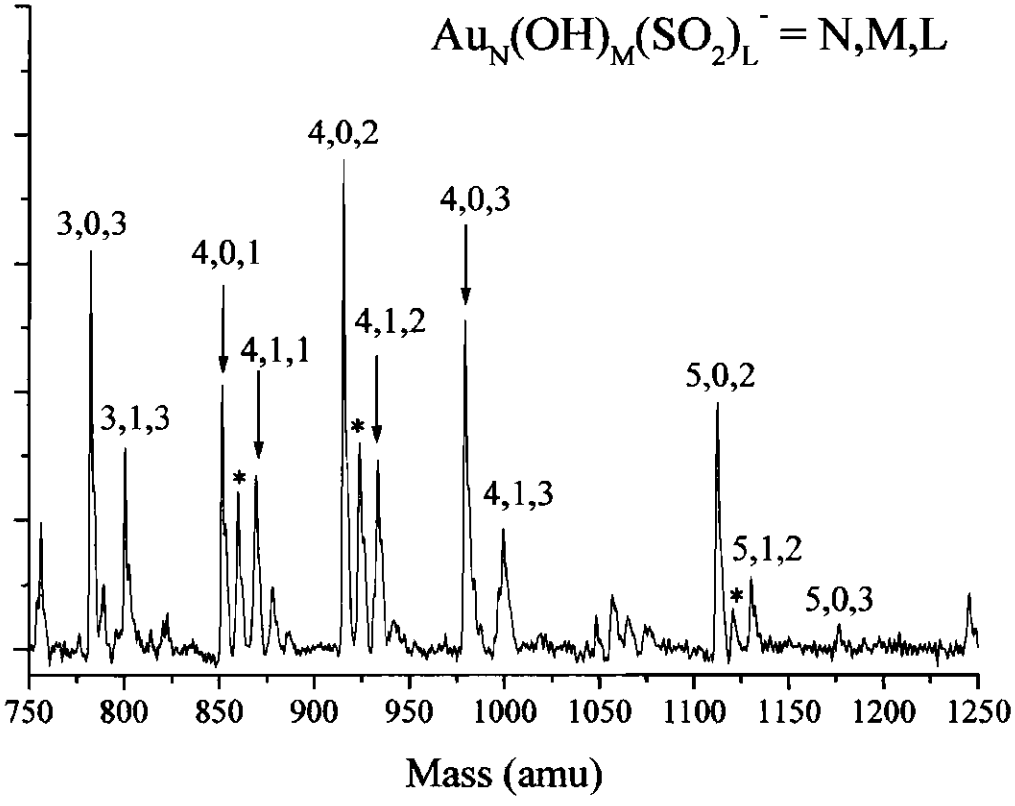

Figure A-14: Reaction of $Au_N(OH)_M^-$ clusters with SO_2

Mass spectrum obtained when the main and secondary gas pulses are temporally overlapped with an SO_2 partial pressure of ~1.1 mbar. The presence of 3 SO_2 adsorbates is apparent on several of the clusters. The peaks marked with asterisks correspond to the metastable loss of H_2O in the first free-flight region of the mass spectrometer, as described previously.[154]

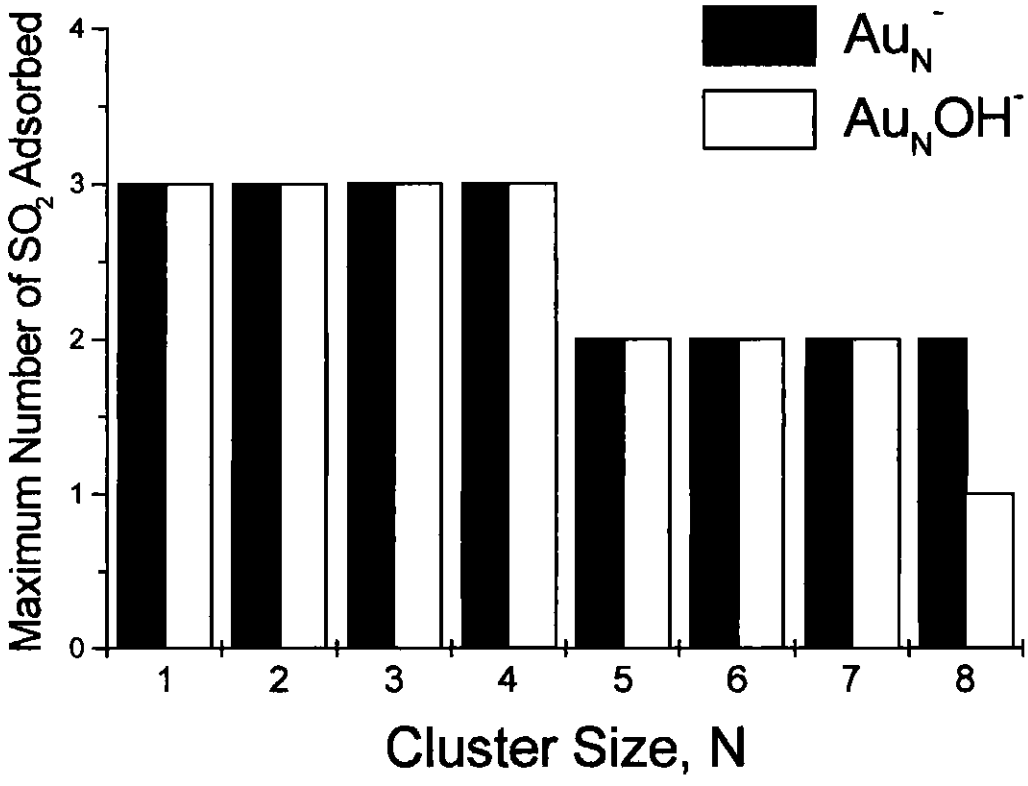

Figure A-15: Maximum number of SO_2 adsorbates (lower pressure)

Largest cluster-adsorbate species observed as a function of cluster size at a reactant partial pressure of ~1 mbar.

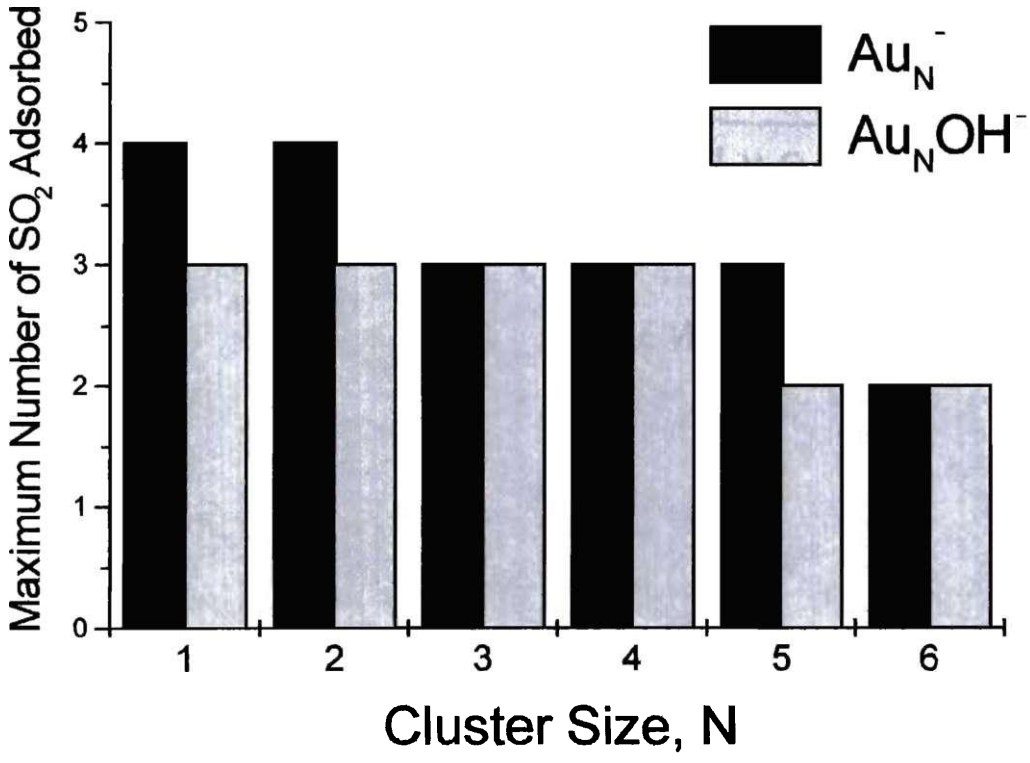

Figure A-16: Maximum number of SO_2 adsorbates (medium pressure)

Largest cluster-adsorbate species observed as a function of cluster size at a reactant partial pressure of ~1.4 mbar.

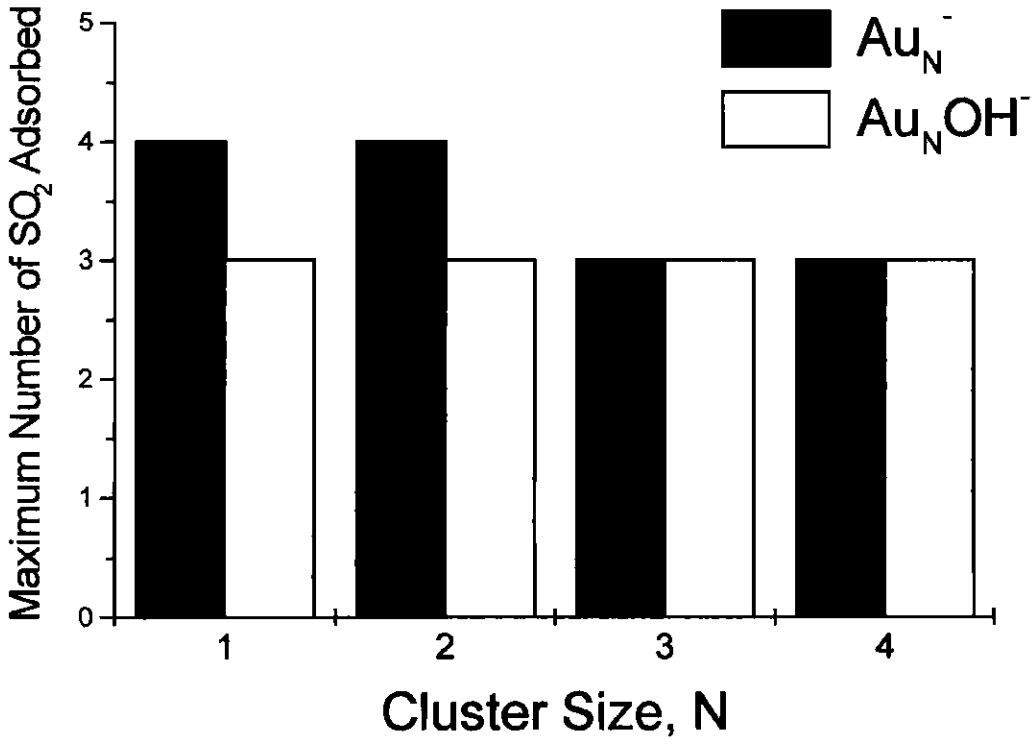

Figure A-17: Maximum number of SO_2 adsorbates (high pressure)

Largest cluster-adsorbate species observed as a function of cluster size at a reactant partial pressure of ~3.2 mbar.

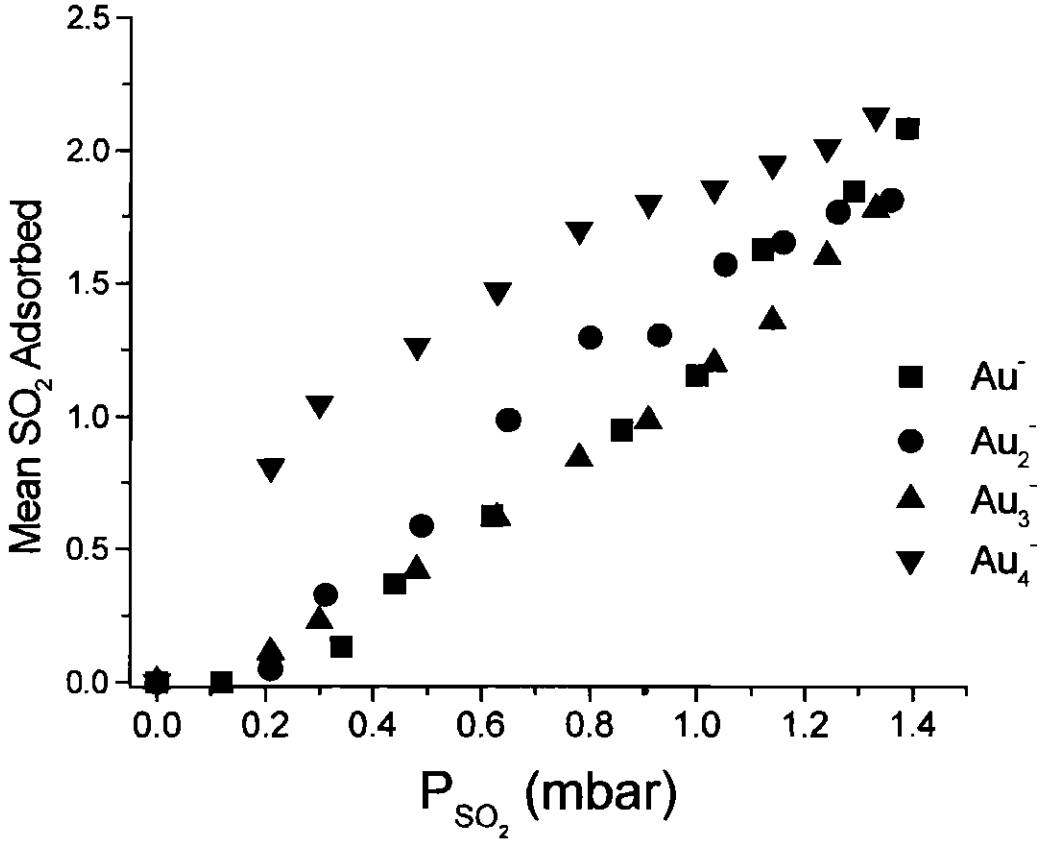

Figure A-18: Variable adsorption of SO_2 on small Au_N^- clusters

Change in mean SO_2 adsorption on small gold cluster anions (N = 1 - 4) as a function of reactant partial pressure. Each of the clusters shows an increase in adsorption with increasing pressure.

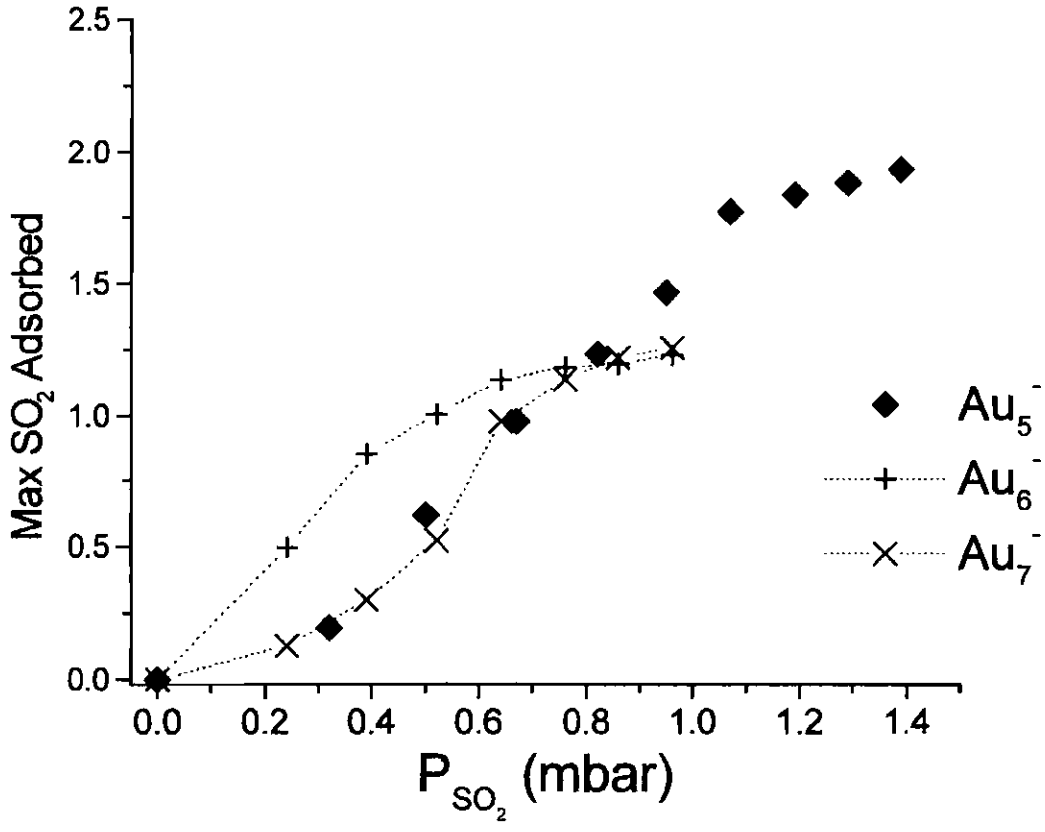

Figure A-19: Variable adsorption of SO_2 on larger Au_N^- clusters

Change in mean SO_2 adsorption on larger gold cluster anions (N = 5 - 7) as a function of reactant partial pressure. In contrast to **Figure A-18**, these cluster species show definite indications of a reluctance to add additional SO_2 molecules.

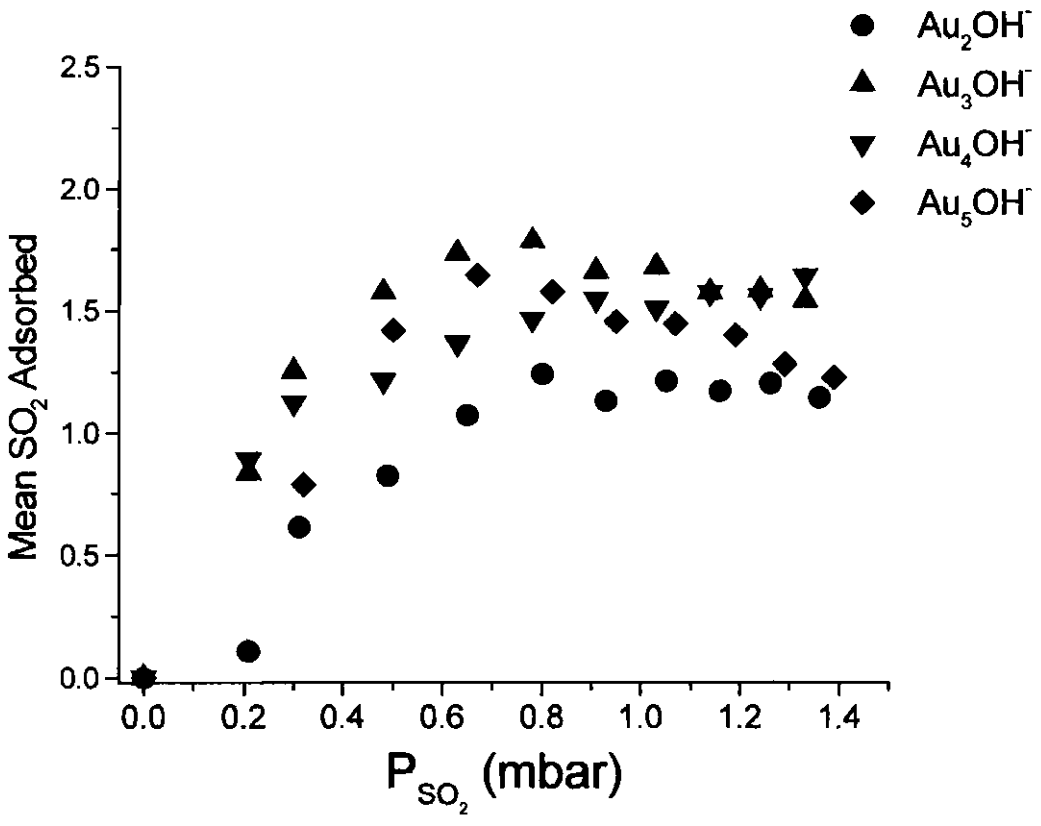

Figure A-20: Variable adsorption of SO_2 on selected Au_NOH^- clusters

Change in mean SO_2 adsorption on small hydrated gold cluster anions (N = 2 - 5) as a function of reactant partial pressure. Each of the clusters shows an increase in adsorption with increasing pressure, until showing a decrease in the mean number of adsorbates, except for Au_4OH^-.

A.4 Discussion

A.4.1 Mass Abundances

The mass abundances shown in **Figures A-3** through **A-13** are interesting in several regards. First, the very active nature of the gold monomer anion towards adsorption of SO_2 is quite surprising. In the gas-phase, this ion is not known to show a great deal of reactivity[226] towards neutral species, with activity towards hexafluorobenzene[227] and S_N2 displacement reactions of alkyl halides[228] being some of the few reactions seen.[228] In contrast, the present results show that Au^- not only is active towards adsorption of SO_2, but adsorbs up to 4 SO_2 molecules in the pressure regimes studied (**Figures A-3** and **A-17**). While the source of this incredible activity is not known, it certainly presents intriguing opportunities for further study. For instance, ion-molecule thermochemical studies could be performed in order to determine the absolute step-wise equilibrium constants of this system as a function of temperature.[229] Studies such as this would provide yet another calibration experiment for groups using fast-flow reactors, as described in Chapter 2.

For the remainder of the bare clusters presented in **Figures A-4** through **A-9**, the activities towards initial SO_2 adsorption are similar, with the maximum abundance of the $Au_N(SO_2)^-$ species appearing at relatively constant SO_2 pressures in the reactor. In each case, a large amount of the single adsorbate species is produced prior to the onset of secondary adsorption, with tertiary adsorption following the same behavior. A notable deviant from the other small, bare gold clusters is Au_4^-, in which the single SO_2

adsorption maximum peaks much earlier, at approximately 0.3 mbar. The corresponding beginning of secondary adsorption also occurs at much lower pressures than the other clusters, indicating that Au_4^- is especially active for SO_2 addition.

The pressure-dependent adsorption characteristics of the hydrated gold cluster anions presented in **Figures A-10** through **A-13** (N = 2 - 5) do not provide as simple an analysis. At lower SO_2 partial pressures, all of the clusters behave very similarly, quickly depleting the bare cluster species and adding SO_2. However, at approximately the same SO_2 partial pressure (and, therefore, overall reactor pressure), while Au_4OH^- behaves much as the non-hydrated clusters, the other hydrated cluster species (N = 2,3,5) begin to show curious behavior. At pressures higher than this onset, an *increase* in the bare (Au_NOH^-) cluster signal is observed, with a corresponding decrease in several of the cluster species possessing adsorbates. This behavior may simply imply that SO_2 is bound more weakly to the hydrated cluster anions than to the bare clusters and the extra collisions endured by the cluster-adsorbate complexes simply fall apart in the flow reactor. However, this explanation raises some interesting questions. First, why does Au_4OH^- act differently than the other clusters, simply adding SO_2 as the reactant partial pressure is increased? Secondly, why does Au_3OH^-, which *does* show an increase in bare cluster intensity, also show a corresponding growth in a cluster species corresponding to $Au_3OH(SO_2)_3^-$? At this point, there are no satisfactory answers to these questions, but they certainly provide impetus for future work on these species.

The maximum adsorption values seen for the Au_N^- and Au_NOH^- clusters at much different SO_2 partial pressures are also very interesting. First, for both the bare and

hydrated gold cluster anions, with increasing cluster size, N, the maximum number of adsorbates is seen to decrease under all of the pressure regimes studied (except for the hydrated clusters under the most extreme conditions, in which there is no decrease). Though one might feel that this is to be expected with the very weak binding energy of SO_2 on the bulk gold surface, it is in direct contrast to that of CO, another weakly bound adsorbate, on similarly-sized, bare gold cluster anions and other cluster anions.[130,230,231] This would seemingly argue against a reaction mechanism dictated by geometric structure, in which larger clusters would conceivably have a larger collision cross-section and presumably more adsorption sites. This decrease in adsorption activity with increasing size also applies to the hydrated cluster anions, though no studies have been done for the Au_NOH^- + CO system to make a direct comparison. The second point of interest concerns the seeming cessation of adsorption after binding a certain number of SO_2 molecules. While the reactant partial pressure change with respect to the maximum number of adsorbates for the larger clusters ($N \geq 5$) is certainly not enough to make a general statement concerning any type of saturation, in the smaller cluster regime, the majority of the clusters show a reluctance towards further adsorption, even over a tremendous pressure increase. For a complete determination of saturation coverages, alternate methods of SO_2 introduction giving higher partial pressures, such as seeding the buffer gas in the main pulsed valve with SO_2,[130,133,192] would likely be needed.

The mean adsorption values plotted in **Figures A-18** through **A-20** provide additional insight into the discussion of the maximum adsorption values described above. **Figure A-18** shows the mean number of SO_2 molecules adsorbed on small Au_N^- clusters (N = 1 -

4). As is readily seen, all of these species (with perhaps the exception of Au_4^-) show a relatively linear increase in number of adsorbates as a function of pressure. After an initial burst of activity (described above), the slope of Au_4^- also is linear. In all cases presented in this figure, the maximum of the plot (at the highest pressure) is a great deal lower than that of the maximum number of adsorbates presented in **Figure A-16**. This fact indicates that, while a certain amount of larger species may be produced, a cluster containing lower numbers of SO_2 adsorbates dominates the mean value, and the maximum values say more about the simple possibility of adding an adsorbate and less about possible saturation or activity of the clusters.

Figure A-19 presents the mean number of SO_2 adsorbates on Au_N^- (N = 5 - 7) clusters. These plots provide some very interesting information concerning the Au_N^- + SO_2 adsorption system. With Au_5^-, there is a gradual rise in mean adsorption with increasing pressure until the slope shows a sharp decrease. As this slope is still increasing, one can read too much into the behavior, so it is important to observe the activity of the surrounding clusters. Au_6^- and Au_7^- provide information with which a definite analysis can be made. In both of the plots showing the adsorption characteristics of these species, an initial rise in activity is followed by a dramatic plateau. This behavior could be indicative of saturation behavior, though, as mentioned above, different experiments would be needed to provide information on absolute saturation. Even so, these plots support the analysis gained from **Figures A-14** through **A-17**, in which adsorption activity decreases with increasing cluster size.

The mean adsorption activity of the hydrated gold cluster anions, Au_NOH^- (N = 2 - 5), are shown in **Figure A-20**. These plots seem to reaffirm the analysis of the pressure-dependent intensity figures shown earlier, as, with the exception of Au_4OH^-, the mean adsorption values show a significant rise before leveling off and beginning a decrease. Once again, the four-atom hydrated gold cluster anion shows behavior that differs from that of its hydrated brethren. Shown even more clearly here than before, the sharp increase in mean number of adsorbates is followed not by a decrease, but by a fairly stable plateau in activity, possibly suggesting saturation of this particular cluster with SO_2.

A.4.2 SO_2 Binding Energetics

In experiments such as these, with moderate transit times in the flow reactor and high buffer gas pressures ($\geq$ 150 mbar) yielding buffer gas collisions on the order of 1 ns^{-1}, it is likely that simple adsorption reactions such as those in (1) are occurring under equilibrium control. In this case, the adsorption free energy is an appropriate measure of the initial activity, which is related to the natural logarithm of the stepwise equilibrium constant, K. A normal approach to determining this value using the Au_N^- + SO_2 system is described by:

$$K = \frac{[Au_N(SO_2)^-]}{P_{SO_2}[Au_N^-]} \qquad (2).$$

The values of the adsorption free energies as a function of cluster size are plotted in **Figure A-21** for several different reactant partial pressures (The results for the hydrated cluster anions were inconclusive and are not shown here). For a reaction occurring under equilibrium conditions, the free energy as a function of size should not change as the reactant partial pressure is changed. For the majority of the clusters, this is indeed the case. For the tetramer, however, an increase in P_{SO2} leads to an increased value of K. At first glance, this could indicate the presence of multiple isomers of Au_4^-, one of which is much more reactive than the other. The presence of isomers would not be unexpected, as that possibility has been predicted previously by Häkkinen and Landman.[99] In general, though, there is an oscillation in free energy, which has been seen for other adsorbates.[133,193] This oscillation can be rationalized using an argument based on electron transfer. With its high electron affinity, SO_2 has been shown to be a strong π-acceptor upon binding to metal species.[216] In this case, the clusters with a lower electron affinity (in this case, the even-N clusters[77]) are better able to donate electron density to the incoming SO_2 molecule. While the odd-N clusters also are able to allow binding by this manner, with their higher electron affinities, this transfer occurs to a lesser extent. This reasoning would suggest that the binding of SO_2 to Au_N^- clusters is determined by cluster electronic structure, rather than geometric structure (as described above).

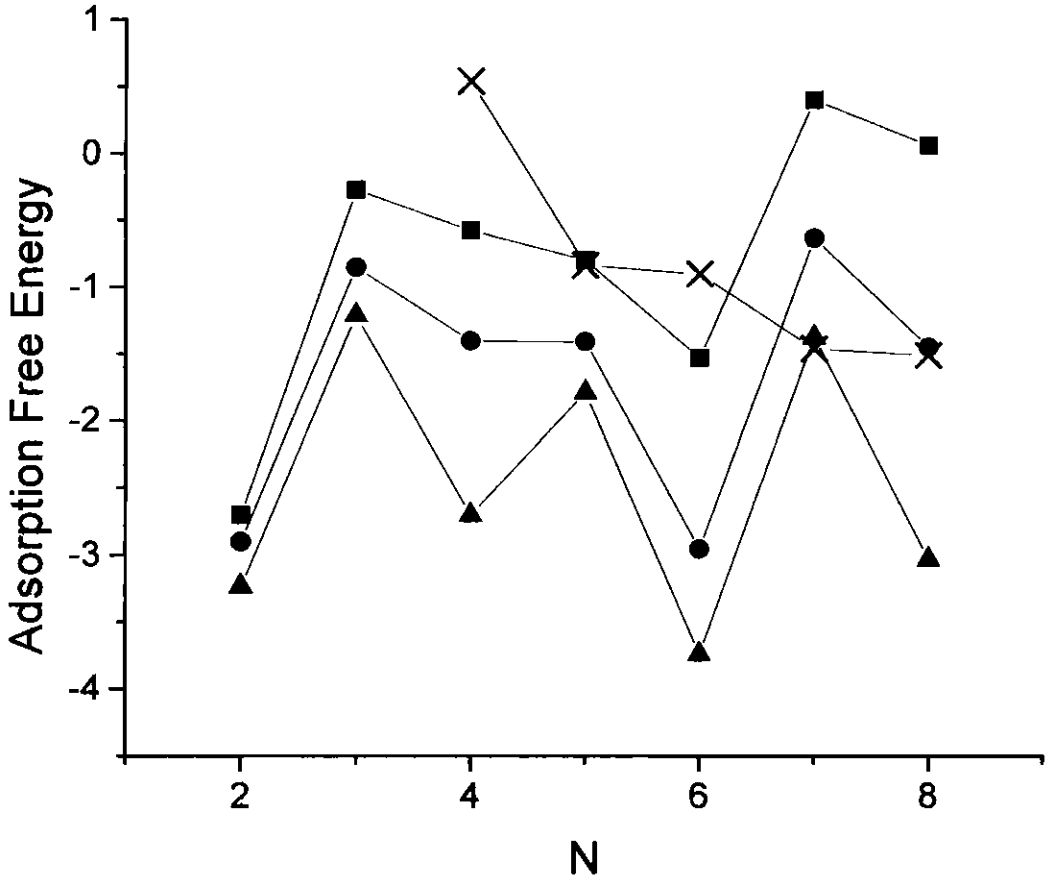

Figure A-21: Adsorption free energy of SO_2 on Au_N^- clusters

The free energy of adsorption (-lnK) as a function of size, N, for 3 different reactant partial pressures. (Squares) 0.08 mbar (Circles) 0.2 mbar (Triangles) 0.3 mbar. The change in the free energy of Au_4^- could indicate the presence of isomers, one which is reactive and one which is not. The crosses represent the free energy of adsorption of CO on Au_N^- clusters at a CO partial pressure of 0.3 mbar and indicate that SO_2 binds much more efficiently under similar conditions.

This simple explanation of the factor behind the adsorption activity certainly could be questioned, as SO_2 is known to bind in several different fashions to metal surfaces[216,219-221] and in inorganic complexes.[217,218] These include η^1-planar, η^1-pyramidal, and η^1-bridging, which each involve bonding through the sulfur atom, η^1 bonding through an oxygen atom, η^2 bonding of both sulfur and an oxygen to a single metal atom, and η^2 bonding involving bridging between two metal centers by both sulfur and oxygen. It could be expected that different forms of binding could not all be explained by the same mechanism. Even so, this explanation provides a first conjecture at a possible binding mechanism, and further theoretical and experimental studies will provide more insight.

It is helpful to study the similarities and differences between SO_2 binding and that of CO on gold cluster anions, Au_N^-, as CO also acts as a σ-donor and π-acceptor when binding to metals. Previously, the adsorption characteristics of CO on this system were studied and the adsorption free energies were calculated.[130] For the same size range studied here, these energies are plotted as crosses in **Figure A-21** at the same highest pressure. SO_2 binds much more efficiently at these partial pressures than CO (with the exception of Au_7^-), probably due to the enhanced π back bonding. This more efficient binding is also apparent from the fact that SO_2 binds very easily to the smaller Au_N^- clusters. In the CO adsorption studies, no evidence of adsorption was seen on the Au_2^- and Au_3^- clusters, even under CO partial pressure conditions in which the larger clusters had achieved saturation.

A.5 Conclusions

The adsorption characteristics of sulfur dioxide on bare and hydrated gas-phase gold cluster anions were studied using pulsed helium flow reactor techniques and time-of-flight mass spectrometry. SO_2 was found to bind on all of the clusters studied, even on the bare gold monomer anion, Au^-. The overall SO_2 adsorption activity is very size dependent, with the smaller clusters adsorbing more SO_2 than their larger counterparts. No complete determination of saturation coverages can be determined, though some of the larger clusters appear to be reluctant to undergo further adsorption at higher reactant partial pressures. A binding mechanism based on electron transfer has been proposed, in which "back bonding" from the cluster to the π^* orbital of the SO_2 molecule takes place, as has been seen in bonding of SO_2 to metal surfaces and in metal-ligand complexes. In relation to the SO_2 reactions occurring on supported gold cluster systems, these results suggest that the gold clusters themselves are capable of adsorbing SO_2 and that adsorption does not only occur at the sites of the cluster-support interface. It is unclear what, if any, effect that the presence of SO_2 would have on the ability of the gas phase clusters to promote CO oxidation.

REFERENCES

1. G.A. Somorjai, Introduction to surface chemistry and catalysis. 1 ed. 1994, New York: John Wiley and Sons, Inc. 667.

2. F. Zaera, Probing catalytic reactions at surfaces. *Prog. Surf. Sci.* **69** (2001) 1-98.

3. J. Xu and J.T. Yates, Catalytic oxidation of CO on Pt (335): a study of the active site. *J. Chem. Phys.* **99** (1993) 725-732.

4. A. Eichler, CO oxidation on transition metal surfaces: reaction rates from first principles. *Surf. Sci.* **498** (2002) 314-320.

5. J. Greeley, J.K. Norskov, and M. Mavrikakis, Electronic structure and catalysis on metal surfaces. *Annu. Rev. Phys. Chem.* **53** (2002) 319-348.

6. S.J. Riley, E.K. Parks, G.C. Nieman, *et al.*, Metal-deficient iron oxide clusters formed in the gas phase. *J. Chem. Phys.* **80** (1984) 1360-1362.

7. D.M. Cox, K.C. Reichmann, D.J. Trevor, *et al.*, CO chemisorption on free gas-phase metal clusters. *J. Chem. Phys.* **88** (1988) 111-119.

8. M.E. Geusic, M.D. Morse, and R.E. Smalley, Hydrogen chemisorption on transition metal clusters. *J. Chem. Phys.* **82** (1985) 590-591.

9. D.J. Trevor, R.L. Whetten, D.M. Cox, *et al.*, Gas-phase platinum cluster reactions with benzene and several hexanes: evidence of extensive dehydrogenation and size-dependent chemisorption. *J. Am. Chem. Soc.* **107** (1985) 518-519.

10. J. Conceicao, R.T. Laaksonen, L.-S. Wang, *et al.*, Photoelectron spectroscopy of transition-metal clusters: correlation of valence electronic structure to reactivity. *Phys. Rev. B* **51** (1995) 4668-4671.

11. M.D. Morse, M.E. Geusic, J.R. Heath, *et al.*, Surface reactions of metal clusters. II. Reactivity surveys with D_2, N_2, and CO. *J. Chem. Phys.* **83** (1985) 2293-2304.

12. M. Andersson, J.L. Persson, and A. Rosen, Reactivity of Fe_n, Co_n, and Cu_n clusters with O_2 and D_2 studied at single-collision conditions. *J. Phys. Chem.* **100** (1996) 12222-12234.

13. P.B. Armentrout, Reactions and thermochemistry of small transition metal cluster ions. *Annu. Rev. Phys. Chem.* **52** (2001) 423-461.

14. S.C. Richtsmeier, E.K. Parks, K. Liu, *et al.*, Gas phase reactions of iron clusters with hydrogen. I. Kinetics. *J. Chem. Phys.* **82** (1985) 3659-3665.

15. R.L. Whetten, D.M. Cox, D.J. Trevor, *et al.*, Free iron clusters react readily with O_2 and H_2S but are inert toward methane. *J. Phys. Chem.* **89** (1985) 566-569.

16. R.L. Whetten, D.M. Cox, D.J. Trevor, *et al.*, Correspondence between electron binding energy and chemisorption reactivity of iron clusters. *Phys. Rev. Lett.* **54** (1985) 1494-1497.

17. E.A. Rohlfing, D.M. Cox, A. Kaldor, *et al.*, Photoionization spectra and electronic structure of small iron clusters. *J. Chem. Phys.* **81** (1984) 3846-3851.

18. M. Andersson and A. Rosen, Catalytic oxidation of hydrogen on free platinum clusters. *J. Chem. Phys.* **117** (2002) 7051-7054.

19. D.M. Cox, P. Fayet, R. Brickman, *et al.*, Abnormally large deuterium uptake on small transition metal clusters. *Cat. Lett.* **4** (1990) 271-278.

20. G. Luttgens, N. Pontius, and P.S. Bechthold, Photon-induced thermal desorption of CO from small metal-carbonyl clusters. *Phys. Rev. Lett.* **88** (2002) 076102.

21. Y. Shi and K.M. Ervin, Catalytic oxidation of carbon monoxide by platinum cluster anions. *J. Chem. Phys.* **108** (1998) 1757-1760.

22. M.B. Knickelbein, Reactions of transition metal clusters with small molecules. *Ann. Rev. Phys. Chem.* **50** (1999) 79-115.

23. T.G. Dietz, M.A. Duncan, D.E. Powers, *et al.*, Laser production of supersonic metal cluster beams. *J. Chem. Phys.* **74** (1981) 6511-6512.

24. D.R. Preuss, S.A. Pace, and J.L. Gole, The supersonic expanison of pure copper vapor. *J. Chem. Phys.* **71** (1979) 3553-3560.

25. A. Hermann, E. Schumacher, and L. Woste, Preparation and photoionization potentials of molecules of sodium, potassium, and mixed atoms. *J. Chem. Phys.* **68** (1978) 2327-2336.

26. J.L. Gole, J.H. English, and V.E. Bondybey, Laser spectroscopy of cooled metal clusters: copper dimer. *J. Phys. Chem.* **86** (1982) 2560-2563.

27. V.E. Bondybey and J.H. English, Laser excitation spectra and lifetimes of Pb_2 and Sn_2 produced by YAG laser vaporization. *J. Chem. Phys.* **76** (1982) 2165-2170.

28. J.B. Hopkins, P.R.R. Langridge-Smith, M.D. Morse, *et al.*, Supersonic metal cluster beams of refractory metals: Spectral investigations of ultracold MO_2. *J. Chem. Phys.* **78** (1983) 1627-1637.

29. F.E. Livingston, The structure and temperature dependence of the molecular adsorption-desorption reactions of water on sodium fluoride clusters and nanocrystals: probing surface processes (1995) University of California, Los Angeles.

30. M. Valden, J. Aaltonene, E. Kuuisto, *et al.*, Molecular beam studies of CO oxidation and CO-NO reactions on a supported Pd catalyst. *Surf. Sci.* **307-309** (1994) 193-198.

31. S.K. Purnell, X. Xu, D.W. Goodman, *et al.*, Adsorption and reaction of $[Re_2(CO)_{10}]$ on ultrathin MgO films grown on a Mo (110) surface: characterization by infrared reflection-absorption spectroscopy and temperature-programmed desorption. *J. Phys. Chem.* **98** (1994) 4076-4082.

32. B.C. Gates, Supported metal clusters: synthesis, structure, and catalysis. *Chem. Rev.* **95** (1995) 511-522.

33. D.W. Goodman, Model studies in catalysis using surface science probes. *Chem. Rev.* **95** (1995) 523-536.

34. A.K. Santra and D.W. Goodman, Oxide-supported metal clusters: models for heterogeneous catalysts. *J. Phys.: Condens. Matter* **14** (2002) R31-R62.

35. C.R. Henry, Surface studies of supported metal catalysts. *Surf. Sci. Rep.* **31** (1998) 235-325.

36. M. Aizawa, S. Lee, and S.L. Anderson, Sintering, oxidation, and chemical properties of size-selected nickel clusters on TiO_2 (110). *J. Chem. Phys.* **117** (2002) 5001-5011.

37. W. Eberhardt, P. Fayet, D.M. Cox, *et al.*, Photoemission from mass-selected monodispersed Pt clusters. *Phys. Rev. Lett.* **64** (1990) 780-783.

38. F. Vanolli, U. Heiz, and W.-D. Schneider, Vibrational coupling of CO adsorbed on monodispersed Ni_{11} clusters supported on magnesia. *Chem. Phys. Lett.* **277** (1997) 527-531.

39. A. Sanchez, S. Abbet, U. Heiz, *et al.*, When gold is not noble: nanoscale gold catalysts. *J. Phys. Chem. A* **103** (1999) 9573-9578.

40. U. Heiz and W.-D. Schneider, Physical chemistry of supported clusters, in Metal clusters at surfaces, K.-H. Meiwes-Broer, Editor. 2000, Springer. p. 237-273.

41. U. Heiz, A. Sanchez, S. Abbet, *et al.*, Tuning the oxidation of carbon monoxide using nanoassembled model catalysts. *Chem. Phys.* **262** (2000) 189-200.

42. U. Heiz, A. Sanchez, S. Abbet, *et al.*, The reactivity of gold and platinum metals in their cluster phase. *Eur. Phys. J. D* **9** (1999) 35-39.

43. U. Heiz, F. Vanolli, A. Sanchez, *et al.*, Size-dependent molecular dissociation on mass-selected, supported metal clusters. *J. Am. Chem. Soc.* **120** (1998) 9668-9671.

44. H. Hakkinen, S. Abbet, A. Sanchez, *et al.*, Structural, electronic, and impurity-doping effects in nanoscale chemistry: supported gold nanoclusters. *Angew. Chem. Int. Ed.* **42** (2003) 1297-1300.

45. U. Heiz, F. Vanolli, L. Trento, *et al.*, Chemical reactivity of size-selected supported clusters: an experimental setup. *Rev. Sci. Instrum.* **68** (1997) 1986-1994.

46. U. Heiz, Size-selected, supported clusters: the interaction of carbon monoxide with nickel clusters. *Appl. Phys. A* **67** (1998) 621-626.

47. M.-H. Schaffner, F. Patthey, and W.-D. Schneider, Size-selected Ag_n and Cu_n clusters supported on MgO (100) films. *Eur. Phys. J. D* **9** (1999) 609-612.

48. C. Binns, Nanoclusters deposited on surfaces. *Surf. Sci. Rep.* **44** (2001) 1-49.

49. A. Cho, Connecting the dots to custom catalysts. *Science* **299** (2003) 1684-1685.

50. M. Haruta, T. Kobayashi, H. Sano, *et al.*, Novel gold catalysts for the oxidation of carbon monoxide at a temperature far below 0°C. *Chem. Lett.* **2** (1987) 405-408.

51. M. Haruta, N. Yamada, T. Kobayashi, *et al.*, Gold catalysts prepared by coprecipitation for low-temperature oxidation of hydrogen and of carbon monoxide. *J. Catal.* **115** (1989) 301.

52. M. Haruta, Size- and support-dependency in the catalysis of gold. *Cat. Today* **36** (1997) 153-166.

53. F. Boccuzzi, A. Chiorino, and S. Tsubota, The oxidation and scrambling of CO with oxygen at room-temperature on Au/ZnO. *Catal. Lett.* **29** (1994) 225-234.

54. F. Boccuzzi, A. Chiorino, and S. Tsubota, FTIR study of carbon monoxide oxidation and scrambling at room temperature over gold supported on ZnO and TiO_2. *J. Phys. Chem.* **100** (1996) 3625-3631.

55. F. Boccuzzi, G. Cerrato, F. Pinna, *et al.*, FTIR, UV-Vis, and HRTEM study of Au/ZrO_2 catalyst. *J. Phys. Chem. B* **102** (1998) 5733-5736.

56. F. Boccuzzi and A. Chiorino, FTIR study of CO oxidation on Au/TiO_2 at 90 K and room temperature. An insight into the nature of the reaction centers. *J. Phys. Chem. B* **104** (2000) 5414-5416.

57. R.S. Cataliotti, G. Compagnini, C. Crisafulli, *et al.*, Low-frequency Raman modes and atomic force microscopy for the size determination of catalytic gold clusters supported on iron oxide. *Surf. Sci.* **494** (2001) 75-82.

58. M.A. Bollinger and M.A. Vannice, A kinetic and DRIFTS study of low-temperature carbon monoxide oxidation over $Au-TiO_2$ catalysts. *Appl. Catal. B: Environ.* **8** (1996) 417-443.

59. S.D. Lin, M. Bollinger, and M.A. Vannice, Low temperature CO oxidation over Au/TiO_2 and Au/SiO_2 catalysts. *Catal. Lett.* **17** (1993) 245-262.

60. K. Ruth, M. Hayes, R. Burch, *et al.*, The effects of SO_2 on the oxidation of CO and propane on supported Pt and Au catalysts. *Appl. Catal. B: Environmental* **24** (2000) L133-L138.

61. L. Guczi, G. Peto, A. Beck, *et al.*, Gold nanoparticles deposited on SiO_2/Si (100): correlation between size, electron structure, and activity in CO oxidation. *J. Am. Chem. Soc.* **125** (2003) 4332-4337.

62. T.S. Kim, J.D. Stiehl, C.T. Reeves, *et al.*, Cryogenic CO oxidation on TiO_2-supported gold nanoclusters precovered with atomic oxygen. *J. Am. Chem. Soc.* **125** (2003) 2018-2019.

63. J.A. Rodriguez, G. Liu, T. Jirsak, *et al.*, Activation of gold on titania: adsorption and reaction of SO_2 on Au/TiO_2 (110). *J. Am. Chem. Soc.* **124** (2002) 5242-5250.

64. T.G. Schaaff and D.A. Blom, Deposition of Au-nanocrystals on TiO_2 crystallites. *Nano Lett.* **2** (2002) 507-511.

65. M. Valden, X. Lai, and D.W. Goodman, Onset of catalytic activity of gold clusters on titania with the appearance of nonmetallic properties. *Science* **281** (1998) 1647-1650.

66. D.A.H. Cunningham, W. Vogel, H. Kageyama, *et al.*, The relationship between the structure and activity of nm-size gold when supported on $Mg(OH)_2$. *J. Catal.* **177** (1998) 1-10.

67. D.A.H. Cunningham, W. Vogel, R.M. Torres-Sanchez, *et al.*, Structural analysis of Au/TiO_2 catalysts by Debye function analysis. *J. Catal.* **183** (1999)

68. Z.-P. Liu, P. Hu, and A. Alavi, Catalytic role of gold in gold-based catalysts: a density functional theory study on the CO oxidation on gold. *J. Am. Chem. Soc.* **124** (2002) 14770-14779.

69. N. Lopez and J.K. Norskov, Theoretical study of the Au/TiO_2(110) interface. *Surf. Sci.* **515** (2002) 175-186.

70. M. Mavrikakis, P. Stoltze, and J.K. Norskov, Making gold less noble. *Cat. Lett.* **64** (2000) 101-106.

71. G. Mills, M.S. Gordon, and H. Metiu, Oxygen adsorption on Au clusters and a rough Au(111) surface: The role of surface flatness, electron confinement, excess electrons, and band gap. *J. Chem. Phys.* **118** (2003) 4198-4205.

72. A. Vittadini and A. Selloni, Small gold clusters on stoichiometric and defected TiO_2 anatase (101) and their interaction with CO: A density functional study. *J. Chem. Phys.* **117** (2002) 353-361.

73. E. Wahlstrom, N. Lopez, R. Schaub, *et al.*, Bonding of gold nanoclusters to oxygen vacancies on rutile TiO_2 (110). *Phys. Rev. Lett.* **90** (2003) 026101.

74. Z. Yang and R. Wu, Origin of positive core-level shifts in Au clusters on oxides. *Phys. Rev. B* **67** (2003) 081403(R).

75. G.C. Bond and D.T. Thompson, Catalysis by gold. *Catal. Rev. Sci. Engng.* **41** (1999) 319-388.

76. M. Haruta, Catalysis of gold nanoparticles deposited on metal oxides. *Cattech* **6** (2002) 102-115.

77. K.J. Taylor, C.L. Pettiette-Hall, O. Cheshnovsky, *et al.*, Ultraviolet photo-electron spectra of coinage metal clusters. *J. Chem. Phys.* (1992) 3319-3327.

78. J. Ho, K.M. Ervin, and W.C. Lineberger, Photoelectron spectroscopy of metal cluster anions: Cu_n^-, Ag_n^-, and Au_n^-. *J. Chem. Phys.* **93** (1990) 6987-7002.

79. G.A. Bishea and M.D. Morse, Resonant two-photon ionization spectroscopy of jet-cooled Au_3. *J. Chem. Phys.* **95** (1991) 8779-8792.

80. O. Cheshnovsky, C.L. Pettiette, and R.E. Smalley, UPS of metal and semiconductor clusters, in Ion and Cluster Ion Spectroscopy and Structure, J.P. Maier, Editor. 1988, Elsevier. p. 373-415.

81. G.F. Gantefor, D.M. Cox, and A. Kaldor, Zero electron kinetic energy spectroscopy of Au_6^-. *J. Chem. Phys.* **96** (1992) 4102-4105.

82. H. Handschuh, G. Gantefor, P.S. Bechthold, *et al.*, A comparison of photoelectron spectroscopy and two-photon ionization spectroscopy: Excited states of Au_2, Au_3, and Au_4. *J. Chem. Phys.* **100** (1994) 7093-7100.

83. J. Li, X. Li, H.-J. Zhai, *et al.*, Au_{20}: a tetrahedral cluster. *Science* **299** (2003) 864-867.

84. K.J. Taylor, C. Jin, J. Conceicao, *et al.*, Vibrational autodetachment spectroscopy of Au_6^-: image-charge-bound states of a gold ring. *J. Chem. Phys.* **93** (1990) 7515-7518.

85. H. Handschuh, C.Y. Cha, H. Moller, *et al.*, Delocalized electronic states in small clusters-comparison of Na_N, Cu_N, Ag_N, and Au_N clusters. *Chem. Phys. Lett.* **227** (1994) 496-502.

86. J. Ziegler, G. Dietrich, S. Krueckeberg, *et al.*, Multicollision-induced dissociation of multiply charged gold clusters, Au_n^{2+}, N = 7–35, and Au_n^{3+}, N = 19–35. *Int. J. Mass Spectrom.* **202** (2000) 47-54.

87. W.D. Knight, K. Clemenger, W.A. deHeer, *et al.*, Electronic shell structure and abundances of sodium clusters. *Phys. Rev. Lett.* **52** (1984) 2141-2143.

88. M.Y. Chou and M.L. Cohen, Electronic shell structure in simple metal clusters. *Phys. Lett.* **113A** (1986) 420-424.

89. M.L. Cohen, M.Y. Chou, W.D. Knight, *et al.*, Physics of metal clusters. *J. Phys. Chem.* **91** (1987) 3141-3149.

90. K.E. Schriver, J.L. Persson, E.C. Honea, *et al.*, Electronic shell structure of group-IIIA metal atomic clusters. *Phys. Rev. Lett.* **64** (1990) 2539-2542.

91. P. Stampfli and K.H. Bennemann, Unified model for the shell structure in the mass spectra of metallic clusters. *Phys. Rev. Lett.* **69** (1992) 3471.

92. M.B. Knickelbein, Electronic shell structure in the ionization potentials of copper clusters. *Chem. Phys. Lett.* **192** (1992) 129-134.

93. C. Jackschath, I. Rabin, and W. Schulze, Electron impact ionization potentials of gold and silver clusters M_n, n<22. *Ber. Bunsenges. Phys. Chem.* **96** (1992) 1200.

94. W.A. deHeer, The physics of simpler metal clusters: experimental aspects and models. *Rev. Mod. Phys.* **65** (1993) 611-676.

95. C.L. Pettiette, S.H. Yang, M.J. Craycraft, *et al.*, Ultraviolet photoelectron spectroscopy of copper clusters. *J. Chem. Phys.* **88** (1988) 5377-5382.

96. D.G. Leopold, J. Ho, and W.C. Lineberger, Photoelectron spectroscopy of mass-selected metal cluster anions. I. Cu_n^-, n = 1 - 10. *J. Chem. Phys.* **86** (1987) 1715-1726.

97. G. Gantefor, C.-Y. Cha, H. Handschuh, *et al.*, Electronic and geometric structure of small mass selected clusters. *J. Elec. Spect. Rel. Phenomena* **76** (1995) 37.

98. K. Balasubramanian and D.-W. Liao, Is Au_6 a circular ring? *J. Chem. Phys.* **94** (1991) 5233-5236.

99. H. Hakkinen and U. Landman, Gold clusters and their anions. *Phys. Rev. B* **62** (2000) R2287-R2290.

100. S. Gilb, P. Weis, and F. Furche, Structures of small gold cluster cations (Au_n^+, n < 14): Ion-mobility measurements versus density functional calculations. *J. Chem. Phys.* **116** (2002) 4094.

101. F. Furche, R. Ahlrichs, P. Weis, *et al.*, The structures of small gold cluster anions as determined by a combination of ion mobility measurements and density functional calculations. *J. Chem. Phys.* **117** (2002) 6982-6990.

102. H. Hakkinen, M. Moseler, and U. Landman, Bonding in Cu, Ag, and Au clusters: relativistic effects, trends, and surprises. *Phys. Rev. Lett.* **89** (2002) 033401.

103. X. Wu, L. Senapati, S.K. Nayak, *et al.*, A density functional study of carbon monoxide adsorption on small cationic, neutral, and anionic gold clusters. *J. Chem. Phys.* **117** (2002) 4010-4015.

104. D.H. Wells, W.N. Delgass, and K.T. Thomson, Density functional theory investigation of gold cluster geometry and gas-phase reactivity with O_2. *J. Chem. Phys.* **117** (2002) 10597.

105. J. Oviedo and R.E. Palmer, Amorphous structures of Cu, Ag, and Au nanoclusters from first principles calculations. *J. Chem. Phys.* **117** (2002) 9548-9551.

106. M.A. Cheeseman and J.R. Eyler, Ionization potentials and reactivity of coinage metal clusters. *J. Phys. Chem.* **96** (1992) 1082-1087.

107. D.M. Cox, R.O. Brickman, K. Creegan, *et al.*, Studies of the chemical properties of size selected metal clusters: kinetics and saturation. *Mat. Res. Soc. Symp. Proc.* **206** (1991) 34-48.

108. D.M. Cox, R. Brickman, K. Creegan, *et al.*, Gold clusters: reactions and deuterium uptake. *Z. Phys. D* **19** (1991) 353-355.

109. M.B. Knickelbein and G.M. Koretsky, Infrared studies of the interactions of methanol with Cu_n, Ag_n, and Au_n. *J. Phys. Chem. A* **102** (1998) 580-586.

110. G.M. Koretsky, M.B. Knickelbein, R. Rousseau, *et al.*, A combined infrared photodissociation and theoretical study of the interaction of ethanol with small gold clusters. *J. Phys. Chem. A* **105** (2001) 11197-11203.

111. M.A. Nygren, P.E.M. Siegbahn, C.-M. Jin, *et al.*, Electronic shell closings in metal cluster plus adsorbate systems: Cu_7^+CO and Cu_{17}^+CO. *J. Chem. Phys.* **95** (1991) 6181-6184.

112. T.H. Lee and K.M. Ervin, Reactions of copper group cluster anions with oxygen and carbon monoxide. *J. Phys. Chem.* **98** (1994) 10023-10031.

113. T.H. Lee, Reactions and bond dissociation energies of bare and ligated copper group anions (1995) University of Nevada, Reno.

114. A.W. Castleman and K.H. Bowen, Clusters: structure, energetics, and dynamics of intermediate states of matter. *J. Phys. Chem.* **100** (1996) 12911-12944.

115. M.T. Bowers, A.G. Marshall, and F.W. McLafferty, Mass spectrometry: recent advances and future directions. *J. Phys. Chem.* **100** (1996) 12897-12910.

116. L.D. Socaciu, J. Hagen, U. Heiz, *et al.*, Reaction mechanism for the oxidation of free silver dimers. *Chem. Phys. Lett.* **340** (2001) 282-288.

117. J. Hagen, L.D. Socaciu, M. Elijazyfer, *et al.*, Coadsorption of CO and O_2 on small free gold cluster anions at cryogenic temperatures: model complexes for catalytic CO oxidation. *Phys. Chem. Chem. Phys.* **4** (2002) 1707-1709.

118. I. Balteanu, O.P. Balaj, B.S. Fox, *et al.*, Very low rate constants of bimolecular CO adsorption on anionic gold clusters: implications for catlytic activity. *Phys. Chem. Phys. Chem.* **5** (2003) 1213-1218.

119. S.W. McElvany, B.I. Dunlap, and A. O'Keefe, Ion molecule reactions of carbon cluster ions with D_2 and O_2. *J. Chem. Phys.* **86** (1987) 715-725.

120. S.W. McElvany, Reactions of carbon cluster ions with small hydrocarbons. *J. Chem. Phys.* **89** (1988) 2063-2075.

121. J.A. Zimmerman, J.R. Eyler, S.B.H. Bach, *et al.*, "Magic number" carbon clusters: ionization potentials and selective reactivity. *J. Chem. Phys.* **94** (1991) 3556-3562.

122. K. Fisher, F. Hopwood, I. Dance, *et al.*, Reactions of small carbon anions with hydrogen sulfide, benzene thiol, and sulfur. *New. J. Chem.* **23** (1999) 609-616.

123. M. Vogel, K. Hansen, A. Herlert, *et al.*, The influence of internal degrees of freedom on the unimolecular decay of the molecule-cluster compound $Au_8^+CH_3OH$. *J. Chem. Phys.* **116** (2002) 9658-62.

124. R. Rousseau, G. Dietrich, S. Krückeberg, *et al.*, Probing cluster structures with sensor molecules: methanol adsorbed onto gold clusters. *Chem. Phys. Lett.* **295** (1998) 41-46.

125. M.B. Sowa and S.L. Anderson, Oxidation of small carbon cluster ions by O_2: effects of structure on the reaction mechanism. *J. Chem. Phys.* **97** (1992) 8164-8172.

126. S.K. Loh, D.A. Hales, L. Lian, *et al.*, Collision-induced dissociation of Fe_n^+ (n = 2 - 10) with Xe: ionic and neutral iron binding energies. *J. Chem. Phys.* **90** (1989) 5466-5485.

127. K.M. Ervin, Experimental techniques in gas-phase ion thermochemistry. *Chem. Rev.* **101** (2001) 391-444.

128. P.B. Armentrout and T. Baer, Gas-phase ion dynamics and chemistry. *J. Phys. Chem.* **100** (1996) 12866-12877.

129. M.E. Geusic, M.D. Morse, S.C. O'Brien, *et al.*, Surface reactions of metal clusters. I: the fast flow cluster reactor. *Rev. Sci. Instrumen.* **56** (1985) 2123-2130.

130. W.T. Wallace and R.L. Whetten, Carbon monoxide adsorption on selected gold clusters: highly size-dependent activity and saturation compositions. *J. Phys. Chem. B* **104** (2000) 10964-10968.

131. W.T. Wallace, A.J. Leavitt, and R.L. Whetten, Comment on: The adsorption of molecular oxygen on neutral and negative Au_N clusters (N = 2-5) [Chem. Phys. Lett. 359 (2002) 493]. *Chem. Phys. Lett.* **368** (2003) 774-777.

132. B.E. Salisbury, Mass spectroscopic characterization of small nanoclusters (1999) Georgia Institute of Technology.

133. B.E. Salisbury, W.T. Wallace, and R.L. Whetten, Low-temperature activitation of molecular oxygen by gold clusters: a stoichiometric process correlated to electron affinity. *Chem. Phys.* **262** (2000) 131-141.

134. E.K. Parks, G.C. Nieman, K.P. Kerns, *et al.*, Reactions of Ni_{38} with N_2, H_2, and CO: cluster structure and adsorbate binding sites. *J. Chem. Phys.* **107** (1997) 1861-1871.

135. E.K. Parks, G.C. Nieman, K.P. Kerns, *et al.*, The thermodynamics of nitrogen adsorption on nickel clusters: Ni_{19}-Ni_{71}. *J. Chem. Phys.* **108** (1998) 3731-3739.

136. L. Zhu, J. Ho, E.K. Parks, *et al.*, Temperature dependence of the reaction of nickel clusters with deuterium. *J. Chem. Phys.* **98** (1993) 2798-2804.

137. B.J. Winter, E.K. Parks, and S.J. Riley, Copper clusters: the interplay between electronic and geometrical structure. *J. Chem. Phys.* **94** (1991) 8618-8621.

138. R.L. Whetten, M.R. Zakin, D.M. Cox, *et al.*, Electron binding and chemical inertness of specific Nb_X clusters. *J. Chem. Phys.* **85** (1986) 1697-1698.

139. E.K. Parks, T.D. Klots, B.J. Winter, *et al.*, Reactions of cobalt clusters with water and ammonia: implications for cluster structure. *J. Chem. Phys.* **99** (1993) 5831-5839.

140. M.L. Homer, F.E. Livingston, and R.L. Whetten, Structure dependence of ammonia adsorption on alkali halide clusters. *J. Am. Chem. Soc.* **114** (1992) 6558-6559.

141. M.L. Homer, F.E. Livingston, and R.L. Whetten, Adsorption reactions of alkali-halide nanocrystals: identification of an important surface defect. *Z. Phys. D* **26** (1993) 201.

142. M.L. Homer, F.E. Livingston, and R.L. Whetten, Molecular adsorption-desorption reactions of ammonia on alkali-halide clusters and nanocrystals. *J. Phys. Chem.* **99** (1995) 7604-7612.

143. M. Doverstal, B. Lindgren, U. Sassenberg, *et al.*, Reaction of small carbon clusters with hydrogen during laser vaporization of graphite. *Z. Phys. D* **19** (1991) 447-449.

144. Q.L. Zhang, S.C. O'Brien, J.R. Heath, *et al.*, Reactivity of large carbon clusters: spheroidal carbon shells and their possible relevance to the formation and morphology of soot. *J. Phys. Chem.* **90** (1986) 525-528.

145. A.J. Leavitt, *personal communication.*

146. E.K. Parks, B.J. Winter, T.D. Klots, *et al.*, The structure of nickel clusters. *J. Chem. Phys.* **94** (1991) 1882-1902.

147. G.M. Koretsky and M.B. Knickelbein, The reactions of silver clusters with ethylene and ethylene oxide: infrared and photoionization studies of $Ag_n(C_2H_4)_m$, $Ag_n(C_2H_4O)_m$ and their deuterated analogs. *J. Chem. Phys.* **107** (1997) 10555-10566.

148. K.A. Zemski, D.R. Justes, and A.W. Castleman, Studies of metal oxide clusters: elucidating reactive sites responsible for the activity of transition metal oxide catalysts. *J. Phys. Chem. B* **106** (2002) 6136-6148.

149. C. Bauer, Y. Koyasu, S. Nakamura, *et al.*, An ab-initio MO study on metal oxide catalytic surfaces. *J. Mol. Struct. (Theochem)* **461** (1999) 391-398.

150. H.-J. Zhai and L.-S. Wang, Electronic structure and chemical bonding of divanadium-oxide clusters (V_2O_x, x = 3 – 7) from anion photoelectron spectroscopy. *J. Chem. Phys.* **117** (2002) 7882-7888.

151. R.B. Wyrwas, A.J. Leavitt, and R.L. Whetten, SOx on VOx: oxidation-state tuning of SO_2 adsorption on vanadium-oxide cluster anions. *J. Phys. Chem.* **submitted** (2003)

152. J.H. Seinfeld and S.N. Pandis, Atmospheric chemistry and physics. 1998, New York: Wiley-Interscience.

153. B.J. Finlayson-Pitts and J.N. Pitts, Chemistry of the upper and lower atmosphere. 2000, New York: Academic Press.

154. W.T. Wallace and R.L. Whetten, Metastability of gold-carbonyl cluster complexes, $Au_N(CO)_M^-$. *Eur. Phys. J. D* **16** (2001) 123-126.

155. P. Milani and W.A. deHeer, Improved pulsed laser vaporization source for production of intense beams of neutral and ionized clusters. *Rev. Sci. Instrum.* **61** (1990) 1835-1838.

156. H. Weidele, U. Frenzel, T. Leisner, *et al.*, Production of "cold/hot" metal cluster ions: a modified laser vaporization source. *Z. Phys. D* **20** (1991) 411-412.

157. W.C. Wiley and I.H. McLaren, Time-of-flight mass spectrometer with improved resolution. *Rev. Sci. Instr.* **26** (1955) 1150-1159.

158. P.M. St.John, C. Yeretzian, and R.L. Whetten, Electron emission mechanism for impact of C_N^- and Si_N^- clusters. *J. Phys. Chem.* **96** (1992) 9100-9104.

159. R.L. Whetten, C. Yeretzian, and P.M. St.John, Cleavage patterns of carbon clusters from impact-induced fragmentation of C_N^-, N = 10 - 50. *Int. J. Mass Spec. Ion Process.* **138** (1994) 63-76.

160. D.S. Cornett, M. Peschke, K. LaiHing, *et al.*, Reflectron time-of-flight mass spectrometer for laser photodissociation. *Rev. Sci. Instrumen.* **63** (1992) 2177-2186.

161. V.I. Karataev, B.A. Mamyrin, and D.V. Shmikk, New method for focusing ion bunches in time-of-flight mass spectrometers. *Sov. Phys.-Tech. Phys.* **16** (1972) 1177-1179.

162. V.A. Mamyrin, V.I. Karateav, D.V. Schmikk, *et al.*, The mass-reflectron, a new non-magnetic time-of-flight mass spectrometer with high resolution. *Sov. Phys. JETP* **37** (1973) 82-89.

163. H. Kuhlewind, H.J. Neusser, and E.W. Schlag, Metastable fragment ions in multi-photon time-of-flight mass spectrometry: decay channels of the benzene cation. *Int. J. Mass Spectrom. Ion Phys.* **51** (1983) 255-256.

164. Y.A. Yang, P. Xia, A.L. Junkin, *et al.*, Direct ejection of clusters from nonmetallic solids during laser vaporization. *Phys. Rev. Lett.* **66** (1991) 1205-1208.

165. Y.J. Twu, C.W.S. Conover, Y.A. Yang, *et al.*, Alkali-halide cluster ions produced by laser vaporization of solids. *Phys. Rev. B* **42** (1990) 5306-5316.

166. X. Li and R.L. Whetten, Ultraviolet absorption bands of ionic compound clusters: onset of crystalline structures in $[Cs_{n+1}I_n]^+$, n = 1 - 13. *J. Chem. Phys.* **98** (1993) 6170-6175.

167. N.G. Gotts, G.v. Helden, and M.T. Bowers, Carbon cluster anions: structure and growth from C_5^- to C_{62}^-. *Int. J. Mass Spect. Ion Process.* **149/150** (1995) 217-229.

168. M. Ohara, M. Suwa, T. Ishigaki, *et al.*, Resonance-enhanced multiphoton electron detachment (REMPED) spectra of C_{10}^- and C_{11}^-. *J. Chem. Phys.* **109** (1998) 1329-1333.

169. M. Kohno, S. Suzuki, H. Shiromaru, *et al.*, Ultraviolet photoelectron spectroscopy on the linear conformer of negatively charged carbon clusters C_n^-. *Chem. Phys. Lett.* **282** (1998) 330-334.

170. J.-D. Grunwaldt and A. Baiker, Gold/titania interfaces and their role in carbon monoxide oxidation. *J. Phys. Chem. B* **103** (1999) 1002-1012.

171. D.A. Outka and R.J. Madix, The oxidation of carbon monoxide on the Au (110) surface. *Surf. Sci.* **179** (1987) 351-360.

172. A.G. Sault and R.J. Madix, Adsorption of oxygen and hydrogen on Au (110)-(1X2). *Surf. Sci.* **169** (1986) 347-356.

173. W.D. Vann, R.L. Wagner, and A.W. Castleman, Gas-phase reactions of nickel and nickel-rich oxide cluster anions with nitric oxide. 2. The addition of nitric oxide, oxidation of nickel clusters and the formation of nitrogen oxide anions. *J. Phys. Chem. A* **102** (1998) 8804-8811.

174. T. Lange, H. Gohlich, U. Naher, *et al.*, Shell-dependent reactivity of sodium clusters with oxygen. *Chem. Phys. Lett.* **192** (1992) 544-546.

175. R.C. Bell, K.A. Zemski, K.P. Kerns, *et al.*, Reactivities and collision-induced dissociation of vanadium oxide cluster cations. *J. Phys. Chem. A* **102** (1998) 1733-1742.

176. C. Yannouleas and U. Landman, Decay channels and appearance sizes of doubly anionic gold and silver clusters. *Phys. Rev. B* **61** (2000) R10587-R10589.

177. M.E. Bartram and B.E. Koel, The molecular adsorption of NO_2 and the formation of N_2O_3 on Au (111). *Surf. Sci.* **213** (1989) 137-156.

178. G. Mills, M.S. Gordon, and H. Metiu, The adsorption of molecular oxygen on neutral and negative Au_N clusters (N = 2-5). *Chem. Phys. Lett.* **359** (2002) 493.

179. S.A. Varganov, R.M. Olson, M.S. Gordon, *et al.*, Reply to a comment: oxygen adsorption on Au clusters by W.T. Wallace, A.J. Leavitt, and R.L. Whetten. *Chem. Phys. Lett.* **368** (2003) 778-779.

180. D. McIntosh and G.A. Ozin, Direct synthesis using gold atoms. Monodioxygen gold, $Au(O_2)$. *Inorg. Chem.* **15** (1976) 2869-2871.

181. H. Huber, D. McIntosh, and G.A. Ozin, A metal atom model for the oxidation of carbon monoxide to carbon dioxide. The gold atom-carbon monoxide-dioxygen

reaction and the gold atom-carbon dioxide reaction. *Inorg. Chem.* **16** (1977) 975-979.

182. D. Stolcic, M. Fischer, G. Gantefor, *et al.*, Direct observation of key reaction intermediates on gold clusters. *J. Am. Chem. Soc.* **125** (2003) 2848-2849.

183. M. Haruta, S. Tsubota, and T. Kobayashi, Low-temperature oxidation of CO over gold supported on TiO_2, α-Fe_2O_3, and Co_3O_4. *J. Catal.* **144** (1993) 175.

184. B.J. Winter, T.D. Klots, E.K. Parks, *et al.*, Chemical identification of icosahedral structure for cobalt and nickel clusters. *Z. Phys. D* **19** (1991) 375-380.

185. C. Brechignac, P. Cahuzac, J. Leygnier, *et al.*, Comparison of reactive nucleation of silver and alkali clusters in the presence of oxygen and water. *Eur. Phys. J. D* **9** (1999) 421-424.

186. U. Ray and M.F. Jarrold, Reactions of silicon cluster ions, Si_n^+ (n=10-65), with water. *J. Chem. Phys* **94** (1991) 2631-2639.

187. L. Poisson, F. Lepetit, J.-M. Mestdagh, *et al.*, Multifragmentation of the $Au(H_20)_{n<10}^+$ cluster ions by collision with helium. *J. Phys. Chem. A* **106** (2002) 5455-5462.

188. L. Poisson, P. Pradel, F. Lepetit, *et al.*, Binding energies of first and second shell water molecules in the $Fe(H_2O)_2^+$, $Co(H_2O)_2^+$, and $Au(H_2O)_2^+$ cluster ions. *Eur. Phys. J. D* **14** (2001) 89-95.

189. D. Feller, E.D. Glendening, and W.A. deJong, Structures and binding enthalpies of $M^+(H_2O)_n$ clusters, M = Cu, Ag, Au. *J. Chem. Phys.* **110** (1999) 1475-1491.

190. H. Hakkinen and U. Landman, Gas-phase catalytic oxidation of CO by Au_2^-. *J. Am. Chem. Soc.* **123** (2001) 9704.

191. V. Bonacic-Koutecky, *personal communication.*

192. W.T. Wallace and R.L. Whetten, Coadsorption of CO and O_2 on selected gold clusters: evidence for efficient room-temperature CO_2 generation. *J. Am. Chem. Soc.* **124** (2002) 7499-7505.

193. W.T. Wallace, R.B. Wyrwas, R.L. Whetten, *et al.*, Oxygen adsorption on hydrated gold cluster anions: experiment and theory. *J. Am. Chem. Soc.* **125** (2003) 8408-8414.

194. C. Lee, W. Yang, and R.G. Parr, Development of the Colle-Salvetti correlation-energy formula into a functional of the electron density. *Phys. Rev. B* **37** (1988) 785.

195. A.D. Becke, Density-functional exchange-energy approximation with correct asymptotic behavior. *Phys. Rev. A* **38** (1988) 3098.

196. A.D. Becke, Density-functional thermochemistry. III. The role of exact exchange. *J. Chem. Phys.* **98** (1993) 5648.

197. D. Andrae, U. Haeussermann, and M. Dolg, Energy-adjusted ab initio pseudopotentials for the 2^{nd}-row and 3^{rd}-row transition elements- Molecular test for Ag_2, Au_2 and RuH, OsH. *Theor. Chim. Acta* **77** (1990) 123.

198. R. Krishnan, J.S. Binkley, and R. Seeger, Self-consistent molecular orbital methods. XX. A basis set for correlated wave functions. *J. Chem. Phys.* **72** (1980) 650.

199. A.D. McLean and G.S. Chandler, Contracted Gaussian basis sets for molecular calculations. I. Second row atoms, Z=11-18. *J. Chem. Phys.* **72** (1980) 5639.

200. K.M. Ervin, *personal communication.*

201. C.W. Baushlicher, S.R. Langhoff, and H. Partridge, Theoretical study of the homonuclear tetramers and pentamers of the group IB metals (Cu, Ag, Au). *J. Chem. Phys.* **93** (1990) 8133.

202. O.D. Haberlen, S.-C. Chung, and M. Stener, From clusters to bulk: a relativistic density functional investigation on a series of gold clusters, Au_n, n = 6,...,147. *J. Chem. Phys.* **106** (1997) 5189.

203. V. Bonacic-Koutecky, J. Burda, R. Mitric, *et al.*, Density functional study of structural and electronic properties of bimetallic silver-gold clusters: comparison with pure silver and gold clusters. *J. Chem. Phys.* **117** (2002) 3120.

204. R. Mitric, C. Burgel, J. Burda, *et al.*, Structural properties and reactivity of bimetallic silver-gold clusters. *Eur. Phys. J. D* (2003) in press.

205. C. Ruggiero and P. Hollins, Adsorption of carbon monoxide on the gold (332) surface. *J. Chem. Soc. Faraday Trans.* **92** (1996) 4829-4834.

206. C. Ruggiero and P. Hollins, Interaction of CO molecules with the Au (332) surface. *Surf. Sci.* **377-379** (1997) 583-586.

207. D. Fischer, W. Andreoni, A. Curioni, *et al.*, Chemisorption on small clusters: can vertical detachment energy measurements provide chemical information? H on Au as a case study. *Chem. Phys. Lett.* **361** (2002) 389-396.

208. O. Echt, P.D. Dao, S. Morgan, *et al.*, Multiphoton ionization of ammonia clusters and the dissociation dynamics of protonated cluster ions. *J. Chem. Phys.* **82** (1985) 4076-4085.

209. J.D. Roth, G.J. Lewis, L.K. Stafford, *et al.*, Exploration of the ionizable metal cluster-electrode surface analogy. *J. Am. Chem. Soc.* **114** (1992) 6159-6164.

210. M. Haruta, When gold is not noble: catalysis by nanoparticles. *Chem. Rec.* **3** (2003) 75-87.

211. P. Schwerdtfeger, Gold goes nano - from small clusters to low-dimensional assemblies. *Angew. Chem. Int. Ed.* **42** (2003) 1892-1895.

212. P.H. Abelson, Funding the nanotech frontier. *Science* **288** (2000) 269.

213. D.A. Mantell, K. Kunimori, S.B. Ryali, *et al.*, The dynamics of CO oxidation on Pt deduced from translational, rotational, and vibrational excitation in product CO_2. *Surf. Sci.* **172** (1986) 281-302.

214. M. Maier-Borst, D.B. Cameron, M. Rokni, *et al.*, Electron diffraction of trapped cluster ions. *Phys. Rev. A* **59** (1999) R3162-R3165.

215. S. Kruckeberg, D. Schooss, M. Maier-Borst, *et al.*, Diffraction of trapped cesium-iodide clusters: the appearance of the bulk structure. *Phys. Rev. Lett.* (2000) in press.

216. J. Haase, Structural studies of SO_2 adsorption on metal surfaces. *J. Phys.: Condens. Matter* **9** (1997) 3647-3670.

217. S. Sakaki, H. Sato, and Y. Imai, Comparison of electronic structure, stereochemistry, and coordinate bonds between Ni(0)-SO_2 complexes and nonmetal SO_2 complexes. *Inorg. Chem.* **24** (1985) 4538-4544.

218. G.J. Kubas and R.R. Ryan, Activation of H_2 and SO_2 by Mo and W complexes: first examples of molecular-H_2 complexes, SO_2 insertion into metal-hydride bonds, and homogeneous hydrogenation of SO_2. *Polyhedron* **5** (1986) 473-485.

219. M. Polcik, L. Wilde, J. Haase, *et al.*, High-resolution XPS and NEXAFS study of SO_2 adsorption on Pt (111): two surface SO_2 species. *Surf. Sci.* **381** (1997) L568-L572.

220. S. Terada, T. Yokoyama, Y. Okamoto, *et al.*, SO_2 adsorption on thin Pd/Ni (111) films studied by X-ray absorption fine structure spectroscopy. *Surf. Sci.* **442** (1999) 141-148.

221. H. Sellers and E. Shustorovich, Chemistry of sulfur oxides on transition metal surfaces: a bond order conservation-Morse potential modeling perspective. *Surf. Sci.* **356** (1996) 209-221.

222. G. Liu, J.A. Rodriguez, J. Dvorak, *et al.*, Chemistry of sulfur-containing molecules on Au (111): thiophene, sulfur dioxide, and methanethiol adsorption. *Surf. Sci.* **505** (2002) 295-307.

223. D.M. Collard and M.A. Fox, Use of electroactive thiols to study the formation and exchange of alkanethiol monolayers on gold. *Langmuir* **7** (1991) 1192-1197.

224. A.J. Leavitt and T.P. Beebe, Chemical reactivity studies of hydrogen-sulfide on Au(111). *Surf. Sci.* **314** (1994) 23-33.

225. F.D. Felice, A. Selloni, and E. Molinari, DFT study of cysteine adsorption on Au(111). *J. Phys. Chem. B* **107** (2003) 1151-1156.

226. http://webbook.nist.gov, .

227. Y.-P. Ho and R.C. Dunbar, Reactions of Au+ and Au- with benzene and fluorine-substituted benzenes. *Int. J. Mass Spectrom.* **182/183** (1999) 175-184.

228. A.K. Chowdhury and C.L. Wilkins, Reactions of atomic gold ions with aliphatic and aromatic hydrocarbons and alkyl halides. *J. Am. Chem. Soc.* **109** (1987) 5336-5343.

229. M.S. El-Shall, K.E. Schriver, R.L. Whetten, *et al.*, Ion-molecule clustering thermochemistry by laser ionization high-pressure mass spectrometry. *J. Phys. Chem.* **93** (1989) 7969-7973.

230. J. Mwakapumba and K.M. Ervin, Reactivity of niobium cluster anions with nitrogen and carbon monoxide. *Int. J. Mass Spectrom. Ion Process.* **161** (1997) 161-174.

231. P.A. Hintz and K.M. Ervin, Nickel group cluster anion reactions with carbon monoxide: rate coefficients and chemisorption efficiency. *J. Chem. Phys.* **100** (1994) 5715-5724.

VITA

William Todd Wallace was born on March 8, 1976 in Riverdale, Georgia (USA). Following his graduation in the spring of 1994 from McIntosh High School in Peachtree City, Georgia, he enrolled at Oxford College of Emory University. After transferring to the State University of West Georgia in the spring of 1997, he began to pursue a degree in chemistry. While at the State University of West Georgia, he was a member of the research group of Professor Andrew Leavitt, studying the chemical reactions of small molecules on metal and ionic surfaces. Graduating with his bachelor of science in chemistry in the spring of 1999, he enrolled at the Georgia Institute of Technology as a graduate student in chemistry, immediately beginning research in the group of Professor Robert Whetten. There, his research focused on the adsorption properties of various gas-phase cluster species. He is currently continuing his work on the adsorption properties of gold clusters and will relocate to the laboratories of Professor D. Wayne Goodman in the fall of 2003 to continue work in surface chemical processes.